3D STATE SPACE ANALYSIS AND FREE-EDGE EFFECT OF PIEZOELECTRIC LAMINATED THICK PLATES

A thesis submitted to the University of Manchester for the degree of

Doctor of Philosophy

in the Faculty of Engineering and Physical Sciences

2014

CHAO HAN

School of Mechanical, Aerospace and Civil Engineering

CONTENTS

WORD COUNT: 43407

LIST OF FIGURES

LIST OF TABLES

LIST OF NOTATIONS

a	Length
b	Width
$BaTiO_3$	Barium titanate
C	Elastic constant
D	Electric displacement vector
e	Piezoelectric constant
E	Electric field vector
d_i	Thickness of each sub-layer in the i^{th} material layer
f_e	Electric body charge
f_i	Body force
h	Thickness
K_i	Number of mathematical sub-layers in the i^{th} material layer
m, n	Vibration wave numbers
N	Number of material layers
P	Total number of mathematical sub-layers
PZT	Lead zirconate titanate
q	Uniformly distributed load
u, v, w	Displacement components
σ	Stress vector
τ	Shear stress
ε	Strain vector

ε_0	Uniform constant axial strain
γ	Shear strain
ν	Poisson's ratio
ϵ	Dielectric constant
ϵ_0	Permittivity of vacuum ($\approx 8.854 \times 10^{-12} F/m$)
$\emptyset$	Electric potential

ABSTRACT

The accurate evaluation of interlaminar stresses is of great significance in the analysis and design of laminated and piezoelectric laminated structures because complex behaviours of these stresses near free edges initiate edge delamination that raises concerns about the structural integrity and reliability. This thesis presented 3D hybrid analyses on the interlaminar stresses to investigate the electromechanical coupling and free edge effects of piezoelectric laminated plates with an emphasis on the realistic distributions of the 3D stress and electric fields near free edges.

In this research, the state space equations for simply-supported and free-edge piezoelectric laminates under transverse loads and infinite long free-edge piezoelectric laminates under uniaxial extension were obtained in the framework of 3D piezoelasticity by considering all the independent elastic and piezoelectric constants. The equations satisfy the traction-free and open-circuit boundary conditions at free edges and the continuity conditions across all interfaces. On the basis of the transfer matrix and recursive solution approaches, 3D exact solutions were sought by a novel non-uniform layer refinement technique to evaluate the accuracy of the finite element method (FEM), and realistic gradients of interlaminar stresses and electric fields were captured. The FEM results were in good agreement with those from the present solutions except for the regions near free edges. For simply-supported and free-edge laminates, stress variations with material properties, geometries and stacking sequences were obtained. The interlaminar stress τ_{xz} was dominant at corners and τ_{yz} also tended to contribute to delamination. In the infinite long free-edge laminates, σ_z, τ_{yz}, E_y and E_z exhibited significant gradients near free edges. Furthermore, the considerable influence of the electromechanical coupling effect on interlaminar stresses revealed that piezoelectric laminates were more susceptible to edge delamination and the application of closed-circuited surface conditions might prevent such edge delamination. The present analytical solution demonstrated an improvement in precision over other 2D analytical and numerical solutions and could serve as a benchmark for the determination of interlaminar stresses and electric fields near the free edges of the piezoelectric laminates.

DECLARATION

No portion of the work referred to in the thesis has been submitted in support of an application for another degree or qualification of this or any other university or other institute of learning.

COPYRIGHT

ACKNOWLEDGEMENTS

First and foremost, I would like to express my sincere gratitude to my supervisor, Dr. Jack Wu, whose expertise, understanding, patience and optimism enlightened me on my PhD research. I also appreciate his valuable guidance and constant encouragement during my academic life and I am so grateful.

I also want to express my gratitude to all the staff of the School of MACE. Special thanks go to Dr. Zhenmin Zou and Dr. Parthasarathi Mandal who gave me very helpful advices and useful comments on my thesis. My sincere appreciation is also extended to Dr. Lu Chen, Dr. Kamis Elmi, Dr. Mark Rainey and Mrs. Edwards for their help and support throughout my study.

Finally, I would like to extend my deepest gratitude to my parents who sacrificed a lot and I could not make it without their dedication and encouragement.

CHAPTER 1 INTRODUCTION

1.1 Background

The use of composite laminates is increasing in various structures that require high strength-to-weight and stiffness-to-weight ratios. One of early applications of composite laminates is related mostly to the high performance products used in the aeronautics field (Nguyen et al., 2013). Aircraft and spacecraft are typical weight-sensitive structures in which composite materials are cost-effective, and in the latest Boeing 787 the usage percentage of fibre-reinforced composite materials reaches 50% by weight. Also to meet the performance and fuel efficiency requirements, the consumption of composites in the automobile industry is growing. To enhance the electrical energy harvest efficiency the blades of wind turbines are normally made of composite laminates and these laminated structures are now playing a major role in the wind energy generation industry (Christou, 2007). Moreover, the applications of laminated structures have been extended to the civil engineering industry to replace conventional materials (such as aluminium and steel). For instance, fibre reinforced polymer (FRP) composites are widely used in construction as structural components due to their strengthening and rehabilitation effects for concrete structures (López et al., 2013).

In recent years, the demand for high-strength and low-density materials, active vibration control and health monitoring of composite laminated structures has generated an increasing number of applications such as design of a multifunctional structure where the multiple properties of materials are exploited in such a way that besides its major designated functionality, the same structural component can accomplish at least one more task (Kapuria et al., 2010). Among various multifunctional structures, under the action of a combination of mechanical and electrical fields, piezoelectric structures have been widely used in many applications such as structural vibration control, precision positioning, medical and aerospace etc. The phenomena of piezoelectricity is a peculiarity of certain class of crystalline

materials and the piezoelectric effect is a linear electromechanical interaction between the mechanical and the electrical state in crystalline materials with no inversion symmetry (Gautschi, 2002). In the direct piezoelectric effect, the internal generation of electrical charge results from an applied mechanical force proportionally. In the inverse piezoelectric effect the application of an electrical field induces mechanical stresses or strains. These two effects represent the coupling between the mechanical and electrical fields (Nye, 1985). Piezoelectric structures can be used in the detection and generation of sonar waves and in ultrasonic transducers for medical imaging. There is also a growing interest evolved with the introduction of piezoelectric ceramics and piezoelectric polymers composites for the structural health monitoring and structural repair (Duan et al., 2010). Composite structures using piezoceramic composites like PZT (lead zirconate titanate) sensors are being developed for damage detection of various structures including beams, plates and pipes. As an emerging application, the piezoelectric structures can convert motion from the human body into electrical power as a piezoelectric energy harvester (White et al., 2001). Most recently, researchers have engineered the piezoelectric effect into graphene which has potential to bring dynamical control to nanoscale electromechanical devices (Ong and Reed, 2012). Generally these piezoelectric structures are available in the form of stacks which can be bonded to or embedded in composite and sandwich laminates to introduce self-sensing and actuation capabilities.

There is no doubt that laminated composites and piezoelectric laminated composites are becoming the preferred structural system in a variety of industrial applications as mentioned above. However, even for the analysis and design of simple laminated composites, one of the most critical failure modes is delamination between adjacent plies and the interlaminar stresses play a crucial role, in particular at the free edges of the composite laminates (Leguillon, 1999). The material discontinuity gives rise to interlaminar stresses at the free edge and those significant stress gradients can result in delamination and failure of laminates at a much lower load level than that predicted by the in-plane failure criteria due to weak transverse normal and shear strengths. To deal with the complex interactions between different material layers at

the interface, Lorriot et al. (2003) performed the edge delamination tests on composite laminates and demonstrated that strong interlaminar stress intensification prevailed near the free edge and contributed to the delamination initiation. Mandell et al. (2003) also indicated that the prediction of delamination in wind turbine blade laminated structures required a complex 3D interlaminar stress state which was rarely analyzed in detail during design.

For those of piezoelectric laminated composite structures, the intrinsic material properties of piezoelectric laminates can induce the electromechanical coupling effect. It is obvious that the so-called free-edge effect and electromechanical effect may exist simultaneously at the interface of different materials in the vicinity of the free edges, which brings more complex phenomena in piezoelectric laminates than those in laminates. Lin et al. (1996) indicated that abrupt voltage variations occurred at the free edge, even in the undamaged case, because the interlaminar stress singularities existed at the free edge, and piezoelectric film sensors were sensitive to various singularities as caused by damage. Shang et al. (2005) also described that these piezoelectric thin films were widely used in micro-electromechanical systems and these devices were often made from multi-layered piezoelectric thin films of dissimilar materials, and numerous interfaces and edges in such devices had a special significance because they might affect the structural performance of these devices. As delamination located along the interface may initiate due to the stress concentration originated from the mismatch of material properties and the brittle nature of piezoelectric materials may raise concerns about the structural integrity and reliability. Therefore, it is essential to predict the free-edge interlaminar stresses through the thickness of the laminated structure accurately.

The presence of material discontinuities in the piezoelectric laminates results in 3D stress and electric fields near the intersections of the interfaces and the free edges. Due to the fact that there is a stress concentration with a possible singularity in the vicinity of the free edge, ad hoc assumptions made on the variations of the field variables (displacements u_i, electric potential $\emptyset$, stress components σ_{ij}, electric displacements D_i) will have significant influences on the accuracy. The analytical

solution of 3D elasticity and piezoelectricity to provide the accurate determination of electromechanical coupling and free-edge effects on these mechanical and electrical variables especially the interlaminar stresses is inevitable in the analysis and design of free-edge piezoelectric laminates. There have been several studies reported on the electromechanical coupling and free-edge effects: 3D finite element analyses of symmetric piezoelectric laminates under uniaxial extension by Mannini and Gaudenzi (2004) and Artel and Becker (2005), and the analytical layerwise solution by Mirzababaee and Tahani (2009). However, owing to the ad hoc assumption on through-thickness variations of the displacements and the electric potential these solutions cannot provide realistic distributions of interlaminar stresses across the thickness accurately.

The state space approach is one of the methods that are particularly suitable for the three-dimensional analysis of laminated structures (Sheng and Ye, 2002). The state space method converts a boundary value problem to an equivalent initial problem in terms of state variables related by a set of first-order differential equation. For instance, a full three-dimensional analysis of a plate and shell generally leads to a set of partial differential equations in three independent spatial variables, where there are boundary/initial conditions compatible with them. The differential equations are considered for each of the laminae in local co-ordinates for the laminated plate (Ye, 2003). A single global partial differential equation system is obtained by assembling all laminae with the continuity of displacements and interlaminar stresses at all interfaces. The application of this method has been developed for static and dynamic analyses of anisotropic plates by many researcher and extensive investigations are presented in the next chapter. However, the main problem is that most of the state space solutions are restricted to the simply-supported or partially clamped boundary conditions and there are no state solutions for predicting the electromechanical and free-edge effects simultaneously.

This research will adopt the state space method and the finite element method to investigate the general electromechanical behaviour of the free-edge piezoelectric laminated plates and aim to clarify the electromechanical coupling and free-edge

effects on the stress and electric fields near the intersection of the interface and the free edge.

1.2 Objectives

The main objectives of the research in this thesis are:

1. To study and review various 2D and 3D plate theories, and experimental and theoretical investigations on the free-edge effect for laminated composite plates and piezoelectric laminated plates. This research is mainly focussed on the realistic distributions of the interlaminar normal and shear stresses through the thickness.
2. To develop 3D analytical state space models for simply-supported and free-edge piezoelectric laminated plates under transverse loads and infinite long piezoelectric laminates under uniaxial extension and evaluate the general electromechanical and free-edge effects on 3D interlaminar stresses and electric fields at interfaces.
3. To evaluate the influences of stacking sequences, material properties, ratios of thickness to in-plane geometric parameters and electric surface conditions on the distributions of 3D interlaminar stresses and electric fields.
4. To develop an accurate and efficient layer refinement technique to delineate the complex electromechanical behaviour of a piezoelectric laminated plate due to the free-edge effect.
5. To use the 3D analytical state space solution to validate and compare with the solutions from the classical laminate plate theory and 3D finite element method by ABAQUS and to assess the accuracy of different plate theories and finite element formulations.

1.3 Thesis outline

This thesis consists of eight chapters which are summarized as follows:

Chapter 1 begins with the research background, presents the aims and objectives and outlines the layout of the thesis.

Chapter 2 reviews the development of 2D and 3D plate theories using analytical and numerical methods and the experimental studies for composite laminated plates and piezoelectric laminated plates. The determination of interlaminar normal and shear stresses at interface of dissimilar material layers is the main concern and the advantages and limitations of each model are discussed. Additionally, various analytical and numerical methods for the solution of the free-edge problem are introduced.

Chapter 3 presents the state space equation of a simply-supported piezoelectric laminated plate with free edges under transverse loads. Based on the theories of 3D linear piezoelasticity, all the boundary conditions and continuity conditions are satisfied and all the elastic and piezoelectric constants are taken into account in the derivation of the equation. To give a more extensive understanding of state space method, transfer matrix and recursive solution approaches, together with the derivations of state equations, are given in details for clarification.

Chapter 4 provides the state equation for an infinite long piezoelectric laminated plate subjected to a uniform axial strain. The state equation guarantees the continuity conditions of interlaminar stresses at the interfaces and fulfills the traction-free boundary conditions at the free edges.

Chapter 5 demonstrates numerical studies on the electromechanical behaviour and free-edge effect of simply-supported free edge piezoelectric laminated plates under transverse loads by implementing a non-uniform layer refinement technique in the state space approach. Different stacking sequences, thickness to length ratios and electric surface conditions are considered and their influences on the distributions of 3D interlaminar stresses and electric fields near the free edge are investigated. In

addition, the results from the present analytical solution are utilized to evaluate the accuracy of the classical laminate plate theory and FEM results.

Chapter 6 presents the influence of different geometric parameters and electrical material properties on the electromechanical behaviour of the piezoelectric laminated plates and beams. As expected, in comparison with the variation of mechanical quantities, the electrical ones are more affected by the electrical material parameters. The significant influence of these geometric and material parameters on the behaviour of the transverse shear stress is captured near the intersection of the interface and the free edge.

Chapter 7 shows how the state space approach can be used to investigate the behaviour of a general cross-ply infinite long piezoelectric laminated plate under uniaxial extension. To assess the influence of piezoelectric coupling effect near free edges, both electromechanical coupled and uncoupled analyses are carried out.

Chapter 8 summarizes the work carried out in this research and draws the main conclusions of this research, and gives recommendations for future work.

CHAPTER 2 LITERATURE REVIEW

2.1 Introduction

In the wake of application of composite laminates in many different fields, numerous theoretical and experimental investigations have been conducted to deal with the heterogeneous anisotropic phenomena and it is becoming more complicated when the electromechanical coupling effect should be taken into account for the piezoelectric laminates. In general the distinctive behaviour of the composite laminated plate can be represented as high transverse deformability at the interface, zigzag effects in the thickness direction and continuity of interlaminar stresses (Fagiano, 2010).

From moderately thick to thin laminates, 2D laminate theories for hybrid plates can be established by making assumptions concerning the kinematics of the deformation or the stress state through the thickness of the laminate. In general, numerous 2D laminate plate theories which have been proposed to describe the kinematics of laminated composite plates can be categorised as: single layer theory and layerwise theory. In single layer theory the number of unknown variables is considered to be independent of the number of constitutive layers, and according to the description of layerwise theory each layer is treated as an independent plate and compatibility of displacements components is imposed as a constraint at each interface. These theories are the most widely used 2D displacement-based plate theories for both elastic and piezoelectric composite plates. Moreover, to overcome the limitations of these theories unified equations have been proposed for mixed single layer and layerwise theories. These unified theories have been formulated in the most general way for users to be capable of choosing the approach and the order of the expansion of displacements and transverse stresses (Carrera and Ciuffreda, 2005). In conjunction with finite element methods, some refined theories have been developed to consider the transverse normal deformability in the presence of potential and thermal fields, satisfy the continuity of transverse stresses at interfaces and account

for the layerwise variation of in-plane displacement as well as the two-way electromechanical coupling (Kapuria et al., 2010). However due to some ad hoc assumptions of 2D laminate theories, several limitations arise. First the accuracy of the stress fields, in particular interlaminar stresses, deteriorates as the laminate becomes thicker. Second the state of stress is often inaccurate at the interfaces wherein material discontinuities occur or near free edges. Hence, a comprehensive treatment of the thick laminate as well as the local region wherein geometric and material discontinuities exist is required. The aforementioned 2D laminate plate theories are based on the displacement formulations, in which only the displacements are assumed as unknown variables of the structural system.

In contrast, 3D approaches are definitely the ideal tool for the analysis of a possible high layerwise inhomogeneity in mechanical and electric properties in the thick hybrid laminates. In addition, due to the presence of material and geometric discontinuities, a 3D stress field arises at the interfaces and in the vicinity of the free edges. Moreover, the coupling effects of electric and pyroelectric fields in piezoelectric laminates have to be considered. An in-depth understanding and accurate analysis of the 3D free-edge stress state of both elastic and piezoelectric composite is thus of necessity in the composite and smart structure engineering. Hence, with no simplified hypothesis on the variation of the field variables such as the displacements, stresses, electric potential and electric displacements through the thickness coordinate, and accounting for the constitutive, kinematics and equilibrium equations for piezoelectric laminated plates, the state space approach, also called hybrid approach (Wu et al., 2010), can provide 3D analytical solutions by satisfying the equilibrium as well as continuity conditions at the interfaces and the boundary conditions. In this thesis the state space approach will be used, in which the displacements and transverse stresses are introduced as state variables of the structural system, and after employing the boundary conditions the displacements and stresses at an arbitrary interface of the laminate can be obtained analytically.

In this chapter, fundamental concepts of 2D and 3D laminated plate theories are given and reviews of relevant articles on laminated plates and piezoelectric

laminated plates are followed. Furthermore, a detailed description of the experimental and theoretical studies on the free-edge effect in general composite laminated structures are presented.

2.2 General plate/shell theories

2.2.1 Single layer theories

Single layer plate theories are derived from the 3D elasticity theory by making decent assumptions wherein displacement components are at least C^1-continuous through the thickness of the laminate. Specifically, the C^1-continuous means the function and its derivative are continuous through the thickness of the laminate. By definition single layer theories are those in which a heterogeneous laminated plate is treated as a statically equivalent single layer with a complex constitutive behaviour and a reduction of a 3D problem to a 2D problem (Reddy, 2004). When the global behaviours of the laminated component such as gross deflection, buckling loads, fundamental vibration frequencies and associated mode shapes are concerned, a global analysis is often carried out by using the classical plate theory (CPT) and first-order shear deformation theory (FSDT) which are two commonly adopted single layer theories. CPT, FSDT and higher-order shear deformation theory (HSDT) can be distinguished by the degree of polynomial functions in the expansion of the displacement components across the thickness coordinate (Figure 2.1).

The assessment of localized regions of the three-dimensional composite laminated structure where the potential failure initiated is desired and an accurate determination of the three-dimensional state of stresses and electric quantities at the ply level is concerned. However, in single layer theories, the displacements are assumed as continuous functions of the thickness coordinate which results in continuous transverse strains. Hence, all stresses including interlaminar stresses in single layer laminate theories are discontinuous between adjacent layers at interfaces of dissimilar materials, contrary to the continuity of interlaminar stresses. This

deficiency is more evident in thick laminates and leads to an erroneous descriptions of results for all stresses and electric quantities.

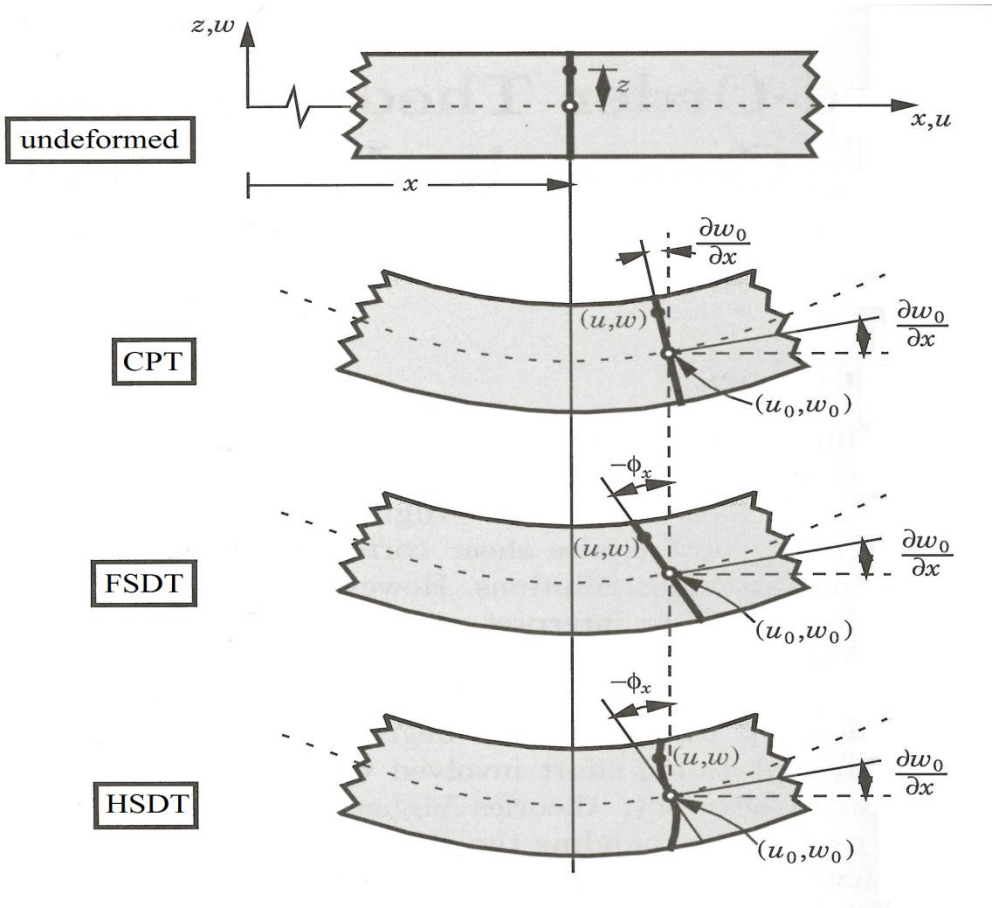

Figure 2.1: Deformation of a transverse normal according to the classical, first–order, and higher-order plate theories (Reddy, 2004)

2.2.1.1 Classical laminated plate theory (CLPT)

The classical laminated plate theory is the simplest laminated plate theory, which was initiated by Kirchhoff in the nineteenth century and developed by Timoshenko et al. (1951) later on. On the basis of the displacement fields the principal assumption in CLPT is that straight lines normal to the mid-plane before deformation remain straight and normal to the plane after deformation. As a result

the effects of both transverse normal and transverse shear strains are neglected, and deformation is due entirely to bending and in-plane stretching. For the orthotropic rectangular laminates with all four edges simply-supported, the transverse displacement and load can be represented in terms of double Fourier expansions that are restricted to those which satisfy the boundary conditions of simply-supported boundary conditions in the Navier method. The substitution of the displacement and load expansions into the governing equation should result in invertible set algebraic equations among the parameters of the displacement expansion. The transverse displacement and load also can be expanded in single Fourier series in the Levy method and the ordinary fourth-order differential equation for plates with two opposite edges simply-supported and the remaining two edges having any possible combination of boundary conditions can be solved by the Ritz, finite difference, and finite element methods (Reddy, 2004). The basic idea of the Levy method is to present a solution that satisfies the boundary conditions along the simply-supported edges exactly, and thereby reduce the two dimensional problem to a one-dimensional problem with respect to the corresponding coordinate. It is worth to mention that this method is widely used and developed for the analysis of laminated plates and piezoelectric laminated plates and the boundary layer effects were also investigated near the various boundary conditions: free, simply-supported, or clamped-supported by Izadi and Tahani (2010) and Kapuria and Kumari (2012).

Due to its simplification, the error induced by ignoring the effect of transverse shear stresses becomes significant when the thickness of the laminated plate increases, and the result deteriorates in the vicinity of free edges and close to the corners of laminated plates. The transverse shear strain may occur even in laminated thin plates and this method can predict deflections and overestimates natural frequencies as well as buckling loads approximately (L ü et al., 2008).

In spite of its deficiency, CLPT can provide as a reference for other composite plate analysis methods and quick predictions for the behaviour of thin plate structures and estimate the global response such as gross deflections, buckling critical loads and natural frequencies. This method also works well for structures which are made out-

of a symmetric and balanced laminate, experiencing pure bending or pure tension. The assumption leads to the simplification of constitutive equations and the reduction in the total number of variables, in consequence, numerous computational time and efforts are saved. In addition, the governing equations can be solved analytically, and CLPT is still widely used as a basic analysis method of composite plates.

Reissner (1961) presented fundamental work to analyze the stiffness behaviour of both bending and stretching in anisotropic elastic plates by using CLPT, and then Whitney and Leissa (1969) obtained a solution to the governing equations of a simply-supported laminated anisotropic plate based on the Kirchhoff assumptions. The earlier studies considering the stiffness of the piezoelectric layers but neglecting the direct piezoelectric effect and shear deformation were carried out by several researchers. Lee (1990) formulated a theory which was capable of incorporating the piezoelectric property of materials into the classical laminate theory. Recently an analytical approach for modelling a circular plate with distributed piezoelectric actuators under static as well as dynamic mechanical or electrical loadings was presented by Sekouri et al. (2004) based on the Kirchhoff plate model. By utilizing the same model as well as shear correction function with a quadratic variation of the electric potential across the piezoelectric layer thickness, Fernandes and Pouget (2006) investigated the static and dynamic responses of an elastic simply-supported composite plate bonded with piezoelectric actuators under cylindrical bending.

Although the transverse normal and shear stresses that play a significant role in the behaviour of composite plates as strain (or stress)-induced failure may occur are neglected in CLPT, the corresponding stresses can be post-computed through 3D elasticity equilibrium equations. However, these equilibrium derived transverse stresses are not accurate when the plates are relatively thick. Also due to the discontinuity of material properties at the interfaces, a highly concentrated inter-laminar stress field can occur in the vicinity of the free edges which will lead to interlaminar failures such as delamination or matrix cracking. In order to achieve an

accurate description of the transverse stresses of composite plates, several other theories have been developed and are presented afterwards.

2.2.1.2 First-order shear deformation theories (FSDTs)

By accounting for transverse shear stresses and still neglecting the transverse normal stress, FSDTs are developed to extend the kinematics of the CLPT to analyze the effect of shear deformation on deflections, stresses, frequencies, and buckling loads. The interlaminar shear stresses derived from the equilibrium equations are quadratic variation through the lamina thickness, whereas those computed from constitutive equations are constant through the lamina thickness (Reddy, 2004). Pioneering work has been done by Reissner (1945) and Mindlin (1964), which is also commonly known as the Mindlin-Reissner theory. This theory was an extension of Kirchhoff-Love plate theory incorporating first-order shear effects and implied a linear in-plane displacements variation and a constant transverse displacement through the thickness. The shear correction factors that depend on the lamination, geometric parameters, loading and boundary conditions were introduced to adjust the transverse shear stiffness of laminates in their models. Later on Srinivas and Rao (1970) developed a linear, small deformation theory of elasticity solution for the free vibration of simply-supported plates. With no restrictions on the thickness variation of stresses or displacements, the formulation yielded a triply infinite spectrum of frequencies, instead of only one doubly infinite spectrum by the thin plate theory and three doubly infinite spectra by Mindlin's thick plate theory. By using FSDT and a single-field displacement finite element model the evaluation of the transverse thermal stresses in laminated plates was conducted by Rolfes et al. (1998).

Furthermore, FSDTs have been applied to piezoelectric laminated plates with direct piezoelectric effect and pyroelectric effect for thermal loading. The temperature distribution was assumed linear through the thickness when the laminate was sufficiently thin, and in accordance with the Reissner-Mindlin theory Noda (2000) established an analytical model of a cross-ply simply-supported laminate accounting

for the effects of transverse shear and coupling among mechanical, thermal, and electrostatic fields. Without a priori assumption of the distribution of the electric potential and temperature across the thickness of the piezothermoelectric rectangular simply-supported plate, FSDT was presented by Kapuria and Dumir (2000) to find the influence of the coupled effects for relatively thick piezoelectric layers. It was concluded that the pyroelectric term had more significant effect than the direct piezoelectric term in case of thermal load, whereas the direct piezoelectric effect was predominant in the potential load case. However, the coupled theories can predict the sensory potential very well for thin to moderately thick plates but none of those 2D theories can give accurate results of all quantities for thick plates.

Most models based on FSDTs are restricted to simply-supported plates and the results deteriorate as the composite plate becomes thicker. In addition, the accuracy of results depends significantly on the shear correction factor. In order to calculate transverse stresses accurately and be capable of predicting the behaviour of thick plates with various boundary conditions and loading conditions, the higher-order shear deformation theories need to be introduced.

2.2.1.3 Higher-order shear deformation theories (HSDTs)

Similar to FSDTs, HSDTs are developed on the basis of the same assumptions as the classical plate theory, except relaxing the straightness and normality of a transverse normal after deformation by using higher-order polynomial functions in the expansion of the displacement components through the thickness of the laminate such as quadratic, cubic, etc. Higher-order theories can give a better description of kinematics. In principle, it is possible to expand the displacement fields in terms of the thickness coordinate up to any desired degree. Nevertheless, due to the increase in algebraic complexity and computational effort induced by higher-orders of polynomial functions, theories higher than third order have not been attempted (Reddy, 2004). The third-order shear deformation theories (TSDTs) discard shear correction coefficients used in FSDTs because the cubic polynomial functions

introduced in the expansion of the displacements result in quadratic variations of the transverse shear strains and transverse shear stresses through the thickness.

Due to the advantages of HSDTs a number of researches on composite plates have been carried out, among which the TSDTs attracted much more attention. Despite neglecting the transverse normal strain, Ambartsumian (1958) initiated the formulation of the transverse shear stresses that varied in the direction of the thickness of the anisotropic shell in accordance with the law of the quadratic parabola. Whitney and Sun (1973) developed a refined laminated plate theory by considering transverse normal stresses and assuming a first-order term to the transverse displacement and second-order terms to the in-plane displacements respectively, and concluded that higher order theory yielded improved results for extensional motion. However, the correction factors were used in their theory and the procedure for determining the value of correction factors which depended on the stacking sequence of the plies and the number of plies as well as the ply properties became tedious. By assuming a cubic variation of in-plane displacements and a quadratic variation of the transverse displacement, Kant and Pandya (1988) developed the TSDTs with finite element method, and the effect of the transverse normal stress in the thickness direction was considered and no shear correction coefficient was required in their study. With respect to the standard Reissner-Mindlin model, the response in these HSDTs was improved by using a higher-order expansion along the thickness co-ordinate for the unknown displacements, but did not include the zigzag effects and guarantee the interlaminar continuity (Carrera, 1996). According to the analysis of thin laminated composite plates carried out by Wu et al. (2005), transverse normal stresses were obtained by integrating three-dimensional local equilibrium equations along the thickness of the laminate and transverse shear stresses were calculated by constitutive equation method directly. It should be noted that for the application of such a plate theory, the accuracy of transverse normal stresses can be improved by refining mesh.

Several in-depth investigations on laminated composite plates using TSDTs have been conducted by Reddy (2004). Solutions for the free flexural vibration of Levy-

type rectangular thick plates based on the Reddy's TSDT were presented by Shahrokh et al. (2011). Lo et al. (2012) proposed an enhanced Reddy's model for composite plates subjected to temperature loads. In this model the transverse normal strain was introduced in the transverse displacement field of Reddy's theory and a triangular plate element was used wherein the C^1 continuity conditions were satisfied.

Based on linear piezoelectricity, Mitchell and Reddy (1995) used a single-layer theory for the mechanical displacement field and modelled the potential function as a layerwise discretization in the thickness direction to include the coupling between mechanical deformations and the charge equations of electrostatics for the simply-supported piezoelectric laminae. However, in their study the transverse normal stress was eliminated from the constitutive relationships and the transverse shear strains were zero at the upper and lower surfaces of the plate, and the traction-free conditions were not satisfied if the piezoelectric effects from components of the in-plane electric field existed. To satisfy exactly the shear traction-free conditions at the top and the bottom of hybrid piezoelectric laminated plates with full simply-supported boundary conditions, Kapuria and Achary (2005) considered the transverse as well as in-plane electric fields and assumed the electric potential as sub-layer wise piecewise linear. The number of sub-layers for discretization of the electric potential and thermal fields was determined by the required accuracy. However, in their coupled consistent TSDT, the transverse displacement was approximated to be uniform and the transverse normal stress was neglected.

2.2.2 Layerwise theories

To avoid the major deficiency of single layer plate theories, the layerwise theories were developed by assuming separate displacement field expansions within each material layer, thus providing a kinematically correct representation of the strain field in discrete layer laminates, and allowing accurate ply-level stresses to be determined. In contrast to single layer plate theories, the displacement components

are assumed C^0 continuity through the laminate thickness and the displacement field exhibits continuous through the thickness but the derivatives of the displacements with respect to the thickness coordinate may be discontinuous at various points through the thickness, leading to possible continuity of interlaminar stresses. Also, in these theories the in-plane displacements are distributed in a layerwise manner through the thickness of thick laminates. Noor and Burton (1989) established a discrete-layer model to predict the displacements and stresses for multilayered composite plates, however, the number of variables was determined by the number of layers at the expense of computational time and their model became impractical for engineering application.

Furthermore, the zigzag behaviour is described as a rapid change in the slope of displacement fields and/or abrupt change in transverse shear modulus in the thickness direction in correspondence with each layer interface (Figure 2.2). This so-called zigzag behaviour can be examined from the exact 3D elasticity solutions obtained by Pagano (1969). From the schematic one-layer and three-layer composite laminates illustrated in Figure 2.2 the general distribution of in-plane stresses, displacements and transverse stresses through the thickness has been given by Carrera (1997). It is depicted that the in-plane stresses are discontinuous at the interfaces, whereas the displacements must be continuous for compatibility reasons and the transverse stresses retain continuous in the thickness *z* direction due to the action-reaction. The displacements should have discontinuous first derivatives corresponding to each interface and thus be expressed as C^0-continuous functions in the thickness direction, thereby allowing for the possibility of continuous transverse stresses. Carrera (1997) has discussed theories in view of the C^0 requirements and pointed out these requirements have been seen as the crucial point in modelling multilayered structures. The C^0 requirements should satisfy the following behaviour: the zigzag effect is included and the interlaminar continuity for the transverse shear stresses is fulfilled a priori.

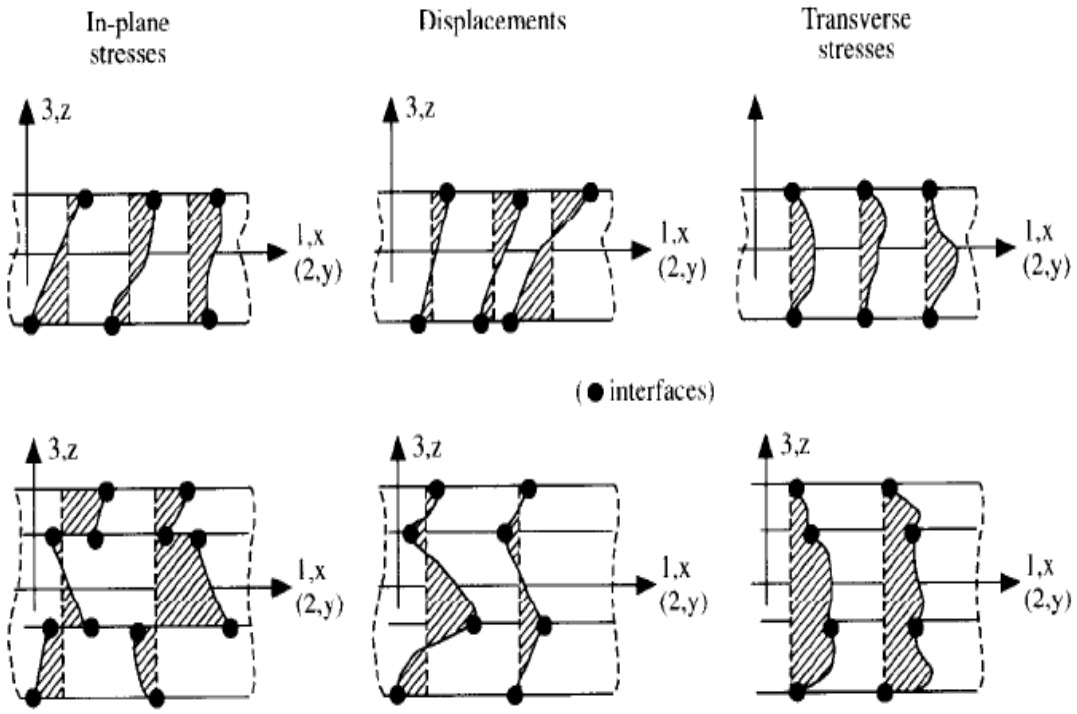

Figure 2.2: Possible scenarios of stress and displacements distributions along the thickness between one-layer and three-layers composite laminate (Carrera, 1997)

When an accurate prediction of the stress state of localized regions between layers like a significant variation in displacement gradients is required, a possible manner of including the zigzag behaviour can be assessed in the framework of single layer and layerwise models. In order to take the number of unknowns independent of the number of layers, Di Sciuva (1986) proposed a linear zigzag model for the in-plane displacements by guaranteeing the continuity of transverse shear stresses at interfaces, whereas the traction free conditions on the upper and lower surfaces were not satisfied. This model was then extended to the cubic zig-zag variations of in-plane displacements through the thickness by Savithri and Varadan (1990), to allow the fulfilment of the top and bottom zero-conditions for the transverse shear stresses.

Reissner (1986) derived a mixed variational equation for three components of displacements and three components of stress in infinitesimal elasticity from a statement of the general variational equation of elasticity. The introduction of the

variational equation for displacements and some stresses allowed for the continuity of the transverse stresses and the discontinuity of the in-plane stresses in the direction of the plate thickness, as a consequence of material property discontinuities. A new HSDT was developed based on Reissner's mixed variational principle. Zigzag shape function and Legendre polynomials were combined to approximate in-plane displacement fields by Toledano and Murakami (1987). However, the Toledano and Murakami's model leads to poor descriptions of the transverse normal stress effects and related consequences (Carrera, 1997) and the transverse stresses cannot be computed directly from constitutive equations. By superposing a linear zig-zag displacement field, with a different slope in each layer, on an overall cubic varying field, another efficient HSDT was also developed in a model presented by Cho and Parmerter (1993). Although the transverse shear stress continuity conditions at the layer interfaces as well as shear free surface conditions were satisfied and the number of the unknowns was independent of the number of layers, the transverse normal strain was neglected in the formulation. By referring to a Reissner's mixed variational theorem, Carrera (1996) extended the standard Reissner-Mindlin plate theory by including the C^0 continuity and adding two zigzag terms for the in-plane displacements. Later on by adopting linear up to fourth order displacement fields in a layerwise analysis, Carrera (2000) carried out a numerical investigation on bending of simply-supported orthotropic plates. It should be noted that he investigated the three manners to compute transverse stresses: a priori evaluation on transverse stresses by employing mixed models formulated on the basis of Reissner's mixed variational theorem, a posteriori evaluation on transverse stresses from Hooke's law and that by using integration of the three-dimensional indefinite equilibrium equations. According to Carrera (2000), the discrepancy among the three manners of evaluating transverse shear stresses was barely dependent on plate thickness ratios and transverse stresses evaluated by integration of the 3D indefinite equilibrium equations have led, in general, to a better description, whereas in some cases such a posteriori procedure could fail to guarantee stress boundary conditions at the top and bottom plate surfaces.

A higher order zigzag theory has been developed by Cho and Oh (2004) to give the accurate prediction of fully coupled mechanical, thermal, and electric responses of smart composite plates. In their assumptions, both in-plane displacements and temperature fields through the thickness were formulated by superimposing linear zigzag field to the smooth globally cubic varying field, and the transverse displacement was considered as smooth parabolic variation and the electric potential was distributed linearly through the thickness. The continuity conditions of transverse shear stresses at the layer interfaces and the shear traction-free conditions at the top as well as bottom surfaces were satisfied for zero in-plane electric field components (Kapuria et al., 2010). It was found that the effect of in-plane electric field components which might be induced by the piezoelectric effect or applied by actuation should not be neglected for the electromechanical coupling analysis of piezoelectric laminated plates, particularly for that of thick plates. By including the in-plane electric field components an efficient zigzag theory of elastic laminated plates (Cho and Parmerter, 1993) has been extended to the analysis of the fully coupled electromechanical response of hybrid piezoelectric plates by Kapuria (2004). In Kapuria's work, a combination of the third-order variation and a layerwise linear zigzag approximation across the thickness was used for the in-plane displacements and a piecewise linear function was assumed for the transverse displacement and electric potential. Although this theory yielded more accurate results than FSDT, the neglect of the transverse normal stress in the constitutive equation still leaded to greater errors in the deflection w in the potential load case than those in the pressure load case.

The single layer and layerwise theories are widely used in the analysis of composite plates and both have their own advantages and disadvantages with respect to accuracy, efficiency and ease of implementation. In order to broaden the range of numerical applications of single layer and layerwise theories, the finite element implementations of these theories have been conducted and many relevant articles have been reviewed Reddy (2004). Models based on single layer theories are often capable of providing a sufficiently accurate prediction of the global response of thin to moderately thick elastic laminated plates as well as piezoelectric laminated plates.

However, these models have difficulties in describing the zigzag effects of the displacements and satisfying the interlaminar continuity of transverse stresses.

In contrast to single layer theories, layerwise theories can represent the zigzag behaviour and fulfill the interlaminar continuity of transverse stresses. Moreover, models based on layerwise theories can lead to a satisfactory assessment of the local response of thin to moderately thick laminated plates, in particular the state of stress in the localized regions where damage initiation is likely. Although layerwise theories have been developed to account for the transverse shear stresses and some of them can calculate transverse shear stresses directly from the constitutive equations, these theories often neglected the transverse normal stress. In some refined higher-order layerwise theories, the improved transverse normal stress can be calculated by integrating the 3D equilibrium equations through the thickness rather than using the constitutive equations directly. As a consequence, unsatisfactory results in the evaluation of the state of stress at the layer level near geometric and material discontinuities will emerge and specifically the transverse normal stress result deteriorates as the plate thickness increases. For high values of the thickness, even though a symmetric layup is considered, the transverse normal stress enforces non-symmetric distributions of stress and displacements along the thickness direction. This asymmetry cannot be described by most of aforementioned models which neglect the transverse normal stress effect (Carrera, 1996). As a consequence, these models may locate the maximum value of transverse shear stresses along the thickness coordinate differently compared with 3D solutions. Furthermore, although all the theories discussed above can deliver some satisfactory results by extending the polynomial functions of the displacement components and electric potential or considering the transverse normal stress effect, ad hoc deficiencies in these theories can lead to more errors for thick plates when the intrinsic material coupling between the transverse normal and in-plane components of the stress field and the electromechanical coupling exist. Therefore, to obtain the accurate global and local response of hybrid laminated plates, an exact analytical solution based on the three-dimensional elasticity and piezoelectricity is essential and necessary.

2.2.3 Three-dimensional solutions for plates

In the three-dimensional solutions the constitutive equations of linear three-dimensional elasticity and piezoelectricity, the kinematic equations (strain-displacement relations and the electric field-potential relations) and the stress equilibrium equations and Gauss's law at all field points are taken into account and continuity at the interfaces and the boundary conditions are also satisfied. The three-dimensional solutions for hybrid plates and shells have attracted researchers' attention for a long time (Kapuria et al., 2010). On one hand these solutions provide in-depth investigations into global and local responses of plates and shells and give accurate predictions on the mechanical or electro-mechanical behaviour, on the other hand they can be treated as benchmarks for evaluating the accuracy of other various two-dimensional theories of plates and shells, resulting in development of other efficient and advanced plate/shell theories.

In general, a system of partial differential equations in three independent spatial variables, along with a set of boundary/initial conditions compatible with them, can be obtained from a full three-dimensional elastic analysis of plates and shells. For a laminated structure, the system of differential equations is established for each of the laminae in their local co-ordinates (Ye, 2003). By employing the continuity of displacements and transverse stresses at interfaces, the differential equations in each local system are assembled to a single global partial differential equation system. With proper approaches, the three-dimensional partial differential equation system can be solved. In the current review of the three-dimensional analysis of laminated plates and piezoelectric laminated plates, three approaches are mainly mentioned for the three-dimensional solutions, namely, the Pagano's approach, the asymptotic approach and state space approach.

2.2.3.1 Pagano's approach

In this approach, researchers put more effort in the variable separation methods to transfer the three-dimensional partial differential equations to a set of ordinary

differential equations with respect to the thickness coordinate. The ordinary differential equations (ODEs) system was then solved analytically.

Pagano (1969) initiated a study on the plane strain problem of the isotropic and orthotropic laminates under the cylindrical bending. By introducing an Airy stress function satisfying the stress equilibrium equations in the formulation, the compatibility equation was expressed as a fourth-order ordinary differential equation in terms of the thickness coordinate only for each individual layer. The 3D solution of laminated plates under cylindrical bending was obtained with the satisfaction of the top and bottom surfaces conditions and continuity of traction and displacement at the interfaces between layers. This approach was extended to the 3D structural behaviours of rectangular bidirectional composites and sandwich plates by Pagano (1970). Moreover, an in-depth investigation has been carried out by Wu and Wardenier (1998) to obtain a three-dimensional solution for a single-layered orthotropic plate with simply supported edges. A sixth-order differential equation governing the transverse displacement w_{mn} was obtained:

$$\frac{d^6 w_{mn}}{dz^6} + A_0 \frac{d^4 w_{mn}}{dz^4} + B_0 \frac{d^2 w_{mn}}{dz^2} + C_0 w_{mn} = 0 \tag{2-1}$$

The three constants, A_0, B_0, C_0 can be determined by the mode shapes considered and the properties of material. There are 14 possible solutions for Equation (2-1) and the nature of the solution is controlled by the sign of the quantity H:

$$H = p^2/4 + q^3/27 \tag{2-2}$$

where

$$\begin{aligned} p &= B_0 - A_0^2/3 \\ q &= C_0 + \frac{A_0}{3}\left(\frac{2A_0^2}{9} - B_0\right) \end{aligned} \tag{2-3}$$

It should be noted that the sign of the quantity H was considered negative only by Pagano (1970), however, Wu and Wandenier (1998) concluded that H can be any real number (positive, negative or zero) determined by the combination of the material, geometry and loading properties in a practical problem and they also presented the explicit expressions of the solutions for all the three cases ($H>0$, $H=0$ and $H<0$).

To account for the transverse shear deformations and rotatory inertia, Srinivas and Rao (1970) adopted the displacement method of elasticity to analyze simply-supported thick laminated orthotropic plates. It was observed that the modular ratio between plies has a significant effect on the errors in the thin plate theory for laminates and mostly errors increase with increasing moduli of outer plies. Moreover, the number of terms needed to maintain a given level of accuracy increased as plate thickness increased. It is worth to mention that since each ply was treated as an individual homogeneous plate, and the number of the simultaneous equations increased with the number of plies P. Usually $6P$ simultaneous equations should be established for each pair of m and n, which were the vibration wave numbers in the x and y direction respectively.

Considering the electromechanical coupling effect, this approach was also implemented for the piezoelectric plates. Based on Pagano's approach, Ray et al. (1992) carried out an exact analysis of the coupled electromechanical behaviour of an infinitely long piezoelectric plate under cylindrical bending (i.e. plane strain state). For the material properties given in their paper, it was found that the quantity $H > 0$. Due to their conclusions, the deformations, stresses and electric potential varied non-linearly the across thickness of thick plates and the non-linearity increased with applied electric potential. Later, Ray et al. (1993) applied a similar formulation to a specific case of an intelligent composite, wherein piezoelectric coefficient e_{33} was set equal to zero and the formulation did not require continuity of the electrostatic potential and normal electric displacement at a layer interface. To remedy these deficiencies, a displacements and electric potential based formulation was established by Heyliger (1994) for bonded laminates of dissimilar piezoelectric

materials. In his study, at each interface between layers, continuity conditions of six elastic variables: u, v, w, σ_z, τ_{xz}, τ_{yz}, and two electrostatic variables: D_z, $\emptyset$ were satisfied.

Recently, Wu and Tsai (2012) developed a modified Pagano method for the static analyses of simply-supported functionally graded (FG) structures. In their modifications, a mixed formulation was adopted to replace the displacement-based one. Based on the successive approximation method proposed by Soldatos and Hadjigeorgiou (1990), the FG plate or shell was artificially divided into a certain number of individual layers with an equal and small thickness, compared with the in-plane dimensions of the plate or the mid-surface radius of the shell. By the refinement manipulation they used, the variable material coefficients of each layer were reasonably approximated to the constant material coefficients in an average thickness sense, reducing the system of thickness-varying differential equations for each individual layer to a system of thickness-invariant differential equations. The general solutions of the system equations were obtained layer-by-layer with a transfer matrix method.

2.2.3.2 Asymptotic approach

Based on the perturbation method, the three-dimensional displacements and stresses can be expressed asymptotically in terms of an appropriate aspect ratio (the thickness divided by a typical in-plane length) which is called dimensionless parameter. The three-dimensional elasticity equations are thereby reduced to a system of partial differential equations with two in-plane independent variables only (Rogers et al., 1995).

In conjunction with other methods, the improved asymptotic approach has been extensively applied for the 3D static and dynamic analyses of piezoelectric laminated as well as FG piezoelectric and magneto-electro-elastic plate/shells. By employing the governing equations in the state space formulation and a combination of transfer matrix method and asymptotic expansion technique, Cheng and Batra

(2000) obtained the three-dimensional solutions for piezoelectric laminates with simply-supported and closed-circuit boundary conditions. Based on the method of perturbation, Wu and Syu (2007) and Wu and Tsai (2009) extended their analyses to the static and dynamic responses of multilayered, hybrid as well as FG piezoelectric shells. It should be noted that the through-thickness distributions of field variables in FG piezoelectric shells revealed different patterns from those in homogeneous piezoelectric shells, and the natural frequencies of shells with open-circuit surface conditions were slightly higher than those of shells with closed-circuit surface conditions.

2.2.3.3 State space approach

The term 'state space' derives from the linear control system where the principal concern is the relationship between inputs (or source) and outputs (or responses) (Ye, 2003). For three-dimensional analyses of laminated plates and shells, the displacements and transverse stresses at the bottom surface of a laminated plate are termed as the initial state of the system. After introducing boundary conditions, the displacements and stresses at the top surface of the plate may be obtained, and the displacements and stresses at an arbitrary interface of the laminate can be traced as the past history of the system. Compared with other aforementioned displacement-based plate theories like CLPT, FSDTs, HSDTs and layerwise theories, in the state space approach the governing equations are formulated on the basis of displacements and transverse stresses. For a homogeneous anisotropic piezoelectric plate or shell, the three-dimensional equations can be represented by a system of partial differential equations (Ye, 2003) as follows:

$$\frac{\partial}{\partial z}\{R\} = [A]\{R\} + \{B\} \tag{2-4}$$

where $\{R\}$ is an unknown state vector comprises eight variables: u, v, w, σ_z, τ_{xz}, τ_{yz}, D_z, $\emptyset$; z is the through thickness coordinate; $[A]$ is a square matrix whose elements are functions of material and geometric constants of the laminate and also partial

differential operators with respect to the other two in-plane coordinates; and $\{B\}$ is a vector associated with, for example, initial stresses, strains, temperatures, etc.

Vlasov (1957) initiated his inspiring work on applying the state variable equation to the solution of the three-dimensional elasticity by using the method of initial functions. Similarly, Bufler (1971) used the transfer matrix method to obtain a suitable and systematic derivation of the governing equations and reduced the partial differential equations to ordinary ones by means of integral transforms, where isotropic plates were considered. Then Iyengar and Pandya (1983) expanded an equation containing differential operators in the form of a Maclaurin series of the coordinate z, thus all the physical quantities appeared to be polynomials of z in the solving procedure, which meant that the original state equation cannot be satisfied exactly.

Because all the physical quantities in the state equation are the compatible quantities of the interfaces, it is convenient to develop the state equation of the whole laminated plate. Abandoning any assumptions of stress and displacement models, Fan and Ye (1990a,b) started applying the state space method to the exact solutions for the statics and dynamics of orthotropic laminated thick plates with simply-supported edges. In their study, the fundamental equations of three-dimensional elasticity can be exactly satisfied and all the elastic constants can also be taken into account, and the number of unknowns included in the final equations was independent of the number of plies. Furthermore, the state equation governing the anisotropic response of simply-supported thick orthotropic rectangular plates subjected to arbitrary loading was deduced by Wu and Wardenier (1998) and a six-order differential equation governing transverse displacement w, compared with the fourth-order one in the classical plate theory, was given for the first time. It was worth to mention that various possible solutions determined by the value of quantity H (negative, zero, positive) were given in this paper and thus transversely isotropic and isotropic cases can be solved analytically.

However, the earlier studies mentioned above are confined to the simply supported case. By imposing the impulse functions and the Dirac functions, Fan and Ding

(1993) presented an exact analytical solution for the statics of thin, moderately thick, and thick laminated cylindrical shells with two clamped edges. The successive approximations method (Soldatos and Hadjigeorgiou, 1990) was adopted to obtain satisfactory precision and controlled error. Comparison was also made between their study and FEM, and it was concluded that their solution satisfied the continuity conditions of stresses and displacements at the interfaces, which the FEM failed. Fan (1998) also solved the bending problem of laminated plates with free edges. In his solution of a plate with free edges, an assumed displacement field was imposed to one of a simply-supported plate. The assumed displacements were so chosen that all displacement components did not vanish at the free edges, while the traction free conditions were satisfied (Dong and Sheng, 2005). Similarly, Sheng and Ye (2005) presented an analytical method to solve the bending problem of angle-plied laminated cylinders subjected to axisymmetrically distributed transverse loads. Due to the recursive formulation used to derive the state equations of laminated cylinders, the dimension of the final state equations did not depend on the number of layers of the cylinder.

In conjunction with other methods, state space approach received a rapturous reception from researchers. Semi-analytical finite elements connected with the state space approach for the static analysis of elastic laminated plates have been proposed by Sheng and Ye (2002). Conventional finite element analyses were based on a representation of the displacement field that guaranteed the continuity of all displacement components across the element boundaries. The stress field derived from the displacement representation by the use of stress-strain relations led to a stress field that was usually discontinuous across element boundaries (Fan, 1998). A combination of the finite element approximation and the analytical solution of the recursive formulation of state equation proposed by Sheng and Ye (2002) eliminated this intrinsic deficiency of conventional FEM and provided continuous distributions of both displacements and transverse stresses across all material interfaces.

Similarly, by combining the classical finite strip method and the state space approach, Attallah et al. (2007) obtained the three-dimensional solutions of

laminated composite plates with simply-supported ends. The simple polynomials in one direction and continuously differentiable smooth series were used in each strip and the series should satisfy a priori the boundary conditions at the ends of the strips. And the state space approach was implemented to describe the variations of displacements and stresses through the thickness direction. Contrary to their result, the analytical solution from Fan (1998) showed that one of the in-plane stress components at the bottom surface of the top ply had an unexpected result. The stress from Fan (1998) underlined in Attallah's paper should be larger than the one at the top surface of the mid ply. This was because the top ply was stiffer than the middle ply and should carry more stresses.

Moreover, to translate the partial differential state equation into the ordinary differential state equation, the variations of the field variables in the in-plane coordinates also can be discretized by the differential quadrature method (DQM) developed by L ü et al. (2008). Although the aforementioned approximations in the in-plane coordinates were combined with the state space approach to make ease of the treatment of various boundary conditions, these 3D semi-analytical methods may encounter challenges in predicting the accurate distributions of stresses and displacements in the vicinity of non-simply-supported edges, i.e. clamped and free edges. Due to the abrupt gradients and possible presence of singularity, more computational effort and possibly numerical instabilities were inevitable.

To develop an efficient analytical methodology for the electromechanical analysis of laminated piezoelectric structures, state space approach has been developed to study electro-elastic responses of a piezoelectric lamina made of $BaTiO_3$ by Lee and Jiang (1996). According to their study, the state space equation for piezoelasticity was structurally the same as the state equation for pure elasticity except for the two additional quantities due to the electric field contribution. The state space equation for pure elasticity was recovered when the piezoelectric constants vanished. From their analysis, an interesting result was obtained that the transverse stresses and electric displacement were not influenced by the electro-elastic coupling. They also

claimed that further studies were required to get the definitive conclusion on this issue.

By adding two extra magnetic quantities (i.e., magnetic flux and magnetic potential) into the state vectors, the exact solutions for three-dimensional, anisotropic magneto-electro-elastic, simply-supported, and multilayered rectangular plates were derived by Pan (2001). For sandwich plates made of the piezoelectric $BaTiO_3$ and magnetostrictive $CoFe_2O_4$, it has been observed that the in-plane electric and magnetic displacements were discontinuous across the interfaces wherein the potentials were continuous, and the stacking sequences had a significant influence on most physical quantities, in particular, on the electric and magnetic quantities.

With the same boundary conditions as the above work, i.e. simply-supported and grounded (closed-circuited) along four edges, Zhong and Shang (2003) assumed that the material properties varied exponentially with spatial position and employed this hypothesis to model the electro-elastic behaviour of a functionally gradient piezoelectric plate. Wen et al. (2011) also developed the governing equations for the functionally graded material by the state space approach in the Laplace transform domain.

In the aforementioned studies the boundary conditions applied on the four edges were simply-supported and close-circuited. Sheng et al. (2007) imposed an assumed displacement field and potential to the two opposite edges which were simply-supported and close-circuited. After the treatment of boundary conditions, two sets of unknown functions contained in the non-homogeneous vector were solved by imposing continuity conditions at interfaces, considering top and bottom surfaces conditions and four edges boundary conditions. The state equation for piezoelectric laminated plates was established. 3D analytical solutions that satisfied the simply-supported and clamped, closed-circuited and open-circuited boundary conditions, were obtained. It should be noted that an FEM solution in which 20-nodes 3D isoparametric elements with $4 \times 4 \times 4$ finite element mesh for a quarter of the plate was used, was also given in their paper for comparison. From the comparison, the FE results violated the continuity conditions at interfaces and there were significant

discrepancies for the transverse stresses at interfaces between two dissimilar material plies. Since a representation of displacements and electric potential in the FE analysis can only guarantee the continuity of all nodal displacements and electric potentials across the element boundaries, the stresses and other electric variables are usually discontinuous across element boundaries or material layers. For a thin or moderately thick plate, a coarse mesh can give satisfactory results on displacements, even stresses except from these near the interfaces of different materials and boundaries. The FEM solutions from Sheng et al. (2007) were obtained by modelling the piezoelectric laminated plate in a coarse mesh. But for a thick plate, a coarse meth led to a poor prediction. Therefore a refined mesh should be applied to the regions located in the vicinity of interfaces and boundaries, which may improve the precision and reconcile the discrepancies.

2.3 Free-edge effects

Due to the presence of a high inhomogeneity in mechanical properties at the interfaces between two dissimilar material layers, the full-scale three-dimensional steep stress gradients occur along the free edges, and this is often referred to as the so-called free-edge effect or boundary-layer effect (Mittelstedt and Becker, 2004) as shown in Figure 2.3. These edge perturbations decay rapidly away from the laminates edges and the localized singular problems of the free-edge stresses may result in premature failure of the laminate, like delamination which is detrimental to the structural reliability and durability of the laminate. Moreover, with the inclusion of the electromechanical coupling effect in piezoelectric laminated plates, the free-edge effect becomes more complicated, in which the concentration of not only the interlaminar stress but also the electric quantities may occur near free edges.

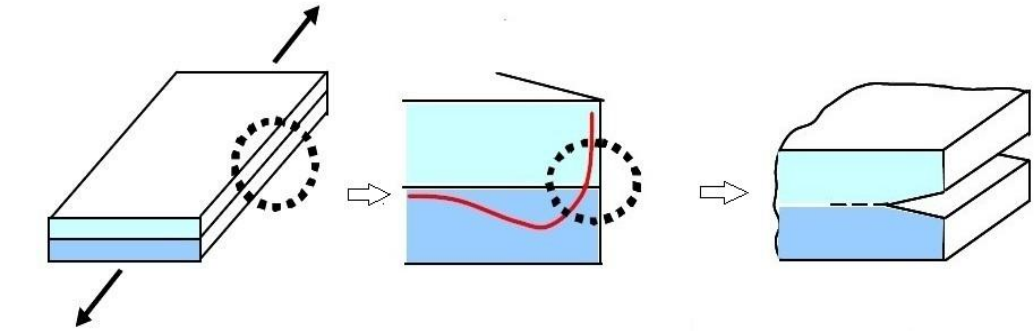

Figure 2.3: General descriptions of the free-edge effects and delamination problem in composite laminates (Chuang, 2003)

Pioneering work was carried out by Hayashi (1967) and the stresses computed from his model were seen to arise at the free edge but rapidly decay to zero at approximately the length of a ply thickness. Hayashi attributed this edge effect of the interlaminar shear stress as the reason for edge delamination. However, the interlaminar normal stress is neglected in his study. Puppo and Evensen (1970) also conducted a similar stress analysis and introduced a separate thin isotropic 'shearing' layer between adjacent plies in order to account for the shearing action between plies. The shearing layer, however, failed to take in-plane or interlaminar normal stresses into account in the analysis of laminates.

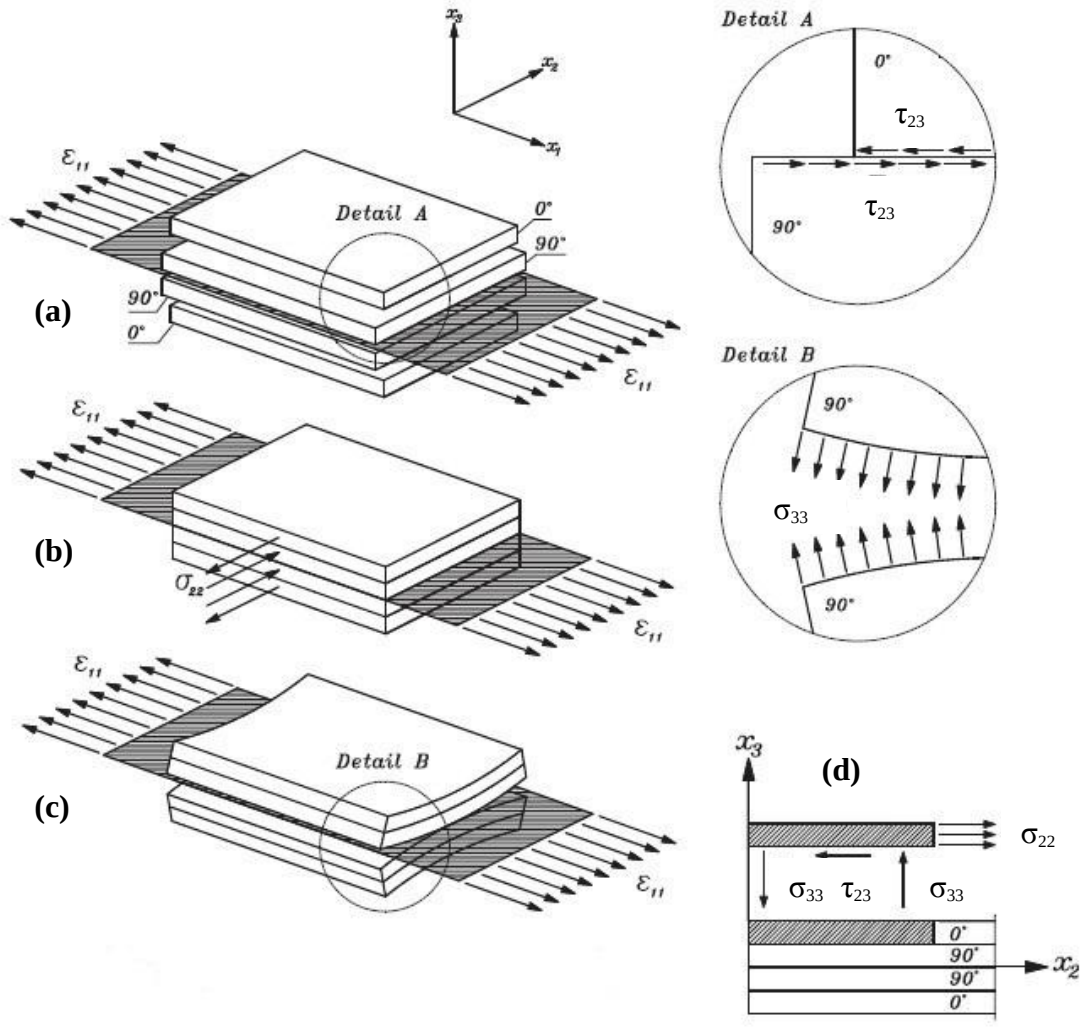

Figure 2.4: The free-edge effect in a cross-ply laminate $[0^{\circ}/90^{\circ}]_s$ under uniaxial extension (Mittelstedt and Becker, 2004).

The accurate descriptions of the 3D elasticity phenomenon of the free-edge effect were proposed by Pipes and Pagano (1970, 1971, 1973) for symmetric laminates subjected to tensile loads (depicted in Figure 2.4(b)). Based on the three-dimensional anisotropic elasticity, field equations for each ply were derived and then the resulting field equations were solved by using the finite difference method. Due to the presence of the interlaminar normal stress and the steep stress gradients in the boundary region, they thought that a possible stress singularity occurred at the

interface of dissimilar materials and the interlaminar shear and normal stresses near free edges might induce delamination.

Pipes and Pagano's inspiring work has triggered an overwhelming amount of various experimental investigations on free-edge delamination and approximate theoretical methods for the determination of the free-edge field in composite laminates. In general, these approximate methods can be categorized as: close-form solutions based on the aforementioned approximate 2D laminate theories (single layer, layerwise), numerical approaches based on 2D/3D elasticity and approximate close-form solutions based on 3D elasticity state space approach.

Numerous relevant literatures on the free-edge effect in composite laminates have been investigated and reviewed exhaustively by Mittelstedt and Becker (2004). As the case depicted in Figure 2.4, the Pagano-Pipes's model is chosen for the assessment of free-edge effects, i.e., a symmetric four-layer laminate strip under a uniaxial extension ε_{11}. To understand the nature of the interlaminar load transfer mechanism, it is informative to examine this cross-ply laminate. We consider the coordinate axes x_1, x_2, x_3 be along the length, width and thickness of the laminate respectively. The interlaminar stresses are denoted by τ_{13}, τ_{23}, and σ_{33}. The in-plane normal stresses σ_{11}, σ_{22} and shear stress τ_{12} can be predicted from CLPT. The laminate strip has thickness of t and the four layers are of equal thickness and is assumed sufficiently long in the x_1 -direction so the strains, stresses and displacements u_2, u_3 become independent from the x_1-axis. If the layers are not bonded together (Figure 2.4(a)), each layer is free to deform individually, and the transverse contraction of the outer 0°-layers contracts more than that of the inner 90°-layers, leading to incompatibility of displacements u_2 in the corresponding layers at the interfaces. However, perfect bonding is used between different layers, thus the displacement distributions at the interfaces must remain compatible. To maintain continuous displacement, one should apply tensile stresses σ_{22} on 0°-layers whereas compressive stresses σ_{22} on 90°-layers (Figure 2.4(b)). The resultant value through the thickness vanishes, i.e. $\int_{-\frac{t}{2}}^{\frac{t}{2}} \sigma_{22} dx_3 = 0$ must be fulfilled through the

laminate thickness. In this case, the absolute values of σ_{22} in 0°-layers and 90°-layers are identical. It should be noted that stresses σ_{22} must attain zero values at the free edges due to traction-free conditions. For equilibrium of forces in the x_2 direction there must be interlaminar shear stresses τ_{23} at the interface of the 0° and 90° layers (Figure 2.4, detail A). Thus, it may be written as $\int_0^{x_2} \tau_{23} d\hat{x}_2 = \int_{\frac{t}{4}}^{\frac{t}{2}} \sigma_{22} dx_3$. It can be seen that these stress resultants do not share a common line of action, thus leading to the bending moment about x_1 axis. Hence, for the equilibrium of this moment interlaminar stress σ_{33} as depicted in Figure 2.4 (Detail B) arises at the interface between 0° and 90° layers. It may be written as $\int_0^{x_2} \sigma_{33} \hat{x}_2 d\hat{x}_2 = \int_{\frac{t}{4}}^{\frac{t}{2}} \sigma_{22}(x_3 - \frac{t}{4}) dx_3$. In order to maintain equilibrium of forces in the x_3-direction, σ_{33} must reverse its sign along the x_2 direction, since the condition $\int_0^{x_2} \sigma_{33} d\hat{x}_2 = 0$ must hold. The interlaminar peeling stress σ_{33} starts to attain a increasing tensile value in the vicinity of the laminate free edge and reaches to its maximum value at the free edge, which is commonly considered as the predominant reason for the onset and propagation of delaminations as depicted in Detail B (Mittelstedt and Becker, 2004) in Figure 2.4. This general description of the free-edge effect in cross-ply laminates yields a three-dimensional state of stress with in-plane stresses as well as interlaminar stresses, in particular the interlaminar normal stress σ_{33}, which is always neglected by most plate theories.

2.3.1 Experimental investigations on free edge effects

In order to evaluate the 3D stress field and the nature of stress concentration that occurs near free edges and the delamination behaviour of composite laminates, a number of experimental investigations have been carried out. The uni-axial loading laminate coupon is used for both experiment and analysis in most delamination studies. The typical tensile specimen configuration is given in Figure 2.5. As mentioned in the previous section, delamination is the mode of matrix dominated

failure that involves ply structural interactions in the laminate. It was found that causes of delamination had been attributed generally to the existence of interlaminar stresses usually occurred near the free edges of the laminate in the experimental study of Bjeletich et al. (1979). They reported test results for a family of six quasi-isotropic graphite-epoxy laminates by altering the stacking sequence of 0^o, $\pm 45^o$ and 90^o plies. It was observed that the tensile strengths varied widely with the stacking sequences and laminates with certain stacking sequences had a higher tendency to delaminate. For instance, the $[90^o/\pm 45^o/0^o]_s$ laminate of the highest strength was found to have a large compressive interlaminar normal stress σ_z while the $[\pm 45^o/0^o/90^o]_s$ laminate of the lowest strength had a large tensile σ_z. Hence, it was thought that the onset of free-edge delamination was induced due to the fact that the tensile σ_z lowered the laminate ultimate strength.

Crossman and Wang (1982) conducted experiments on a series of T300/934 $[\pm 25^o/90^o_{n*}]_s$ graphite/epoxy laminates under axial tension to investigate the thickness effect of one ply on edge delamination, and n^* was the number of plies and varied from 1/2 to 8, while all other laminate parameters remained the same. These laminate series was chosen for their experiments due to its well documented propensity for delamination under tensile loading. A cross-sectional view of delamination crack of a $[\pm 25^o/90^o_{1/2}]_s$ laminate specimen is illustrated in Figure 2.6. It was clear that free-edge delamination initiated near the mid-plane and propagated through the 90 ply into the laminate interior. Several secondary cracks had also formed near the delamination crack tip. The tensile strain required to initiate delamination in the 90^o ply depended on the thickness of the 90^o ply and for $n^* \leq 3$ delamination occurred at the free edges of the specimens.

Figure 2.5: Typical tensile specimen configuration

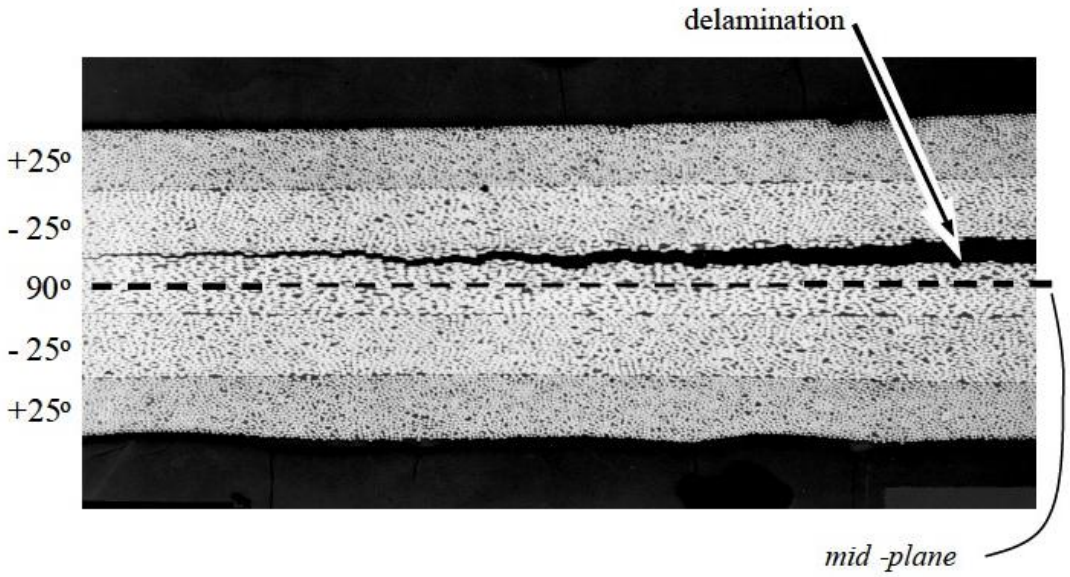

Figure 2.6: Cross-sectional view of delamination crack at the free-edge of a $[\pm 25^{o}/90^{o}_{1/2}]_s$ laminate under tension (Crossman and Wang, 1982)

Recently edge delamination tests on various carbon/epoxy G947/M18 laminates under axial tensile loadings have been performed by Lagunegrand et al. (2006a). It was found that for the $[\pm 10^{o}_{n*}]_s$ laminates with n*=1,2,3,4 plies the interlaminar stress τ_{xz} was dominant at the interface on the free edge of the laminate and drastically decreased when moving away from the free edge. The general behaviour of $[\pm 10^{o}_{n*}]_s$ laminates was perfectly linear up to delamination and interlaminar crack growth was very unstable and failure occurred instantaneously after crack initiation at the free edge. The behaviour of $[\pm 20^{o}_{n*}]_s$ laminates was similar to that of $[\pm 10^{o}_{n*}]_s$ laminates whereas the behaviour of $[\pm 30^{o}_{n*}]_s$ laminates was non-linear and delamination was less unstable. Moreover, for $[15^{o}_{2n*}/90^{o}_{n*}/-15^{o}_{2n*}]_s$ laminates (n*=1,2,3,4), both the interlaminar normal stress σ_z and shear stress τ_{xz} were

significant near the free edge and it was not sufficient to predict delamination initiation precisely by considering the interlaminar shear stress effect only.

Furthermore, Lagunerand et al. (2006b) carried out an experimental study to investigate and identify the influence of the interlaminar normal stress on the free-edge delamination initiation in composite laminates. A four point bending test on a sandwich beam (length=400mm, width=20mm) was designed in order to load the interface of composite laminated skins either with a tensile or a compressive uniform stress field. It was found that for $[\pm 10^{o}_{n*}]_s$ laminated skin the stress level for free-edge delamination initiation had appeared to be the same for both tensile and compressive loading, and for $[15^{o}_{2}/90^{o}/-15^{o}_{2}]_s$ and $[30^{o}_{2}/90^{o}/-30^{o}_{2}]_s$ laminates loading the specimen in tension led to tensile interlaminar normal stresses while a compressive loading on the laminated skin induced compressive ones. They indicated that the delamination onset stress level was different when loading the interface in tension or in compression and a negative interlaminar normal stress increased the resistance of the delamination initiation.

By utilizing the novel sandwiched cantilever specimen Shang et al. (2005) performed the delamination tests to study the interface strength of PZT thin films on a silicon substrate. It was revealed from their experiment that delamination initiated at the free edge on the interface between the thin chromium layer and PZT layer, and fracture occurred abruptly after the initiation and there was no evidence of slow stable crack growth in all the tests. Meanwhile, the experimental results implied that strong stress intensification prevailed over the region near the vicinity of the interface and the free edge, and the tensile interlaminar normal stress concentration was observed.

The mechanisms of delamination at the free edge are influenced by the fibre orientation, ply stacking sequence, thickness, loading and boundary conditions. An in-depth understanding of the nature of the interlaminar stresses in the neighbourhood of the interface and free edge is the key to a proper delamination analysis. From the experimental investigations it is found that such free-edge delamination induced by significant interlaminar stresses occurs not only in

composite laminates but also in piezoelectric laminates, which brings more difficulties in the theoretical analysis, as introduced in the following subsection. An accurate evaluation of these interlaminar stresses near the free edge is necessary and a rigorous solution needs to be sought.

2.3.2 Analytical solutions to free-edge effects

In the study of Krishna Murty and Hari Kumar (1989) a higher-order theory approach has been formulated and the laminate has been modelled as a single layer by assuming polynomials through the laminate thickness. To satisfy the zero shear condition at the surface of the plate, the corresponding shear strains were set to zero. The interlaminar stresses, however, were discontinuous at the interfaces of dissimilar plies, because the thickness variations of the displacements were assumed a priori. By introducing a warp deformation mode for the near-edge displacements, Becker (1993) also utilized a higher-order laminated plate theory to solve the free edge problem. Displacements were assumed with the addition of warping deformation modes in forms of the trigonometric functions through the thickness. The warping terms were especially adjusted to the respective free-edge effect situations (Mittelstedt and Becker, 2004). In analogy with the usual procedure in CLPT the equilibrium was fulfilled in an average sense for appropriate stress resultants after integration through the laminate thickness. The boundary conditions at the free edges were satisfied in an integral sense.

The edge-effect problem of laminates subjected to extension is actually a quasi-three-dimensional problem and its stress analysis can be restricted to a general two-dimensional cross-section of the laminates (Tahani and Nosier, 2003). Tahani and Nosier (2003) adopted a displacement-based layerwise theory to study the behaviour of interlaminar stresses in general cross-ply laminates under uniaxial extension and thermal loading. Through the thickness, each layer was discretized in several mathematical layers and the field variables were interpolated with linear Lagrange polynomials. Later by using the similar approach of Reddy's layerwise theory,

Tahani and Nosier (2004) developed the analytical solutions for the edge-effect problem of general cross-ply laminates in various loading cases. It should be noted that there were repeated zero eigenvalues in the characteristic equations of the set of governing equations of equilibrium and some small artificial terms were employed to make these characteristic eigenvalues become distinct in Tahani and Nosier's solutions. Recently Nosier and Maleki (2008) presented an analytical solution for the assessment of interlaminar stresses in a long laminated plate under extension by using an improved FSDT along with Reddy's layerwise theory. However, in these aforementioned layerwise theories, the resultant stress fields fulfilled the boundary conditions at free edges in an integral sense and the interlaminar shear stress did not vanish at free edges, contrary to the traction-free conditions. Moreover, the computational effort was increasing with an increasing number of numerical layers.

On the other hand, the stress-based layerwise solutions to the problems of the complete state of stress, in particular the interlaminar stresses at free edges in composite laminates were derived with the combination of the force balance method and the principle of minimum complementary energy by Kassapoglou and Lagace (1987). The stress shapes were assumed a priori in terms of exponential functions and then Kassapoglou (1990) developed this approach by assuming the stresses as unknown functions. The continuity of interlaminar stresses at the laminate interfaces was guaranteed and the traction-free boundary conditions were satisfied as well. Recently a new layerwise stress model, which is called LS1 model (layerwise stress model with first-order membrane stress approximation per layer), has been extended to deal with the general non-delaminated and delaminated multilayered plates under uniaxial extension by Saeedi et al. (2012a). In their model, each layer was treated as a Reissner-Mindlin plate and the layers were linked together by interfacial stresses considered as polynomial functions of z whose coefficients were expressed in terms of generalized stresses of the model. The comparison with 3D FEM showed that this model was capable and efficient to predict the behaviour of free-edge effect and provide the estimation of interlaminar stresses rather than the determination of stress fields at the interfaces except near singularities. To overcome this drawback, based on an irregular layerwise mesh, a refined LS1 model was proposed to evaluate the

initiation and propagation of delamination in multilayered plates under uniaxial extension by Saeedi et al. (2012b).

To give an accurate description of the 3D elasticity problem of the interlaminar stresses, in particular the interlaminar normal stress at the free edge, several approximate analytical methods have been carried out. Wang et al. (2000) studied the stress decay problem in cross-ply laminates due to edge boundary effects by adopting state space approach. In contrast to the usual layerwise approach, this approach led to the solution of determinants independent of the number of laminae. However, the traction-free conditions at the free edges were not satisfied in this method. To fulfill all the traction-free conditions, Zhang et al. (2006, 2007) presented an approximate close form solution of the 3D elasticity equations for the free-edge and cracking effect in cross-ply and angle-ply composite laminates under extension and thermal loading. This semi-analytical method accounted for all independent material properties and continuity of interlaminar stress field. In the formulation, a Fourier series expansion was applied in the in-plane transverse direction, while an exact analytical solution for the variation in the thickness direction was obtained by using the state space approach and layer refinement. Moreover, the convergence was assessed by the Fourier terms and layer refinement.

Recently Tahani and Andakhshideh (2012) has employed the 3D multi-term extended Kantorovich method (3DMTEKM) to investigate analytically the interlaminar stresses in moderately thick rectangular laminated plates with arbitrary laminations and boundary conditions under transverse loads. The 3DMTEKM was utilized to reduce the governing equations based on the principle of minimum potential energy to a three sets of ordinary differential equations and the derived sets of ordinary differential equations were solved analytically. With the same approach, Andakhshideh and Tahani (2013) presented analytical solutions to determine the interlaminar stresses in general rectangular laminates with finite dimensions subjected to various loading conditions, such as axial stress, shear stress, bending, torsion and thermal loads. Nevertheless, the traction-free conditions at free edges were only satisfied in an integral sense.

2.3.3 Numerical solutions to free-edge effects

In 2D plate/shell theories, the variations of the displacement or stress variables through the thickness direction are assumed a priori and the boundary conditions at the free edges are generally satisfied only in an integral sense. Being a 3D stress concentration problem with possible singularity, any approximation and assumption on the variation of state variables will lead to prominent bearing on the accuracy (Kapuria et al., 2010). Thus, to determine the 3D stresses at the free edges of elastic composite under tension, bending and thermal loading, numerical methods have been developed and employed.

As mentioned above, Pipes and Pagano (1970) initiated the finite difference method to obtain the 3D solution for a free-edge stress field in the laminated strip under uniaxial tension. A thorough investigation on the mechanism of interlaminar load transfer for the cross-ply composite laminate was conducted by Pipes (1980). His finite difference solution showed that the interlaminar shear stress grew abruptly to a finite value in the vicinity of the free edge and vanished at the free edge and in the inner region. In addition, the finite difference solution which predicted finite values of the interlaminar normal stress at the free edge and the large gradient in the function in this region suggested the possible occurrence of a singularity. These phenomena may attribute to the mismatch in the longitudinal Poisson's ratio of 0° and 90° layers.

Wang and Crossman (1977) investigated the Pagano-Pipes problem with emphasis placed on assessing the stress field closest to the interfaces and free edges. Generalized plane strain and three-node triangular finite elements were adopted, and a denser mesh approach was also used in the vicinity of the free edge region for an accurate prediction of the 3D laminate stress field. Icardi and Bertetto (1995) used a 20-noded, quadratic interpolation, isoparametric brick element and a 15-noded, quadratic interpolation, singular wedge element generated from a 20-noded brick element based on special shape functions by coalescing nodes. The tentative continuous interlaminar stresses were obtained and the stress-free conditions were nearly automatically satisfied by employing a predictor corrector procedure in their

solution. Ye et al. (2004) combined the traditional finite element method with the state space approach to solve the free-edge effect problem. Based on a mixed variational principle, the in-plane variations of displacements and stresses were approximated by the traditional finite element method while the through-thickness distributions were represented by using state space approach.

Carreira et al. (2002) developed a layerwise model, called Multiparticle Models of Multilayered Materials, and their study dealt with the validation by means of finite element calculations. Since the finite element stresses were mean element values and not calculated at the desired interface, they introduced what they called finite element generalised forces, which were deduced from the 3D equilibrium equations. For the singular behaviour of the stresses in the vicinity of the free edges or the microcrack, they found the maximum value of stresses was rendered meaningless due to mesh dependence. In the convergence study they excluded a region where the finite element calculations were mesh-dependent and the calculated stresses had no meanings, and found that the generalised shear stresses converged regardless of the mesh used, as long as at a distance (1% of the width in the *y* direction away from the edge). Based on the layerwise model of Carreira et al. (2002), a new layerwise finite element was applied for the analysis of the free-edge stresses of composite laminates subjected to uniaxial extension and uniform temperature by Nguyen and Caron (2006). It is interesting to note that in their study increasing the subdivisions number was useful to reproduce shape distribution but their solution was incapable of capturing the stress singularity at the interface. By means of an finite element model with solid elements of the software ABAQUS, the submodelling technique was used to analyze the free edge effects of composite laminates by Romera et al. (2013). In the submodelling technique, the global model was analyzed with a coarse mesh. Then the submodel with a more fine mesh was extracted from the global model and analyzed by using the displacements which were the interpolated values of the nodal displacements obtained in the previous analysis of the global model. This mesh refinement technique has been selected to optimize the high computational effort.

2.3.4 Free-edge and electromechanical coupling effects on piezoelectric laminated plates

The evaluation of the 3D field stress becomes of particular interest when the electromechanical coupling effect is concerned, leading to more complex phenomena in the vicinity of free edges. Izadi and Tahani (2010) derived the governing equations for the general cross-ply piezoelectric laminated Levy-type plates with two kinds of boundary conditions: fully simply-supported, two opposite edges simply-supported and the others free. In estimating the boundary-layer effect, the second-order shear deformation plate theory was used to represent the displacement field, and also the electric potential was assumed to vary linearly in the *z* direction through each layer. By this assumption only the transverse component E_z of the electric field exists and the absence of the other two electric field components E_x and E_y leads to an inaccurate prediction of electromechanical behaviour of piezoelectric laminated plates, particularly in the vicinity of free edges where possible stresses and electric fields singularities occur.

With a compromise between accuracy and computational efficiency, the coupled efficient layerwise theory, also known as the zigzag theory (ZIGT) (Kapuria, 2004) has been developed for static electromechanical analyses of piezoelectric composite cross-ply plates. In this theory the transverse normal stress was omitted in the constitutive equation. As a result, greater errors were induced in the potential load case than those in the pressure load case. Even in the pressure load the results tended to deteriorate when the span-to-thickness ratio decreased to 5. Recently, by using the improved zigzag theory (IZIGT) Kapuria and Kumari (2012) studied the boundary-layer effects in the cross-ply rectangular piezoelectric composite plates with Levy-type boundary conditions. According to Heyliger (1994), the electric potential follows a nearly quadratic variation across the thickness of a piezoelectric layer. So in Kapuria and Kumari's paper the electric potential was approximated as a piecewise quadratic, wherein the two-way electromechanical coupling due to the direct piezoelectric effect was considered. They concluded that the electric boundary conditions at the edge significantly altered the strength of edge effect and the

strongest effects occurred at the free edges rather than the simply-supported edges. However, the inherent deficiency in their formulation still existed, such as neglect of the interlaminar normal stress, traction-free condition at the free edges was satisfied in an integral sense.

Mannini and Gaudenzi (2004) investigated the numerical performance of a cantilever beam composed of two actuating piezoelectric layers perfectly bonded to a passive substructure. The multi-layer higher-order finite element approach was used and the static interaction between a laminate and distributed piezoelectric actuators was considered in their finite element model. Due to the nature of the stress field, a dense mesh was used near the free end of the beam in order to perform a more accurate analysis where a high stress concentration was predicted. It was seen from the distributions of the interlaminar stresses along the length of the beam, the interlaminar shear stress was quite small from the fixed end to the inner region, and increased abruptly to a finite value close to the free end and vanished at the free end. The interlaminar normal stress converted its sign near the free edge and arose to a finite value at the free end. Also, a 3D finite element model was constructed for analyzing interlayer stresses of a laminated beam with two piezoelectric cover sheets and one elastic core by Yang et al. (2006). In their work, the influence of geometrical and material parameters was addressed. The interlayer stress level and concentration were reduced when the relatively thick ratio of piezoelectric sheet was used. On the contrary, thin piezoelectric sheets often induced relatively large interlayer stress level and concentration near the free edge of the beam.

A finite difference method was adopted by Zhang et al. (2003) to obtain a coupled electromechanical analysis of a piezoelectric layer bonded to an elastic substrate near free edges. The numerical results of the electric fields indicated clearly that the electric field intensity exhibited a significant disturbance near the edges of the piezoelectric layer in the cases of actuator and sensor. It was suggested that a significant error could be caused by the assumption of a homogeneous electric field that neglected the spatial variation in the piezoelectric layer. A spatial gradient of the electric potential near the edges was also observed and a much higher magnitude of

the electric potential gradient induced by the edge effect was found in the sensor case. Moreover, there was a prominent interlaminar stress concentration near the edges, and the tensile interlaminar normal stress, which was much higher than the interlaminar shear stress, was found to contribute to the delamination initiation.

Furthermore, based on the Pipe-Pagano's model, Artel and Becker (2005) considered the effect of electromechanical coupling on the interlaminar stresses and the electric field intensity components at free edges of laminated plates with piezoelectric material properties. In their finite element model, symmetric cross-ply and angle-ply laminates were investigated under uniaxial extension. It was shown that the coupling effect for cross-ply laminates resulted in significantly higher interlaminar stresses near the free edges, whereas the coupling effect for the angle-ply laminate was of minor significance. It is worth to mention that the coupling effect may trigger the presence of the singular electric field intensity in the vicinity of the free edges.

Tahani and Mirzababaee adopted a coupled fourth-order single layer theory (Tahani and Mirzababaee, 2009) and a coupled layerwise theory (Mirzababaee and Tahani, 2009) to obtain analytical solutions for Artel and Becker's piezoelectric laminated plate under uniaxial tension. In the study of Tahani and Mirzababaee (2009), except for the inner region where the interlaminar stresses vanished, the results in the vicinity of the free edges did not show good agreement with those of Artel and Becker (2005) and those of Mirzababaee and Tahani (2009). In addition, the through-thickness distributions of interlaminar stresses were not given and the traction-free conditions cannot be satisfied at the free edges. It should be noted that numerical values of the uncoupled interlaminar normal stress through thickness obtained by Artel and Becker (2005) did not agree with those obtained by Wang and Crossman (1977), Spilker and Chou (1980) and Mirzababaee and Tahani (2009). This problem draws the author's attention and there must be a decent description of electromechanical effects on the free edge interlaminar stresses and electric quantities. Further investigations are necessary and analytical solutions will be sought in this thesis.

2.4 Summary

As an alternative to the 3D elasticity and piezoelectricity and a compromise between the accuracy and computation efficiency, 2D laminate theories has gained widespread popularity from researchers. 2D laminate theories can provide predictions to some global responses of thin laminated composites, such as displacements and vibration frequencies. However, these theories yield only average through thickness values for the in-plane stresses and gives no or unsatisfactory descriptions about the important inter-laminar tractions (Ye, 2002).

In the review of previous and current theoretical and experimental studies, it is established that free-edge delamination induced by significant interlaminar stresses occurs not only in composite laminates but also in piezoelectric laminates, which brings more difficulties in structural analysis. Also the presence of material discontinuities and electromechanical coupling effect at the free edges in piezoelectric laminates leads to a more complicated 3D stress and electric field. Since the localized and complex phenomenon with a possible 3D stress and electric field singularity arises at the intersection of the interface and the free edge, any approximation and assumption on the variation of state variables will have a significant influence on the accuracy.

In the following investigation of this thesis, the state space approach based on the theories of 3D elasticity and piezoelectricity will be adopted to obtain the 3D analytical solutions that satisfy both mechanical and electric boundary conditions and the continuity conditions between different laminates. The solutions to the problems of the free edge effect in the piezoelectric laminate subjected to bending and in-plane extension, as main concerns, are presented in Chapters 3 and 4, respectively. Numerical analyses and validations are given in Chapters 5, 6 and 7.

CHAPTER 3 STATE SPACE METHOD FOR SIMPLY-SUPPORTED PIEZOELECTRIC LAMINATES WITH FREE EDGES UNDER TRANSVERSE LOADS

3.1 Introduction

In the extensive and in-depth review of the aforementioned literature, most of the three-dimensional solutions are restricted to piezoelectric laminates which are simply-supported and electrically grounded. However, this kind of boundary condition do not exhibit the well-known singular effects observed near traction-free edges and little research effort has been devoted so far for the development of the 3D analytical models for evaluating the bending behaviour as well as edge-effect of the piezoelectric laminated thick plate with free edges. Due to electromechanical coupling and free-edge effects in the piezoelectric laminate, the accurate estimation of the global behaviour of the plate, especially the localized interlaminar stresses and electric field intensity components in the immediate vicinity of the intersection of the interface and the free edge is of crucial importance. Any assumptions such as neglecting shear strains, assuming constant shear strains through the thickness, assuming linear electric potential through the thickness or the traction-free boundary conditions satisfied only in an integral sense, will lead to a poor description of global response even yield inaccurate results in the possible singular region very near the free edge.

In contrast to most 2D plate theories, state space approach preserves the interlaminar stresses as the state vectors in the formulation with respect to the theories of 3D elasticity and piezoelectricity. Moreover, all the independent elastic and piezoelectric constants for the orthotropic and piezoelectric materials are taken into account and the continuity conditions between different layers are also satisfied by using the transfer matrix and recursive solution approaches. In this chapter, with appropriate boundary functions (Dong and Sheng, 2005) the state space equations

are formulated to obtain the 3D analytical solutions for the bending problems of the thick rectangular piezoelectric laminated plates with two opposite free edges. Since the eight state variables employed in the state equations directly represent the boundary conditions on the top and bottom surfaces, exact solutions can be presented for different mechanical and electrical surface conditions.

3.2 Formulation of fundamental state space method for a piezoelectric plate

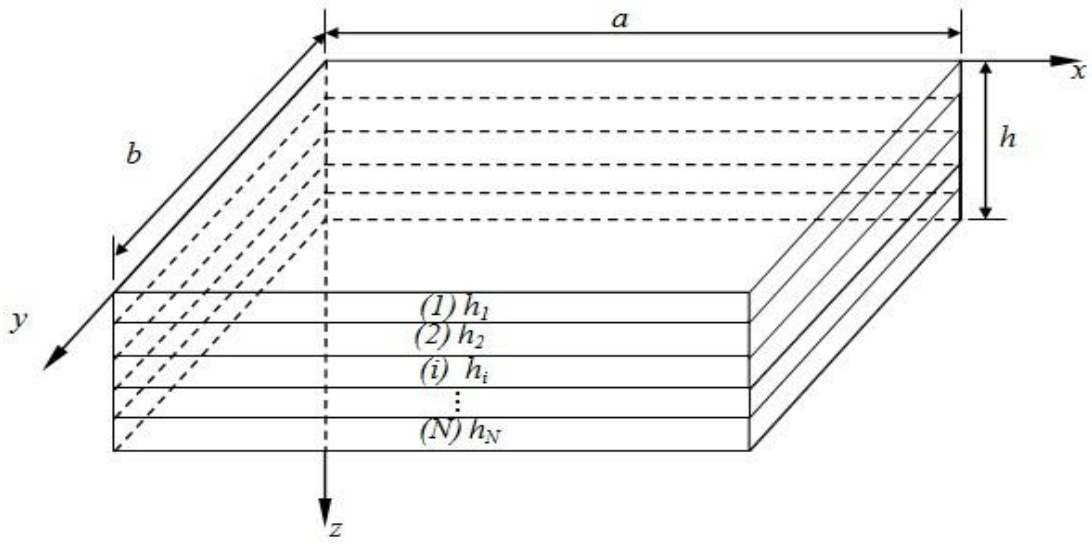

Figure 3.1 Geometry and coordinate system of a piezoelectric laminated plate

Consider a homogeneous orthotropic piezoelectric plate of uniform thickness *h*, length *a*, width *b* (Figure 3.1). The principal elastic directions of plate coincide with the axes of the chosen rectangular coordinate system and the full coupled three-dimensional piezoelectric-elastic constitutive relations of an orthotropic piezoelectric lamina can be expressed as (Nye, 1976)

$$\{\sigma\} = [C]\{\varepsilon\} - [e]^T\{E\} \tag{3-1}$$

$$\{D\} = [e]\{\varepsilon\} + [\in]\{E\} \tag{3-2}$$

Explicit forms of Equation (3-1) and Equation (3-2) are given as follows:

$$\begin{Bmatrix}\sigma_x\\ \sigma_y\\ \sigma_z\\ \tau_{yz}\\ \tau_{xz}\\ \tau_{xy}\end{Bmatrix} = \begin{bmatrix}C_{11} & C_{12} & C_{13} & 0 & 0 & 0\\ C_{12} & C_{22} & C_{23} & 0 & 0 & 0\\ C_{13} & C_{23} & C_{33} & 0 & 0 & 0\\ 0 & 0 & 0 & C_{44} & 0 & 0\\ 0 & 0 & 0 & 0 & C_{55} & 0\\ 0 & 0 & 0 & 0 & 0 & C_{66}\end{bmatrix}\begin{Bmatrix}\varepsilon_x\\ \varepsilon_y\\ \varepsilon_z\\ \gamma_{yz}\\ \gamma_{xz}\\ \gamma_{xy}\end{Bmatrix} - \begin{bmatrix}0 & 0 & e_{31}\\ 0 & 0 & e_{32}\\ 0 & 0 & e_{33}\\ 0 & e_{24} & 0\\ e_{15} & 0 & 0\\ 0 & 0 & 0\end{bmatrix}\begin{Bmatrix}E_x\\ E_y\\ E_z\end{Bmatrix} \tag{3-3}$$

$$\begin{Bmatrix}D_x\\ D_y\\ D_z\end{Bmatrix} = \begin{bmatrix}0 & 0 & 0 & 0 & e_{15} & 0\\ 0 & 0 & 0 & e_{24} & 0 & 0\\ e_{31} & e_{32} & e_{33} & 0 & 0 & 0\end{bmatrix}\begin{Bmatrix}\varepsilon_x\\ \varepsilon_y\\ \varepsilon_z\\ \gamma_{yz}\\ \gamma_{xz}\\ \gamma_{xy}\end{Bmatrix} + \begin{bmatrix}\in_{11} & 0 & 0\\ 0 & \in_{22} & 0\\ 0 & 0 & \in_{33}\end{bmatrix}\begin{Bmatrix}E_x\\ E_y\\ E_z\end{Bmatrix} \tag{3-4}$$

where $\{\sigma\}$, $\{\varepsilon\}$, $\{E\}$ and $\{D\}$ are, respectively, stress, strain, electric field, and electric displacement vectors. $[C]$, $[e]$ and $[\in]$ are elastic, piezoelectric and electric permittivity constants, respectively. For a piezoelectric material, the electrical and mechanical constitutive equations are coupled. A strain ε in the materials induces a polarization $e\varepsilon$ by the direct piezoelectric effect. Conversely, an applied electric field E tends to align the internal dipoles, inducing stress $-eE$ in the material by the inverse piezoelectric effect.

The linear strain-displacement relations and the electric field-electric potential relations can be written as:

$$\begin{aligned}&\varepsilon_x = \frac{\partial u}{\partial x}, \quad \varepsilon_y = \frac{\partial v}{\partial y}, \quad \varepsilon_z = \frac{\partial w}{\partial z},\\ &\gamma_{yz} = \frac{\partial w}{\partial y} + \frac{\partial v}{\partial z}, \quad \gamma_{xz} = \frac{\partial u}{\partial z} + \frac{\partial w}{\partial x}, \quad \gamma_{xy} = \frac{\partial u}{\partial y} + \frac{\partial v}{\partial x},\\ &E_x = -\frac{\partial \emptyset}{\partial x}, \quad E_y = -\frac{\partial \emptyset}{\partial y}, \quad E_z = -\frac{\partial \emptyset}{\partial z}.\end{aligned} \tag{3-5}$$

where u, v and w represent displacements in the x, y and z directions, respectively. $\emptyset$ is electric potential.

The equilibrium equations of elasticity and the Gaussian law of electrostatics can be written, respectively, as follows:

$$\begin{aligned}
&\frac{\partial \sigma_x}{\partial x}+\frac{\partial \tau_{xy}}{\partial y}+\frac{\partial \tau_{xz}}{\partial z}+f_x=0\,,\\
&\frac{\partial \tau_{xy}}{\partial x}+\frac{\partial \sigma_y}{\partial y}+\frac{\partial \tau_{yz}}{\partial z}+f_y=0\,,\\
&\frac{\partial \tau_{xz}}{\partial x}+\frac{\partial \tau_{yz}}{\partial y}+\frac{\partial \sigma_z}{\partial z}+f_z=0\,,
\end{aligned} \tag{3-6}$$

$$\frac{\partial D_x}{\partial x}+\frac{\partial D_y}{\partial y}+\frac{\partial D_z}{\partial z}-f_e=0\,. \tag{3-7}$$

Under electric body charge f_e and body forces $f_i\ (i=x,y,z)$. For laminated structure the interlaminar stresses are prominent and continuous at the interface of materials thus chosen as state vectors in the formulation. By eliminating the in-plane stresses σ_x, σ_y, τ_{xy}, and the in-plane electric displacements D_x, D_y in the *x*-*y* plane, the differentials of the displacements *u*, *v*, *w*, and the transverse stresses σ_z, τ_{xz}, τ_{yz}, and electric variables D_z, $\emptyset$, with respect to the *z* coordinate can be derived.

First let $\alpha=\frac{\partial}{\partial x}$, $\beta=\frac{\partial}{\partial y}$, under the condition of zero electric body charge f_e as well as body forces f_i, the following relations (see Appendix A) can be obtained from Equation (3-5) and the third equations of the matrix in Equations (3-3) and (3-4).

$$\frac{\partial}{\partial z}\begin{Bmatrix} w \\ \emptyset \end{Bmatrix}=\begin{bmatrix} k_1\alpha & k_2\beta & k_3 & k_4 \\ k_5\alpha & k_6\beta & k_7 & k_8 \end{bmatrix}\begin{Bmatrix} u \\ v \\ D_z \\ \sigma_z \end{Bmatrix} \tag{3-8}$$

The coefficients k_i in the matrix are the constants that are solely determined by the material properties of the laminate. By substituting Equation (3-8) into Equations (3-3) and (3-4), the in-plane stresses and electric displacements are presented:

$$\begin{Bmatrix}\sigma_x\\ \sigma_y\\ \tau_{xy}\end{Bmatrix}=\begin{bmatrix}k_9\alpha & k_{10}\beta & k_{11} & k_{12}\\ k_{13}\alpha & k_{14}\beta & k_{15} & k_{16}\\ k_{17}\beta & k_{17}\alpha & 0 & 0\end{bmatrix}\begin{Bmatrix}u\\ v\\ D_z\\ \sigma_z\end{Bmatrix} \tag{3-9}$$

$$\begin{Bmatrix}D_x\\ D_y\end{Bmatrix}=\begin{bmatrix}k_{18} & 0 & k_{19}\alpha\\ 0 & k_{20} & k_{21}\beta\end{bmatrix}\begin{Bmatrix}\tau_{xz}\\ \tau_{yz}\\ \emptyset\end{Bmatrix} \tag{3-10}$$

All the constants are given as follows:

$$\begin{aligned}
&k_1=\frac{-e_{31}e_{33}-C_{13}\in_{33}}{e_{33}^2+C_{33}\in_{33}},\quad k_2=\frac{-e_{32}e_{33}-C_{23}\in_{33}}{e_{33}^2+C_{33}\in_{33}},\quad k_3=\frac{e_{33}}{e_{33}^2+C_{33}\in_{33}}\\
&k_4=\frac{\in_{33}}{e_{33}^2+C_{33}\in_{33}},\quad k_5=\frac{C_{33}e_{31}-C_{13}e_{33}}{e_{33}^2+C_{33}\in_{33}},\quad k_6=\frac{C_{33}e_{32}-C_{23}e_{33}}{e_{33}^2+C_{33}\in_{33}}\\
&k_7=\frac{-C_{33}}{e_{33}^2+C_{33}\in_{33}},\quad k_8=\frac{e_{33}}{e_{33}^2+C_{33}\in_{33}},\quad k_9=C_{11}+k_1C_{13}+k_5e_{31}\\
&k_{10}=C_{12}+k_2C_{13}+k_6e_{31},\quad k_{11}=k_3C_{13}+k_7e_{31},\quad k_{12}=k_4C_{13}+k_8e_{31}\\
&k_{13}=C_{12}+k_1C_{23}+k_5e_{32},\quad k_{14}=C_{22}+k_2C_{23}+k_6e_{32},\quad k_{15}=k_3C_{23}+k_7e_{32}\\
&k_{16}=k_4C_{23}+k_8e_{32},\quad k_{17}=C_{66},\quad k_{18}=\frac{e_{15}}{C_{15}},\quad k_{19}=-\frac{e_{15}^2}{C_{55}}-\in_{11},\quad k_{20}=\frac{e_{24}}{C_{44}}\\
&k_{21}=-\frac{e_{24}^2}{C_{44}}-\in_{22},\quad k_{22}=\frac{1}{C_{55}},\quad k_{23}=-\frac{e_{15}}{C_{55}},\quad k_{24}=\frac{1}{C_{44}},\quad k_{25}=-\frac{e_{24}}{C_{44}}
\end{aligned} \tag{3-11}$$

Considering the equilibrium equations of elasticity and the Gaussian law of electrostatics (Equations (3-6) and (3-7)), and Equations (3-3), (3-8), (3-9) and (3-10), yields the following first-order partial differential equation:

$$\frac{\partial}{\partial z}\{R\}=[A]\{R\} \tag{3-12}$$

$\{R\}$ represents the state vector of a piezoelectric plate and contains the mechanical and electric variables which need to fulfill the continuity conditions at the interface of the laminates. And the state vector $\{R\}$ can be expressed as:

$$\{R\} = [u \quad v \quad D_z \quad \sigma_z \quad \tau_{xz} \quad \tau_{yz} \quad \emptyset \quad w]^T \tag{3-13}$$

The system matrix $[A]$ has the following form:

$$[A] = \begin{bmatrix} 0 & A_1 \\ A_2 & 0 \end{bmatrix} \tag{3-14}$$

where

$$[A_1] = \begin{bmatrix} k_{22} & 0 & k_{23}\alpha & -\alpha \\ 0 & k_{24} & k_{25}\beta & -\beta \\ -k_{18}\alpha & -k_{20}\beta & -k_{19}\alpha^2 - k_{21}\beta^2 & 0 \\ -\alpha & -\beta & 0 & 0 \end{bmatrix} \tag{3-15}$$

$$[A_2] = \begin{bmatrix} -k_9\alpha^2 - k_{17}\beta^2 & (-k_{10}-k_{17})\alpha\beta & -k_{11}\alpha & -k_{12}\alpha \\ (-k_{17}-k_{13})\alpha\beta & -k_{17}\alpha^2 - k_{14}\beta^2 & -k_{15}\beta & -k_{16}\beta \\ k_5\alpha & k_6\beta & k_7 & k_8 \\ k_1\alpha & k_2\beta & k_3 & k_4 \end{bmatrix} \tag{3-16}$$

3.3 Boundary conditions and analytical solutions

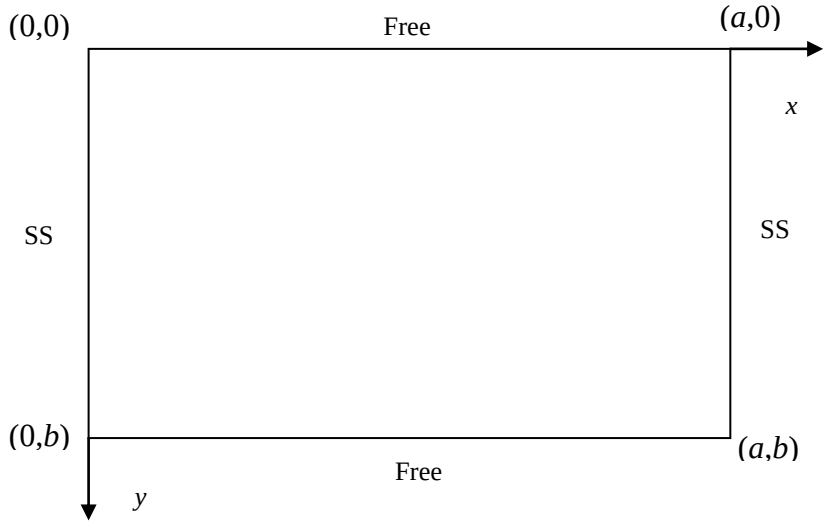

Figure 3.2 Boundary conditions of a piezoelectric laminated plate

For a piezoelectric laminated plate with simply-supported (SS) and electrical close-circuited at x=0, a and free edges at y=0, b (Figure 3.2), the following boundary conditions must be satisfied:

$$\sigma_x = v = w = \phi = 0, \qquad at\ \ x = 0, x = a \tag{3-17}$$

$$\sigma_y = \tau_{xy} = \tau_{yz} = D_y = 0, \qquad at\ \ y = 0, y = b \tag{3-18}$$

In general, the displacements of each layer can be expressed as:

$$u(x,y,z) = \tilde{u}(x,y,z) + f_1(y)u^{(0)}(x,z) + f_2(y)u^{(a)}(x,z) \tag{3-19}$$

$$v(x,y,z) = \tilde{v}(x,y,z) + g_1(y)v^{(0)}(x,z) + g_2(y)v^{(b)}(x,z) \tag{3-20}$$

Since there are two opposite free boundary conditions at y=0 and y=b, and the other two simply-supported boundary conditions at x=0 and x=a, boundary functions can be assumed as follows:

$$u(x,y,z) = \tilde{u}(x,y,z) + \frac{b}{2}\left(1 - \frac{y}{b}\right)^2 \alpha v^{(0)}(x,z) - \frac{b}{2}\left(\frac{y}{b}\right)^2 \alpha v^{(b)}(x,z) \tag{3-21}$$

$$v(x,y,z) = \tilde{v}(x,y,z) + \left(1 - \frac{y}{b}\right) v^{(0)}(x,z) + \frac{y}{b} v^{(b)}(x,z) \tag{3-22}$$

From above equations $v^{(0)}(x,z)$ and $v^{(b)}(x,z)$ are the unknown boundary functions which can be determined by the given boundary conditions and they have the following forms:

$$\begin{aligned} v^{(0)}(x,z) &= \sum_m v_m^{(0)}(z) \sin \zeta x \\ v^{(b)}(x,z) &= \sum_m v_m^{(b)}(z) \sin \zeta x \end{aligned} \tag{3-23}$$

The six elastic state variables can be expressed in terms of eigen-functions given by Dong and Sheng (2005) in the analysis of laminated plates and for the electromechanical analysis, the other two electric state variables also can be expressed in terms of eigen-functions:

$$\begin{aligned}
\tilde{u} &= \sum_m \sum_n \tilde{u}_{mn}(z)\cos\zeta x\cos\eta y, & \tau_{xz} &= \sum_m \sum_n X_{mn}(z)\cos\zeta x\cos\eta y \\
\tilde{v} &= \sum_m \sum_n \tilde{v}_{mn}(z)\sin\zeta x\sin\eta y, & \tau_{yz} &= \sum_m \sum_n Y_{mn}(z)\sin\zeta x\sin\eta y \\
\sigma_z &= \sum_m \sum_n Z_{mn}(z)\sin\zeta x\cos\eta y, & w &= \sum_m \sum_n w_{mn}(z)\sin\zeta x\cos\eta y \\
D_z &= \sum_m \sum_n D_{mn}(z)\sin\zeta x\cos\eta y, & \emptyset &= \sum_m \sum_n \emptyset_{mn}(z)\sin\zeta x\cos\eta y
\end{aligned} \tag{3-24}$$

The functions included in the two unknown boundary components from Equations (3-21) and (3-22) can be expressed in terms of eigen-functions as follows:

$$\begin{aligned}
1-\frac{y}{b} &= \sum_{n=1}^{\infty}\frac{2}{n\pi}\sin\eta y, & (1-\frac{y}{b})^2 &= \frac{1}{3}+\sum_{n=1}^{\infty}\frac{4}{n^2\pi^2}\cos\eta y \\
\frac{y}{b} &= \sum_{n=1}^{\infty}\frac{-2\cos n\pi}{n\pi}\sin\eta y, & (\frac{y}{b})^2 &= \frac{1}{3}+\sum_{n=1}^{\infty}\frac{4\cos n\pi}{n^2\pi^2}\cos\eta y
\end{aligned} \tag{3-25}$$

where $\zeta = \frac{m\pi}{a}$, $\eta = \frac{n\pi}{b}$, and m and n are the vibration wave numbers in the x and y direction respectively.

An assumed displacement field is imposed to a simply supported plate to represent the displacements of a piezoelectric plate with free edges and the introduction of eigen-functions in the series is to satisfy the given boundary conditions. By introducing Equations (3-21)-(3-25) to the first-order partial differential Equation (3-12), the first-order non-homogeneous ordinary differential equation for each pair of m and n is obtained and the derivation of this equation is given in Appendix B:

$$\frac{d}{dz}\{R_{mn}(z)\} = [\bar{A}]\{R_{mn}(z)\} + \{B_{mn}(z)\} \tag{3-26}$$

where

$$\{R_{mn}(z)\} = [\tilde{u}_{mn}(z) \quad \tilde{v}_{mn}(z) \quad D_{mn}(z) \quad Z_{mn}(z) \quad X_{mn}(z) \quad Y_{mn}(z) \quad \emptyset_{mn}(z) \quad w_{mn}(z)]^T \tag{3-27}$$

$$[\bar{A}] = \begin{bmatrix} 0 & \bar{A}_1 \\ \bar{A}_2 & 0 \end{bmatrix} \tag{3-28}$$

$$[\bar{A}_1] = \begin{bmatrix} k_{22} & 0 & k_{23}\zeta & -\zeta \\ 0 & k_{24} & -k_{25}\eta & \eta \\ k_{18}\zeta & -k_{20}\eta & k_{19}\zeta^2 + k_{21}\eta^2 & 0 \\ \zeta & -\eta & 0 & 0 \end{bmatrix} \tag{3-29}$$

$$[\bar{A}_2] = \begin{bmatrix} k_9\zeta^2 + k_{17}\eta^2 & (-k_{10}-k_{17})\zeta\eta & -k_{11}\zeta & -k_{12}\zeta \\ (-k_{17}-k_{13})\zeta\eta & k_{17}\zeta^2 + k_{14}\eta^2 & k_{15}\eta & k_{16}\eta \\ -k_5\zeta & k_6\eta & k_7 & k_8 \\ -k_1\zeta & k_2\eta & k_3 & k_4 \end{bmatrix} \tag{3-30}$$

$$B_{mn} = \begin{Bmatrix} \frac{b\cdot\zeta}{6}\cdot\frac{dF_{m0}(z)}{dz} \\ 0 \\ 0 \\ 0 \\ -[\frac{k_9\cdot b\cdot\zeta^3}{6} + \frac{k_{10}\cdot\zeta}{b}]\cdot F_{m0}(z) \\ 0 \\ [\frac{k_5\cdot b\cdot\zeta^2}{6} + \frac{k_6}{b}]\cdot F_{m0}(z) \\ [\frac{k_1\cdot b\cdot\zeta^2}{6} + \frac{k_2}{b}]\cdot F_{m0}(z) \end{Bmatrix}, (n = 0, m \neq 0) \tag{3-31}$$

$$B_{mn} = \left\{ \begin{array}{c} \frac{2 \cdot b \cdot \zeta}{n^2\pi^2} \cdot \frac{dF_{mn}(z)}{dz} \\ \frac{2}{n\pi} \cdot \frac{dF_{mn}(z)}{dz} \\ 0 \\ 0 \\ -\frac{2 \cdot k_9 \cdot b \cdot \zeta^3}{n^2\pi^2} \cdot F_{mn}(z) \\ \frac{2 \cdot k_{13} \cdot \zeta^2}{n\pi} \cdot F_{mn}(z) \\ \frac{2 \cdot k_5 \cdot b \cdot \zeta^2}{n^2\pi^2} \cdot F_{mn}(z) \\ \frac{2 \cdot k_1 \cdot b \cdot \zeta^2}{n^2\pi^2} \cdot F_{mn}(z) \end{array} \right\}, (n \neq 0, m \neq 0) \tag{3-32}$$

where

$$F_{mn}(z) = (\cos n\pi) v_m^{(b)}(z) - v_m^{(0)}(z) \tag{3-33}$$

The solution to non-homogeneous state equation with respect to the thickness coordinate z is presented as:

$$\{R_{mn}(z)\} = [G_{mn}(z)]\{R_{mn}(0)\} + \{H_{mn}(z)\}, \quad z \in [0, h] \tag{3-34}$$

where

$$\begin{aligned} [G_{mn}(z)] = e^{[\bar{A}]\cdot z} &= [I] + [\bar{A}] \cdot z + \frac{1}{2!}[\bar{A}]^2 \cdot z^2 + \frac{1}{3!}[\bar{A}]^3 \cdot z^3 + \cdots \\ &= \alpha_0(z)[I] + \alpha_1(z)[\bar{A}] + \alpha_2(z)[\bar{A}]^2 + \cdots + \alpha_{k-1}(z)[\bar{A}]^{k-1} \end{aligned} \tag{3-35}$$

$$\{H_{mn}(z)\} = \int_0^z e^{[\bar{A}]\cdot(z-\tau)} \{B_{mn}(\tau)\} d\tau \tag{3-36}$$

$[G_{mn}(z)]$ is called the transfer matrix of the homogeneous plate which represents the relationship between the initial state vector on the top surface and any other state vector at coordinate z and $\{H_{mn}(z)\}$ is the non-homogeneous vector. The $\alpha_i(z)$ (i=0,

1, 2, …k-1, k is the order of the matrix $[\bar{A}]$) are unknown scalar functions of z. They can be determined by replacing the matrix $[\bar{A}]$ with the eigenvalues λ_i (the i^{th} eigenvalue) of $[\bar{A}]$ in Equation (3-35) on the basis of the Cayley-Hamilton theorem (Charef and Boucherma, 2011). The unknown boundary functions and their derivatives are included in the non-homogeneous vector $\{B_{mn}(z)\}$. In order to solve the non-homogeneous equation, the determination of non-homogeneous vector $\{B_{mn}(z)\}$ is inevitable.

Consider the piezoelectric laminated plate consists of N different material layers. For an arbitrary layer i, the non-homogeneous ordinary differential equation by following the same procedure as described above can be presented as

$$\frac{d}{dz}\{R_{mn}(z)\}_i = [\bar{A}_i]\{R_{mn}(z)\}_i + \{B_{mn}(z)\}_i \tag{3-37}$$

The solution to the non-homogeneous ordinary differential Equation (3-37) can be obtained if the non-homogeneous vector $\{B_{mn}(z)\}_i$ is determined. As shown in Equations (3-31) and (3-32), the non-homogeneous vector $\{B_{mn}(z)\}_i$ contains unknown boundary functions and their derivatives.

A subdivision approach is subsequently carried out to meet the accuracy requirement of the solution. In this approach, the i^{th} physical layer is divided into K_i thin mathematical sub-layers and the thickness of each sub-layer is $d_{i,j}$. If the fictitious sub-layer is sufficiently thin, it is reasonable to assume that the unknown boundary functions are linearly distributed within the thin layers in the local coordinate z_i and they can be written as:

$$\begin{aligned} &v_{i,j}^{(0,b)}(z) = v_{i,j}^{(0,b),u} \cdot \left(1 - \frac{z}{d_{i,j}}\right) + v_{i,j}^{(0,b),l} \cdot \left(\frac{z}{d_{i,j}}\right) \\ &z \in \left[0, d_{i,j}\right], i = 1,2,\cdots N, j = 1,2,\cdots K_i \end{aligned} \tag{3-38}$$

where the subscript i,j denotes the j^{th} thin mathematical layer in the i^{th} physical layer of the piezoelectric laminated plate. $v_{i,j}^{(0,b),u}$, $v_{i,j}^{(0,b),l}$ are the end values of $v_{i,j}^{(0,b)}(z)$ at

the upper (u) and lower (l) surfaces of the j^{th} thin sub-layer, respectively. K_i denotes the number of thin mathematical sub-layers within the i^{th} layer. For a relatively thick plate, the number of division depends on the desired accuracy according to Fan (1998). As a consequence the errors induced by assumptions in Equation (3-38) are controllable.

For an arbitrary mathematical sub-layer j in the i^{th} layer, the state equation and its solution can be presented as:

$$\frac{d}{dz}\{R_{mn}(z)\}_{i,j} = [\bar{A}_i]\{R_{mn}(z)\}_{i,j} + \{B_{mn}(z)\}_{i,j} \tag{3-39}$$

$$\{R_{mn}(z)\}_{i,j} = [G_{mn}(z)]_{i,j}\{R_{mn}(0)\}_{i,j} + \{F_{mn}(z)\}_{i,j}, \quad z \in [0, d_{i,j}] \tag{3-40}$$

The non-homogeneous vector $\{B_{mn}(z)\}_{i,j}$ in Equation (3-39) can be determined by substituting Equation (3-38) into Equations (3-31) and (3-32).

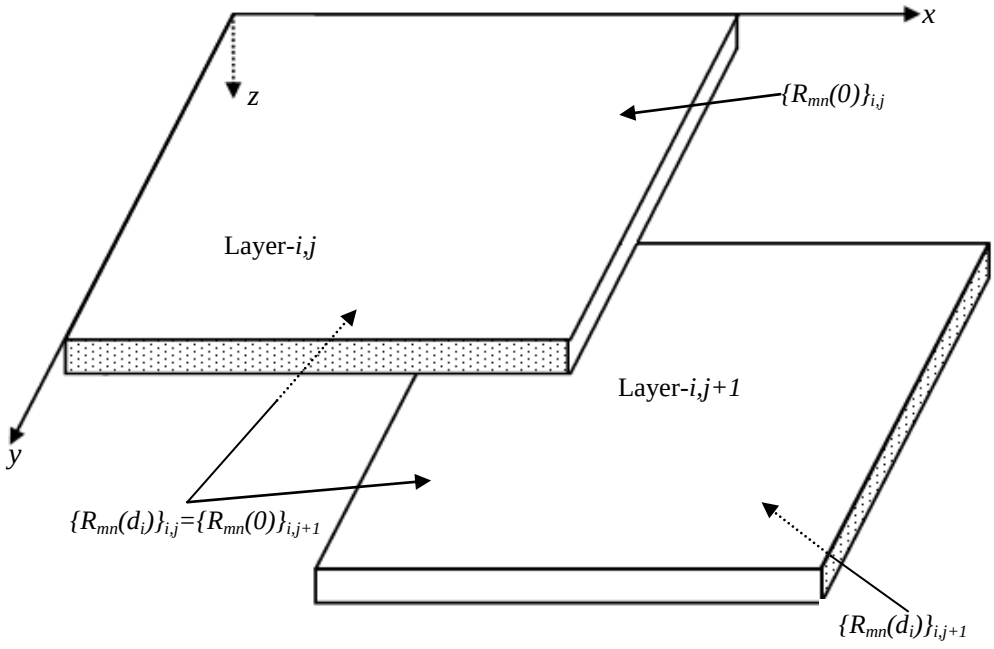

Figure 3.3: Continuity condition of state vectors at the interface of adjacent layers

The continuity condition at the interface of adjacent sub-layers is illustrated in Figure 3.3 and there is an analogous continuity condition at the interface of the adjacent physical layers. These continuity conditions are given:

$$\left\{R_{mn}\left(d_{i,j}\right)\right\}_{i,j} = \{R_{mn}(0)\}_{i,j+1} \tag{3-41}$$

$$\{R_{mn}(h_i)\}_i = \{R_{mn}(0)\}_{i+1} \tag{3-42}$$

By using Equation (3-41) recursively the relationship between the state vectors of the bottom surface and those of the top surface for the i^{th} layer is presented as

$$\{R_{mn}(h_i)\}_i = [M_i]\{R_{mn}(0)\}_i + \{\bar{M}_i\} \tag{3-43}$$

where

$$[M_i] = \prod_{j=K_i}^{1}\left[G_{mn}\left(d_{i,j}\right)\right]_{i,j}, \tag{3-44}$$

$$\begin{aligned}\{\bar{M}_i\} = &\left(\prod_{j=K_i}^{2}\left[G_{mn}\left(d_{i,j}\right)\right]_{i,j}\right)\left\{F_{mn}\left(d_{i,1}\right)\right\}_{i,1} + \left(\prod_{j=K_i}^{3}\left[G_{mn}\left(d_{i,j}\right)\right]_{i,j}\right)\left\{F_{mn}\left(d_{i,2}\right)\right\}_{i,2} \\ &+ \cdots + \left\{F_{mn}\left(d_{i,K_i}\right)\right\}_{i,K_i}.\end{aligned} \tag{3-45}$$

By employing Equations (3-42) and (3-43) recursively the relationship between the state vectors of the bottom and top surfaces of the plate can be obtained

$$\{R_{mn}(h_N)\} = [M]\{R_{mn}(0)\} + \{\bar{M}\} \tag{3-46}$$

$\{R_{mn}(0)\}$ and $\{R_{mn}(h_N)\}$ are the state vectors of the top and bottom surfaces of the piezoelectric plate, respectively. $[M]$ is the state transfer matrix and the non-homogeneous vector $\{\bar{M}\}$ comprises the unknown boundary coefficients $v_{i,j}^{(0,b),u}$ and $v_{i,j}^{(0,b),l}$. There are $2 \times (K_1 + K_2 + \cdots + K_N + 1)$ unknown coefficients by employing the continuity conditions at the interfaces of all layers. The unknown coefficients need to be determined by the given mechanical and electric boundary conditions at the four edges and the surface conditions on the top and bottom surfaces of the piezoelectric plate.

3.4 Boundary conditions at top and bottom surfaces of the piezoelectric laminated plate

The top and bottom surfaces of the piezoelectric laminated plate are subjected to both mechanical and electric surface conditions, in this study two types of surface conditions are employed.

3.4.1 Open-circuit surface condition

First, the top and bottom surfaces of the laminated piezoelectric plate are open-circuited, and the top surface is under a uniformly distributed load q_0. These surface conditions can be presented in terms of state variables as:

$$[D_{mn}(0) \quad Z_{mn}(0) \quad X_{mn}(0) \quad Y_{mn}(0)]^{\mathrm{T}} = [0 \quad -q_{mn} \quad 0 \quad 0]^{\mathrm{T}} \tag{3-47}$$

$$[D_{mn}(h_N) \quad Z_{mn}(h_N) \quad X_{mn}(h_N) \quad Y_{mn}(h_N)]^{\mathrm{T}} = [0 \quad 0 \quad 0 \quad 0]^{\mathrm{T}} \tag{3-48}$$

where $q_{mn}=4q_0/(m\pi)$ when n=0, and $q_{mn}=0$ when n=2, 4, 6 ⋯:

According to Equations (3-46)-(3-48), the following linear algebraic equation can be obtained

$$\begin{bmatrix} M_{31} & M_{32} & M_{37} & M_{38} \\ M_{41} & M_{42} & M_{47} & M_{48} \\ M_{51} & M_{52} & M_{57} & M_{58} \\ M_{61} & M_{62} & M_{67} & M_{68} \end{bmatrix} \begin{Bmatrix} \tilde{u}_{mn}(0) \\ \tilde{v}_{mn}(0) \\ \emptyset_{mn}(0) \\ w_{mn}(0) \end{Bmatrix} = q_{mn} \begin{Bmatrix} M_{34} \\ M_{44} \\ M_{54} \\ M_{64} \end{Bmatrix} - \begin{Bmatrix} \bar{M}_3 \\ \bar{M}_4 \\ \bar{M}_5 \\ \bar{M}_6 \end{Bmatrix} \tag{3-49}$$

3.4.2 Closed-circuit surface condition

In the second surface condition, the same mechanical load is applied but the top and bottom surfaces are grounded. The state variables on the corresponding surfaces can be expressed as

$$[Z_{mn}(0) \quad X_{mn}(0) \quad Y_{mn}(0) \quad \emptyset_{mn}(0)]^{\mathrm{T}} = [-q_{mn} \quad 0 \quad 0 \quad 0]^{\mathrm{T}} \tag{3-50}$$

$$[Z_{mn}(h_N) \quad X_{mn}(h_N) \quad Y_{mn}(h_N) \quad \emptyset_{mn}(h_N)]^{\mathrm{T}} = [0 \quad 0 \quad 0 \quad 0]^{\mathrm{T}} \tag{3-51}$$

Considering Equations (3-46), (3-50) and (3-51), the following linear algebraic equation is shown as

$$\begin{bmatrix} M_{41} & M_{42} & M_{43} & M_{48} \\ M_{51} & M_{52} & M_{53} & M_{58} \\ M_{61} & M_{62} & M_{63} & M_{68} \\ M_{71} & M_{72} & M_{73} & M_{78} \end{bmatrix} \begin{Bmatrix} \tilde{u}_{mn}(0) \\ \tilde{v}_{mn}(0) \\ D_{mn}(0) \\ w_{mn}(0) \end{Bmatrix} = q_{mn} \begin{Bmatrix} M_{44} \\ M_{54} \\ M_{64} \\ M_{74} \end{Bmatrix} - \begin{Bmatrix} \bar{M}_4 \\ \bar{M}_5 \\ \bar{M}_6 \\ \bar{M}_7 \end{Bmatrix} \tag{3-52}$$

Equations (3-49) and (3-52) are two sets of linear algebra equations in terms of different state vectors, respectively. The unknown boundary coefficients are contained in the term $\bar{M}$ and need to be determined by introducing boundary conditions along the edges of the laminate as given in Equations (3-17) and (3-18).

The expressions of $\sigma_x, \sigma_y, \tau_{xy}, \tau_{yz}, D_y$ are given as follows

$$\begin{aligned} \sigma_x = & \sum_m \sum_n [-k_9 \cdot \zeta \cdot \tilde{u}_{mn}(z) + k_{10} \cdot \eta \cdot \tilde{v}_{mn}(z) + k_{11} \cdot D_{mn}(z) \\ & + k_{12} \cdot Z_{mn}(z)] \sin \zeta x \cos \eta y \\ & + \sum_m \{-\frac{k_9}{2} \cdot b \cdot [(1 - \frac{y}{b})^2 + \left(\frac{y}{b}\right)^2] \cdot \zeta^2 - \frac{2k_{10}}{b}\} v_m^{(0)}(z) \sin \zeta x \end{aligned} \tag{3-53}$$

$$\begin{aligned} \sigma_y = & \sum_m \sum_n [-k_{13} \cdot \zeta \cdot \tilde{u}_{mn}(z) + k_{14} \cdot \eta \cdot \tilde{v}_{mn}(z) + k_{15} \cdot D_{mn}(z) \\ & + k_{16} \cdot Z_{mn}(z)] \sin \zeta x \cos \eta y \\ & + \sum_m \{[-\frac{k_{13}}{2} \cdot b \cdot (1 - \frac{y}{b})^2 \cdot \zeta^2 - \frac{k_{14}}{b}] \cdot v_m^{(0)}(z) \\ & + [-\frac{k_{13}}{2} \cdot b \cdot (\frac{y}{b})^2 \cdot \zeta^2 + \frac{k_{14}}{b}] \cdot v_m^{(b)}(z)]\} \sin \zeta x \end{aligned} \tag{3-54}$$

$$\tau_{xy} = \sum_m \sum_n [-k_{17} \cdot \eta \cdot \tilde{u}_{mn}(z) + k_{17} \cdot \zeta \cdot \tilde{v}_{mn}(z)] \cos \zeta x \sin \eta y \tag{3-55}$$

$$D_y = \sum_m \sum_n [k_{20} \cdot Y_{mn}(z) - k_{21} \cdot \eta \cdot \emptyset_{mn}(z)] \sin \zeta x \sin \eta y \tag{3-56}$$

According to Equations (3-9), (3-10), (3-21), (3-22) and (3-24), the simply supported boundary conditions are fulfilled automatically. The boundary conditions at the free edges are also satisfied considering Equations (3-24), (3-55) and (3-56) except for σ_y. Detailed verifications of the boundary conditions are given in Appendix C and the remaining boundary condition to be determined is

$$\sigma_y = 0, \qquad at \;\; y = 0, y = b \tag{3-57}$$

When y=0

$$\begin{aligned} \sigma_y = \sum_n & [-k_{13} \cdot \zeta \cdot \tilde{u}_{mn}(z) + k_{14} \cdot \eta \cdot \tilde{v}_{mn}(z) + k_{15} \cdot D_{mn}(z) + k_{16} \cdot Z_{mn}(z)] \\ & + (-\frac{k_{13} \cdot b \cdot \zeta^2}{2} - \frac{k_{14}}{b}) \cdot v_m^{(0)}(z) + \frac{k_{14}}{b} \cdot v_m^{(b)}(z) = 0 \end{aligned} \tag{3-58}$$

When y=b

$$\begin{aligned} \sigma_y = \sum_n & (-1)^n [-k_{13} \cdot \zeta \cdot \tilde{u}_{mn}(z) + k_{14} \cdot \eta \cdot \tilde{v}_{mn}(z) + k_{15} \cdot D_{mn}(z) + k_{16} \cdot Z_{mn}(z)] \\ & + (\frac{k_{13} \cdot b \cdot \zeta^2}{2} + \frac{k_{14}}{b}) \cdot v_m^{(b)}(z) - \frac{k_{14}}{b} \cdot v_m^{(0)}(z) = 0 \end{aligned} \tag{3-59}$$

Due to the symmetry, $v_m^{(0)}(z) = -v_m^{(b)}(z)$, thus only the boundary condition at *y=0* needs to be satisfied, thus the following condition is obtained:

$$\sigma_y = \sum_n [-k_{13}\cdot\zeta\cdot\tilde{u}_{mn}(z)+k_{14}\cdot\eta\cdot\tilde{v}_{mn}(z)+k_{15}\cdot D_{mn}(z)+k_{16}\cdot Z_{mn}(z)] + (-\frac{k_{13}\cdot b\cdot\zeta^2}{2}-\frac{2k_{14}}{b})v_m^{(0)}(z) = 0 \quad (3\text{-}60)$$

The state variables at the top surface for open-circuit and closed-circuit surface conditions are given as follows, respectively.

$$\begin{Bmatrix}\tilde{u}_{mn}(0)\\ \tilde{v}_{mn}(0)\\ D_{mn}(0)\\ Z_{mn}(0)\end{Bmatrix} = \begin{bmatrix}M_{11}(z) & M_{12}(z) & M_{17}(z) & M_{18}(z)\\ M_{21}(z) & M_{22}(z) & M_{27}(z) & M_{28}(z)\\ M_{31}(z) & M_{32}(z) & M_{37}(z) & M_{38}(z)\\ M_{41}(z) & M_{42}(z) & M_{47}(z) & M_{48}(z)\end{bmatrix}\begin{bmatrix}M_{31} & M_{32} & M_{37} & M_{38}\\ M_{41} & M_{42} & M_{47} & M_{48}\\ M_{51} & M_{52} & M_{57} & M_{58}\\ M_{61} & M_{62} & M_{67} & M_{68}\end{bmatrix}^{-1}$$
$$\times\left(\begin{bmatrix}M_{33} & M_{34} & M_{35} & M_{36}\\ M_{43} & M_{44} & M_{45} & M_{46}\\ M_{53} & M_{54} & M_{55} & M_{56}\\ M_{63} & M_{64} & M_{65} & M_{66}\end{bmatrix}\begin{Bmatrix}0\\ q_{mn}\\ 0\\ 0\end{Bmatrix}-\begin{Bmatrix}\bar{M}_3\\ \bar{M}_4\\ \bar{M}_5\\ \bar{M}_6\end{Bmatrix}\right) \quad (3\text{-}61)$$
$$-\left(\begin{bmatrix}M_{13}(z) & M_{14}(z) & M_{15}(z) & M_{16}(z)\\ M_{23}(z) & M_{24}(z) & M_{25}(z) & M_{26}(z)\\ M_{33}(z) & M_{34}(z) & M_{35}(z) & M_{36}(z)\\ M_{43}(z) & M_{44}(z) & M_{45}(z) & M_{46}(z)\end{bmatrix}\begin{Bmatrix}0\\ q_{mn}\\ 0\\ 0\end{Bmatrix}+\begin{Bmatrix}\bar{M}_1(z)\\ \bar{M}_2(z)\\ \bar{M}_3(z)\\ \bar{M}_4(z)\end{Bmatrix}\right)$$

$$\begin{Bmatrix}\tilde{u}_{mn}(0)\\ \tilde{v}_{mn}(0)\\ D_{mn}(0)\\ Z_{mn}(0)\end{Bmatrix} = \begin{bmatrix}M_{11}(z) & M_{12}(z) & M_{13}(z) & M_{18}(z)\\ M_{21}(z) & M_{22}(z) & M_{23}(z) & M_{28}(z)\\ M_{31}(z) & M_{32}(z) & M_{33}(z) & M_{38}(z)\\ M_{41}(z) & M_{42}(z) & M_{43}(z) & M_{48}(z)\end{bmatrix}\begin{bmatrix}M_{41} & M_{42} & M_{43} & M_{48}\\ M_{51} & M_{52} & M_{53} & M_{58}\\ M_{61} & M_{62} & M_{63} & M_{68}\\ M_{71} & M_{72} & M_{73} & M_{78}\end{bmatrix}^{-1}$$
$$\times\left(\begin{bmatrix}M_{44} & M_{45} & M_{46} & M_{47}\\ M_{54} & M_{55} & M_{56} & M_{57}\\ M_{64} & M_{65} & M_{66} & M_{67}\\ M_{74} & M_{75} & M_{76} & M_{77}\end{bmatrix}\begin{Bmatrix}q_{mn}\\ 0\\ 0\\ 0\end{Bmatrix}-\begin{Bmatrix}\bar{M}_4\\ \bar{M}_5\\ \bar{M}_6\\ \bar{M}_7\end{Bmatrix}\right) \quad (3\text{-}62)$$
$$-\left(\begin{bmatrix}M_{14}(z) & M_{15}(z) & M_{16}(z) & M_{17}(z)\\ M_{24}(z) & M_{25}(z) & M_{26}(z) & M_{27}(z)\\ M_{34}(z) & M_{35}(z) & M_{36}(z) & M_{37}(z)\\ M_{44}(z) & M_{45}(z) & M_{46}(z) & M_{47}(z)\end{bmatrix}\begin{Bmatrix}q_{mn}\\ 0\\ 0\\ 0\end{Bmatrix}+\begin{Bmatrix}\bar{M}_1(z)\\ \bar{M}_2(z)\\ \bar{M}_3(z)\\ \bar{M}_4(z)\end{Bmatrix}\right)$$

By considering Equations (3-12), (3-60), (3-61) and (3-62), the unknown boundary coefficients for each electric surface condition can be solved.

3.5 Conclusions

To fulfill the continuity conditions between different layers of laminates, three displacement components, electrical potential, three interlaminar stresses, and transverse electric displacements are chosen as state variables. On the basis of the theories of 3D elasticity and piezoelectricity, the non-homogeneous state equation including the unknown boundary coefficients is established. The relationship between the state variables on the top surface and those on an arbitrary interface is obtained by using the transfer matrix. By introducing the loading and boundary conditions on the plate, the unknown boundary coefficients in the non-homogeneous vectors can be solved simultaneously. It is worth to mention that it is innovative to introduce the two electric state variables (D_z and ϕ) in terms of eigen-functions in the state equation to solve the bending problem of simply-supported and free-edge piezoelectric laminates. Moreover, new associated electric boundary conditions are also given and the layer refinement approach is carried out to meet the accuracy requirement of the solution.

Since the 3D state space solution can take into account all the independent elastic and piezoelectric constants and satisfy both mechanical and electric boundary conditions and guarantee the continuity conditions, the accurate determination of the electromechanical coupling in the piezoelectric laminates under the mechanical and electrical loading can be revealed.

CHAPTER 4 STATE SPACE METHOD FOR INFINITE LONG PIEZOELECTRIC LAMINATES WITH FREE EDGES UNDER UNIAXIAL EXTENSION

4.1 Introduction

In the previous chapter, the state space method has been extended to the simply-supported piezoelectric laminated plate with two opposite free edges under transverse loads. The formulation admits the traction-free boundary conditions at the free edges and is applicable to thick and thin piezoelectric laminated plates. Inspired by the work performed by Zhang et al. (2006) on the cross-ply laminated composite under uniform extension and thermal loading, to consider the electromechanical coupling behaviour and electric boundary conditions the state equations for a piezoelectric laminated plate subjected to uniaxial extension are formulated in this chapter.

4.2 Formulation of fundamental state space approach

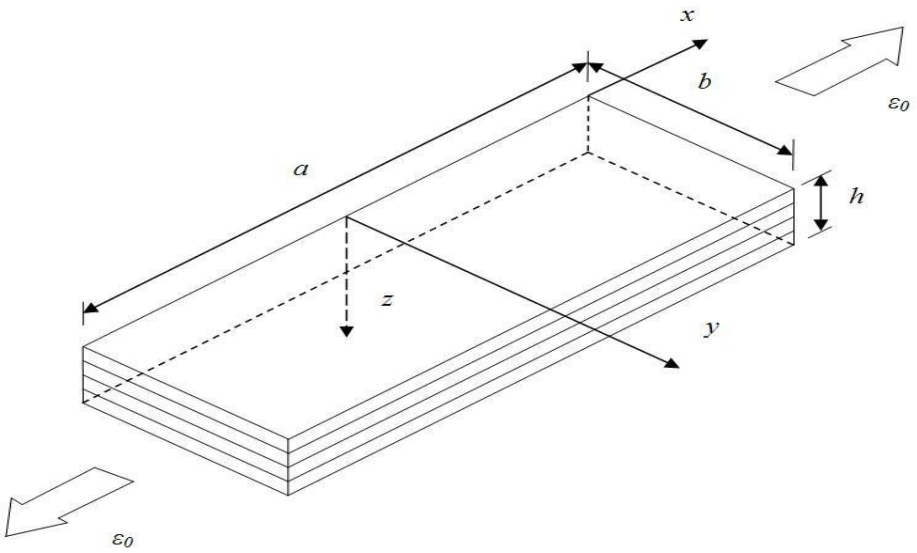

Figure 4.1: Geometry and coordinate system of a piezoelectric laminated plate

As depicted in Figure 4.1, a rectangular piezoelectric laminated plate is subjected to a uniform constant axial strain ε_0 and it is assumed to have constant thickness h, width b and length a. The principal elastic directions of the plate coincide with the axes of the chosen rectangular coordinate system and the fully coupled three-dimensional constitutive relations of an orthotropic piezoelectric lamina are exactly the same as those of Equations (3-1)-(3-4).

Due to the uniform extension ε_0 and infinite length in the x direction, the state variables are independent from the longitudinal coordinate x, as a consequence, the linear strain-displacement relations of elasticity and the electric field-electric potential relations can be written as:

$$\begin{aligned}
&\varepsilon_x = \frac{\partial u}{\partial x} = \varepsilon_0\,, \quad \varepsilon_y = \frac{\partial v}{\partial y}\,, \quad \varepsilon_z = \frac{\partial w}{\partial z}\,, \\
&\gamma_{yz} = \frac{\partial w}{\partial y} + \frac{\partial v}{\partial z}\,, \quad \gamma_{xz} = \frac{\partial u}{\partial z} + \frac{\partial w}{\partial x} = 0, \quad \gamma_{xy} = \frac{\partial u}{\partial y} + \frac{\partial v}{\partial x} = 0\,, \\
&E_x = -\frac{\partial \emptyset}{\partial x} = 0\,, \quad E_y = -\frac{\partial \emptyset}{\partial y}\,, \quad E_z = -\frac{\partial \emptyset}{\partial z}\,.
\end{aligned} \tag{4-1}$$

where u, v and w represent displacements in the x, y and z directions, respectively. $\emptyset$ is electric potential.

By considering the condition of zero electric body charge f_e and body forces f_i, the equilibrium equations of elasticity and the Gaussian law of electrostatics can be expressed, respectively, as follows:

$$\begin{aligned}
&\sigma_{x,x} = 0\,, \\
&\sigma_{y,y} + \tau_{yz,z} = 0\,, \\
&\tau_{yz,y} + \sigma_{z,z} = 0\,,
\end{aligned} \tag{4-2}$$

$$D_{y,y} + D_{z,z} = 0\,. \tag{4-3}$$

From Equations (3-3), (3-4) and (4-1), it can be concluded that $\tau_{xz} = 0$, $\tau_{xy} = 0$, $D_x = 0$ and other 9 state variables v, w, σ_x, σ_y, σ_z, τ_{yz}, D_y, D_z, $\emptyset$ are all independent of *x*. They can be expressed as $v(y,z)$, $w(y,z)$, $\sigma_x(y,z)$, $\sigma_y(y,z)$, $\sigma_z(y,z)$, $\tau_{yz}(y,z)$, $D_y(y,z)$, $D_z(y,z)$, $\emptyset(y,z)$.

The interlaminar stresses $\sigma_z(y,z)$ and $\tau_{yz}(y,z)$ are significant and continuous at the interface of dissimilar materials thus chosen as state vectors in the formulation. By eliminating the in-plane stresses σ_x and σ_y, and the in-plane electric displacement D_y in the *x*-*y* plane, the differentials of the displacements *v* and *w*, and the transverse stresses σ_z and τ_{yz}, and the electric variables D_z and $\emptyset$, with respect to the *z* coordinate can be derived.

Let $\beta = \frac{\partial}{\partial y}$, from Equation (4-1) and the third equations of the matrix in Equations (3-3) and (3-4), the following relations (Appendix C) can be obtained:

$$\frac{\partial}{\partial z}\begin{Bmatrix} w \\ \emptyset \end{Bmatrix} = \begin{bmatrix} k_1'\beta & k_2' & k_3' \\ k_5'\beta & k_6' & k_7' \end{bmatrix}\begin{Bmatrix} v \\ \sigma_z \\ D_z \end{Bmatrix} + \begin{Bmatrix} k_4' \\ k_8' \end{Bmatrix}\varepsilon_0 \tag{4-4}$$

By substituting Equation (4-4) into Equations (3-3) and (3-4), the in-plane stresses and electric displacement are presented:

$$\begin{Bmatrix} \sigma_x \\ \sigma_y \end{Bmatrix} = \begin{bmatrix} k_9'\beta & k_{10}' & k_{11}' \\ k_{13}'\beta & k_{14}' & k_{15}' \end{bmatrix}\begin{Bmatrix} v \\ \sigma_z \\ D_z \end{Bmatrix} + \begin{Bmatrix} k_{12}' \\ k_{16}' \end{Bmatrix}\varepsilon_0 \tag{4-5}$$

$$D_y = k_{17}' \cdot \tau_{yz} + k_{18}' \cdot \beta\emptyset \tag{4-6}$$

The coefficients k_i' in the matrix are the constants that are only determined by the material property of the laminate. All the constants k_i' are given as follows:

$$k_1^{'}=\frac{-e_{32}e_{33}-C_{23}\in_{33}}{e_{33}^2+C_{33}\in_{33}},\quad k_2^{'}=\frac{\in_{33}}{e_{33}^2+C_{33}\in_{33}},\quad k_3^{'}=\frac{e_{33}}{e_{33}^2+C_{33}\in_{33}}$$

$$k_4^{'}=\frac{-e_{31}e_{33}-C_{13}\in_{33}}{e_{33}^2+C_{33}\in_{33}},\quad k_5^{'}=\frac{C_{33}e_{32}-C_{23}e_{33}}{e_{33}^2+C_{33}\in_{33}},\ k_6^{'}=\frac{e_{33}}{e_{33}^2+C_{33}\in_{33}}$$

$$k_7^{'}=\frac{-C_{33}}{e_{33}^2+C_{33}\in_{33}},\quad k_8^{'}=\frac{C_{33}e_{31}-C_{13}e_{33}}{e_{33}^2+C_{33}\in_{33}},\quad k_9^{'}=C_{12}+k_1^{'}C_{13}+k_5^{'}e_{31}$$

$$k_{10}^{'}=k_2^{'}C_{13}+k_6^{'}e_{31},\quad k_{11}^{'}=k_3^{'}C_{13}+k_7^{'}e_{31},\quad k_{12}^{'}=C_{11}+k_4^{'}C_{13}+k_8^{'}e_{31} \tag{4-7}$$

$$k_{13}^{'}=C_{22}+k_1^{'}C_{23}+k_5^{'}e_{32},\quad k_{14}^{'}=k_2^{'}C_{23}+k_6^{'}e_{32},\quad k_{15}^{'}=k_3^{'}C_{23}+k_7^{'}e_{32}$$

$$k_{16}^{'}=C_{12}+k_4^{'}C_{23}+k_8^{'}e_{32},\quad k_{17}^{'}=\frac{e_{24}}{C_{44}},\quad k_{18}^{'}=-\frac{e_{24}^2}{C_{44}}-\in_{22},$$

$$k_{19}^{'}=\frac{1}{C_{44}},\quad k_{20}^{'}=-\frac{e_{24}}{C_{44}},\quad k_{21}^{'}=-1.$$

Considering the equilibrium equations of elasticity and the Gaussian law of electrostatics and Equations (3-3), (4-4), (4-5) and (4-6), yields the following first-order non-homogeneous partial differential equation:

$$\frac{\partial}{\partial z}\{R\}=[A]\{R\}+\{B\} \tag{4-8}$$

$\{R\}$ represents the state vector of the piezoelectric plate and contains the mechanical and electric variables which need to fulfill the continuity conditions at the interface of the laminates. And the state vector $\{R\}$ can be expressed as:

$$\{R\}=[v\quad D_z\quad \sigma_z\quad \tau_{yz}\quad \emptyset\quad w]^T \tag{4-9}$$

The system matrix $[A]$ has the following form:

$$[A]=\begin{bmatrix}0 & A_1\\ A_2 & 0\end{bmatrix} \tag{4-10}$$

where

$$[A_1]=\begin{bmatrix}k_{19}^{'} & k_{20}^{'}\beta & k_{21}^{'}\beta\\ -k_{17}^{'}\beta & -k_{18}^{'}\beta^2 & 0\\ -\beta & 0 & 0\end{bmatrix} \tag{4-11}$$

$$[A_2] = \begin{bmatrix} -k_{13}'\beta^2 & -k_{15}'\beta & -k_{14}'\beta \\ k_5'\beta & k_7' & k_6' \\ k_1'\beta & k_3' & k_2' \end{bmatrix} \tag{4-12}$$

And the non-homogeneous vector $\{B\}$ is written as

$$\{B\} = \begin{Bmatrix} 0 \\ 0 \\ 0 \\ 0 \\ k_8' \\ k_4' \end{Bmatrix} \varepsilon_0 \tag{4-13}$$

4.3 Boundary conditions and analytical solution

The piezoelectric laminate has the traction-free and electric open-circuit boundary conditions at y=0, b. The following boundary conditions must be satisfied:

$$\sigma_y = \tau_{xy} = \tau_{yz} = D_y = 0, \qquad at \;\; y = 0, y = b \tag{4-14}$$

The displacement $v(y,z)$ of each layer can be expressed as:

$$v(y,z) = \tilde{v}(y,z) + (1 - \frac{2y}{b}) \cdot v^{(0)}(z) \tag{4-15}$$

where $v^{(0)}(z)$ is the unknown boundary function which can be determined by imposing traction free conditions and open-circuit conditions on the free edges. The six state variables can be expressed in terms of eigen-functions as follows:

$$\tilde{v}(y,z)=\sum_{n}\tilde{v}_n(z)\sin\eta y,\qquad \tau_{yz}(y,z)=\sum_{n}Y_n(z)\sin\eta y$$
$$D_z(y,z)=\sum_{n}D_n(z)\cos\eta y,\qquad \emptyset(y,z)=\sum_{n}\emptyset_n(z)\cos\eta y \tag{4-16}$$
$$\sigma_z(y,z)=\sum_{n}Z_n(z)\cos\eta y,\qquad w(y,z)=\sum_{n}w_n(z)\cos\eta y$$

The assumed eigen-functions in the series are so chosen that the traction-free and open-circuit boundary conditions at free edges can be satisfied automatically. The function contained in the unknown boundary component from Equation (4-15) is a linear function which can guarantee sufficiently accurate results (Fan, 1998) and can be expressed in terms of eigen-functions as follows:

$$y=-\sum_{n=0}^{\infty}\frac{2b\cos n\pi}{n\pi}\sin\eta y \tag{4-17}$$

where $\eta=\frac{n\pi}{b}$, since a uniformly distributed extension is applied, displacement *v* is zero at *y=b/2*.

By introducing Equations (4-15)-(4-17), for an arbitrary *n* the first-order non-homogeneous ordinary differential equation is obtained and the detailed derivation of this equation is given in Appendix D:

$$\frac{d}{dz}\{R_n(z)\}=[\bar{A}]\{R_n(z)\}+\{\bar{B}_n(z)\} \tag{4-18}$$

where

$$\{R_n(z)\}=[\tilde{v}_n(z)\quad D_n(z)\quad Z_n(z)\quad Y_n(z)\quad \emptyset_n(z)\quad w_n(z)]^T \tag{4-19}$$

$$[\bar{A}]=\begin{bmatrix}0 & \bar{A}_1\\ \bar{A}_2 & 0\end{bmatrix} \tag{4-20}$$

$$[\bar{A}_1] = \begin{bmatrix} k_{19}^{'} & -k_{20}^{'}\eta & -k_{21}^{'}\eta \\ -k_{17}^{'}\eta & k_{18}^{'}\eta^2 & 0 \\ -\eta & 0 & 0 \end{bmatrix} \tag{4-21}$$

$$[\bar{A}_2] = \begin{bmatrix} k_{13}^{'}\eta^2 & k_{15}^{'}\eta & k_{14}^{'}\eta \\ k_{5}^{'}\eta & k_{7}^{'} & k_{6}^{'} \\ k_{1}^{'}\eta & k_{3}^{'} & k_{2}^{'} \end{bmatrix} \tag{4-22}$$

The non-homogeneous vectors are expressed as follows:

$$\bar{B}_n(z) = \begin{Bmatrix} 0 \\ 0 \\ 0 \\ 0 \\ -\frac{2}{b} \cdot k_5^{'} \cdot v^{(0)}(z) + k_8^{'} \cdot \varepsilon_0 \\ -\frac{2}{b} \cdot k_1^{'} \cdot v^{(0)}(z) + k_4^{'} \cdot \varepsilon_0 \end{Bmatrix}, (n = 0) \tag{4-23}$$

$$\bar{B}_n(z) = \begin{Bmatrix} \frac{-2\,(1+\cos n\pi)}{n\pi} \cdot \frac{dv^{(0)}(z)}{dz} \\ 0 \\ 0 \\ 0 \\ 0 \\ 0 \end{Bmatrix}, (n \neq 0) \tag{4-24}$$

The solution of the non-homogeneous state equation with respect to the thickness coordinate z is presented as:

$$\{R_n(z)\} = [G_n(z)]\{R_n(0)\} + \{F_n(z)\} \tag{4-25}$$

where

$$\begin{aligned} [G_n(z)] = e^{[\bar{A}]\cdot z} &= [I] + [\bar{A}] \cdot z + \frac{1}{2!}[\bar{A}]^2 \cdot z^2 + \frac{1}{3!}[\bar{A}]^3 \cdot z^3 + \cdots \\ &= \alpha_0(z)[I] + \alpha_1(z)[\bar{A}] + \alpha_2(z)[\bar{A}]^2 + \cdots + \alpha_{k-1}(z)[\bar{A}]^{k-1} \end{aligned} \tag{4-26}$$

$$\{F_n(z)\} = \int_0^z e^{[\bar{A}]\cdot(z-\tau)} \{\bar{B}_n(\tau)\} d\tau \tag{4-27}$$

The transfer matrix of the homogeneous plate $[G_n(z)]$ represents the relationship between the initial state vector on the top surface and any other state vector at the coordinate z and $\{F_n(z)\}$ is the non-homogeneous vector. The coefficient $\alpha_i(z)$ (i=0, 1, 2, …k-1, k is the order of the matrix $[\bar{A}]$) are unknown scalar functions of z. They can be determined by replacing the matrix $[\bar{A}]$ with the eigenvalues λ_i (the i^{th} eigenvalue) of $[\bar{A}]$ in Equation (4-26) on the basis of the Cayley-Hamilton theorem. The unknown boundary function and its derivatives are contained in the non-homogeneous vector $\{\bar{B}_n(z)\}$. In order to solve the non-homogeneous equation, the determination of non-homogeneous vector $\{\bar{B}_n(z)\}$ is necessary.

Suppose the piezoelectric laminated plate consists of N different layers. For an arbitrary layer i, the non-homogeneous ordinary differential equation by following the same procedure as described above can be presented as:

$$\frac{d}{dz}\{R_n(z)\}_i = [\bar{A}_i]\{R_n(z)\}_i + \{\bar{B}_n(z)\}_i \tag{4-28}$$

When the non-homogeneous vector $\{\bar{B}_n(z)\}_i$ is determined, the solution to the non-homogeneous ordinary differential Equation (4-28) can be solved. The non-homogeneous vector $\{\bar{B}_n(z)\}_i$ contains the unknown boundary function and its derivatives as shown in Equations (4-23) and (4-24).

In order to meet the accuracy requirement of the solution in practice, a subdivision approach may be needed to solve the unknown boundary function. In this approach, the i^{th} physical layer is further divided into K_i thin mathematical sub-layers and the thickness of each sub-layer is $d_{i,j}$. With sufficiently thin fictitious sub-layers, the unknown boundary function can be assumed to be linearly distributed within the thin layers in the local coordinate z_i and it can be expressed as:

$$v_{i,j}^{(0,b)}(z) = v_{i,j}^{(0,b),u} \cdot \left(1 - \frac{z}{d_{i,j}}\right) + v_{i,j}^{(0,b),l} \cdot \left(\frac{z}{d_{i,j}}\right),$$
$$z \in \left[0, d_{i,j}\right], i = 1,2,\cdots N, j = 1,2,\cdots K_i \tag{4-29}$$

where the subscript i,j denotes the j^{th} thin mathematical layer in the i^{th} physical layer of the piezoelectric laminated plate. $v_{i,j}^{(0,b),u}$, $v_{i,j}^{(0,b),l}$ are the end values of $v_{i,j}^{(0,b)}(z)$ at the upper (u) and lower (l) surfaces of the j^{th} thin sub-layer, respectively. K_i denotes the number of thin mathematical sub-layers within the i^{th} layer. For a relatively thick plate, the number of division depends on the desired accuracy (Fan, 1998). It also should be mentioned that $v^{(0)}(z) = -v^{(b)}(z)$ is applied due to the symmetric loading and boundary conditions and thus only one unknown boundary function $v^{(0)}(z)$ needs to be determined.

For an arbitrary mathematical sub-layer j in the i^{th} layer, the state equation and its solution can be presented as:

$$\frac{d}{dz}\{R_n(z)\}_{i,j} = [\bar{A}_i]\{R_n(z)\}_{i,j} + \{\bar{B}_n(z)\}_{i,j} \tag{4-30}$$

$$\{R_n(z)\}_{i,j} = [G_n(z)]_{i,j}\{R_n(0)\}_{i,j} + \{F_n(z)\}_{i,j}, \quad z \in [0, d_{i,j}] \tag{4-31}$$

The non-homogeneous vector $\{\bar{B}_n(z)\}_{i,j}$ in Equation (4-30) can be determined by substituting Equation (4-29) into Equations (4-23) and (4-24).

The continuity condition of state vectors at the interfaces of adjacent layers (depicted in Figure 3.3) and the continuity condition at the interfaces of adjacent sub-layers need to be satisfied, and these continuity conditions are written as:

$$\{R_n(h_i)\}_i = \{R_n(0)\}_{i+1} \tag{4-32}$$

$$\left\{R_n(d_{i,j})\right\}_{i,j} = \{R_n(0)\}_{i,j+1} \tag{4-33}$$

By using Equation (4-33) recursively the relationship between the state vector of the bottom surface and that of the top surface for the i^{th} layer is presented as:

$$\{R_n(h_i)\}_i = [M_i]\{R_n(0)\}_i + \{\bar{M}_i\} \tag{4-34}$$

where

$$[M_i] = \prod_{j=K_i}^{1} \left[G_n(d_{i,j})\right]_{i,j}, \tag{4-35}$$

$$\{\bar{M}_i\} = \left(\prod_{j=K_i}^{2} \left[G_n(d_{i,j})\right]_{i,j}\right)\{F_n(d_{i,1})\}_{i,1} + \left(\prod_{j=K_i}^{3} \left[G_n(d_{i,j})\right]_{i,j}\right)\{F_n(d_{i,2})\}_{i,2} + \cdots + \{F_n(d_{i,K_i})\}_{i,K_i}. \tag{4-36}$$

Similarly, considering Equations (4-32) and (4-34) the relationship between the state vectors of the bottom and top surfaces of the plate can be established:

$$\{R_n(h_N)\} = [M]\{R_n(0)\} + \{\bar{M}\} \tag{4-37}$$

$\{R_n(0)\}$ and $\{R_n(h_N)\}$ are the state vectors of the top and bottom surfaces of the piezoelectric plate, respectively. $[M]$ is the state transfer matrix and the non-homogeneous vector $\{\bar{M}\}$ comprises the unknown boundary coefficients $v_{i,j}^{(0,b),u}$ and $v_{i,j}^{(0,b),l}$. There are $(K_1 + K_2 + \cdots + K_N + 1)$ unknown coefficients by employing the continuity conditions at all the interfaces of layers. As mentioned before, the unknown coefficients need to be determined by the traction-free and open-circuited boundary conditions at the free edge and the surface conditions on the top and bottom surfaces of the piezoelectric laminate.

4.4 Boundary conditions at top and bottom surfaces of piezoelectric laminated plate

The top and bottom surfaces of the piezoelectric laminate are subjected to both mechanical and electric surface conditions and two types of boundary conditions are considered in this study.

4.4.1 Open-circuit surface condition

First, the top and bottom surfaces of the laminated piezoelectric laminate are considered as traction-free and open-circuited and they can be presented in terms of state variables as

$$[D_n(0) \quad Z_n(0) \quad Y_n(0)]^{\mathrm{T}} = [0 \quad 0 \quad 0]^{\mathrm{T}} \tag{4-38}$$

$$[D_n(h_N) \quad Z_n(h_N) \quad Y_n(h_N)]^{\mathrm{T}} = [0 \quad 0 \quad 0]^{\mathrm{T}} \tag{4-39}$$

Considering Equations (4-37)-(4-39), the following linear algebraic equation can be obtained

$$\begin{bmatrix} M_{21} & M_{25} & M_{26} \\ M_{31} & M_{35} & M_{36} \\ M_{41} & M_{45} & M_{46} \end{bmatrix} \begin{Bmatrix} \tilde{v}_n(0) \\ \emptyset_n(0) \\ w_n(0) \end{Bmatrix} = - \begin{Bmatrix} \bar{M}_2 \\ \bar{M}_3 \\ \bar{M}_4 \end{Bmatrix} \tag{4-40}$$

4.4.2 Closed-circuit surface condition

For the second surface condition, the top surface and the bottom surface are both grounded, leading to the closed-circuit boundary conditions. Moreover, the traction-free conditions are imposed on both surfaces. Such surface conditions can be written as:

$$[Z_n(0) \quad Y_n(0) \quad \emptyset_n(0)]^{\mathrm{T}} = [0 \quad 0 \quad 0]^{\mathrm{T}} \tag{4-41}$$

$$[Z_n(h_N) \quad Y_n(h_N) \quad \emptyset_n(h_N)]^{\mathrm{T}} = [0 \quad 0 \quad 0]^{\mathrm{T}} \tag{4-42}$$

According to Equations (4-37), (4-41) and (4-42), the following linear algebraic equation is shown as:

$$\begin{bmatrix} M_{31} & M_{32} & M_{26} \\ M_{41} & M_{42} & M_{46} \\ M_{51} & M_{52} & M_{56} \end{bmatrix} \begin{Bmatrix} \tilde{v}_n(0) \\ D_n(0) \\ w_n(0) \end{Bmatrix} = - \begin{Bmatrix} \bar{M}_3 \\ \bar{M}_4 \\ \bar{M}_5 \end{Bmatrix} \tag{4-43}$$

There are two sets of linear algebra equations in terms of different state vectors in Equations (4-40) and (4-43), respectively. The unknown boundary coefficients are

included in the term $\bar{M}$ and need to be determined by introducing boundary conditions along the edges of the laminate.

The expressions of σ_y and D_y are given as follows:

$$\sigma_y = \sum_n [k_{13}^{'} \cdot \eta \cdot \tilde{v}_n(z) + k_{14}^{'} \cdot Z_n(z) + k_{15}^{'} \cdot D_n(z)] \cos \eta y + k_{16}^{'} \cdot \varepsilon_0 - k_{13}^{'} \cdot \frac{2}{b} \cdot v^{(0)}(z) \tag{4-44}$$

$$D_y = \sum_n [k_{17}^{'} \cdot \eta \cdot Y_n(z) - k_{18}^{'} \cdot \eta \cdot \emptyset_n(z)] \sin \eta y \tag{4-45}$$

It is apparent that from Equations (4-6) and (4-16), $\tau_{xy} = \tau_{yz} = D_y = 0$ are satisfied automatically along the free edges at *y=0, b.* The remaining boundary condition to be fulfilled at the free edges is:

$$\sigma_y = 0, \quad \text{at } y=0, y=b \tag{4-46}$$

Due to the symmetry, $v^{(0)}(z) = -v^{(b)}(z)$, thus only the boundary condition at y=0 needs to be determined, and the following condition is obtained:

$$\sigma_y = \sum_n [k_{13}^{'} \cdot \eta \cdot \tilde{v}_n(z) + k_{14}^{'} \cdot Z_n(z) + k_{15}^{'} \cdot D_n(z)] + k_{16}^{'} \cdot \varepsilon_0 - k_{13}^{'} \cdot \frac{2}{b} \cdot v^{(0)}(z) = 0 \tag{4-47}$$

The state variables at the top surface for open-circuit and closed-circuit surface conditions are presented:

$$\begin{Bmatrix} \widetilde{v}_n(0) \\ D_n(0) \\ Z_n(0) \end{Bmatrix} = -\begin{bmatrix} M_{11}(z) & M_{15}(z) & M_{16}(z) \\ M_{21}(z) & M_{25}(z) & M_{26}(z) \\ M_{31}(z) & M_{35}(z) & M_{36}(z) \end{bmatrix} \begin{bmatrix} M_{21} & M_{25} & M_{26} \\ M_{31} & M_{35} & M_{36} \\ M_{41} & M_{45} & M_{46} \end{bmatrix}^{-1} \begin{Bmatrix} \bar{M}_2 \\ \bar{M}_3 \\ \bar{M}_4 \end{Bmatrix} + \begin{Bmatrix} \bar{M}_1(z) \\ \bar{M}_2(z) \\ \bar{M}_3(z) \end{Bmatrix} \quad (4\text{-}48)$$

$$\begin{Bmatrix} \widetilde{v}_n(0) \\ D_n(0) \\ Z_n(0) \end{Bmatrix} = -\begin{bmatrix} M_{11}(z) & M_{12}(z) & M_{16}(z) \\ M_{21}(z) & M_{22}(z) & M_{26}(z) \\ M_{31}(z) & M_{32}(z) & M_{36}(z) \end{bmatrix} \begin{bmatrix} M_{31} & M_{32} & M_{36} \\ M_{41} & M_{42} & M_{46} \\ M_{51} & M_{52} & M_{56} \end{bmatrix}^{-1} \begin{Bmatrix} \bar{M}_3 \\ \bar{M}_4 \\ \bar{M}_5 \end{Bmatrix} + \begin{Bmatrix} \bar{M}_1(z) \\ \bar{M}_2(z) \\ \bar{M}_3(z) \end{Bmatrix} \quad (4\text{-}49)$$

For each electric surface condition, the unknown boundary coefficients can be determined by considering Equations (4-25), (4-47), (4-48) and (4-49).

4.5 Conclusions

This chapter dealt with the application of the state space method to the piezoelectric laminated plate under uniaxial extension and presented a new analytical solution that accounts for all the independent elastic and piezoelectric constants and guarantees the continuity conditions of all interlaminar stresses across interfaces between different material layers and traction-free boundary conditions at the free edges. The two electric state variables in terms of eigen-functions are employed in the state equation to account for the electromechanical coupling and free edge effects for the first time.

CHAPTER 5 NUMERICAL ANALYSIS OF SIMPLY-SUPPORTED PIEZOELECTRIC LAMINATES WITH FREE EDGES UNDER TRANSVERSE LOADS

5.1 Introduction

As mentioned in Chapter 3, many three-dimensional solutions are focussed on the piezoelectric laminates with fully simply-supported and electrically grounded boundary conditions where no singular effect is observed. Such solutions can be used for validating new or improved plate theories and finite element formulations (Vel and Batra, 2000). At the free edge of the piezoelectric laminate, both the traction-free mechanical boundary condition and the open-circuit electric boundary condition wherein the normal component of the electric displacement vanishes should be satisfied. Moreover, considering the electromechanical coupling effect and material discontinuity the three-dimensional analysis of the static behaviour of the piezoelectric laminated plate becomes more complicated by comparison with those of laminated plates. By using the exact analytical solution obtained in Chapter 3, the three-dimensional numerical analysis on the general behaviour and the electromechanical as well as edge effects of simply-supported piezoelectric laminated plates with free edges is carried out in this chapter.

5.2 Simply-supported three-layered laminated piezoelectric plate with free edges

In this section, particular attention is paid to the accurate description of the coupling electromechanical field in the thick plate. As shown in Figure 5.1, a three-layered laminated piezoelectric plate is considered: the length a is the same as the width b and the total thickness is h, and $h_1=h_3=0.2h$ for the two identical face layers and $h_2=0.6h$ for the core layer. This plate is simply-supported (SS) and grounded at $x=0$

and $x=a$, and free at $y=0$ and $y=b$. In addition, a uniformly distributed pressure q is applied on the top surface of the plate.

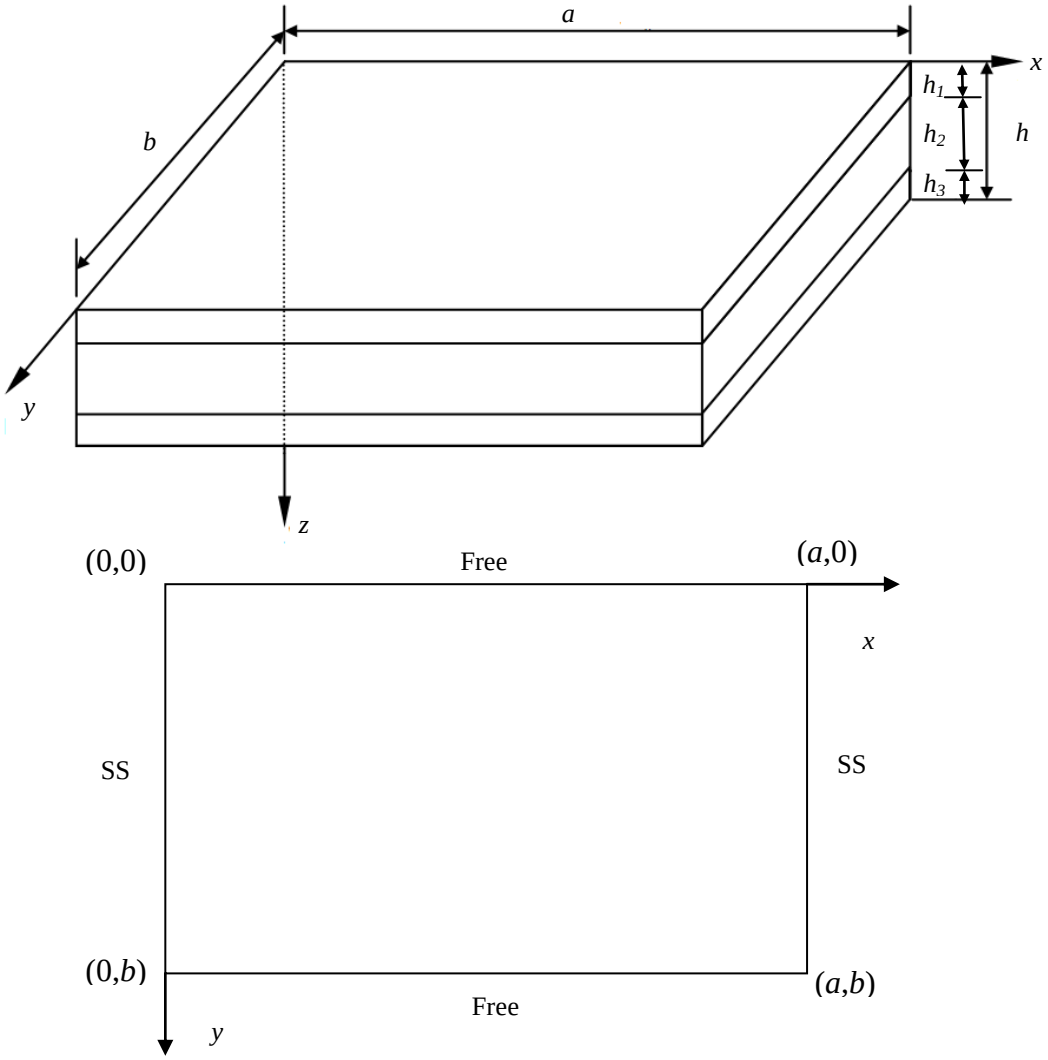

Figure 5.1: Geometry and coordinate system of a three-layered piezoelectric laminate

The material $BaTiO_3$ given by Lee and Jiang (1996) is chosen for the core layer (Table 5.1). According to Sheng et al. (2007) the two face layers are distinguished by the ratio of $\delta = C_{ij}^{(F)}/C_{ij}^{(C)}$, $\lambda = e_{ij}^{(F)}/e_{ij}^{(C)}$ and $\kappa = \epsilon_{ij}^{(F)}/\epsilon_{ij}^{(C)}$, where F and C denote face and core, respectively. In the section, $\delta = 4$, $\lambda = 2$ and $\kappa = 1$ are taken in the analysis of this three-layered piezoelectric laminate.

Table 5.1: Mechanical and electrical properties of $BaTiO_3$ (Lee and Jiang, 1996)

Elastic Stiffness (GPa)	Piezoelectric Coefficients (C/m^2)	Dielectric Properties (CV/m)
$C_{11}=C_{22}=166$ $C_{12}=77$ $C_{33}=162$ $C_{13}=C_{23}=78$ $C_{44}=C_{55}=43$ $C_{66}=43$	$e_{31}=e_{32}=-4.4$ $e_{33}=18.6$ $e_{24}=e_{15}=11.6$	$\epsilon_{11}=1.12\times10^{-8}$ $\epsilon_{22}=1.12\times10^{-8}$ $\epsilon_{33}=1.26\times10^{-8}$

The present results are compared with those from the finite element analysis performed by ABAQUS. And the following non-dimensionalization is adopted in presenting the analytical and numerical results:

$$
\begin{aligned}
&(\bar{u},\bar{v},\bar{w}) = \frac{C_{11}^{C}}{qh}(u,v,w),\\
&\left(\bar{\sigma}_x,\bar{\sigma}_y,\bar{\sigma}_z,\bar{\tau}_{xz},\bar{\tau}_{yz}\right) = \left(\sigma_x,\sigma_y,\sigma_z,\tau_{xz},\tau_{yz}\right)/q,\\
&\left(\bar{\emptyset}\right) = \frac{e_{33}^{C}}{qh}\emptyset,\\
&\left(\bar{E}_x,\bar{E}_y,\bar{E}_z\right) = \frac{e_{33}^{C}}{q}\left(E_x,E_y,E_z\right),\\
&\left(\bar{D}_x,\bar{D}_y,\bar{D}_z\right) = \frac{C_{11}^{C}}{qe_{33}^{C}}\left(D_x,D_y,D_z\right).
\end{aligned}
\tag{5-1}
$$

To assess the influence of thickness to length ratio *h/a* on the coupling electromechanical response in the thick piezoelectric laminated plate, corresponding analytical models are established with respect to different *h/a*, which is taken as 0.2, 0.4 and 0.6. Moreover, both open-circuit and closed-circuit surface conditions are considered to investigate the 3D variations of the mechanical and electrical quantities.

5.2.1 The finite element model

In the immediate vicinity of material layer interfaces and free edges, the 3D electromechanical coupling effect and the free-edge effect in a piezoelectric laminate lead to a more complex phenomenon due to the existence of material and geometric discontinuities at the intersection of the interface and the free edge in composite laminates. In order to provide faithful results to validate the present 3D state space solution, the finite element method was developed and implemented by a commercial FEM package ABAQUS.

5.2.1.1 Element types and boundary conditions

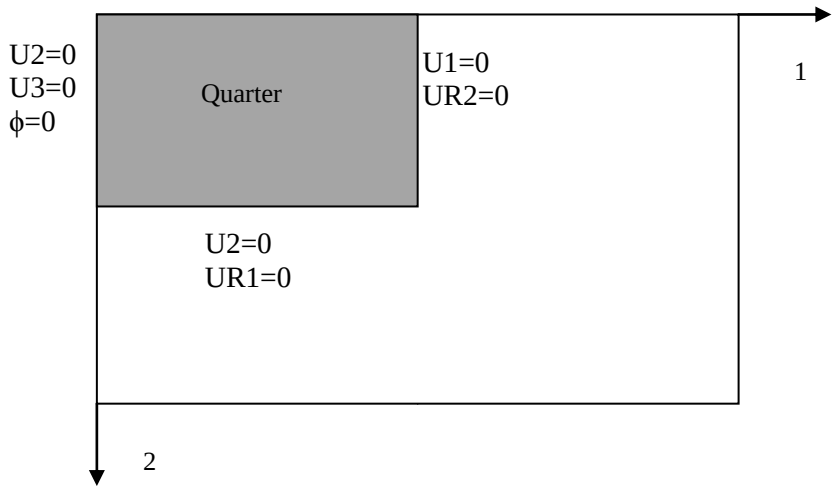

Figure 5.2: Boundary conditions of a three-layered piezoelectric laminate in finite element modelling

In the ABAQUS element library, there are many different types of elements including hexahedron (brick), shell, contact and beam elements. Among numerous successful applications of finite element simulations to study the behaviour of composite structures, Wu and Kamis (2012) carried out an extensive and comparative investigation on the numerical techniques in analyzing the 3D static behaviour of composite laminated plates with clamped edges by choosing various

types of elements. In their study, the thick shell element S8R (the 8-node quadratic shell element with reduced integration), the 3D solid elements C3D8 (3D 8-node linear brick element) and C3D20 (3D 20-node quadratic brick element) were utilized in the simulations for comparison. The comparison between the results from the exact solution and those from FEM indicates that C3D20 provides higher accuracy than C3D8 and captures stress concentrations more effectively particularly in the case of bending-dominated problems where the shear locking phenomenon is commonly associated with C3D8 (ABAQUS, 2010).

Moreover, the ABAQUS/Standard has the capability to perform a fully coupled piezoelectric analysis and provides the piezoelectric elements which have both displacements and electric potentials as degrees of freedom. C3D20E element which is a 20-node quadratic piezoelectric brick element with displacement degrees of freedom and an additional electric potential degree of freedom was offered by ABAQUS/Standard and these degrees of freedom allow fully coupled electromechanical analyses. In addition, regular stress/displacement elements can be used in parts of the model where piezoelectric effects are not taken into account.

In the present research, thick piezoelectric laminated plates with free edges are considered and significant stress gradients may take place due to the free-edge effect. Due to the fact that both electromechanical coupling and free-edge effects arise in the 3D analysis of the piezoelectric laminated plate, and through the comparative modelling with the aforementioned shell and brick elements, it is found that C3D20 is suitable for representing the general behaviour of the composite laminated plate and also gives an accurate prediction of stress gradients at the clamped and free edges. Hence, the 20-node quadratic piezoelectric brick element is chosen. Similar to displacement and rotation degrees of freedom, the electric potential at a node (degree of freedom 9) should also be prescribed with an appropriate boundary condition as shown in Figure 5.2. Moreover, perfect bonding is assumed between the physical layers, and tie connection was chosen to simulate such interaction to merge the nodes at the interfaces.

5.2.1.2 Mesh convergence

In the finite element modelling, a finer mesh theoretically results in a more accurate solution on the basis of algorithm itself. However, as mesh is made finer, the more computational effort is inevitable and computational cumulative error will increase. To balance the accuracy and computing resources satisfactorily, a sensitivity analysis was conducted to determine the appropriate element number of mesh.

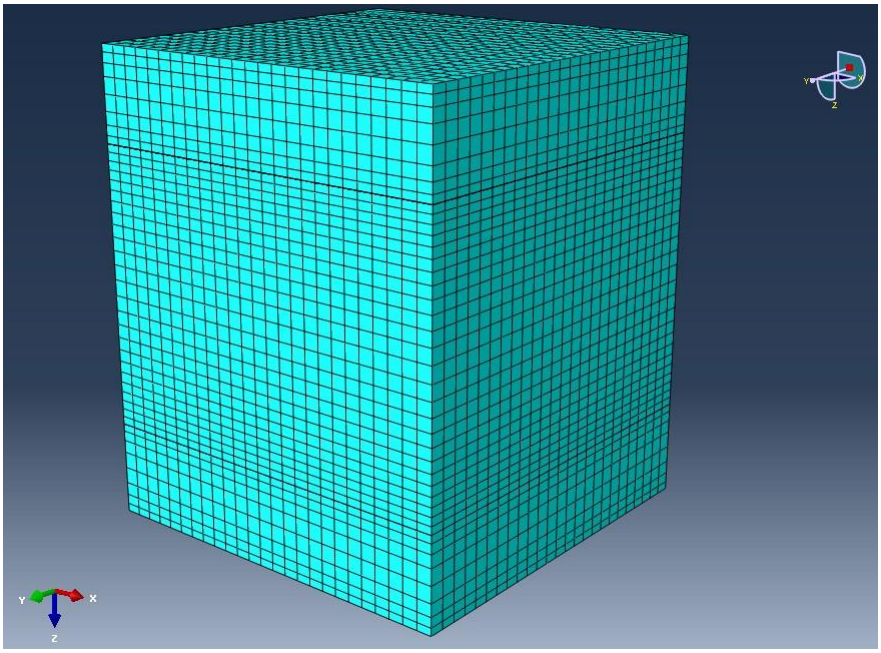

Figure 5.3: Biased mesh of one quarter of the three-layered piezoelectric laminated thick plate with h/a=0.6

In the mesh sensitivity study, the three-layered piezoelectric laminated thick plate with h/a=0.6 is chosen. Due to symmetries in geometries, material properties and loading and boundary conditions, only one quarter of the piezoelectric laminate needs to be analyzed (Figure 5.2). The dimension of this plate is given as: a=10mm, b=10mm and h=0.6. In general, to get more reasonable results, it is necessary to refine the mesh in the regions close to the surfaces or interfaces. In ABAQUS, the biased mesh allows the user to define the size of the coarsest and finest elements or

the number of elements and the ratio of the two sizes. The mesh size can be chosen from the maximum to minimum. By using this biased mesh, it is convenient to refine the mesh in the concerned region and retain the coarse mesh away from this region. Figure 5.3 illustrates the double biased meshes that are applied in the three-layered piezoelectric laminated plate with a biased ratio of two. It is clear that the size of the finest elements at the surfaces of each layer is half of that of the coarsest elements in the middle of each layer in the *z* direction. The numerical result and computational time of the finite element simulation were obtained with an Intel Core i7 (3.40GHz) processer and 16GB RAM.

Table 5.2: Mesh options for one quarter of the three-layered piezoelectric laminated plate with h/a=0.6

Mesh Option	Mesh Size	Total Element No.	CPU Time (sec)
A	0.015×0.015×0.015	43560	600
B	Coarsest: 0.02×0.02×0.02 Finest: 0.02×0.02×0.005	34375	380
C	Coarsest: 0.02×0.02×0.02 Finest: 0.02×0.02×0.01	25625	300
D	0.02×0.02×0.02	18750	180
E	0.03×0.03×0.03	5780	55

This stacked solid model consists of three layers through the thickness and each single-layer has the same mesh in the *x* and *y* directions but the non-uniform discretization in the *z* direction. The results from different mesh options are shown in Table 5.2 and Figure 5.4. In this case, for comparison the biased ratio (BR), i.e. the ratio between the maximum and the minimum size of elements in the *z* direction, is taken as 1 (Mesh option A, Mesh option D and Mesh option E), 2 (Mesh option C), 4 (Mesh option B) respectively as shown in Table 5.2.

For the displacement-based finite element method the convergence of the displacements is faster than that of stresses. Hence, the through-thickness distributions of the interlaminar shear stress τ_{xz} at x=0 and y=0 for each mesh option

are evaluated and compared with the present analytical solution by using the state space analysis (SSA). From Figure 5.4, it is found that the consistency between the finite element result and the result from the analytical solution is good. Since the interlaminar stresses and electric field intensity components near the intersection of the interface and the free edge from FEM are only adopted to be compared with the present analytical results and the computational time also needs to be considered, the optimal mesh option C will be used in the following FEM simulations of this chapter.

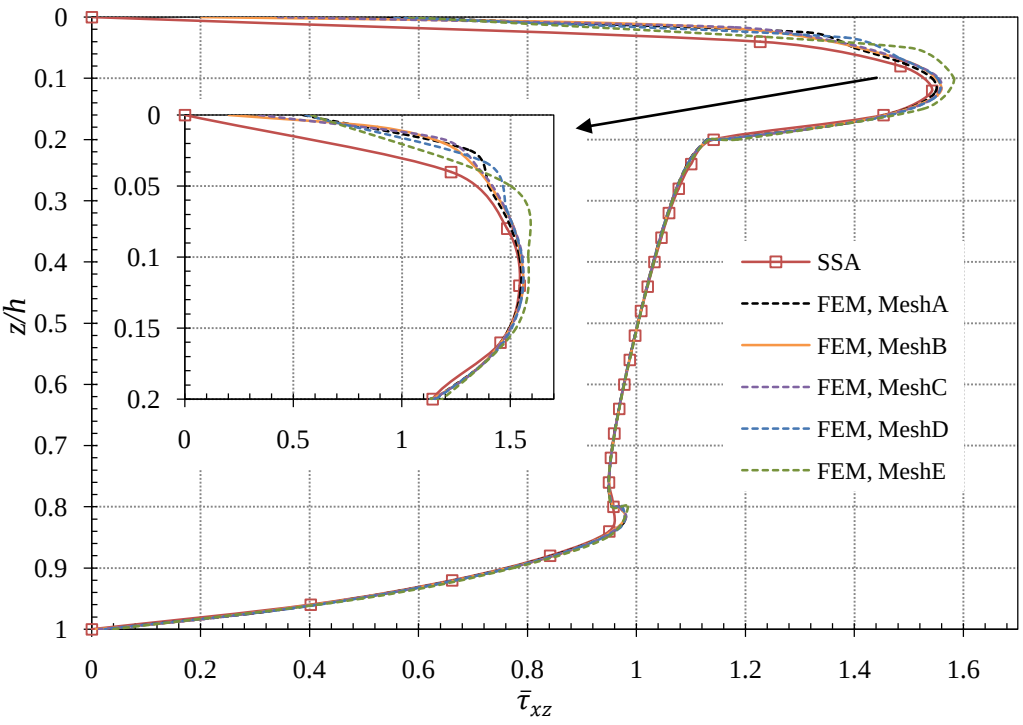

Figure 5.4: Mesh sensitivity for one quarter of the three-layered piezoelectric laminated thick plate with h/a=0.6

5.2.2 Analytical results

This case of the simply-supported three-layered piezoelectric laminated plate with free edges is used to test the reliability and accuracy of the present analytical solution from SSA by comparing its results with the corresponding numerical results

obtained from FEM. Since this research dealt with the electromechanical coupling and free edge effect on the interlaminar stresses, it is essential to capture the possible singular behaviours of these stresses as well as electric fields.

Table 5.3: Influence of layer refinement on mechanical and electrical quantities

Layer Refinement	$\bar{w}$ at x=a/2, y=b/2, z/h=0	$\bar{\sigma}_x$ at x=a/2, y=b/2, z/h=0	$\bar{E}_x$ at x=a/4, y=b/2, z/h=0.2	$\bar{D}_x$ at x=a/4, y=b/2, z/h=0	$\bar{\phi}$ at x=a/2, y=b/2, z/h=0	$\bar{\tau}_{xz}$ at x=0, y=b/2, z/h=0.2	Difference $\bar{\tau}_{xz}$
6+18+6= 30	1.68570	-3.60368	-0.15184	-0.94606	0.13068	0.91939	N/A
5+15+5= 25	1.68563	-3.60374	-0.15182	-0.94614	0.13069	0.91908	0.03%
4+12+4= 20	1.68550	-3.60385	-0.15179	-0.94619	0.13070	0.91862	0.08%

As discussed in Chapter 3, each material layer is divided into fictitious sub-layers *K* in the analysis of the thick plate. Theoretically, the approximate solution obtained can be arbitrarily close to the exact three-dimensional solution if the number of sub-layers and the sinusoidal displacement mode numbers *m* and *n* are all sufficiently large. Owing to the improvement in accuracy, this subdivision approach has been adopted by researchers like Fan and Sheng (1992) and Fan (1998), and details of the convergence of the solution can be found in their work. It is also worth to mention that in their studies a uniform layer refinement was adopted in each physical layer with the same thickness and this uniform layer refinement can provide desired accuracy for the analysis of thick orthotropic laminated plates. Moreover, in this study, the values of *m*=1,3,5,7,9.....29 and *n*=0,2,4,6,8.....200 are considered.

To evaluate this subdivision approach, the configuration of layer refinements and comparison for *h/a*=0.6 are given in Table 5.3. For example, the first layer refinement means that the top and bottom layer are divided into 6 sub-layers separately and the core layer comprises 18 sub-layers and the total number of subdivision for this plate is 30. When the laminated plate is divided into 20 sub-layers, all the given mechanical and electrical results converge to those obtained by

utilizing 30 sub-layers and the difference is found in the fourth decimal place. The convergence of the SSA solution is observed from the table and the present solution can produce very accurate results even using the coarse subdivision where the difference of τ_{xz} is 0.08%. It is also shown that the convergence of τ_{xz} at the boundary is slightly slower than those of other results in the inner region of the plate. For the three-layered laminated plate, all results are obtained by choosing P=25 which can guarantee sufficient accuracy.

The present study is mostly concerned with the accurate determination of the coupling electromechanical field along the thickness coordinate z, in particular at the interfaces between two dissimilar materials in the piezoelectric laminated plate. For this numerical example, there are six physical interfaces: the upper surface of the top layer, the lower surface of the top layer, the upper surface of the core layer, the lower surface of the core layer, the upper surface of the bottom layer and the lower surface of the bottom layer, which are denoted by T+, T-, C+, C-, B+ and B- respectively.

From the relatively thin (h/a=0.2) to thick (h/a=0.6) plates, there is good agreement between the SSA results and those from FEM as shown in Table 5.4. In the state space method, the displacements are chosen as the state variables in the state equations and the continuity conditions can be satisfied. As the primary nodal degrees of freedom in the analysis of FEM, the displacements are directly determined at the nodes and continuous across the element interfaces.

In the 3D analysis of a piezoelectric laminated plate, the transverse displacement is not constant and varies in the z direction. It is clear that even when h/a=0.2 the transverse displacement at the middle of the plate changes through the thickness. The discrepancies become more noticeable when the ratio of thickness to length increases and the transverse displacement at the top surface is 8% greater than that at the bottom surface for h/a=0.4, and 27% for h/a=0.6. Moreover, the variation of the transverse displacement at the free edge is analogous to that at the middle of the plate while the transverse displacement at the free edge is quantitatively larger.

Table 5.4: Displacements under open-circuit conditions against different *h/a*

		h/a=0.2		*h/a*=0.4		*h/a*=0.6	
		SSA	FEM	SSA	FEM	SSA	FEM
$\bar{u}$	T+	8.65587	8.65859	1.08362	1.08327	0.36854	0.36834
x=*a*/4	T-	4.22733	4.22744	0.26201	0.26183	-0.04640	-0.04617
y=0	C+	4.22733	4.22744	0.26201	0.26183	-0.04640	-0.04617
	C-	-4.50203	-4.50242	-0.40390	-0.40403	-0.07135	-0.07147
	B+	-4.50203	-4.50242	-0.40390	-0.40403	-0.07135	-0.07147
	B-	-8.93861	-8.94106	-1.20725	-1.20698	-0.39713	-0.39675
$\bar{v}$	T+	-5.12257	-5.13001	-0.859493	-0.85452	-0.34152	-0.33457
x=*a*/2	T-	-3.17423	-3.18645	-0.56248	-0.56440	-0.22991	-0.22858
y=0	C+	-3.17423	-3.18645	-0.56248	-0.56440	-0.22991	-0.22858
	C-	2.78755	2.79668	0.35894	0.35849	0.08410	0.08389
	B+	2.78755	2.79668	0.35894	0.35849	0.08410	0.08389
	B-	4.79266	4.80099	0.71276	0.71103	0.23645	0.23524
$\bar{w}$	T+	44.49340	44.49492	4.67566	4.67522	1.68563	1.68570
x=*a*/2	T-	44.77880	44.78071	4.69825	4.69819	1.66085	1.66136
y= *b*/2	C+	44.77880	44.78071	4.69825	4.69819	1.66085	1.66136
	C-	44.48480	44.48689	4.38421	4.38381	1.28150	1.28045
	B+	44.48480	44.48689	4.38421	4.38381	1.28150	1.28045
	B-	44.13410	44.13608	4.29551	4.29503	1.24070	1.23958
$\bar{w}$	T+	53.97340	54.04047	5.43569	5.43376	1.87579	1.87173
x=*a*/2	T-	54.18480	54.24935	5.43067	5.42541	1.83160	1.82385
y=0	C+	54.18480	54.24935	5.43067	5.42541	1.83160	1.82385
	C-	53.92500	53.99593	5.15271	5.15455	1.48568	1.48507
	B+	53.92500	53.99593	5.15271	5.15455	1.48568	1.48507
	B-	53.64370	53.71428	5.08706	5.08856	1.45683	1.45580

In the finite element analysis, the stresses are computed at the Gauss point nearest to the locations at which the stresses can be evaluated by the present solution analytically. Although with mesh refinement the Gauss point locations get closer to the node point locations to which the element interface is related, these locations

never become the nodal locations. In addition, the strain continuity across the interfaces is not ensured. Hence along a boundary common to two elements, the stresses take different values on the two sides of the interfaces of two adjacent elements. From Table 5.5, the discontinuities of the in-plane stresses at the interfaces are remarked for both SSA and FEM results.

Table 5.5: In-plane stresses under open-circuit conditions against different *h/a*

		h/a=0.2		*h/a*=0.4		*h/a*=0.6	
		SSA	FEM	SSA	FEM	SSA	FEM
$\bar{\sigma}_x$	T+	-22.9948	-22.97600	-6.51815	-6.49623	-3.60374	-3.58040
x=*a*/2	T-	-12.4607	-12.46830	-2.57983	-2.58079	-0.63538	-0.63317
y=*b*/2	C+	-3.37548	-3.37703	-0.90962	-0.90980	-0.43873	-0.43845
	C-	3.14322	3.14409	0.65186	0.65181	0.16689	0.16639
	B+	12.66530	12.66840	2.71796	2.71801	0.83348	0.83283
	B-	23.16850	23.17290	6.75155	6.75328	3.45021	3.44963
$\bar{\sigma}_x$	T+	-22.42550	-22.41070	-5.72897	-5.70857	-2.93949	-2.91991
x=*a*/2	T-	-11.25620	-11.21880	-1.84836	-1.80448	-0.22068	-0.16787
y=0	C+	-3.09567	-3.04806	-0.78887	-0.73919	-0.41679	-0.36582
	C-	2.87791	2.84833	0.51869	0.50541	0.12583	0.11045
	B+	11.65890	11.59520	2.13992	2.11234	0.58431	0.54984
	B-	22.79820	22.80660	6.15620	6.15706	3.07817	3.07721
$\bar{\sigma}_y$	T+	-4.60462	-4.58379	-0.89679	-0.88775	-0.43243	-0.43914
x=*a*/2	T-	-2.06947	-2.06560	0.07064	0.06622	0.36018	0.34561
y=*b*/2	C+	-0.77768	-0.77634	-0.24701	-0.24805	-0.18984	-0.19375
	C-	0.57643	0.57613	0.02947	0.03028	-0.05398	-0.05349
	B+	2.39812	2.39649	0.22839	0.23192	-0.05003	-0.04665
	B-	4.92002	4.91640	1.28075	1.28868	0.68107	0.68842

Table 5.6: Interlaminar stresses under open-circuit conditions against different *h/a*

		h/a=0.2		*h/a*=0.4		*h/a*=0.6	
		SSA	FEM	SSA	FEM	SSA	FEM
$\bar{\sigma}_z$	T+	-1.02120	-1.00036	-1.02120	-1.00015	-1.02120	-1.00006
*x=a/*2	T-	-0.87703	-0.87765	-0.88917	-0.89008	-0.92713	-0.92912
y=b/2	C+	-0.87703	-0.87640	-0.88917	-0.88930	-0.92713	-0.92828
	C-	-0.12393	-0.12313	-0.13664	-0.13661	-0.17110	-0.17201
	B+	-0.12393	-0.12180	-0.13664	-0.13578	-0.17110	-0.17150
	B-	0.00000	0.00260	0.00000	0.00190	0.00000	0.00225
$\bar{\tau}_{xz}$	T+	0.00000	0.01513	0.00000	0.05341	0.00000	0.08788
x=0	T-	2.60019	2.64192	1.34333	1.35805	0.91908	0.93055
y=b/2	C+	2.60019	2.64192	1.34333	1.34666	0.91908	0.92190
	C-	2.43860	2.44072	1.17589	1.17686	0.74651	0.74694
	B+	2.43860	2.44880	1.17589	1.17944	0.74651	0.74864
	B-	0.00000	0.01033	0.00000	0.00324	0.00000	0.00211
$\bar{\tau}_{yz}$	T+	0.00000	0.00037	0.00000	0.00006	0.00000	0.00001
x=a/2	T-	0.18963	0.19109	0.04253	0.04008	0.00388	-0.00060
y=b/4	C+	0.18963	0.19021	0.04253	0.03998	0.00388	-0.00062
	C-	0.19135	0.19216	0.07992	0.08191	0.05047	0.05310
	B+	0.19135	0.19302	0.07992	0.08224	0.05047	0.05339
	B-	0.00000	0.00114	0.00000	0.00043	0.00000	0.00039

Due to the action-reaction, the continuity conditions must hold between the interlaminar stress fields of adjacent layers at the interface. In Table 5.6, the interlaminar stresses obtained by the SSA solution are continuous but those obtained by FEM show discontinuous at layer interfaces as expected. With much effort on mesh refinement, the discrepancy between the discontinuous interlaminar stresses at the interface can be reduced and the error introduced can be negligible as shown in this table. Nevertheless, this deficiency in interlaminar stresses may lead to poor results in the vicinity of the intersection of the interface and the free edge. It is also

observed that FEM cannot guarantee the traction-free conditions at the surfaces and with improved mesh refinement this difference can also be reduced but never be eliminated. Moreover, shear deformation tends to be of greater concern when the ratio between the thickness and length is increasing and shearing may become significant in locations of bending-stress concentrations. The SSA solution can capture the stress distribution more accurately than those solutions based on thin-plate theories.

The comparisons between the SSA and FEM results on the electric quantities are given in Appendix F. It is apparent that the electric potential obtained by the SSA solution is consistent with that from FEM in the middle of the plate and at the free edge. In the FEM modelling the 20-node quadratic piezoelectric solid element with displacement DOFs and an additional electric potential DOF 9 at each node was used and these DOFs allow fully coupled electromechanical analyses. Like displacements, the nodal electric potential is determined directly, thus continuous at the interface. There is no significant difference in the electric field intensity components between the SSA and FEM results. It is interesting to note that a small difference in E_y at the interface is observed for $h/a=0.6$ when the free edge is approached, which suggests that the mismatch of material near the free edge may result in the singular behaviour of stresses or electric fields. Also the discrepancy between the SSA and FEM results will become more notable in the immediate vicinity of the interface and the free edge. Similar to the electric field intensity components discussed above, there is a small difference in D_y at the interface for the thick plate. Moreover the horizontal electric displacements are discontinuous across the interfaces, whereas the vertical electric displacement is chosen as the state variable in the state space equation and retains continuous.

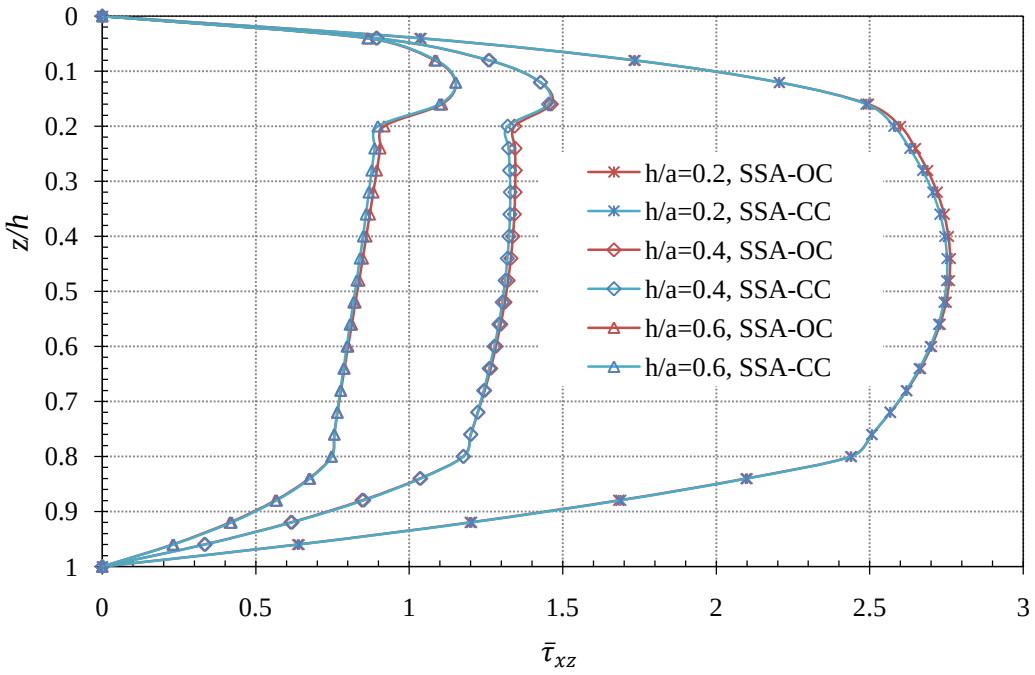

Figure 5.5: Distributions of interlaminar shear stress $\bar{\tau}_{xz}$ under open-circuit (OC) and closed-circuit (CC) conditions in three-layered piezoelectric laminates

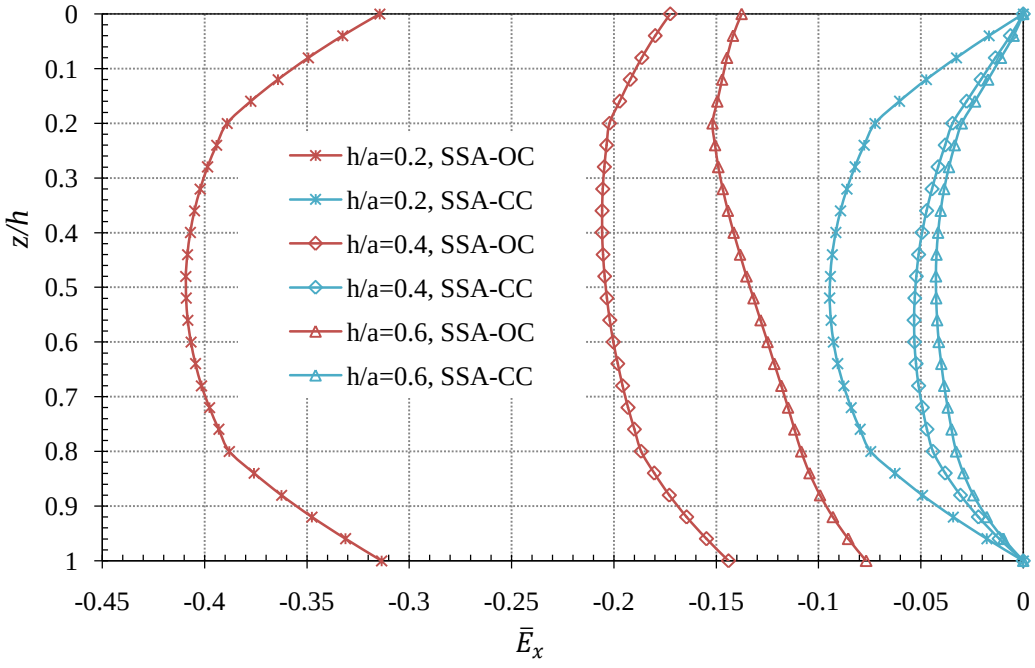

Figure 5.6: Distributions of electric field intensity component $\bar{E}_x$ under open-circuit (OC) and closed-circuit (CC) conditions in three-layered piezoelectric laminates

The SSA result in the closed-circuit surface condition is also obtained and compared with that from FEM and they are in good agreement. From Figure 5.5, it is found that different electric surface conditions do not have strong influences on the interlaminar shear stress τ_{xz}. As expected, the electrical quantities are strongly affected by the electric surface conditions in Figure 5.6.

5.3 A non-uniform layer refinement technique

In the previous section, the uniform layer refinement technique was adopted and each physical layer was divided uniformly. Similarly in the other state space approaches by Zhang et al. (2006) and Sheng et al. (2007) each physical layer of the laminate was also divided uniformly into appropriate sub-layers with identical thickness. As regards the finite element models, significant mesh refinements are required near the interfaces and free edges in ABAQUS simulation and they provide very close estimation and significant gradients of the interlaminar stresses.

It is conceivably hypothesised that the accuracy of the model is improved with an enhanced layer refinement. By compromising the accuracy and efficiency, the enhanced layer refinement should be applied to the region close to the intersection of the interface and the free edge, where the free-edge effect is most concerned. As a consequence, a non-uniform layer refinement technique is proposed to give a better prediction of the electromechanical and free-edge effect in the piezoelectric laminate. To avoid more computational efforts, the number of sub-layers in each physical layer is the same as that in the uniform layer refinement technique illustrated in Figure 5.7(a), whereas the thicknesses of the mathematical sub-layers are reduced in the vicinity of the interfaces between dissimilar physical layers in the non-uniform layer refinement technique. In this new technique, the reduction of thicknesses of the mathematical sub-layers means that more mathematical sub-layers are assumed in a small region very near the interface where a high inhomogeneity in mechanical and electric properties exists while less mathematical sub-layers are proposed far from the interfaces. It is shown in Figure 5.7(b) that the non-uniform layer refinement

technique is used near the interface of two adjacent physical layers which have different material orientations and there is no need to use this technique for the interface of two adjacent layers with the same material orientation.

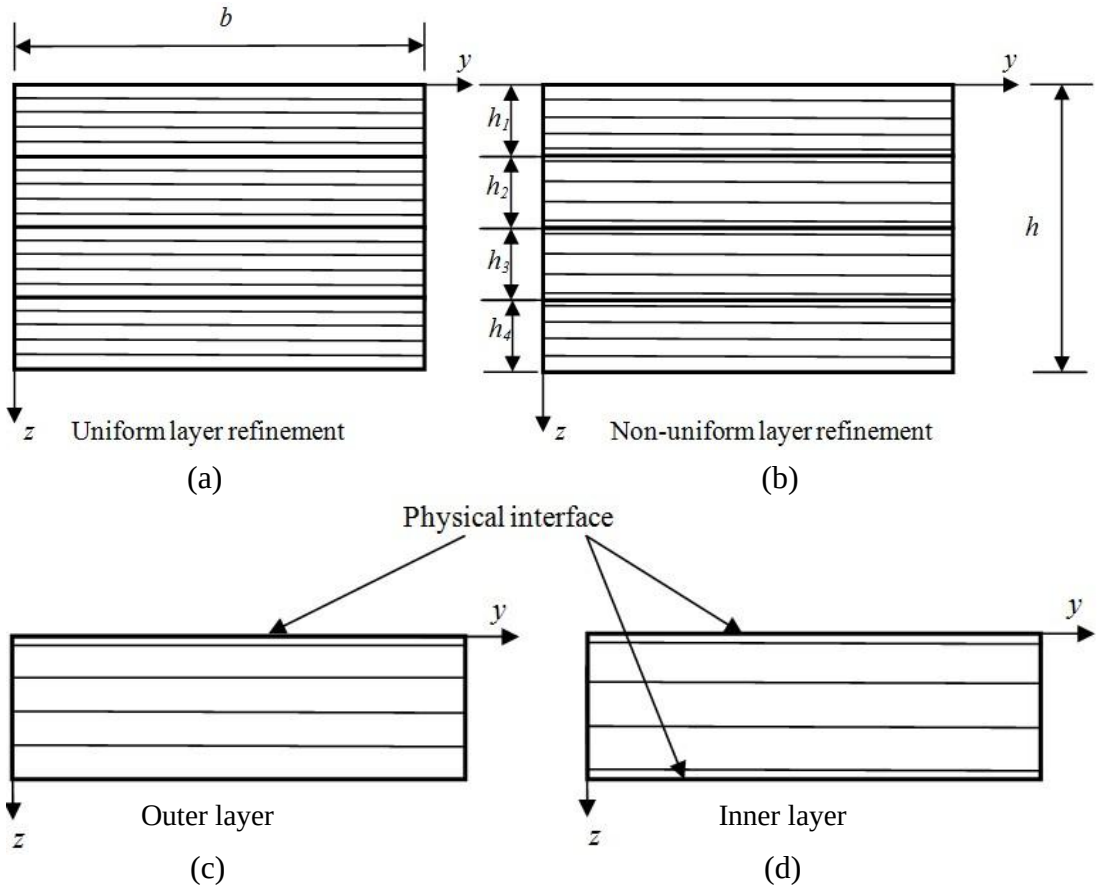

Figure 5.7: Uniform and non-uniform layer refinement techniques through the thickness of a laminate

In order to validate the non-uniform layer refinement technique, comparisons are made between the present new technique and the uniform layer refinement technique and ABAQUS. To evaluate the influence of layer refinements on the results, especially those near the free edge, the same numerical example: the thick three-layered piezoelectric laminated plate with h/a=0.6 is considered with uniform and non-uniform layer refinements. The non-uniform layer refinement technique preserves the same number of mathematical sub-layers in each physical layer as that in the uniform layer refinement technique. However, the thickness of the adjacent

sub-layer near the interface in the non-uniform layer refinement is reduced to one-tenth of that in the uniform one and the thickness of remaining sub-layers is identical in the outer physical layer (Figure 5.7(c)) and the inner physical layer (Figure 5.7(d)). The geometrical parameters and material properties in the previous section are also taken into account.

Table 5.7: Comparison between uniform and non-uniform layer refinement techniques

Layer Refinement	$\bar{w}$ at x=a/2, y=b/2, z/h=0	$\bar{\sigma}_x$ at x=a/2, y=b/2, z/h=0	$\bar{\tau}_{xz}$ at x=0, y=b/2, z/h=0.2	$\bar{\tau}_{yz}$ at x=a/2, y=b/4, z/h=0.2	$\bar{E}_y$ at x=a/2, y=b/4, z/h=0.2	$\bar{E}_x$ at x=a/4, y=b/2, z/h=0.2	$\bar{\emptyset}$ at x=a/2, y=b/2, z/h=0
Uniform	1.68563	-3.60374	0.91908	0.00388	0.00179	-0.15182	0.13069
Non-uniform	1.68570	-3.60329	0.91893	0.00317	0.00194	-0.15080	0.13066

From Table 5.7, the results from the non-uniform layer refinement are consistent with those of the uniform layer refinement. It is clear that the electromechanical quantities from the inner region of the plate are less affected by the layer refinement than those near the free edge or simply-supported edge. It seems that the interlaminar shear stress τ_{yz} and the electric field intensity component E_y are sensitive to the layer subdivision close to the intersection of the interface and the free edge.

As illustrated in Figures 5.8 and 5.9, the distributions along the interface and through the thickness indicate the noticeable stress and electric field gradients near the free edge with respect to different thickness to length ratios. In these two figures, the left column gives the distributions across the width *b* and at *z/h*=0.2 along the interface between the top and core layers. Specifically, the distribution of τ_{xz} at the simply-supported edge (*x/a*=0) and the distributions of τ_{yz} and E_y at *x/a*=0.5 are assessed. The right column shows the through-thickness distributions of τ_{xz} at *y/b*=0 and τ_{yz} and E_y at *y/b*=0.009, respectively.

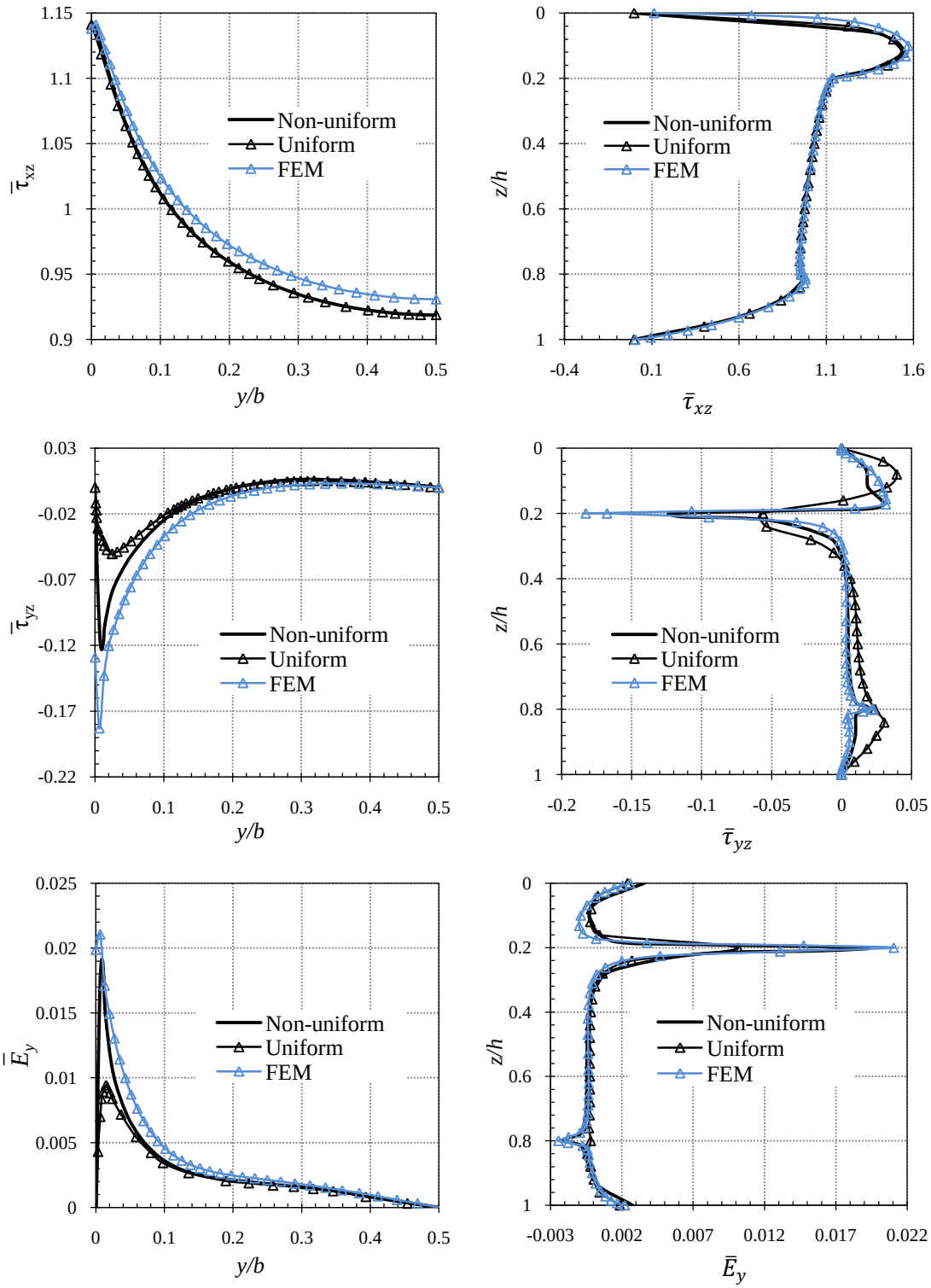

Figure 5.8: Distributions of interlaminar shear stresses and electric field intensity component by using the non-uniform and uniform layer refinement techniques when *h/a*=0.6

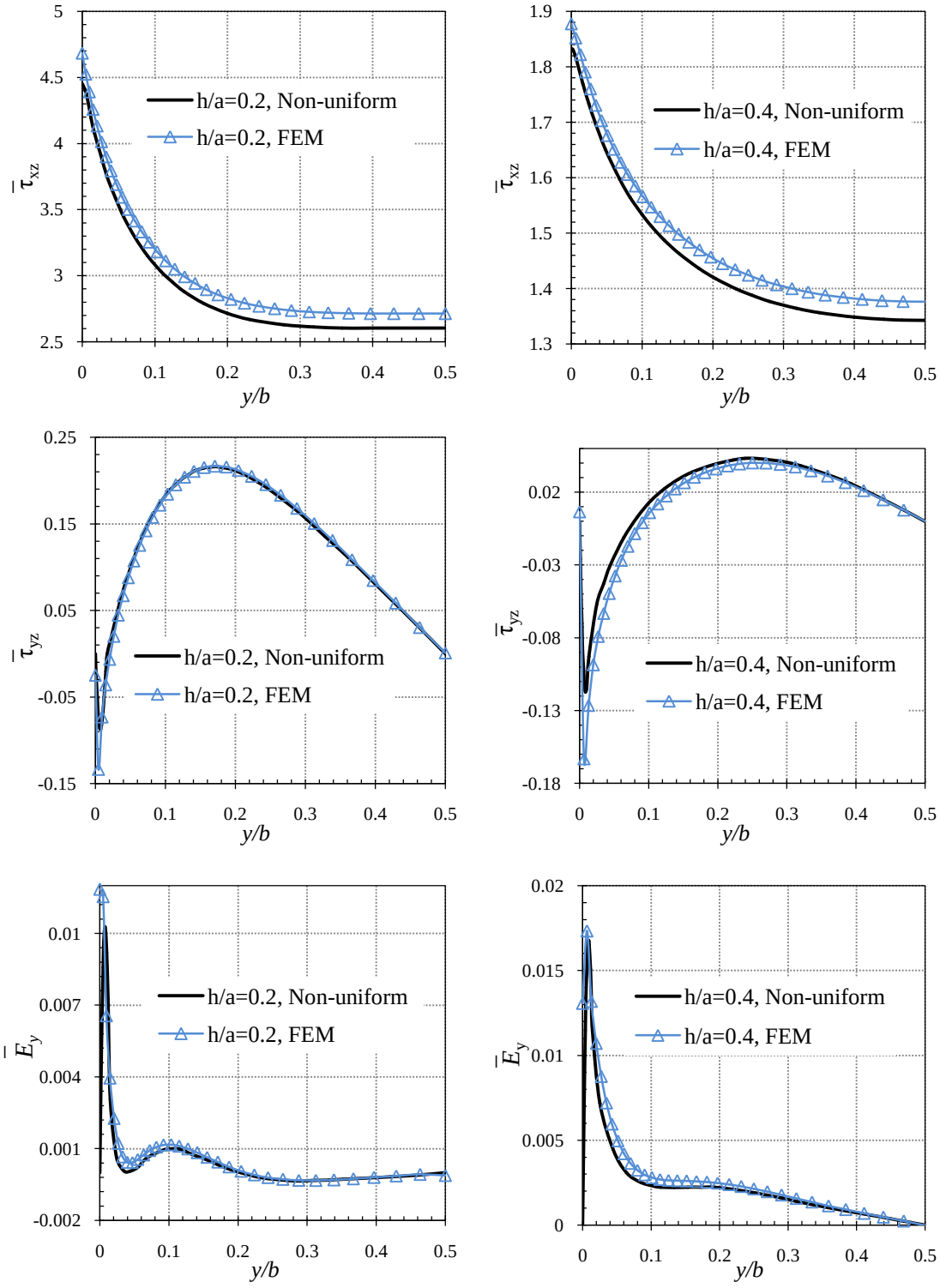

Figure 5.9: Distributions of interlaminar shear stresses and electric field intensity component along the interface when *h/a*=0.2 (left) and *h/a*=0.4 (right)

It is clear that when the free edge is approached, τ_{yz} and E_y change dramatically. It is shown that they rise towards the free edge, but decrease rather suddenly to zero at $y=0$ in the present analysis, whereas the traction-free condition ($\tau_{yz} = 0\ at\ y = 0$) cannot be fulfilled in FEM because of significant stress gradients. The results from the non-uniform layer refinement can predict this steep gradient behaviour very near the free edge compared to those from the uniform layer refinement which has been verified by FEM. The interlaminar shear stress τ_{xz} is dominant at the simply-supported edges for all three thickness to span ratios and the magnitude of τ_{xz} is much larger than that of shear stress τ_{yz} and similarly the magnitude of E_x (Table 5.7) is also much larger than that of E_y.

Although there are significant gradients of τ_{yz} and E_y in the vicinity of the free edge compared to the absence of these two quantities in the middle of the plate, they are still quantitatively smaller than τ_{xz} and E_x. However, the analysis of the edge effect and electromechanical coupling effect on the behaviour of piezoelectric laminates is still of necessity. Due to different material properties, stacking sequences and kind of boundary conditions as well as loading conditions, the influence of these two quantities may become stronger.

Furthermore, the finite element solution obtained by ABAQUS can demonstrate significant stress and electric field gradients with an enhanced mesh refinement in the vicinity of the free edge. To obtain such special description of the free-edge and electromechanical coupling effects, the non-uniform layer refinement technique was proposed. Although there are differences between the uniform and non-uniform layer refinement results near the free edge where a possible singularity occurs, they both predict the interlaminar stresses and electric field intensity components gradients at the intersection of the interface and the free edge. However, the non-uniform layer refinement results show much stronger gradients than the uniform layer refinement results. With more mathematical sub-layers towards the interface of two different adjacent physical layers, the small region near the interface is relatively refined, leading to a more accurate prediction of the stresses and electric fields distributions. As a consequence, this new technique can be used to capture the

possible singular behaviour of stresses and electric fields in the piezoelectric laminated plate.

5.4 Comparison with Levy solutions

As a benchmark for classical plate theory (CLPT) and various 2D plate and shell theories, the present 3D state space piezoelasticity solution can assess the accuracy of FEM and also be used to evaluate errors caused by various assumptions in different plate theories. As a case study, the results from one of existing classical plate solutions-Levy solution, are compared with those from the present 3D state space solution and FEM in this section.

Generally, a Levy solution can be developed for plates with two opposite edges simply supported and the remaining two edges having any possible combination of boundary conditions: free, simply support, or fixed support. Analytical solutions for rectangular laminated plates with Levy-type boundary conditions have been obtained by Reddy (2004) based on the CLPT. For simplicity, the same three-layered laminated plate model in the previous section is analyzed but only the mechanical property is considered in this case. The influence of the thickness to length ratio *h/a* on the static response of the laminated plate is evaluated and the ratio is chosen as 0.05, 0.1 (due to the thin plate requirement for the CLPT-Levy solution) and 0.2. Moreover, the ratio of $\delta = C_{ij}^{(F)}/C_{ij}^{(C)}$ is taken as 4.

In the CLPT, the plane-stress state is assumed and the transverse shear and transverse normal strains are neglected. As shown in Table 5.8 the accuracy of the in-plane stresses and transverse displacement predicted by the CLPT deteriorates as the laminate becomes thicker. Even in the thin plates, the discrepancies between the CLPT results and the present results are noticeable. It is observed that the FEM results are consistent with the present state space analytical results. The CLPT underestimates the maximum central deflection of the laminated plate. For the practical design of simply-supported thick laminated plates with free edges, 3D analytical solutions are required.

Table 5.8: In-plane stresses and transverse displacement against different *h/a*

		h/a=0.05			*h/a*=0.1			*h/a*=0.2		
		CLPT	SSA	FEM	CLPT	SSA	FEM	CLPT	SSA	FEM
$\bar{\sigma}_x$	T+	-349.57	-351.04	-351.00	-87.40	-88.51	-88.49	-21.85	-22.97	-22.96
x=*a*/2	T-	-209.74	-209.15	-209.19	-52.44	-51.66	-51.69	-13.11	-12.36	-12.37
y=*b*/2	C+	-52.44	-52.61	-52.61	-13.11	-13.23	-13.24	-3.28	-3.40	-3.41
	C-	52.44	52.31	52.31	13.11	12.94	12.94	3.28	3.11	3.11
	B+	209.74	209.42	209.42	52.44	51.92	51.93	13.11	12.61	12.61
	B-	349.57	351.24	351.24	87.40	88.72	88.73	21.85	23.20	23.19
$\bar{\sigma}_y$	T+	-112.24	-75.17	-75.08	-28.06	-17.89	-17.84	-7.01	-3.94	-3.90
x=*a*/2	T-	-67.84	-44.47	-44.42	-16.84	-10.09	-10.07	-4.21	-1.72	-1.70
y=*b*/2	C+	-16.84	-11.44	-11.42	-4.21	-2.84	-2.83	-1.05	-0.75	-0.74
	C-	16.84	11.17	11.17	4.21	2.57	2.58	1.05	0.48	0.48
	B+	67.84	44.85	44.84	16.84	10.47	10.48	4.21	2.11	2.12
	B-	112.24	75.53	75.50	28.06	18.25	18.27	7.01	4.31	4.32
$\bar{w}$	T+	7884.16	9879.81	9879.77	492.76	650.25	650.24	30.80	48.97	48.97
x=*a*/2	T-	7884.16	9887.83	9887.80	492.76	652.17	652.17	30.80	49.38	49.38
y=*b*/2	C+	7884.16	9887.83	9887.80	492.76	652.17	652.17	30.80	49.38	49.38
	C-	7884.16	9887.46	9887.40	492.76	651.81	650.93	30.80	49.02	49.02
	B+	7884.16	9887.46	9887.40	492.76	651.81	650.93	30.80	49.02	49.02
	B-	7884.16	9879.35	9879.30	492.76	649.79	649.79	30.80	48.51	48.51

As a 3D analytical solution, the present state space solution provides accurate descriptions of the static response for thin to thick laminates with free-edge boundary conditions. In addition, when considering the electromechanical coupling effect the more complicated state of stress and electric field would be expected.

5.5 Edge effects of simply-supported cross-ply piezoelectric laminated plate with free edges

The three-layered piezoelectric laminated plate with two opposite edges simply-supported and the other two edges free has been investigated in the previous section. The influence of edge effect on the electromechanical quantities has been illustrated with respect to different thickness to length ratios. The result indicates the existence of significant interlaminar shear stresses and electric field gradients near the free edges.

In the analysis of the three-layered piezoelectric laminated plate, the interlaminar normal stress is compressive at the interface for all models with different thickness to length ratios. However, with different material properties and stacking sequences, tensile interlaminar normal stress could emerge at the interface. It is still interesting to evaluate the edge effect and the electromechanical coupling effect with different stacking sequences. There are four stacking sequences $[0^\circ/90^\circ]_s$, $[90^\circ/0^\circ]_s$, $[0^\circ/90^\circ/0^\circ/90^\circ]$ and $[90^\circ/90^\circ/90^\circ/0^\circ]$. These general cross-ply laminates are subjected to a uniformly transverse distributed load on the top surface, and the open-circuit surface condition is applied to both top and bottom surfaces.

As illustrated in Figure 5.10 the rectangular piezoelectric laminate has length *a*, width *b* and thickness *h*, with *a/b*=2.5 and *h/b*=0.25. Each lamina is assumed to be of the same thickness and the employed virtual material by Artel and Becker (2005) is a piezoelectric composite material with the mechanical properties of T300/Epoxy and the piezoelectric and electrical properties of PZT-5A. The material properties of this piezoelectric lamina are given in Table 5.9. Material with the presented properties may be realized by the use of piezoelectric fibres in a resin matrix.

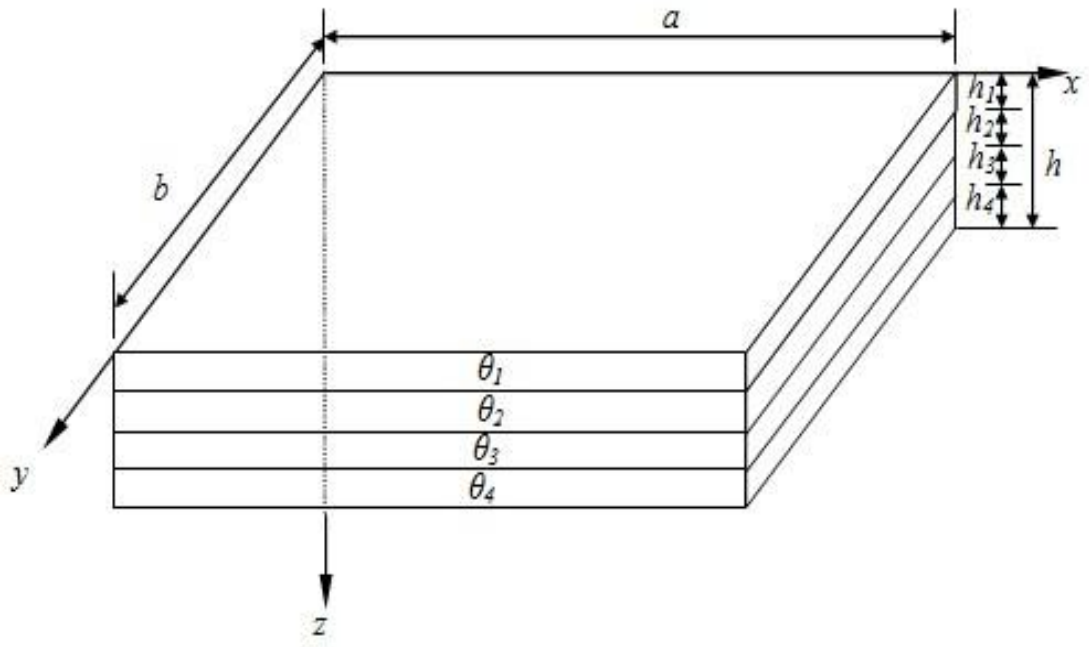

0^o	90^o	0^o	90^o
90^o	0^o	90^o	90^o
90^o	0^o	0^o	90^o
0^o	90^o	90^o	0^o
L1	L2	L3	L4

Figure 5.10: Geometry and coordinate system of a general four-layered cross-ply piezoelectric laminate and four stacking sequences

Table 5.9: Mechanical and electrical properties of a piezoelectric lamina

Elastic Stiffness (GPa)	Piezoelectric Coefficients (C/m^2)	Dielectric Properties (CV/m)
$C_{11}=137$	$e_{31}=e_{32}=-5.4$	$\epsilon_{11}=\epsilon_{22}=1730\epsilon_0$
$C_{12}=C_{13}=3.75$	$e_{33}=15.8$	$\epsilon_{33}=1700\epsilon_0$
$C_{22}=C_{33}=10.9$	$e_{24}=e_{15}=12.3$	$\epsilon_0=8.859\times10^{-12}$
$C_{23}=3$		
$C_{44}=3.97$		
$C_{55}=C_{66}=5$		

All the numerical results shown in this section are presented by means of the following non-dimensional parameters:

$$
\begin{aligned}
&(\bar{u}, \bar{v}, \bar{w}) = \frac{C_{11}}{qh}(u, v, w), \\
&\left(\bar{\sigma}_x, \bar{\sigma}_y, \bar{\sigma}_z, \bar{\tau}_{xz}, \bar{\tau}_{yz}\right) = \left(\sigma_x, \sigma_y, \sigma_z, \tau_{xz}, \tau_{yz}\right)/q, \\
&\left(\bar{\emptyset}\right) = \frac{e_{33}}{qh}\emptyset, \\
&\left(\bar{E}_x, \bar{E}_y, \bar{E}_z\right) = \frac{e_{33}}{q}\left(E_x, E_y, E_z\right), \\
&\left(\bar{D}_x, \bar{D}_y, \bar{D}_z\right) = \frac{C_{11}}{q e_{33}}\left(D_x, D_y, D_z\right).
\end{aligned}
\tag{5-2}
$$

As discussed in the previous section, interlaminar stresses must conform to the continuity at the interface between two dissimilar materials and there are some difficulties in employing the continuity of interlaminar stresses in C^0 interpolated elements in FEM. And the nodal values of the stresses are generally retrievable at Gauss points using constitutive relations or variationally consistent procedures in conventional Lagrangian formulation. However, the interlaminar stress failure is likely to initiate at the interface between layers with material discontinuities in laminates, the accurate determination of interlaminar stresses is desired at the interface rather than Gauss points. Accurate extrapolation technique from Gauss points is usually required in conventional finite element procedures to achieve an appropriate level of accuracy of the interlaminar stress fields at the element nodes. Inaccuracy in the recovered interlaminar stress distributions may be obtained at the interfaces between the layers in the case of high out-of-plane stress gradients (Fagiano, 2010).

Similarly, Whitcomb et al. (1982) concluded that the finite element solutions were accurate everywhere except very near a stress discontinuity or a singularity. And the region of inaccuracy was limited to about two elements and refined meshes were required in such small region to generate reliable distributions of interlaminar

stresses through the thickness in particular achieve the interlaminar continuity of the transverse stresses. Also, it was evident that by decreasing mesh size the finite element solution converged everywhere except very near the intersection of the interface and the free edge. Their study indicated that accurate and valid results might be obtained by finite element methods in the neighbourhood of singularities. Consequently, for the sake of comparison with FEM results, the point y=0.0025b which is in the immediate vicinity of the free edge is chosen for the distributions of σ_z. In addition, for the purpose of abbreviation, L1, L2, L3 and L4 are chosen to denote the four stacking sequences: $[0^\circ/90^\circ]_s$, $[90^\circ/0^\circ]_s$, $[0^\circ/90^\circ/0^\circ/90^\circ]$ and $[90^\circ/90^\circ/90^\circ/0^\circ]$, respectively as shown in Figure 5.10.

Figure 5.11 illustrates the variations of the interlaminar normal stress σ_z along the interface (z=3h/4) and through the thickness at x=a/2 for the $[0^\circ/90^\circ]_s$, $[90^\circ/0^\circ]_s$, $[0^\circ/90^\circ/0^\circ/90^\circ]$, $[90^\circ/90^\circ/90^\circ/0^\circ]$ laminates. There is good agreement between the SSA results and FEM results and they both predict the steep stress gradients very near the interfaces and free edges. It is also noted that the SSA results are consistent with those of FEM in the inner region and there is a slight difference near the interface where the SSA results are smaller than those of FEM.

Tensile interlaminar normal stress σ_z is found in all laminates and it is apparent that for the $[0^\circ/90^\circ]_s$ and $[90^\circ/90^\circ/90^\circ/0^\circ]$ laminate, σ_z at the interface (z=3h/4) is compressive in the interior region of the laminate and reverses its sign and rises to a high positive value very near the free edge (y=0.0025b). Due to the interlaminar normal stress concentration, delamination damage can be initiated near the intersection of the interface and the free edge and leads to a significant loss of strength and stiffness. Among these four cross-ply piezoelectric laminates, the $[90^\circ/90^\circ/90^\circ/0^\circ]$ one is more vulnerable to delamination damage.

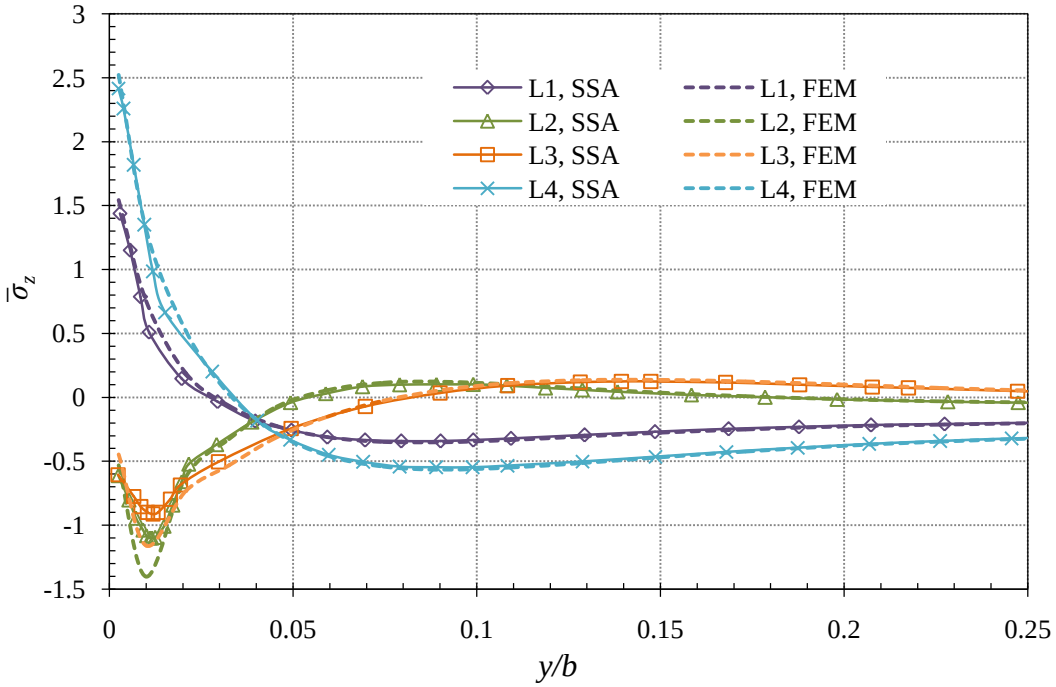

(a) Along the interface

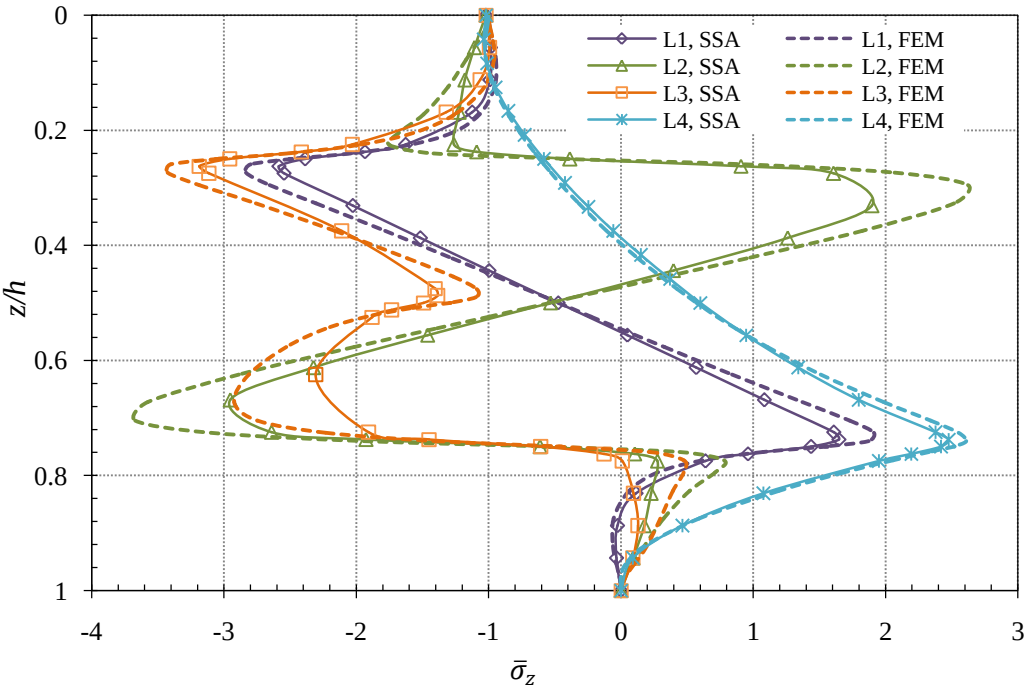

(b) Through the thickness

Figure 5.11: Variations of interlaminar normal stress $\bar{\sigma}_z$ in the general cross-ply laminates under uniformly distributed loading and open-circuit conditions

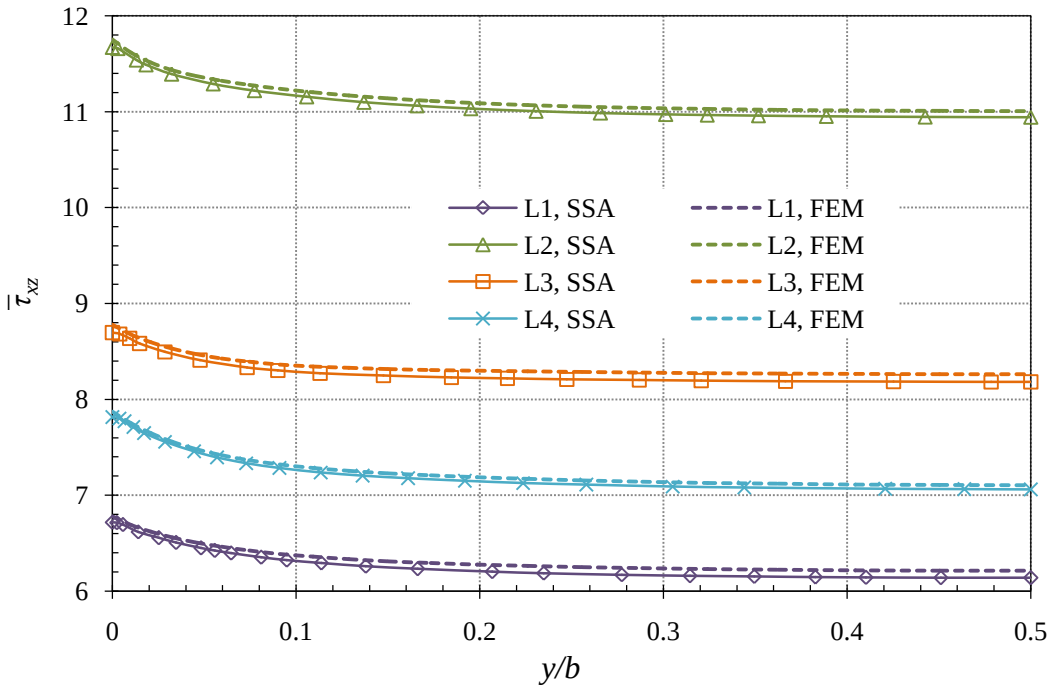

(a) Along the interface

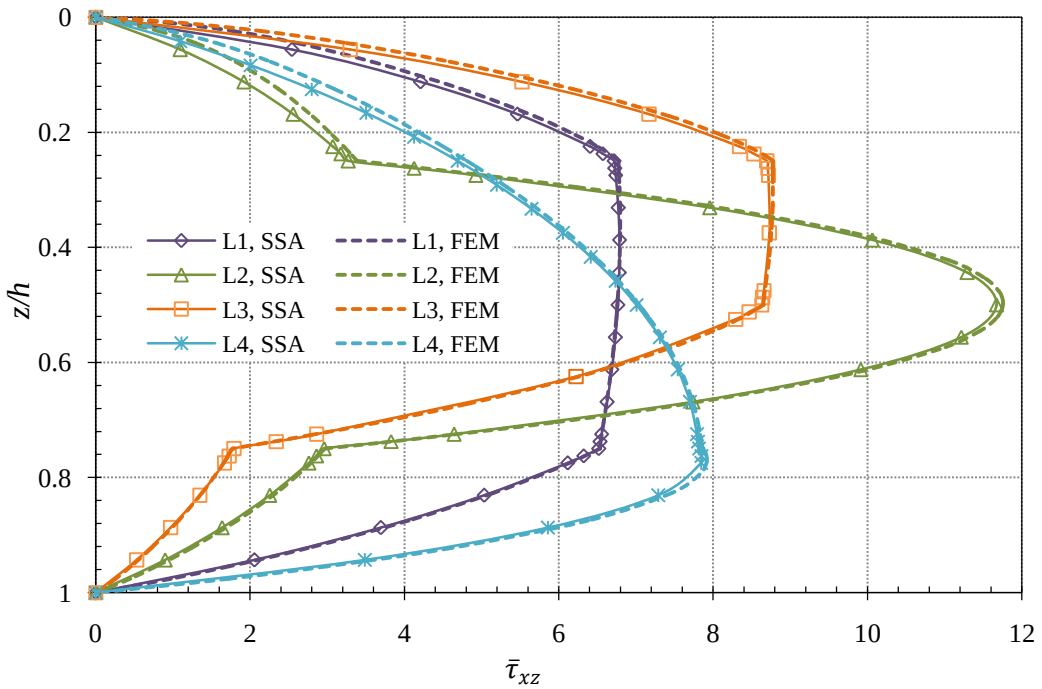

(b) Through the thickness

Figure 5.12: Variations of interlaminar shear stress $\bar{\tau}_{xz}$ in the general cross-ply laminates under uniformly distributed loading and open-circuit conditions

As expected, the interlaminar shear stress τ_{xz} attains a higher value in the boundary region (simply-supported edge) in Figure 5.12. Under the same loading and boundary conditions, the maximum τ_{xz} is observed at the middle plane (z=h/2) of the $[90^\circ/0^\circ]_s$ piezoelectric laminate. Moreover, from Figure 5.12 (a) it is shown that τ_{xz} is still increasing steadily when approaching the free edge and reaches the maximum value at the corner of the laminate.

The distributions of the interlaminar shear stress τ_{yz} along the interface (z=3h/4) and through the thickness at x=a/2 are depicted in Figure 5.13. Similarly, to investigate the immediate vicinity of the free edge, the point y=0.0125b is considered. It is shown that τ_{yz} in the $[90^\circ/0^\circ]_s$ and $[0^\circ/90^\circ/0^\circ/90^\circ]$ laminates grows more abruptly and reaches a higher value near the intersection of the interface and the free edge than that in the $[0^\circ/90^\circ]_s$ and $[90^\circ/90^\circ/90^\circ/0^\circ]$ laminates. In the analysis of the three-layered piezoelectric laminates, τ_{xz} is approximately ten times higher than τ_{yz}, while in this case τ_{xz} is only five times greater. It seems due to the possible singular behaviour the influence of τ_{yz} near the interface and free edge is not negligible and this shear stress tends to contribute to the delamination of the piezoelectric laminate.

Analogous to the variation of the interlaminar shear stress τ_{yz}, the electric field intensity component E_y also exhibits sharp variations at the interface (z=3h/4) and very near the free edge (y=0.0125b) in Figure 5.14. It is obvious that E_y in the $[90^\circ/0^\circ]_s$ and $[0^\circ/90^\circ/0^\circ/90^\circ]$ laminates shows a notably steeper gradient than that in the other two laminates near the free edge and decays in the inner region of the laminate. It is also worth to mention that there is good agreement between the SSA result and FEM result except for the region very near the free edge.

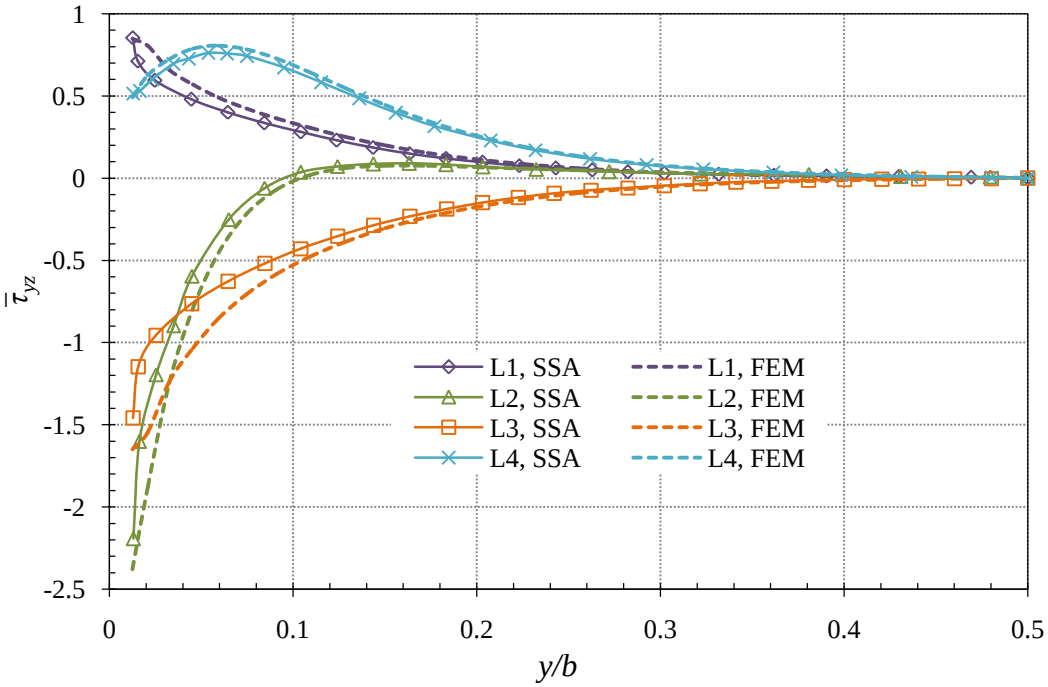

(a) Along the interface

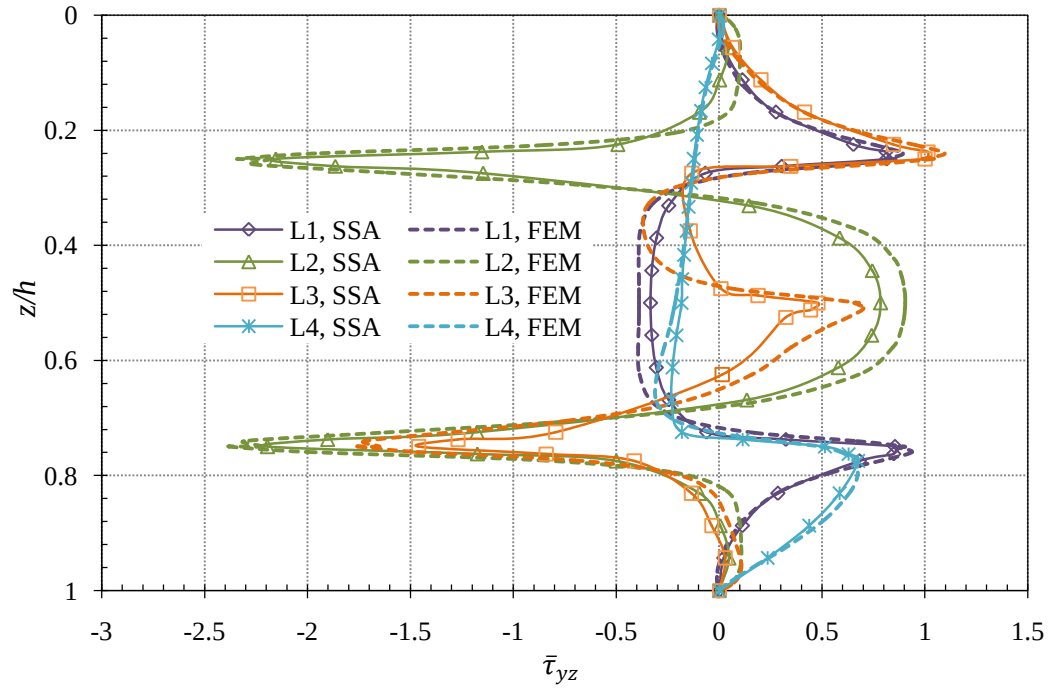

(b) Through the thickness

Figure 5.13: Variations of interlaminar shear stress $\bar{\tau}_{yz}$ in the general cross-ply laminates under uniformly distributed loading and open-circuit conditions

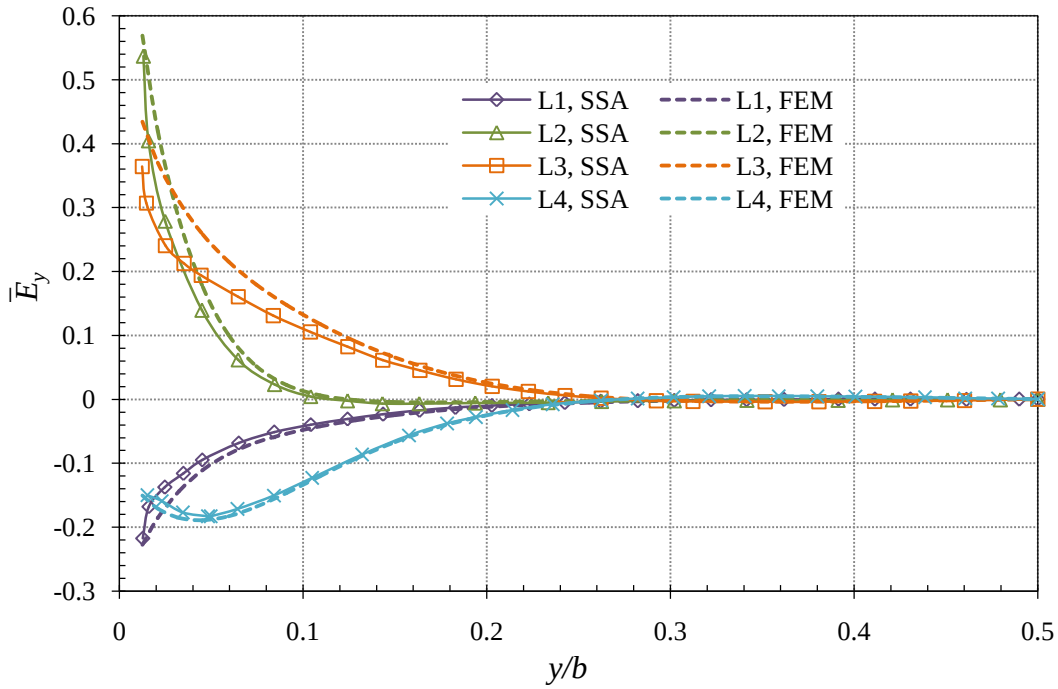

(a) Along the interface

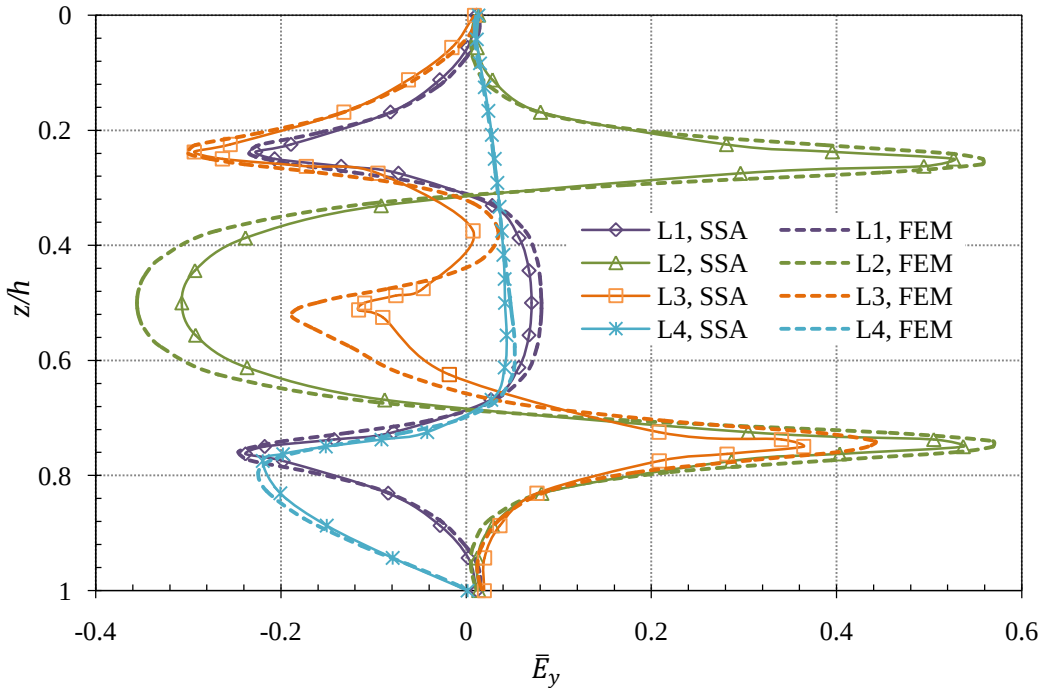

(b) Through the thickness

Figure 5.14: Variations of electric field intensity component $\bar{E}_y$ in the general cross-ply laminates under uniformly distributed loading and open-circuit condition

The results of this investigation show that all three interlaminar stresses exhibit apparent gradient behaviours near the intersection of the interface and the free edge. Among them the transverse shear stress τ_{xz} demonstrates the largest magnitude of the interlaminar stresses along the free edges. The most obvious finding to emerge from this investigation is that the tensile interlaminar normal stress was verified in the general cross-ply piezoelectric laminates and the largest tensile interlaminar normal stress at the interface was found in the $[90^\circ/90^\circ/90^\circ/0^\circ]$ laminate. Similar to τ_{yz}, the rapid variation of the electric field intensity component E_y is detected in a neighbourhood of concentration near the interface and the free edge.

5.6 Conclusions

This chapter has presented a series of numerical studies to analyze the electromechanical behaviour of simply-supported piezoelectric laminated plates with free edges under mechanical transverse loads.

The present analytical solution from state space analysis can predict the coupled electromechanical response of the thick three-layered piezoelectric laminates with different thickness to length ratios. The validity and accuracy of the present analytical solution have been verified in comparison with the FEM results. To capture the steep variations of the interlaminar stresses and electric field intensity components near the intersection of the interface and the free edge, the non-uniform layer refinement has been introduced and implemented in the state space approach for the first time. This novel technique allowed more mathematical sub-layers in the small region near the interface to improve the accuracy of the local mechanical and electrical quantities without increasing the total number of sub-layers and was a possible compromise between the accuracy and computation efficiency for the analysis of the free-edge effect. Moreover, the existing analytical Levy solution by CLPT was compared with the present SSA solution and FEM for the simply-supported laminated plates with free edges. It was found that CLPT gave poor predictions of the in-plane stresses and underestimated the maximum central

deflection. As a result, the present 3D analytical solution is required in the design and analysis of simply-supported and free-edge laminated and piezoelectric laminated structures.

Furthermore, for the three-layered piezoelectric laminated plates the interlaminar stress τ_{xz} was dominant at the simply-supported edge and reached the maximum value at the corners. Although τ_{yz} exhibited a significant gradient near the free edge, it was quantitatively smaller than τ_{xz}. However with different material properties, geometries and stacking sequences the contributions from interlaminar stresses σ_z and τ_{yz} cannot be neglected compared with τ_{xz} in the four-layered cross-ply piezoelectric laminated plates. In the immediate vicinity of the intersection and the free edge, steep gradients of these stresses were observed and tensile σ_z was found. The significant variations of interlaminar stresses near the free edge tended to contribute to edge delamination. Among the four stacking sequences, the $[90^\circ/90^\circ/90^\circ/0^\circ]$ laminate was found to be more vulnerable to edge delamination due to its highest tensile interlaminar normal stress at the interface. In order to prevent such edge delamination, the edge reinforcement or edge modification should be utilized in practical design.

The 3D piezoelectric brick element in the commercial FE package like ABAQUS can provide accurate distributions of the field variables in the piezoelectric laminate. Due to the weak transverse normal and shear strengths in composites/piezoelectric composites, the interlaminar stress fields at the element nodes need to be intensively investigated and the accuracy of those stresses is mostly desired. However, these interlaminar stresses in FEM are different on the two sides of the interfaces of adjacent elements so they are discontinuous at the interface between dissimilar material layers. Although this discrepancy between the two adjacent elements can be reduced by using a refined mesh, the Gauss point location can never become the nodal location at the interface. It was found that this discontinuity of interlaminar stresses at the interface was negligible in the inner region of the piezoelectric laminated plate, however, when approaching the immediate vicinity of the free edge where a possible stress concentration was expected, this discontinuous behaviour

might become more significant and the results from that small region deteriorated, in particular with a high inhomogeneity in mechanical and electric material properties in the piezoelectric laminates.

Compared with FEM, the present analytical solution can guarantee the continuity of the interlaminar stresses at interfaces and all the mechanical and electrical variables are computed directly from the interface of sub-layers with an appropriate layer refinement. The present 3D analytical solution showed an improvement in precision over other 2D analytical and numerical solutions for determining interlaminar stresses as well as electric fields not only in the inner region but also near the intersection of the interface and the free edge of the piezoelectric laminates and could serve as a benchmark for estimating the accuracy of these analytical and numerical methods.

CHAPTER 6 EFFECTS OF GEOMETRIC PARAMETERS AND ELECTRICAL PROPERTIES

6.1 Introduction

In order to make an appropriate design for laminated piezoelectric plates, the effects of several geometric and piezoelectric parameters on the electromechanical response of laminated plates will be investigated in this chapter. For example, by reducing the width to thickness ratio, the 3D plate solution obtained in the previous chapter will be simplified to an exact solution for a laminated beam structure. This can be used to compare with some of 2D solutions. In addition, various electrical material properties are also selected to evaluate their influence on the mechanical and electrical components of the plates.

6.2 Simply-supported single-layered piezoelectric beam

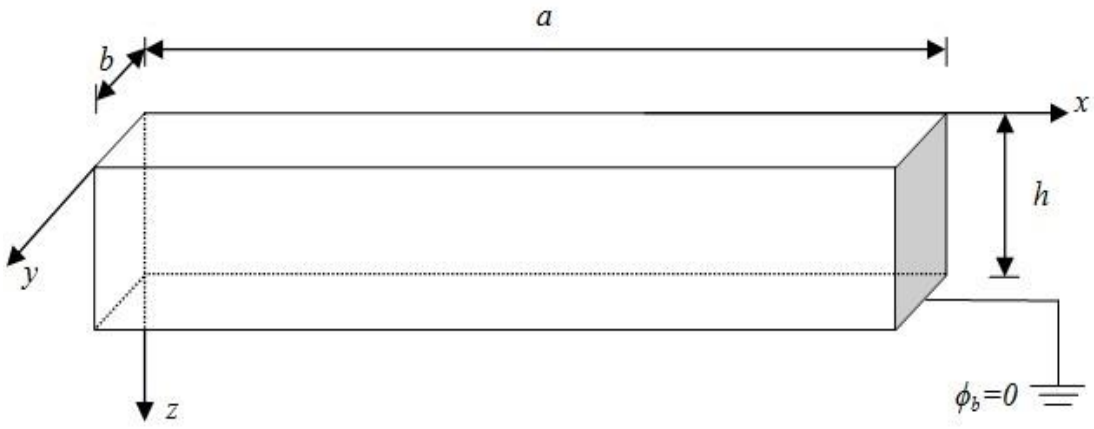

Figure 6.1: Simply-supported piezoelectric beam under a uniformly distributed load

A simply-supported piezoelectric plate with two opposite free edges can be regarded as a simply-supported beam when *a* is sufficiently large and its width *b* is smaller than its thickness *h* (Figure 6.1). As a 3D analytical solution for the piezoelectric

plate with free edges, the state space solution in the previous chapter provides an alternative to accurately assess the bending behaviour of the simply-supported piezoelectric beam without any assumptions and simplifications. More specifically, the 3D plate model is used directly to analyze the simply-supported piezoelectric beam problem by accounting for all the independent elastic and piezoelectric constants.

Based on the theories of 2D elasticity and piezoelectricity, Lin et al. (2000) investigated the problem of a simply-supported piezoelectric beam under a uniformly distributed transverse load and obtained the analytical close-form solution. In their analytical beam model (Figure 6.1), since b is negligible in magnitude compared with the other dimensions, the plane stress state in x-z plane is assumed, where the normal stress σ_y and the shear stresses τ_{xy} and τ_{zy} directed perpendicular to the x-z plane are considered to be zero.

To verify the accuracy and efficiency of the present solution with those of Lin et al. (2000), the following parameters are given for a numerical example of the piezoelectric single-layer beam presented by Lin et al. (2000): the length a is 0.3 m, the width b is 0.002 m and the thickness h is 0.02 m. The uniform distributed load is 10 N/m^2 and is applied on the top surface of the beam while the bottom surface is traction-free and grounded. The lamina is made of PZT-4 material which has the following mechanical and electrical properties in Table 6.1.

Table 6.1: Mechanical and electrical properties of PZT-4 (Lin et al., 2000)

Elastic Stiffness (GPa)	Piezoelectric Coefficients (C/m^2)	Dielectric Properties (CV/m)
$C_{11}=C_{22}=139$	$e_{31}=e_{32}=-6.98$	$\epsilon_{11}=6\times10^{-9}$
$C_{12}=77.8$	$e_{33}=13.84$	$\epsilon_{22}=6\times10^{-9}$
$C_{33}=113$	$e_{24}=e_{15}=13.44$	$\epsilon_{33}=5.47\times10^{-9}$
$C_{13}=C_{23}=74.3$		
$C_{44}=C_{55}=25.6$		
$C_{66}=30.6$		

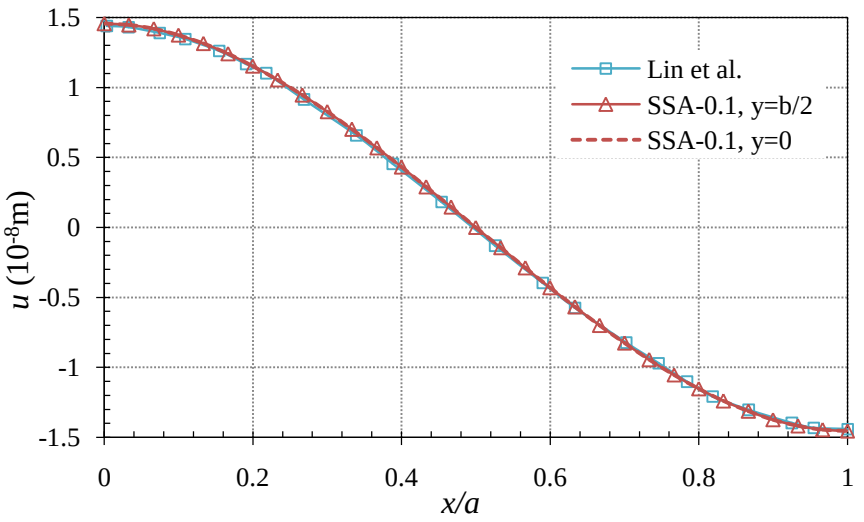

(a) z=0

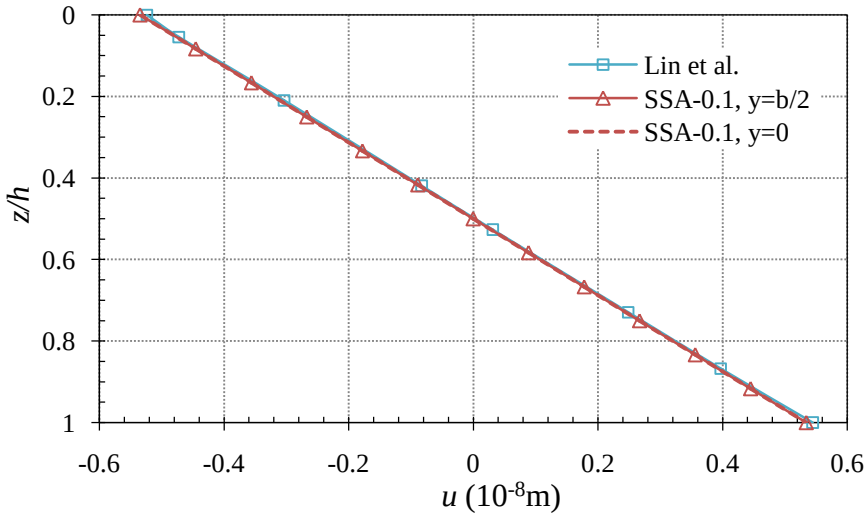

(b) $x = \frac{5}{8}a$

Figure 6.2: Distributions of in-plane displacement u (a) along the length (b) through the thickness

As mentioned, in the piezoelectric beam model of Lin et al. (2000), the width b is smaller than the thickness h, a plane stress state assumption is hence made. And all variables are independent of y. However, despite the relatively small value of width b compared with the length a and thickness h, all variables that demonstrate negligible variations across the y direction are retained in the 3D state space plate

model. It is expected that there is a difference between the results from these two analytical models. Those analytical results from the state space analysis (SSA) for the bending problem of the piezoelectric beam with b/h=0.1 is abbreviated as SSA-0.1 in Figures 6.2-6.9. Due to the consideration for different positions of the beam, a further labelling such as y=b/2 and y=0 is added in the relevant curves of these figures correspondingly.

Figures 6.2 and 6.3 give the distributions of the in-plane displacement u and transverse displacement w along the length and through the thickness. It is shown that the findings of the present analytical study are consistent with those of Lin et al. (2000). Compared to the transverse displacement, the in-plane displacement is much smaller and distributed linearly through the thickness. The transverse deflection is approximately two-order larger in magnitude than the longitudinal displacement. Lin's beam model with the plane-stress assumption did give a similar result as that of the 3D analysis, however, the deflection w is larger (Figure 6.3 (b)) in Lin's beam model which again did not support the opinion that the effect of various plate assumptions is to increase the stiffness of the structure and, therefore, yields lower deflections. Wu and Wardenier (1998) have proved that the displacements obtained from approximate theories may be either over- or under-estimated.

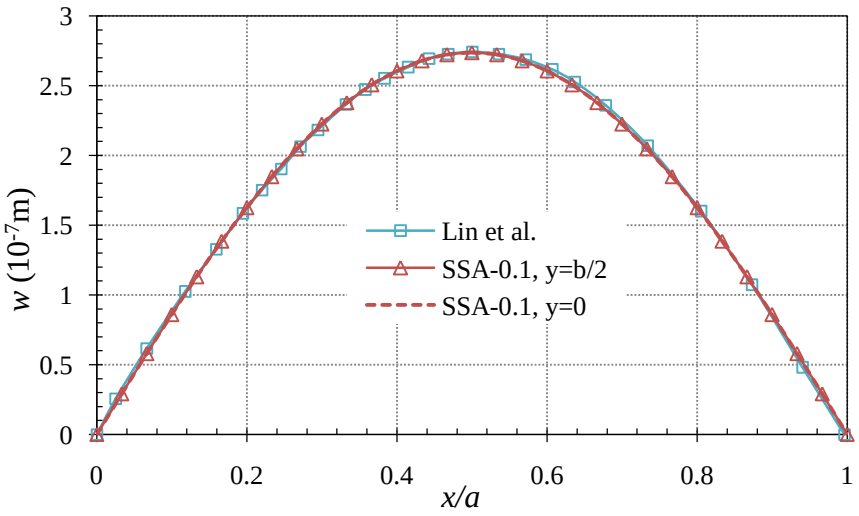

(a) $z = \frac{h}{2}$

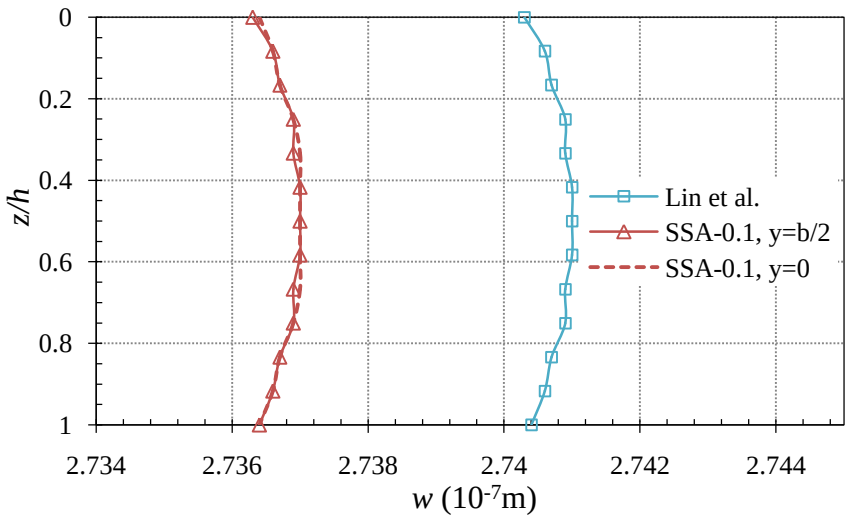

(b) $x = \frac{a}{2}$

Figure 6.3: Distributions of transverse displacement *w* (a) along the length (b) through the thickness

Since the transverse normal strain ε_z and shear strain γ_{xz} are considered in the solution of the present study and Lin et al. (2000) whereas such transverse normal and shear strains are often neglected in most 2D plate theories, the variation of transverse displacement *w* is not constant through the thickness even in the thin beam and it is also observed that there is a maximum transverse displacement *w* at the middle surface of the beam perpendicular to the *z*-axis rather than at the top or bottom surface. This variation of transverse displacement across the thickness of the orthotropic plate has been investigated by Fan (1998) and Wu and Wardenier (1998). According to their studies, the influence of the thickness of the plate subjected to a uniformly distributed pressure cannot be neglected in the analysis of moderately thick plate and the maximum transverse displacement across the thickness varies with respect to different *h/a* or Young's modulus ratio. This behaviour of a moderately thick piezoelectric plate has been investigated thoroughly in the previous section. Moreover, due to the sufficiently small ratio *b/h*, there is no significant difference between the results at *y*=*b*/2 and those at *y*=0.

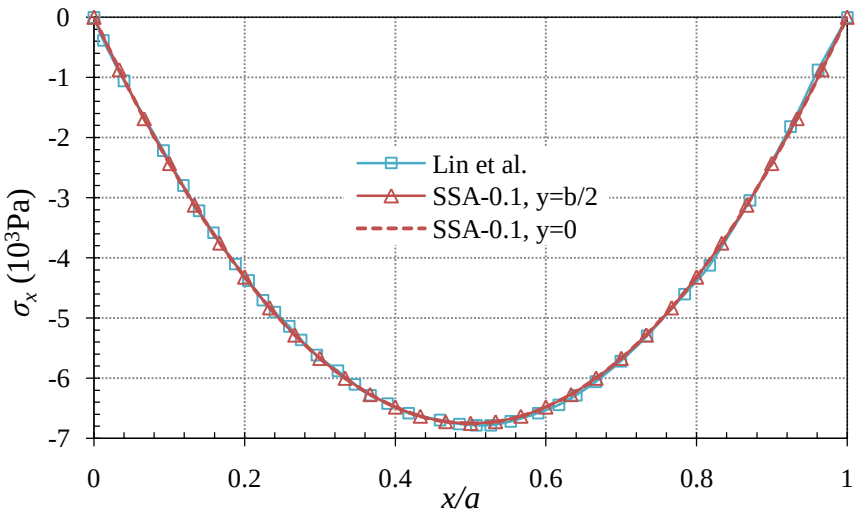

(a) $z=0$

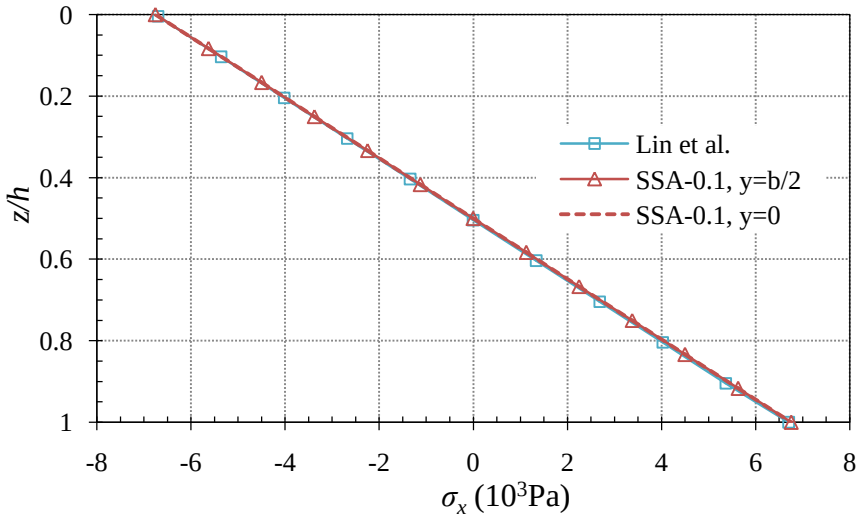

(b) $x = \frac{a}{2}$

Figure 6.4: Distributions of in-plane stress σ_x (a) along the length (b) through the thickness

As depicted in Figure 6.4, the maximum in-plane normal stress σ_x is found at the middle of the beam, where the top surface is under compression while the bottom surface is subjected to tension. It is also observed that there is a maximum transverse

shear stress τ_{xz} in the vicinity of the simply-supported edges (Figure 6.5). The present results agree well with those of Lin et al. (2000) and no significant discrepancy between the results at *y=b/2* and those at *y=0* is observed in both figures.

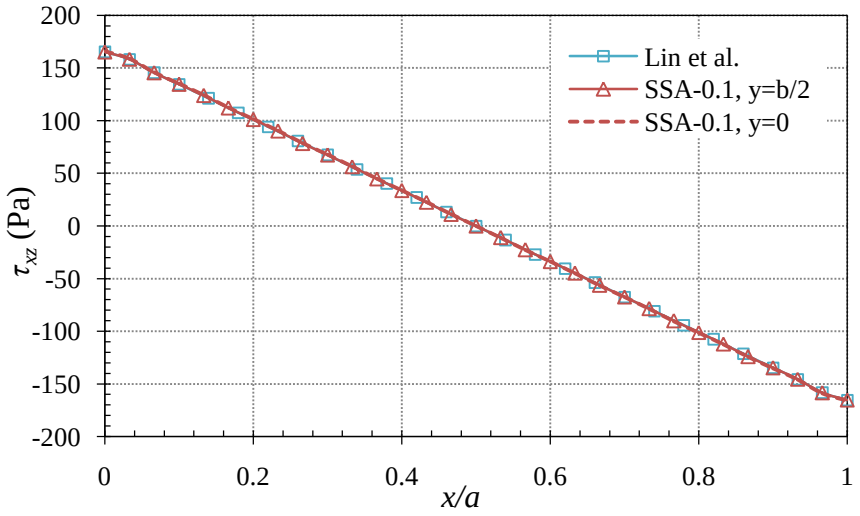

(a) $z = \frac{h}{4}$

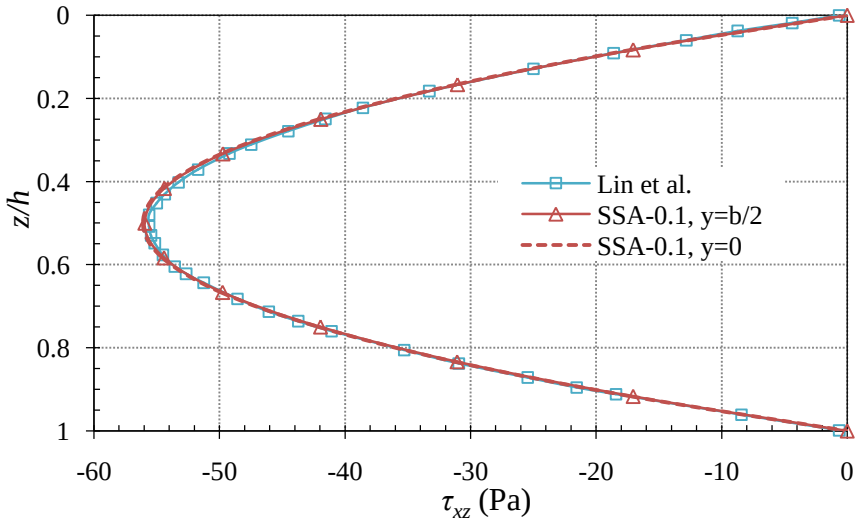

(b) $x = \frac{5}{8}a$

Figure 6.5: Distributions of transverse shear stress τ_{xz} (a) along the length (b) through the thickness

The 3D electromechanical coupling behaviour is also taken into account, and it is shown in Figure 6.6 that for both present results and those of Lin et al. (2000) the electric potential ∅ exhibits polynomial distributions across the length and the thickness of the piezoelectric beam.

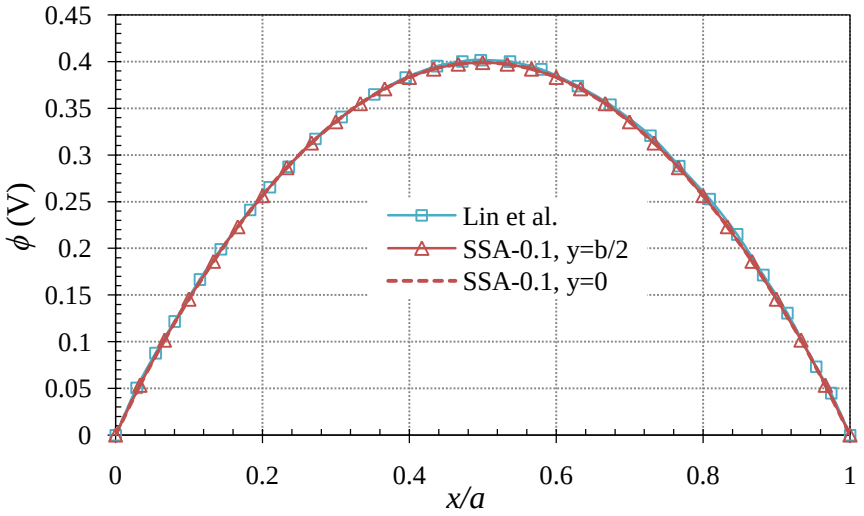

(a) $z=0$

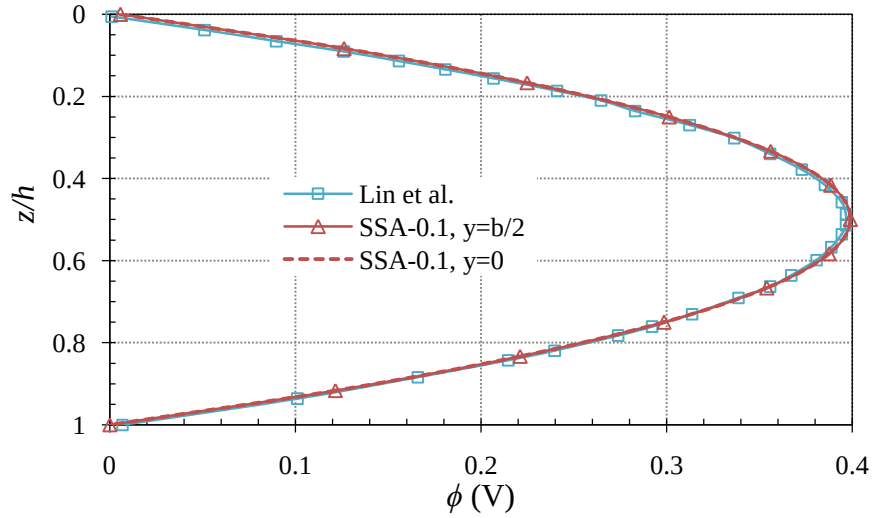

(b) $x = \frac{a}{2}$

Figure 6.6: Distributions of electrical potential ϕ (a) along the length (b) through the thickness

Analogous to SSA-0.1, the present results are also given for the piezoelectric beams with b/h=0.5 and b/h=1, which are abbreviated as SSA-0.5 and SSA-1 respectively. As illustrated in Figure 6.7, when b/h=0.1 there is no noticeable difference between the present results at $y=b/2$ and those at y=0 for the distributions of transverse shear stress τ_{xz}. However, the discrepancies between the results at $y=b/2$ and those at y=0 become greater as the width b is increased in the SSA-0.5 and SSA-1 cases. The value of the transverse shear stress τ_{xz} at the intersection of the free edge and simply-supported edge is approximately 33% larger than that at the middle of the simply-supported edge in SSA-1 case and the assumption of plane stress state is not appropriate and could make an inaccurate prediction of the state of the stresses and electrical quantities, especially the transverse shear stresses. Moreover, the accurate determination of τ_{xz} is essential due to the fact that the strength of the material along the longitudinal direction of fibres are normally significantly higher than the transverse shear strength of the laminae and the possible shear failure may occur.

The variables in the y-direction which are neglected due to the plane stress state assumption also can be obtained in the present solution. The distributions of the in-plane displacement v and transverse shear stress τ_{yz} through the thickness are illustrated in Figures 6.8 and 6.9. The width of beam b is still much smaller than the length a so these variables in the y-direction are in small orders of magnitude compared to those in the x-direction. It can be seen that the displacement v is two-order smaller in magnitude than the displacement u but does not vanish. As b/h increases, v and τ_{yz} exhibit significant growths and the contribution from the y direction is not negligible, and the behaviour of the structure tends to be like that of a plate. Since the present solution is obtained on the basis of the 3D state space plate theory, the 3D distributions of stresses and electrical quantities can be accounted for, even for beam models. As a consequence, the present solution provides alternative means for evaluating the full 3D state of stresses and electrical quantities in the analysis of piezoelectric beams.

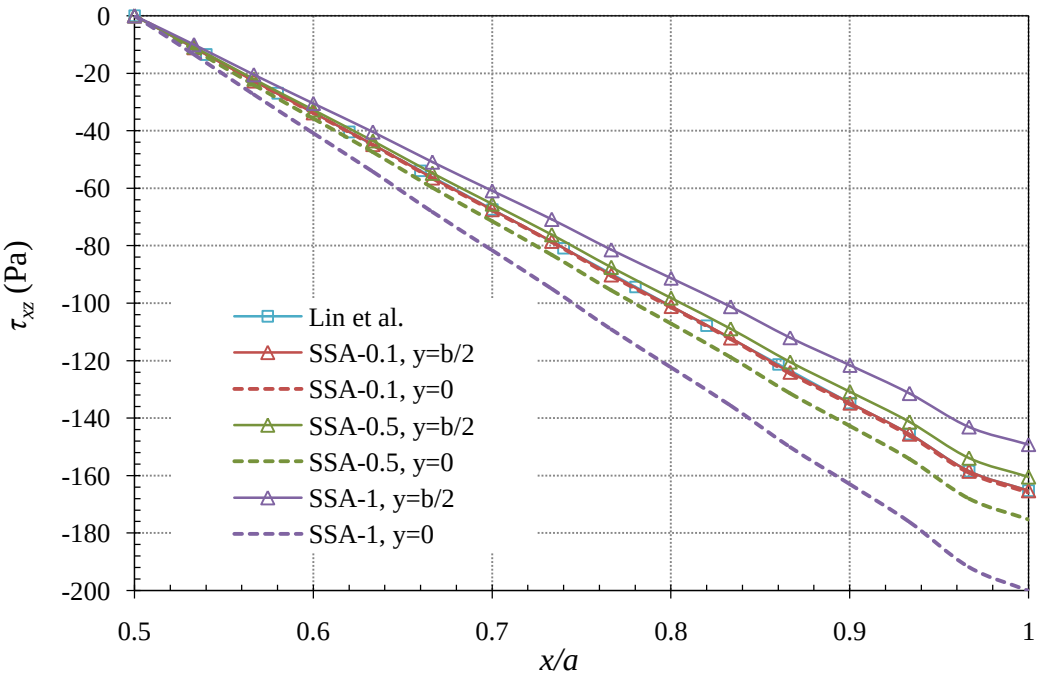

(a) $z = \frac{h}{4}$

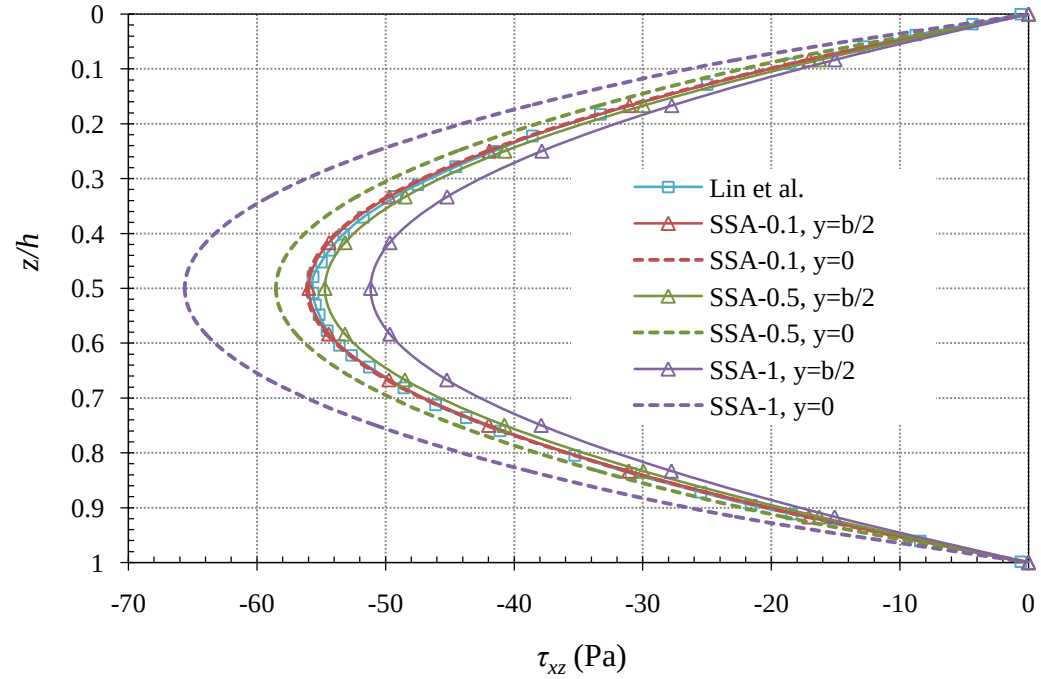

(b) $x = \frac{5}{8}a$

Figure 6.7: Distributions of transverse shear stress τ_{xz} (a) along the length (b) through the thickness with different *b/h*

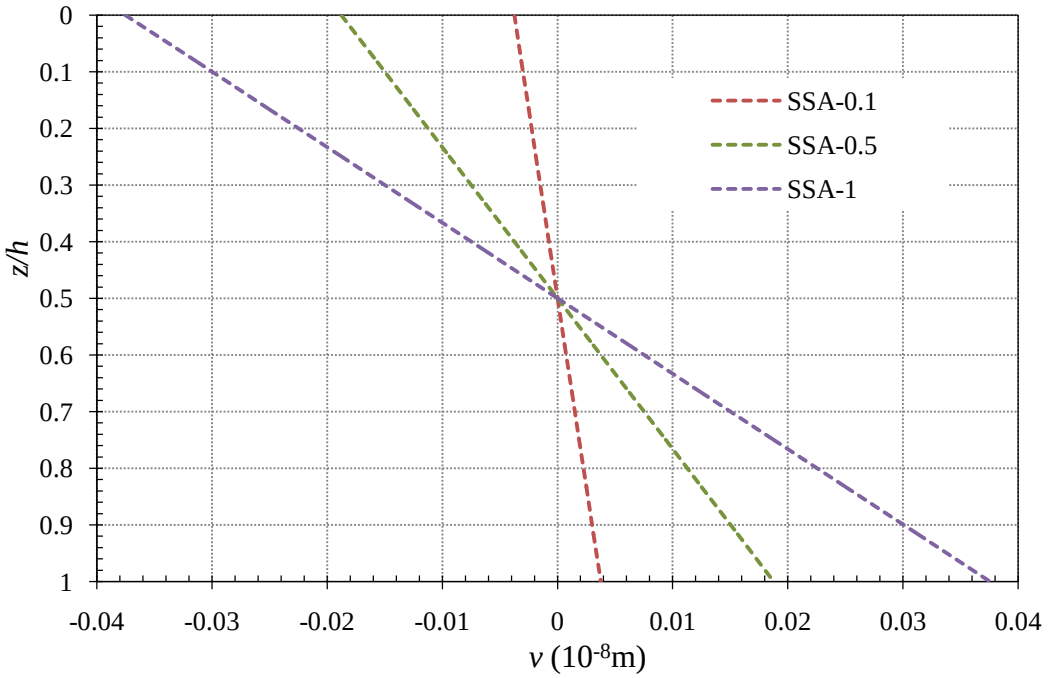

Figure 6.8: Distributions of in-plane displacement v through the thickness with different b/h at $x=a/2$ and $y=0$

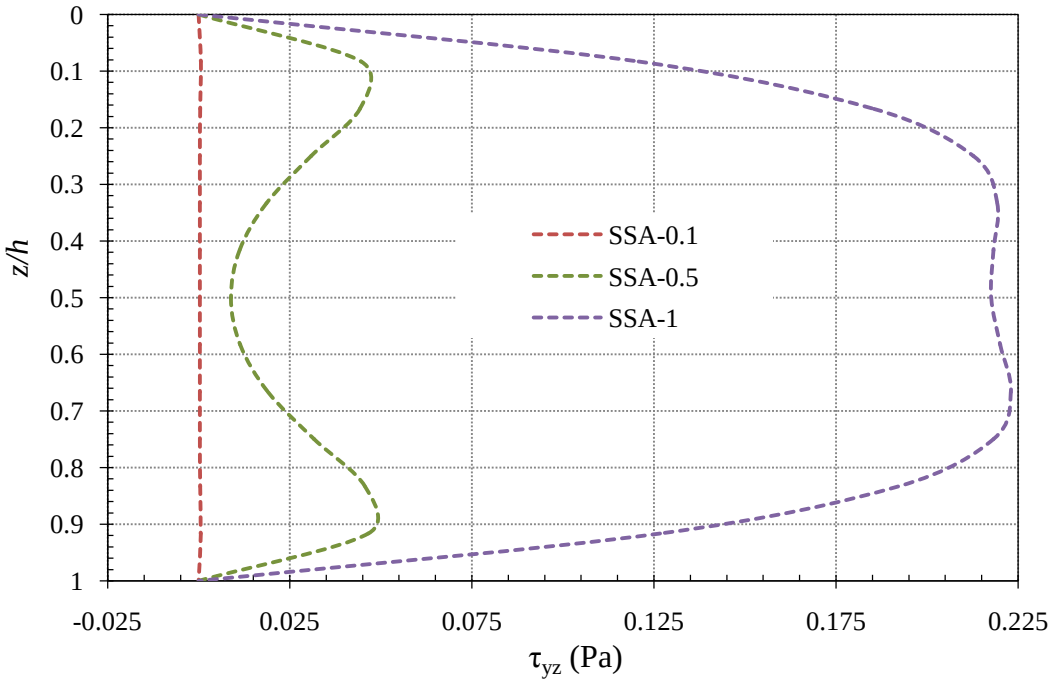

Figure 6.9: Distributions of transverse shear stress τ_{yz} through the thickness with different b/h $x=a/2$ and $y=b/4$

6.3 Three-layered piezoelectric laminated plate with different electrical properties

Based on three-layered piezoelectric laminated plates in Chapter 5, the influence of different electrical properties on the mechanical and electrical responses is presented here. This plate has the same geometry, loading and boundary conditions as those in Chapter 5 and the thickness to length ratio is 0.6. The two face layers are also distinguished by the ratio of $\delta = C_{ij}^{(F)}/C_{ij}^{(C)}$, $\lambda = e_{ij}^{(F)}/e_{ij}^{(C)}$ and $\kappa = \epsilon_{ij}^{(F)}/\epsilon_{ij}^{(C)}$, where F and C denote face and core, respectively. In this section, only the electrical property parameters for the two face layers are changed, where $\delta = 1$, $\lambda = 1, 2, 3, 4$ and $\kappa = 1, 2, 3, 4$. In addition, the same non-dimensionalization is used.

For the sake of brevity, w (a/2, b/2, 0), σ_x (a/2, b/2, 0), τ_{xz} (0, 0, h/5), ϕ (a/2, b/2, 0), D_z (0, 0, h/5) and E_z (0, 0, h) are chosen. It is shown in Figure 6.10 that all components are affected by different λ and κ. It is clear that the variations of electrical properties have a stronger influence on the electrical response than the mechanical one as expected.

From Figure 6.11 (a) it is apparent that the transverse shear stress τ_{yz} shows a stronger gradient when λ increases in the vicinity of the free edge for $\kappa = 1$. When $\lambda = 1$ and $\kappa = 1$, this three-layered plate is treated as a single-layered plate because the two face layers and the core layer have the same material properties. As λ varies there are material discontinuities at the interface between the face and core layers and these material discontinuities may induce the shear stress concentration at the free edge. Moreover, as illustrated in Figure 6.11 (b) the maximum value of the transverse shear stress declines when κ increases for $\lambda = 4$. The distributions of the transverse shear stress τ_{yz} through the thickness are also given in Figure 6.12. To delineate the significant gradient near the free edge, the distribution at y=0.009b is chosen. It is observed that a steep variation occurs at the interface.

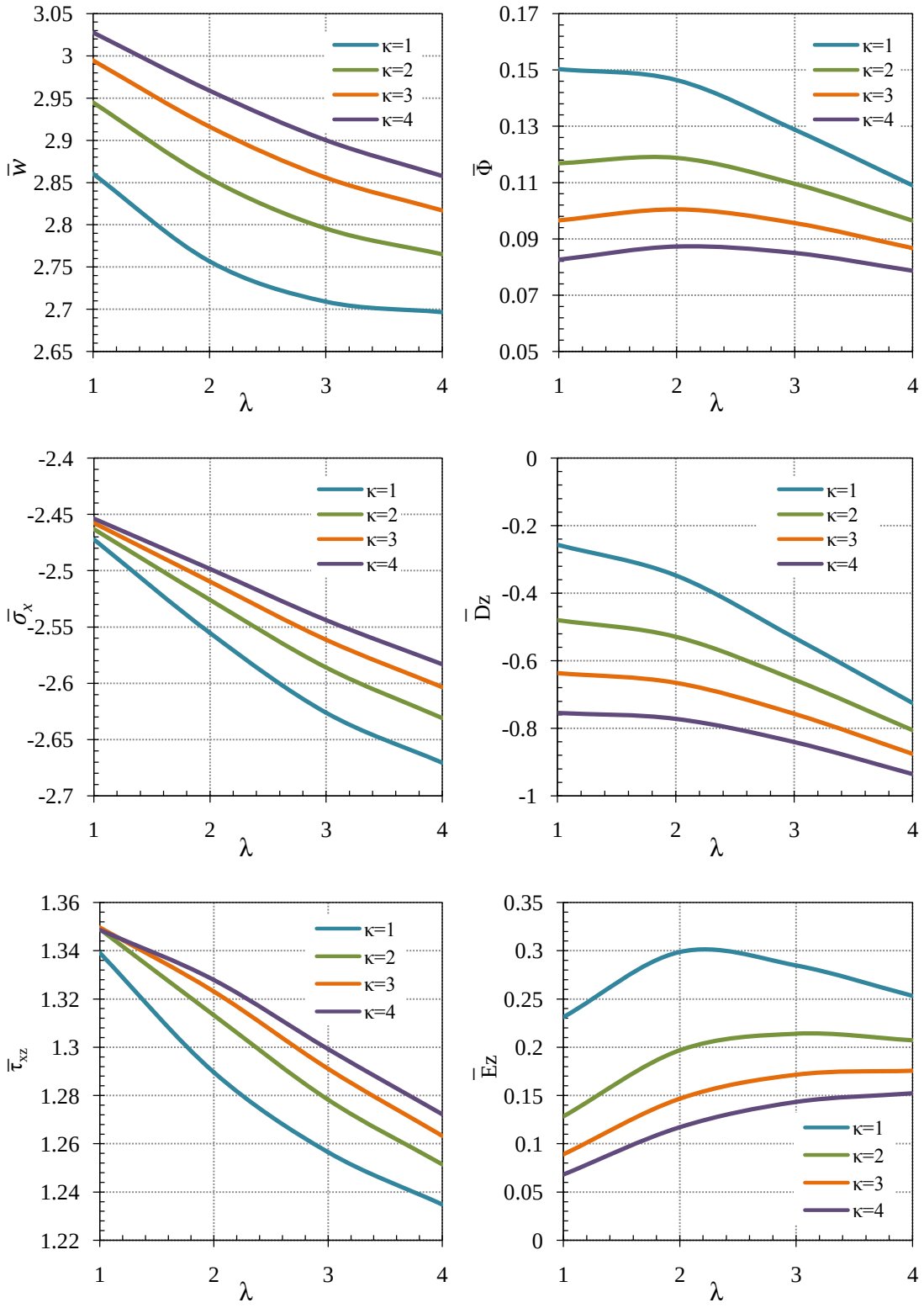

Figure 6.10: Variations of physical quantities with various λ and κ.

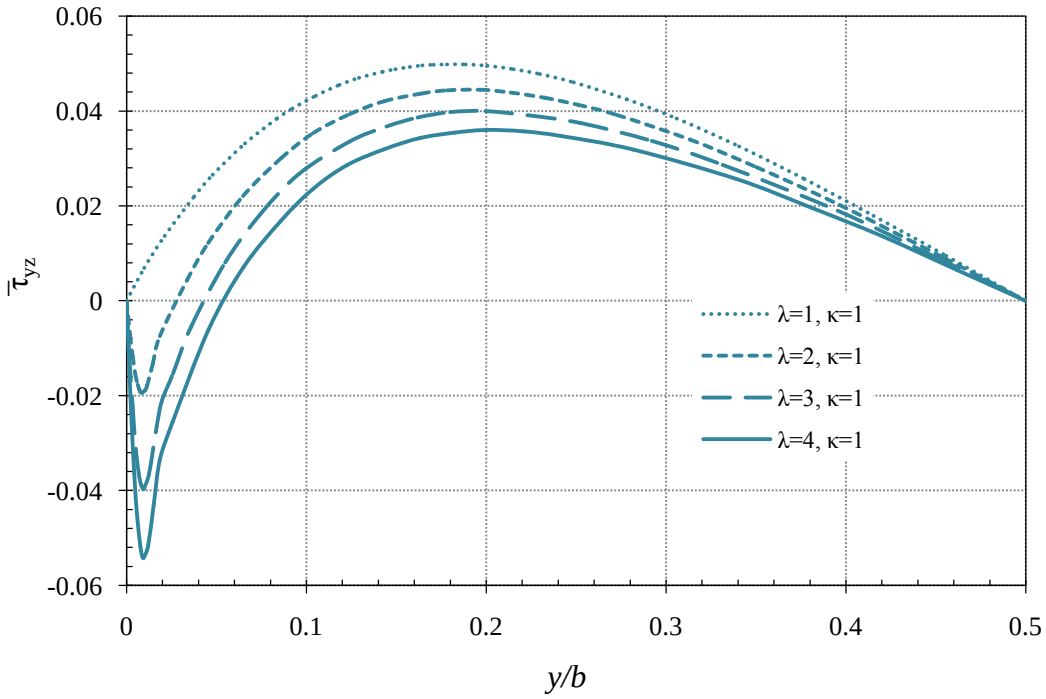

(a)

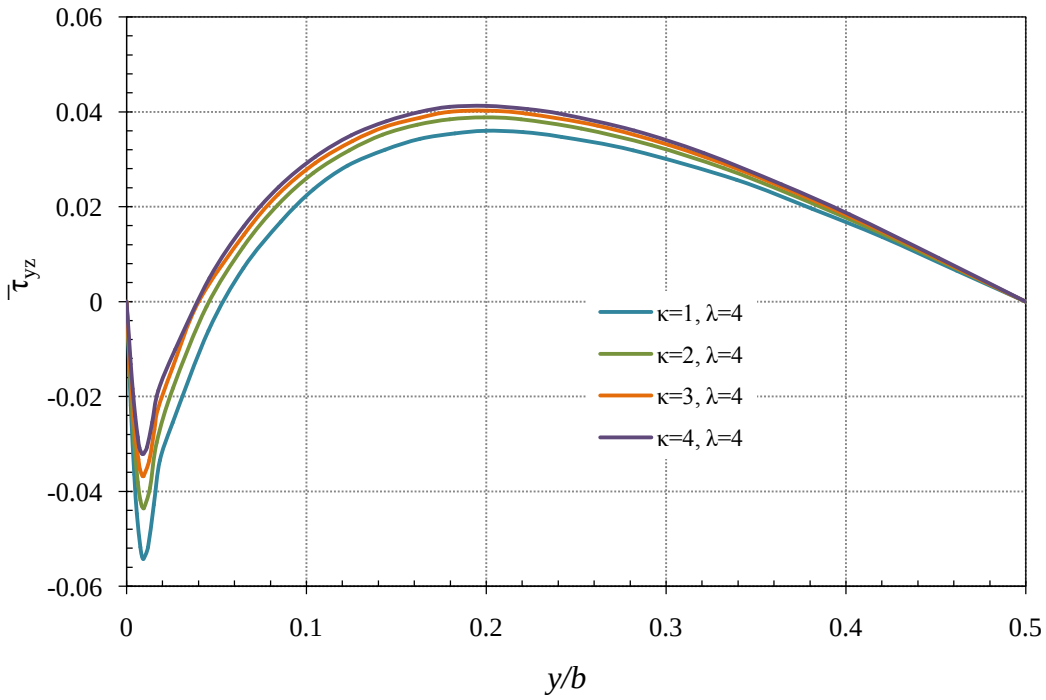

(b)

Figure 6.11: Distributions of transverse shear stress $\bar{\tau}_{yz}$ along the interface at z=0.2h with various λ and κ.

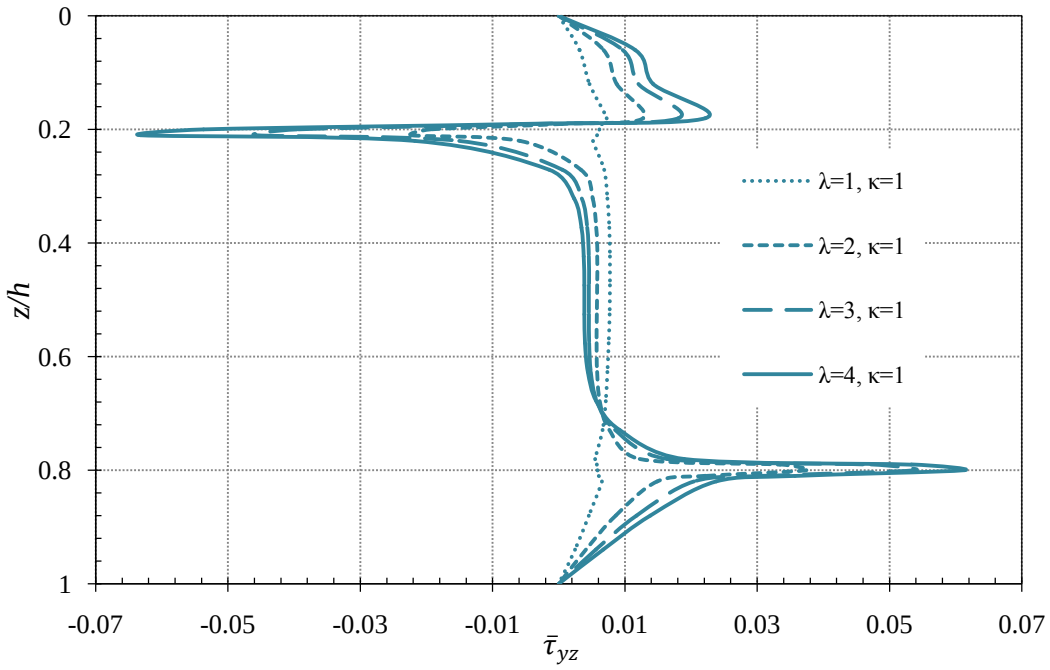

(a)

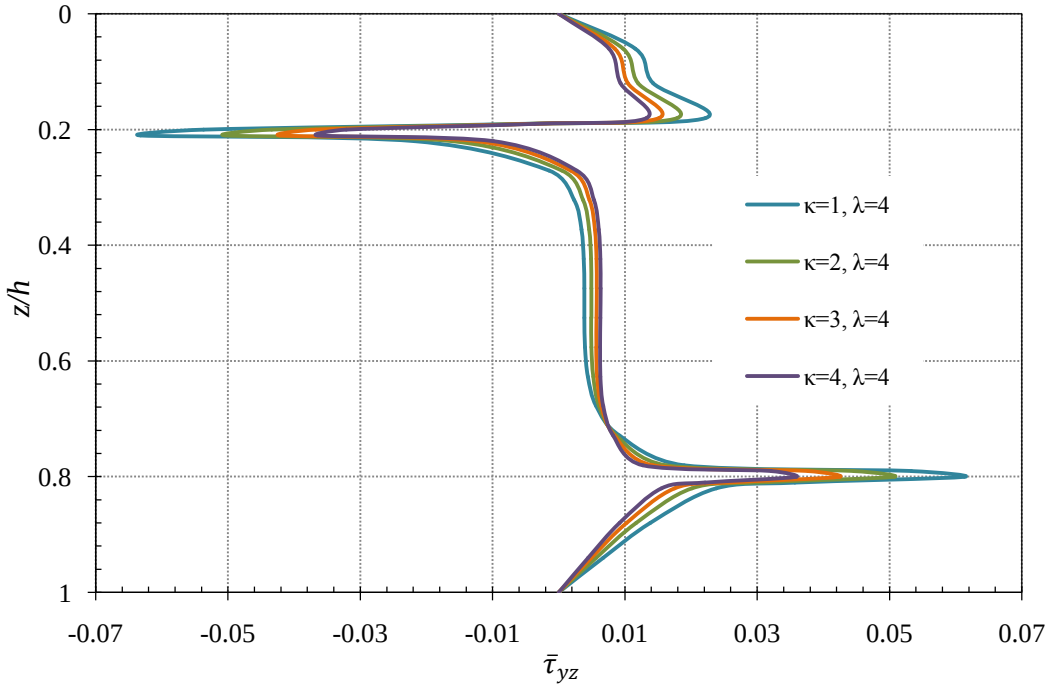

(b)

Figure 6.12: Distributions of transverse shear stress $\bar{\tau}_{yz}$ through the thickness at y=0.009b with various λ and κ.

6.4 Conclusions

With various width to thickness ratios the present solution accounts for all geometric parameters and elastic and electric constants for the orthotropic and piezoelectric material and can be used to analyze the 3D electromechanical behaviour of piezoelectric beams exactly. By comparing the present 3D solution with a 2D analytical solution, it was found that the solution based on the 2D theory was not accurate when the width to thickness ratio *b/h* increased, and the variables in the *y* direction increased dramatically and the contribution from the *y* direction should be taken into account, especially for the transverse shear stress τ_{xz}. The value of τ_{xz} at the intersection of the free edge and simply-supported edge was approximately 33% larger than that at the middle of the simply-supported edge when *b/h*=1 and the assumption of plane stress state would lead to a poor prediction of behaviours of the transverse shear stresses. For the design and analysis of laminated and piezoelectric laminated beams the present 3D plate analysis should be considered in order to account for the edge effect which cannot be predicted by these 2D theories.

It was also observed that the electrical quantities were more affected by the electrical material parameters compared to the mechanical ones. The significant influence of these parameters on the singular behaviour of the transverse shear stress τ_{yz} was captured near the intersection of the interface and the free edge by using the 3D state space approach. By increasing the dielectric ratio κ the transverse shear stress τ_{xz} which was much larger than τ_{yz} rose slightly, whereas the maximum value of τ_{yz} at the interface declined.

CHAPTER 7 NUMERICAL ANALYSIS OF INFINITE LONG PIEZOELECTRIC LAMINATES WITH FREE EDGES UNDER UNIAXIAL EXTENSION

7.1 Introduction

It is well known that the free-edge effect and delamination in laminated composites have been investigated by many researchers and a number of analytical, semi-analytical, and numerical methods have been established subsequently. Among these researches, a particular problem where general cross-ply laminates are subjected to uniform axial extension, has drawn more attention and a detailed description of this problem has been given and discussed exclusively in the literature review.

Numerous published researches have attempted to investigate and explain a possible stress singularity at the free edges between the layers with different materials, for example, Pipes and Pagano (1970); Wang and Crossman (1977); Tahani and Nosier (2002); Zhang et al. (2006); Artel and Becker (2005); Mirzababaee and Tahani (2009). According to Tahani and Nosier (2002), no exact elasticity solution to the free-edge problem is yet known to exist and all conclusions drawn with respect to the singularity of stresses are merely based upon approximate analytical and numerical studies. Artel and Becker (2005) adopted 20-noded isoparametric displacement based volume elements with refined free edge modelling and investigated the electromechanical coupling effects on the interlaminar stresses and the electric field intensities near the free edges in laminates with piezoelectric material properties under a uniformly axial extension. In their finite element model, general symmetric laminate lay-ups were considered with and without electromechanical coupling. Based on the layerwise laminate theory as well as the principle of minimum total potential energy, the same problem has been studied and comparisons with the results of Artel and Becker (2005) also have been made by Mirzababaee and Tahani (2009). In their comparisons, except for the regions close to

the free edge, there are several decent agreements between the results of Mirzababaee and Tahani (2009) and those of Artel and Becker (2005). Nevertheless, for the cross-ply piezoelectric laminates there are some discrepancies for the variations of interlaminar stresses along the interfaces in particular the distributions of interlaminar normal stresses through the thickness. The coupling effect on the free edge interlaminar stresses at the interface of dissimilar piezoelectric materials is such a complex phenomenon that the aforementioned solutions can provide some satisfactory predictions of the interlaminar stresses and electric field intensities, however approaching the free edge may result in the deteriorating descriptions of these electromechanical variables.

Furthermore, it is pointed out that the aforementioned methods employed are focussed on the symmetric cross-ply composite piezoelectric laminates and the solutions they obtained are neither general nor accurate enough. Although symmetry of a laminate about the mid-plane is often desirable to avoid coupling between bending and extension, some practical applications require unsymmetric laminates to achieve specific design requirements and further investigation on the unsymmetric laminates is necessary and important for the application requirement. By using the analytical solutions obtained in Chapter 4, a numerical analysis of general symmetric cross-ply lay-ups can be conducted in comparison with the results of Artel and Becker (2005) and those of Mirzababaee and Tahani (2009). Further analytical investigation on other stacking sequences of the cross-ply piezoelectric laminates, is also carried out and the corresponding numerical examples are subsequently given for the first time. In addition to considering the open-circuit surface condition which has been employed by previous studies, the closed-circuit surface condition will be taken into account in the present analysis. Moreover, the present approach has the capability to predict and illustrate the variations of electromechanical variables at the interfaces and along the thickness of the piezoelectric laminate and can be used to evaluate the accuracy of ABAQUS simulation.

7.2 Open-circuit surface condition

For the 3D analysis of a free-edge piezoelectric laminated plate problem subjected to a uniform axial strain ε_0 along the x direction, there are four traction-free boundary conditions: two free edges at $y=0$ and $y=b$, and two top and bottom surfaces at $z=0$ and $z=h$. For the top and bottom surfaces, two types of electric boundary conditions can be imposed: open-circuit condition and closed-circuit condition. The former electric surface condition is considered in this section and the latter one will be given in the next section.

To evaluate the accuracy and efficiency of the present method, four numerical examples are presented for the general cross-ply piezoelectric laminated plates. Specifically, for a four-layered laminate which has an infinite length in the x-axis, the width b is chosen ten times larger than the thickness h, and the thickness of each layer in the laminate is identical (Figure 7.1). Moreover, ε_0 is taken as 0.1%.

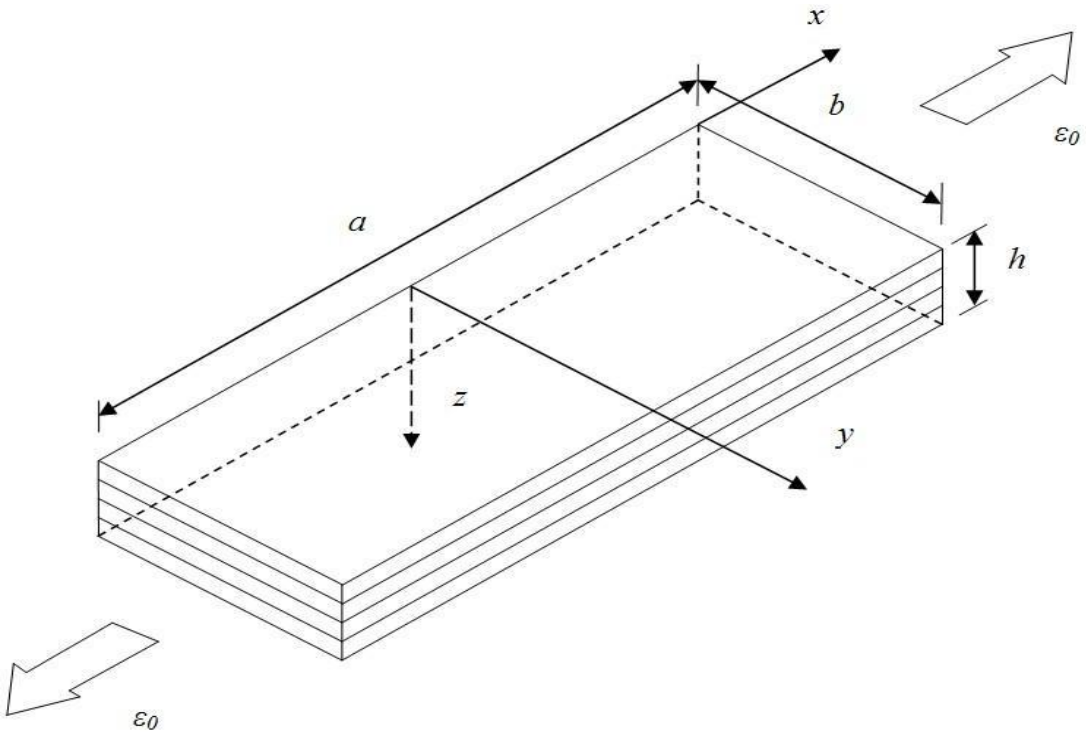

Figure 7.1: Nomenclature of a piezoelectric laminated plate

There are four stacking sequences $[0^\circ/90^\circ]_s$, $[90^\circ/0^\circ]_s$, $[0^\circ/90^\circ/0^\circ/90^\circ]$ and $[90^\circ/90^\circ/90^\circ/0^\circ]$ with and without electromechanical coupling respectively. Due to the symmetry, stresses and electric field intensity components are symmetric or antisymmetric across the width of laminates with respect to *y* coordinate. In addition, the homogeneous orthotropic material is the combination of the mechanical properties of a T300/Epoxy and the piezoelectric and electrical properties of a PZT-5A. This material property is given in Table 5.9.

In the present state space analysis the unknown boundary function contained in the non-homogeneous vectors is a function of *z*. The actual physical layer in a laminate can be treated as if it is made of as many mathematical sub-layers as necessary. For a single sufficiently thin layer, excellent accuracy can be achieved by assuming that the function is linearly distributed with respect to *z* coordinate. By introducing this subdivision technique in each layer, the total number of fictitious sub-layers *P* is determined. As the number *P* is increased, the accuracy of the model is also improved. In general, the number of subdivisions used can be different from layer to layer.

According to the previous convergence tests against different number of sub-layers *P* conducted by Zhang et al. (2006) and Sheng et al. (2007), a uniform layer refinement was adopted in each physical layer with the same thickness. Refined subdivisions can be employed near the interface where interlaminar stresses and electric field intensity components become prominent, as a consequence the proposed non-uniform layer refinement in Chapter 5 will be adopted to analyze the electromechanical coupling and free-edge effect on the piezoelectric laminates with a uniform axial strain.

7.2.1 Numerical results of symmetric cross-ply laminates

In order to validate the present method, two symmetric lay-ups $[0^\circ/90^\circ]_s$ and $[90^\circ/0^\circ]_s$ laminates subjected to a uniform axial strain with and without electromechanical coupling are thoroughly investigated and comparisons are made

between the present analytical solution and those from Artel and Becker (2005) and Mirzababaee and Tahani (2009). For the purpose of abbreviation, **A & B (2005)** and **M & T (2009)** are used to denote Artel and Becker (2005) and Mirzababaee and Tahani (2009) in the following figures, respectively. It is still worth to mention that in the coupled analysis the state space equation for piezoelasticity should be adopted due to the electromechanical coupling, and in the uncoupled analysis the state space equation for pure elasticity should be employed by setting the piezoelectric constants to zero.

In addition, a 3D finite element modelling is performed by ABAQUS for comparison. Because of the symmetries in the problem, only one quarter of the laminate is modelled. A 20-node quadratic piezoelectric brick element C3D20E is employed and the mesh at the intersection of the interface and the free edge is highly refined to obtain a more accurate prediction of the free edge effect.

These two cases are chosen for demonstrating one more application of the present approach and providing an in-depth understanding of the electromechanical coupling behaviour as well as the influence of such coupling effect on the interlaminar stresses and electric field intensity components in the vicinity of the free edges.

According to the state space approach proposed in this study, the interlaminar stresses and electric field intensity components are determined by adopting both the constitutive equations and the equilibrium equations simultaneously in the frame of the linear piezoelasticity. Due to the nature of the symmetric cross-ply laminates and infinite length in the x direction, some mechanical and electrical variables: τ_{xy}, τ_{xz}, D_x and E_x are expected to vanish, and the detailed explanation has been given in Chapter 4.

7.2.1.1 $[0^{\circ}/90^{\circ}]_s$ laminate

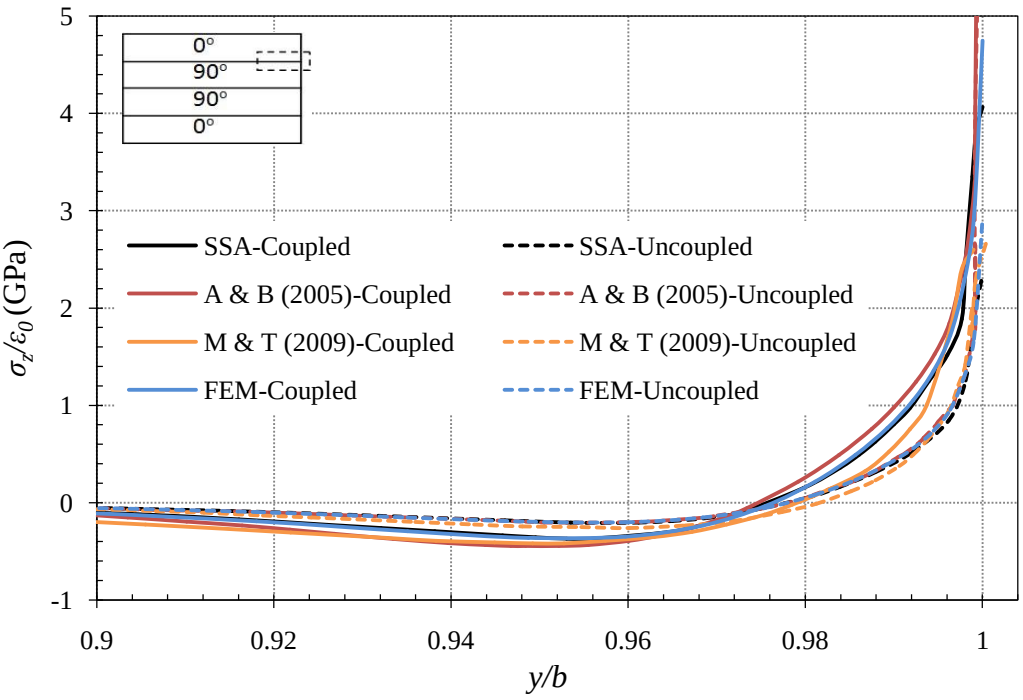

Figure 7.2: Distributions of interlaminar normal stress σ_z at the $0^{\circ}/90^{\circ}$ interface in the $[0^{\circ}/90^{\circ}]_s$ laminate

Distributions of stresses and electric field intensity components at the $0^{\circ}/90^{\circ}$ interface in a $[0^{\circ}/90^{\circ}]_s$ laminate are presented for the electromechanical coupled and uncoupled cases. The numerical results and comparison in Figure 7.2 illustrate that there is good agreement between present SSA results and those of Artel and Becker (2005), Mirzababaee and Tahani (2009) and FEM for the electromechanical coupled and uncoupled cases. It is interesting to note that SSA results and those of Artel and Becker (2005), Mirzababaee and Tahani (2009) and FEM provide similar distributions of the interlaminar normal stress for $y/b > 0.9$, and they also give close predictions in the inner region of the laminates. It is apparent from Figure 7.2 that the interlaminar normal stress σ_z shows a singular behaviour at the intersection of the interface and the free edge and ascends to a very large value at the free edge for the coupled and uncoupled cases. It is shown that for both coupled and

uncoupled cases the interlaminar normal stress σ_z is quite small in the interior region and then it reverses its sign to positive (tensile) and increases dramatically near the free edge. This notable behaviour of σ_z tends to contribute to the delamination of the laminated plate for not only the uncoupled case but also the coupled case. Moreover, as shown in this figure the interlaminar normal stress σ_z in the vicinity of the free edge in the coupled piezoelectric case is approximately two times larger than that in the uncoupled case. This significant gradient of σ_z indicates that the free-edge effect is more prominent in the piezoelectric laminate than the laminate without electromechanical coupling and this coupling effect has a significant influence on the 3D behaviour of interlaminar stresses near free edges.

The aforementioned solutions can provide the sufficiently accurate distribution of the interlaminar normal stress from the inner region up to $y/b = 0.98$ except in the vicinity of the free edge at a distance of about 2% (between $y/b = 0.98$ and $y/b = 1$) of the laminate. They also can capture a singular behaviour near the free edge or at the free edge, although the interlaminar normal stress values obtained at the singularity point are quite different from each other. Due to the singularity, the magnitude of σ_z at the $0^\circ/90^\circ$ interface-edge corners of laminates will continue to grow with the increasing value of P (Tahani and Nosier, 2003). In addition, the stress values around the singularity point are rendered meaningless because of the mesh dependence in 3D FE model (Carreira et al., 2002). Therefore, the maximum values of the interlaminar normal stress at the free edge obtained from different methods are impossible and inappropriate for comparison. Although the maximum value of the interlaminar normal stress at the singularity point is uncertain and can be any large finite value in the frame of different methods, the integral of the interlaminar stress σ_z over the y direction must be zero in order to maintain equilibrium of forces in the z direction. In the sense of mathematics, this behaviour is analogous to that of Dirac delta function. The delta function is sometimes thought of as an infinitely high and infinitely thin spike at the origin, with total area unit one under the spike. The behaviour of Dirac delta function gives a good explanation that in spite of any maximum value of the interlaminar normal stress σ_z at the singularity

point, the integral of zero over the *y* direction must be satisfied. Although the stress values at the singularity points are meaningless, the accurate description of the stress distributions in the vicinity of the free edge is essential and may provide the prediction of the possible failure for the coupled and uncoupled piezoelectric laminated plates. For instance, according to Lagunegrand et al. (2006) and Saeedi et al. (2012) there are the delamination stress criteria based on stress values at a specific distance from the singularity point or the average stress criteria considering the average of interlaminar stresses over a characteristic distance from the singularity point.

Since a stress singularity exists at the intersection of the interface and the free edge, this singular point presents difficulties in numerical and approximate analytical methods and those different methods certainly behave differently near such singular points in a small region. The differences in magnitude of the peak stress are expected, but not the difference in the sign (Whitcomb et al., 1982).

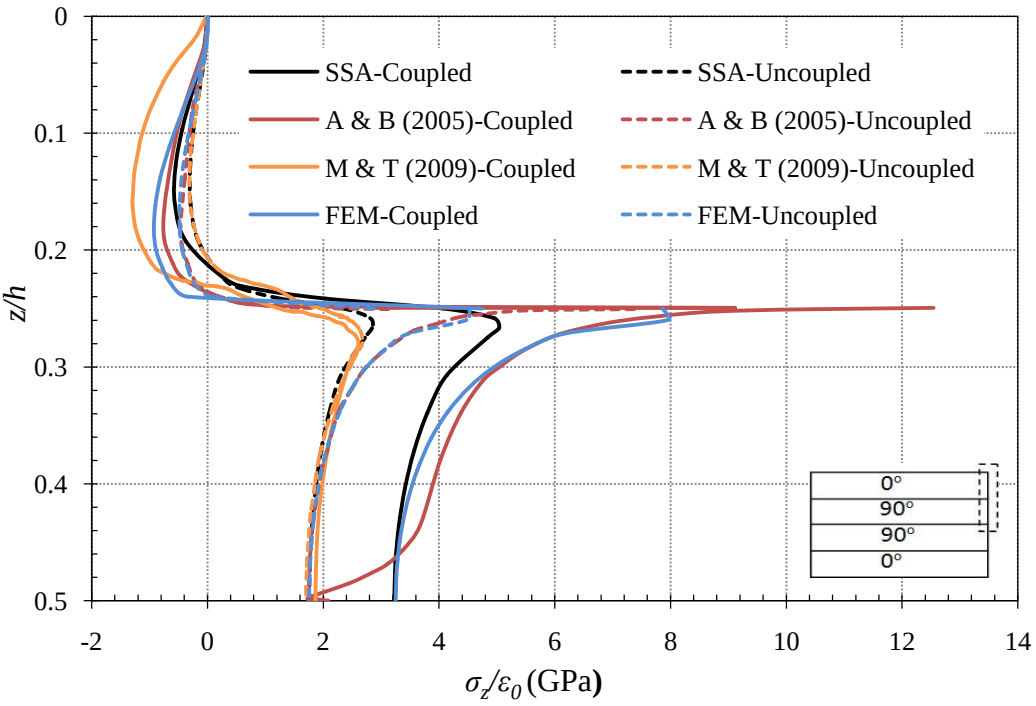

Figure 7.3: Variations of interlaminar normal stress σ_z through the thickness in the $[0^{\circ}/90^{\circ}]_s$ laminate along the free edge

The variations of the interlaminar normal stress σ_z through the thickness in a $[0^\circ/90^\circ]_s$ laminate along the free edge for the coupled and uncoupled cases are depicted in Figure 7.3. It is shown that the SSA uncoupled result is consistent with that of Mirzabaee and Tahani (2009) through the thickness while in decent agreement with the result of Artel and Becker (2005) and FEM through the thickness except for the region close to the interface at $z/h = 0.25$. From the result of Artel and Becker (2005) and FEM the interlaminar normal stress σ_z changes steeply in this small region and tends to approach the SSA result and that of Mirzabaee and Tahani (2009) away from the interface.

For the coupled cases, in general, there are decent agreements between the SSA result and those of Artel and Becker (2005), Mirzabaee and Tahani (2009) and FEM within the upper layer except at the interface ($0 \leq z/h < 0.25$). In the upper layer, the coupled result of Mirzabaee and Tahani (2009) is approximately two times larger than their uncoupled one while within the core layer ($0.25 \leq z/h \leq 0.5$), there is no difference between their coupled result and uncoupled one. However, it is clear from Figure 7.3 that unlike the description of Mirzabaee and Tahani (2009) even within the core layer ($0.25 \leq z/h \leq 0.5$) the coupled results of the SSA solution and Artel and Becker (2005) as well as FEM are at least approximately two times larger than the uncoupled ones, respectively. In addition, it is also worth to mention that the SSA coupled result is in decent agreement with that of FEM through the free edge. It is shown that not only does the piezoelectric effect have a remarkable influence on the free edge effect of the upper layer, but it also affects that of the core layer significantly.

Furthermore there are similarities between the coupled and uncoupled results of FEM and those of Artel and Becker (2005) because these analyses are both performed by using finite element method but with different types of element and mesh refinement. Even for the region close to the interface at $z/h = 0.25$, they both provide similar descriptions. However in the frame of the finite element method, both results cannot guarantee the continuity conditions of the interlaminar stress. As a result, it is clear from Figure 7.3 that for both results of FEM and Artel and Becker

(2005) the interlaminar normal stress σ_z exhibits discontinuous at the intersection of the interface and the free edge. Despite a refined mesh approach applied in the vicinity of the free edge and the interface of different layers for both analyses, such discrepancies in the finite element method cannot be eliminated. Theoretically, σ_z should be continuous due to the action-reaction at the interface of adjacent dissimilar layers. The FE method fails to give a continuous value of the stress because it is associated with the treatment to the nodal forces (average) in FE and a selection of integration points in the adjacent elements with free edges Nevertheless, the 3D finite element method is still a powerful alternative to the analytical solutions for the analysis of the interlaminar stress near the free edge and the interface in piezoelectric laminates, and the comparison between SSA results and those of FEM is valid and useful, in particular when there is no published results by other authors.

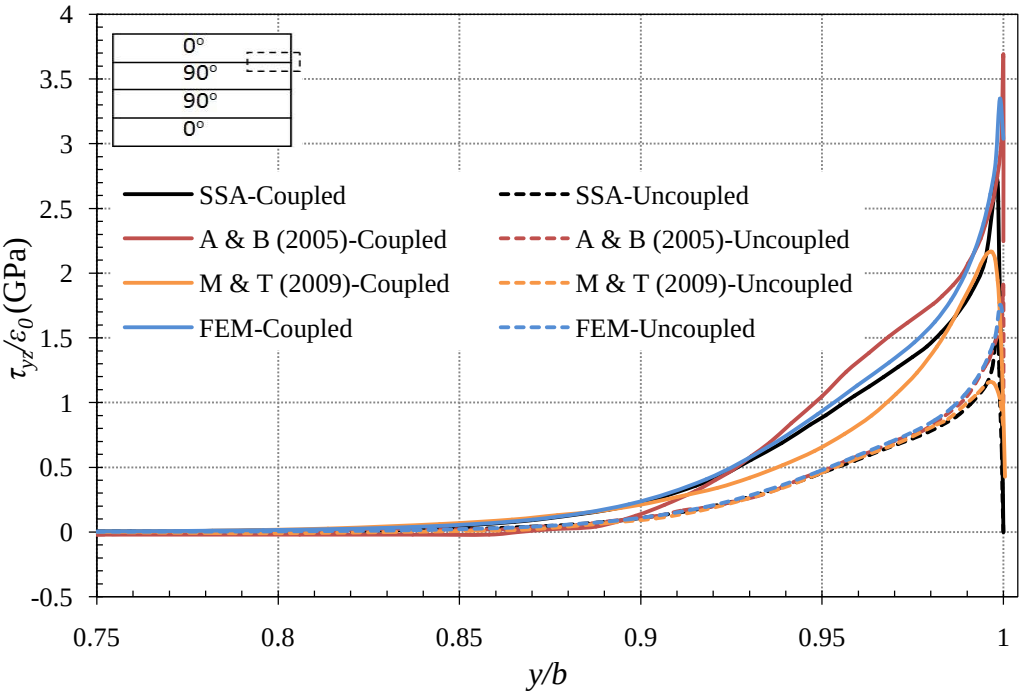

Figure 7.4: Distributions of interlaminar shear stress τ_{yz} at the $0^{\circ}/90^{\circ}$ interface in the $[0^{\circ}/90^{\circ}]_s$ laminate

Figure 7.4 above illustrates the distributions of the interlaminar shear stress τ_{yz} at the $0^{\circ}/90^{\circ}$ interface along the y coordinate in a $[0^{\circ}/90^{\circ}]_s$ laminate. Except for the region where the free-edge effect dominates ($0.99 \leq y/b \leq 1$), the SSA results agree with those of Artel and Becker (2005), Mirzababaee and Tahani (2009) and FEM for the electromechanical coupled and uncoupled cases. Analogous to the uncoupled cases, it is shown that in coupled cases the interlaminar shear stress τ_{yz} rises towards the free edge but decreases dramatically at the free edge. It is also observed from the plots that the SSA results and those of Mirzababaee and Tahani (2009) are smaller than those of Artel and Becker (2005) and FEM near the free edge for both coupled and uncoupled cases. Moreover, all the plots for the interlaminar shear stress τ_{yz} indicate that the result in the coupled analysis is qualitatively similar to that in the uncoupled analysis but approximately two times larger.

It should be noted that due to the traction free boundary conditions imposed on the free edges the interlaminar shear stress τ_{yz} must vanish at the free edges, which is observed from the SSA results. Contrary to expectations, this traction free boundary condition cannot be fulfilled in the results of Artel and Becker (2005), Mirzababaee and Tahani (2009) and FEM. The traction free boundary condition is satisfied except at the intersection of the interface and the free edge by the numerical models of Artel and Becker (2005) and FEM due to the significant stress gradients near the free edge. According to Whitcomb et al. (1982), the region of boundary condition violation is restricted to the two elements nearest to the singular point and this region can be made as small as desired through mesh refinement. Mirzababaee and Tahani (2009) mentioned that despite improvement in the number of sub-layers in each lamina, the numerical value of τ_{yz} may never become zero at the free edge. This phenomenon may be attributed to two reasons: (1) the generalized stress resultant rather than the interlaminar shear stress τ_{yz} is prescribed at the free edge in the formulations of FE method and Mirzababaee and Tahani (2009), thus the boundary condition is only satisfied in the sense of integral (resultant force); (2) the implementation of the shear deformation continuity at the free edge would lead to the stress discontinuity at the

interface of the dissimilar materials. The variations of the interlaminar shear stress τ_{yz} through the thickness in a $[0^{\circ}/90^{\circ}]_s$ laminate near the free edge are given in Figure 7.5. The singular points on the y-axis with respect to corresponding maximum numerical values of the interlaminar shear stress τ_{yz} in Figure 7.4 are different for the SSA results, and those of Mirzababaee and Tahani (2009) and FEM but all these singular points are very close and in a small range very near the free edge ($0.995b < y < b$). For the sake of comparison, $y = 0.999b$ is chosen for these results. The plots for τ_{yz} show that the results from FEM seem to be consistent with those of the SSA solution except in the regions very close to the interface of dissimilar layers for both coupled and uncoupled cases and they both exhibit significant stress gradients. However, the difference between the result of the SSA solution and FEM and that of Mirzababaee and Tahani (2009) is noticeable in the coupled cases.

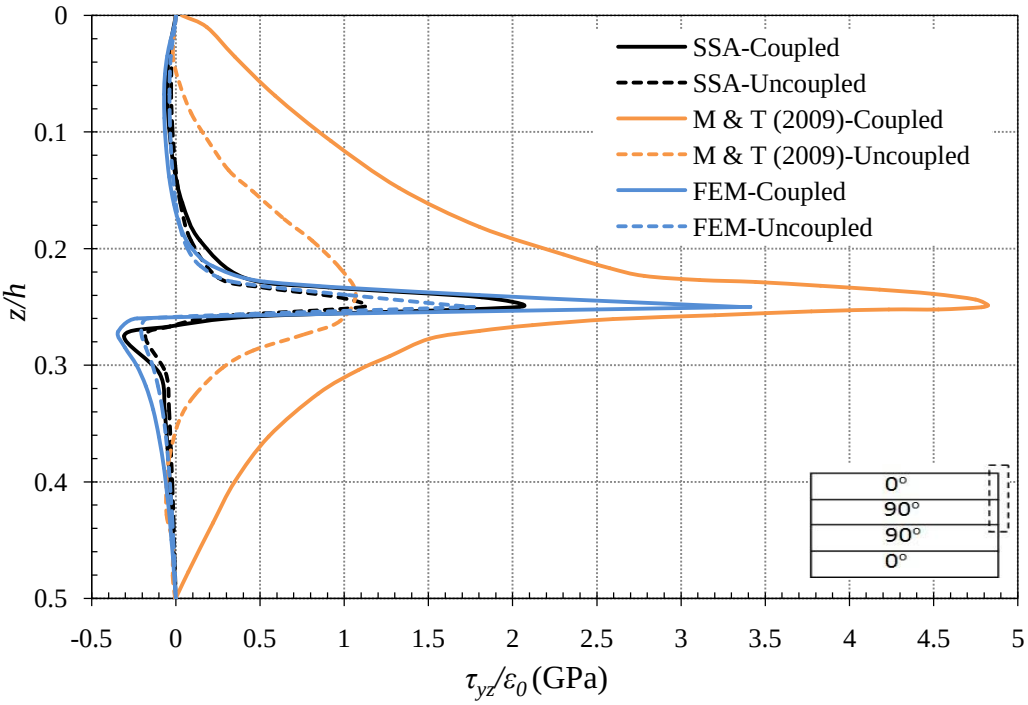

Figure 7.5: Variations of interlaminar shear stress τ_{yz} through the thickness in the $[0^{\circ}/90^{\circ}]_s$ laminate near the free edge at y =0.999b

From the plots for coupled cases in Figure 7.5, there is a significant difference between the result of Mirzababaee and Tahani (2009) and those of the SSA solution and FEM. For τ_{yz} Mirzababaee and Tahani (2009) showed approximately five times larger in the coupled case than the uncoupled one. The results of the SSA solution and FEM only gave about two times larger in the corresponding analyses. It should be mentioned that the maximum value of the interlaminar shear stress τ_{yz} along the interface from Mirzababaee and Tahani (2009) (Figure 7.4) is approximately half of their maximum value of τ_{yz} through the thickness (Figure 7.5). It is apparent that their results of τ_{yz} are not consistent in these two figures.

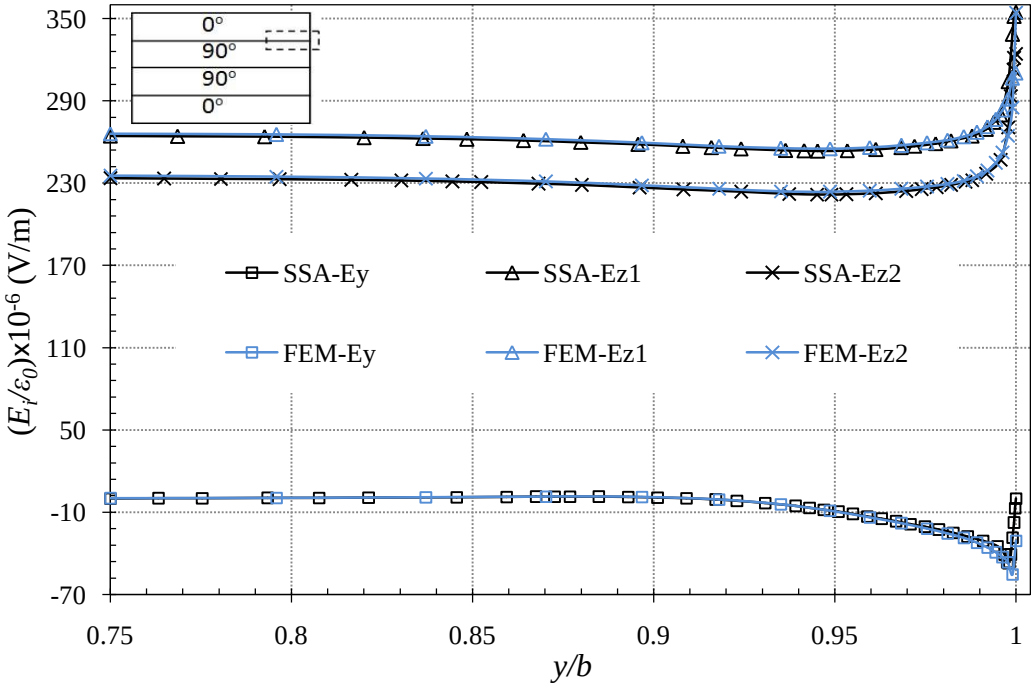

Figure 7.6: Distributions of electric field intensity components E_y and E_z at the $0^\circ/90^\circ$ interface in the $[0^\circ/90^\circ]_s$ laminate

It is observed that the interlaminar normal stress and shear stress exhibit significant stress gradients in the vicinity of the free edges for both coupled and uncoupled cases. Electrical quantities also may have singular behaviours and show such strong gradients near the intersection of the interface and the free edge. For an infinite long piezoelectric laminate in this study, it has been proved in Chapter 4 that the electric field intensity component E_x is zero. Therefore the remaining two electric field intensity components E_y and E_z are analyzed. Figure 7.6 illustrates the distributions of electric field intensity components E_y and E_z at the $0^\circ/90^\circ$ interface along the y coordinate in a $[0^\circ/90^\circ]_s$ laminate. The results from FEM are consistent with the SSA results and they both indicate strong electric field changes near the free edges for E_y and E_z.

Electric field intensity component E_y is quite small in the inner region where y/b is not larger than 0.9. Then it is growing gradually and increasing abruptly in a small region ($y/b \geq 0.99$). After approaching a finite value, E_y declines and seems to be vanishing at the free edge. The observed difference between the result from FEM and that of the SSA solution is not significant, however, it is still worth to mention that E_y in FEM shows a little bit more significant gradient than that in the present analysis very near the free edge and has a tendency to decrease to zero but attains a smaller finite value at the free edge. In the present analysis the electric field intensity component E_y vanishes at the free edge. It seems that there is a singularity in the immediate vicinity of the intersection of the interface and the free edge.

The electric field intensity component E_z in the SSA result and FEM result is discontinuous along the interfaces between 0° layer and 90° layer. In Figure 7.6, E_{z1} denotes electric field intensity component E_z at the bottom surface of layer-1 (0° layer) and E_{z2} denotes E_z at the top surface of layer-2 (90° layer). Unlike the distribution of E_y, E_z retains a high value in the inner region of the laminate along the interface and increases sharply, and attains a very large value at the intersection of the interface and the free edge.

The distributions of the electric field intensity components E_y and E_z along the interface are similar to those of the interlaminar stresses τ_{yz} and σ_z. They both show apparent gradients and singular behaviours at the intersection of the interface and the free edge. It should be noted that the SSA result disagreed with those of Artel and Becker (2005), and Mirzababaee and Tahani (2009) in magnitude. The SSA result and that of FEM are three orders of magnitude greater than those results from Artel and Becker (2005) and Mirzababaee and Tahani (2009) while the shapes of these plots are similar qualitatively.

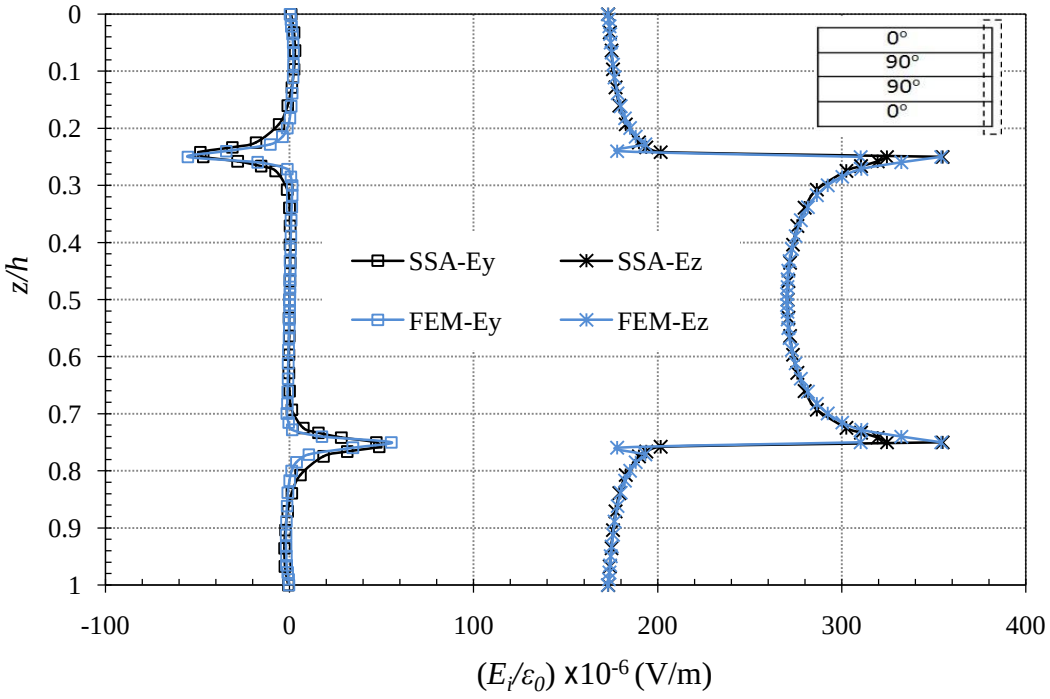

Figure 7.7: Variations of electric field intensity components E_y and E_z through the thickness in the $[0^{\circ}/90^{\circ}]_s$ laminate

Analogous to the variations of the interlaminar shear stress τ_{yz} through the thickness, the electric field component E_y at $y = 0.999b$ are chosen for the thickness distributions in the SSA result and that of FEM, respectively. It is shown that the electric field disturbance occurs at the interfaces (Figure 7.7). It is interesting to note that both the discontinuity and steep gradient of E_z are observed at the intersections of the interface and the free edge.

It should be noted that the discrepancy on the interlaminar normal stress σ_z emerges between the SSA solution and other aforementioned solutions when the free edge is approached. Similarly these discrepancies on the interlaminar shear stress τ_{yz} and the electric field intensity components E_y and E_z still exist in the immediate vicinity of intersection of the interface and the free edge, respectively. Despite these discrepancies on the interlaminar stresses and electric field intensity components, these solutions do capture the qualitative nature of distributions of those variables in the vicinity of the free edge.

7.2.1.2 $[90^{\circ}/0^{\circ}]_s$ laminate

The distributions of interlaminar stresses and electric field intensity components in a $[90^{\circ}/0^{\circ}]_s$ laminate are also illustrated for the electromechanical coupled and uncoupled cases. It is revealed from the comparisons in Figure 7.8 that the SSA results in coupled and uncoupled cases are consistent with those of Artel and Becker (2005), Mirzababaee and Tahani (2009) and FEM.

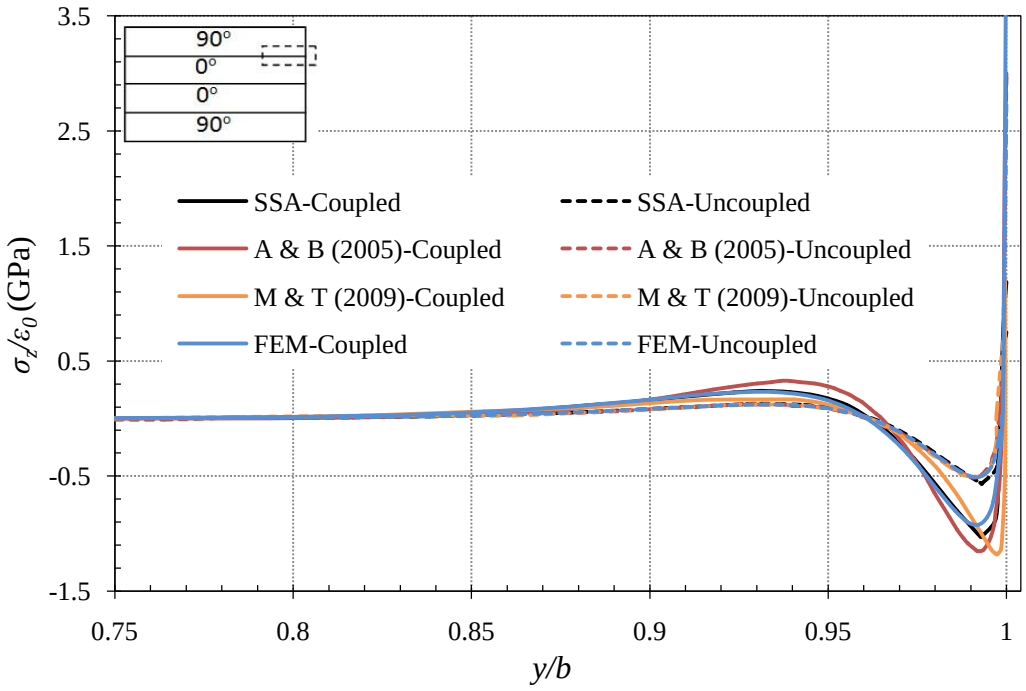

Figure 7.8: Distributions of interlaminar normal stress σ_z at the 90°/0° interface in the $[90^\circ/0^\circ]_s$ laminate

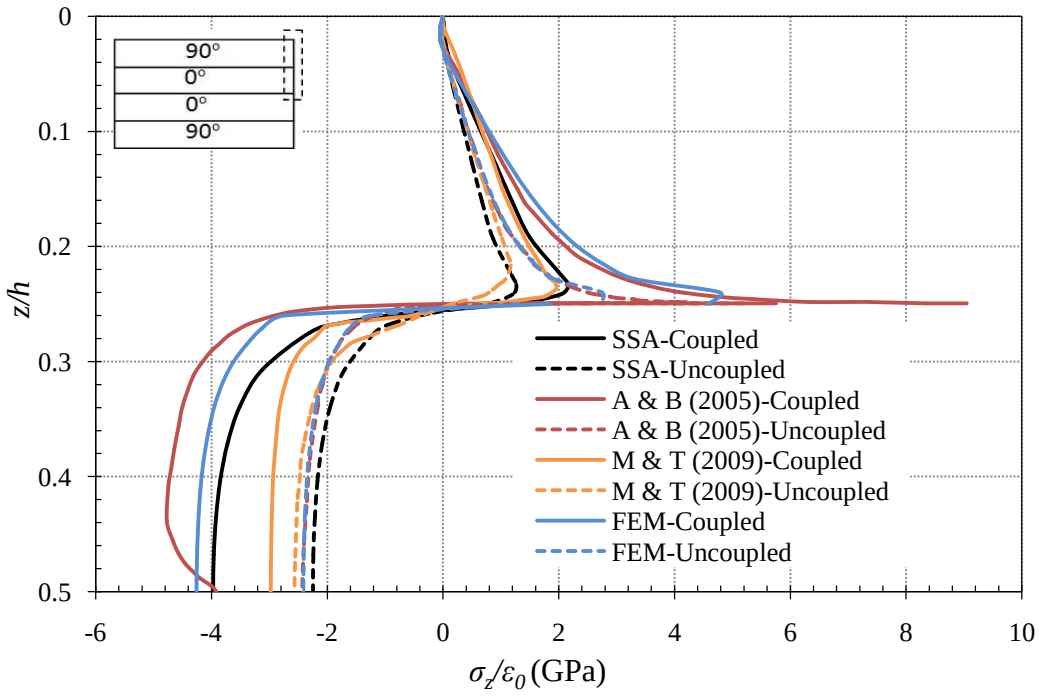

Figure 7.9: Variations of interlaminar normal stress σ_z through the thickness in the $[90^\circ/0^\circ]_s$ laminate along the free edge

Similar to the distribution of the interlaminar normal stress σ_z in $[0^\circ/90^\circ]_s$, σ_z in $[90^\circ/0^\circ]_s$ is small in the inner region of a laminate and also converts its sign to positive and ascends abruptly very near the free edge, and then reaches a finite value at the free edge for both coupled and uncoupled cases. It is shown that σ_z tends to increase in negative when $y > 0.95b$, and attains a higher negative value than that in $[0^\circ/90^\circ]_s$. It is found that the interlaminar normal stress gradient in $[90^\circ/0^\circ]_s$ is more significant than that in $[0^\circ/90^\circ]_s$. Also the interlaminar normal stress in the vicinity of the free edge in the coupled case is approximately two times larger than that in the uncoupled one.

For both coupled and uncoupled cases, the interlaminar normal stresses in the analyses of Artel and Becker (2005) and FEM exhibit stronger gradients than those in the analysis of the SSA solution and Mirzabaee and Tahani (2009) when the interface is approached (Figure 7.9). Except for the region close to the interface, decent agreements between the present results and other results are observed.

As mentioned above, the free-edge effect is prominent in the vicinity of the intersection of the interface and the free edge. The distributions of the interlaminar shear stress τ_{yz} at the $90^\circ/0^\circ$ interface along the *y* direction in Figure 7.10 illustrate that the stress disturbance occurs near the free edge. The coupled and uncoupled results in the present analysis are in general agreement with those in other analyses. Also the results in $[90^\circ/0^\circ]_s$ are quantitatively similar to those in $[0^\circ/90^\circ]_s$ while having opposite signs. Moreover, the interlaminar shear stresses with respect to different possible singular points along the *y* coordinate are different and for comparison the variations of these stresses through the thickness at y =0.999b are plotted in Figure 7.11. It is clear from these two figures that the interlaminar shear stresses in the coupled analysis are qualitatively similar to those in the uncoupled analysis but approximately twice larger.

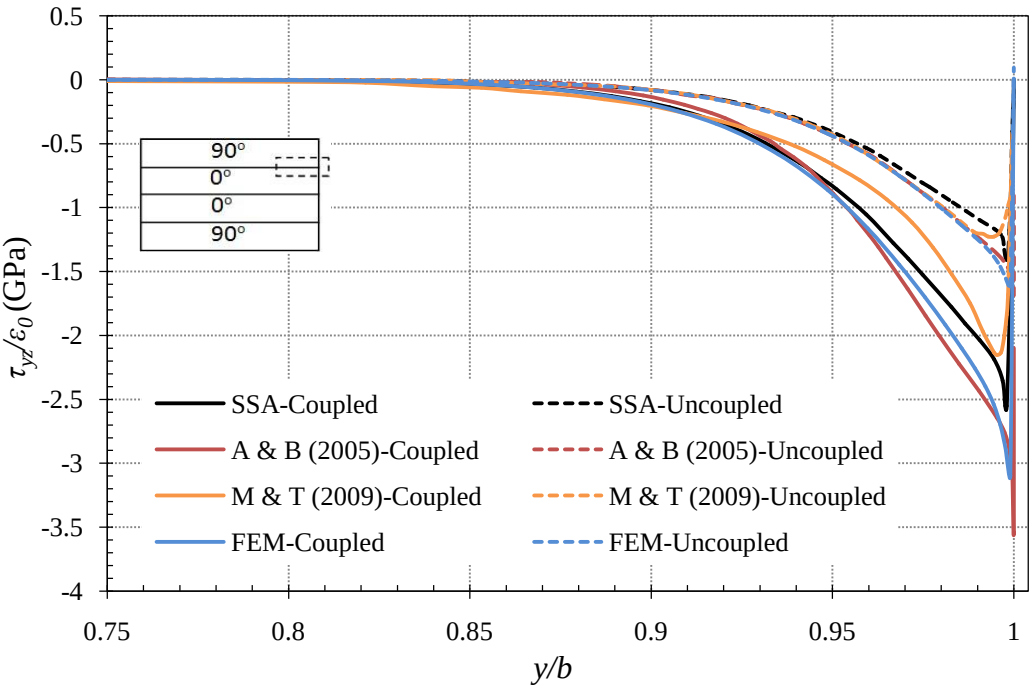

Figure 7.10: Distributions of interlaminar shear stress τ_{yz} at the $90^{\circ}/0^{\circ}$ interface in the $[90^{\circ}/0^{\circ}]_s$ laminate

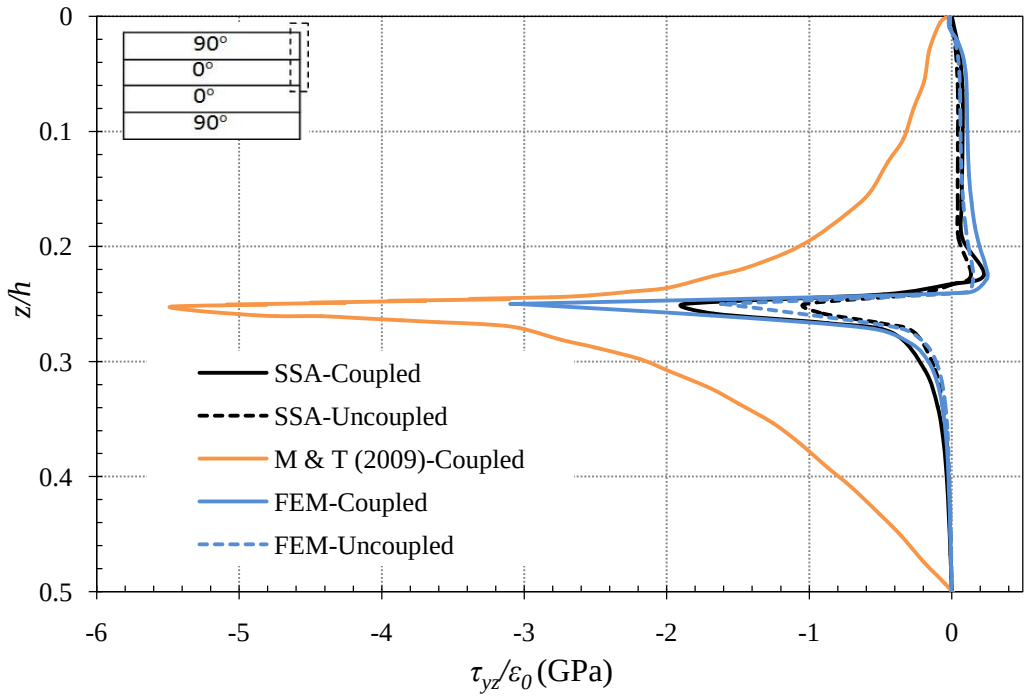

Figure 7.11: Variations of interlaminar shear stress τ_{yz} through the thickness in the $[90^{\circ}/0^{\circ}]_s$ laminate at $y = 0.999b$

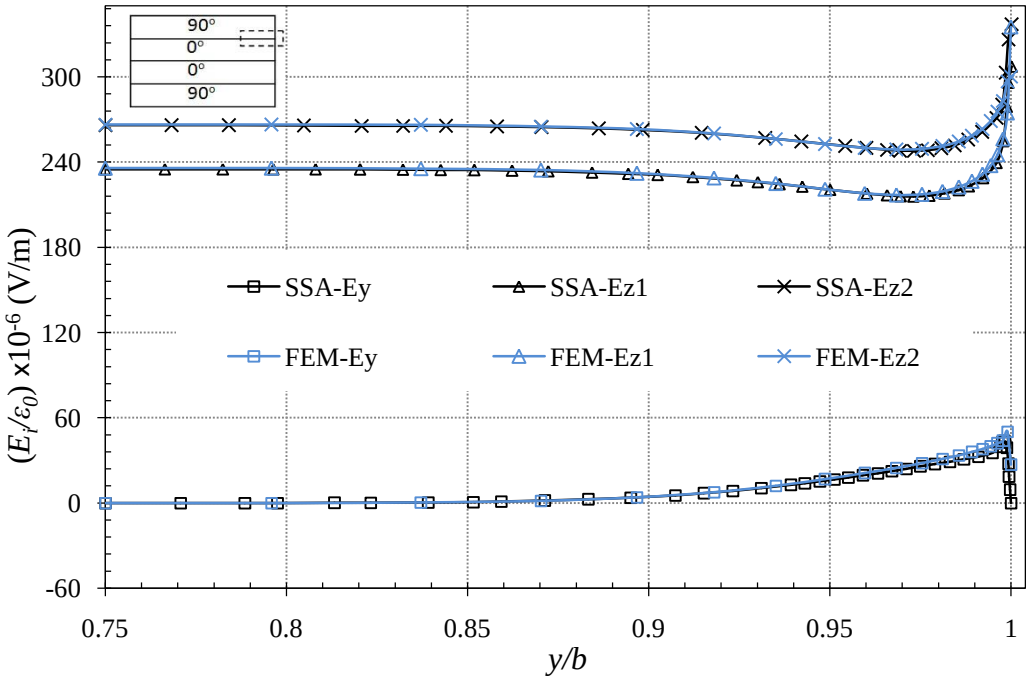

Figure 7.12: Distributions of electric field intensity components E_y and E_z at the $90^{\circ}/0^{\circ}$ interface in the $[90^{\circ}/0^{\circ}]_s$ laminate

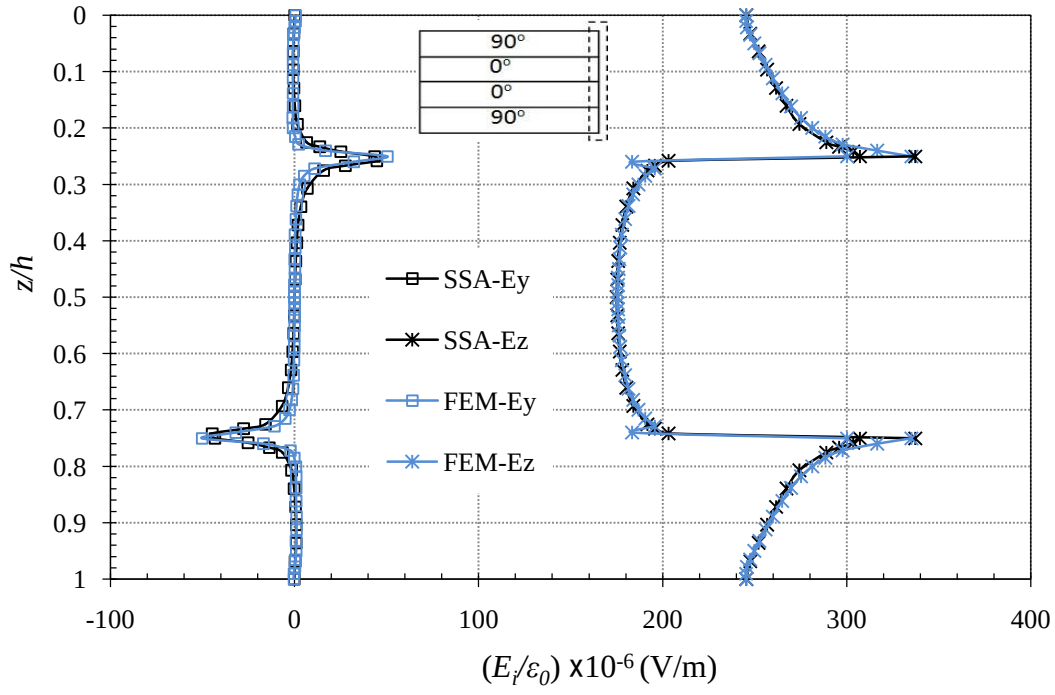

Figure 7.13: Variations of electric field intensity components E_y and E_z through the thickness in the $[90^{\circ}/0^{\circ}]_s$ laminate

There are good agreements between the electric field intensity components E_y and E_z in the present analysis and those obtained by FEM. In addition possible singularities can be found near the intersections of the interface and the free edge as depicted in Figures 7.12 and 7.13.

The comparisons between the SSA results using the non-uniform layer refinement and other published and FEM results for the $[0^\circ/90^\circ]_s$ and $[90^\circ/0^\circ]_s$ piezoelectric laminates demonstrate that the singularity arises from the vicinity of the interface and the free edge. It is apparent that the SSA results show good agreement with other results except for the region very near the free edge where some differences are observed from the variations of interlaminar stresses and electric field intensity components through the thickness. These differences become more notable in a small region ($0.98 \leq y/b \leq 1$) where the free edge effect plays a dominant role. Thus to get an in-depth understanding of the electromechanical and free edge effects on the stress and electric fields, the through thickness variations of interlaminar stresses and electric field intensity components with respect to different y near the free edge in the $[0^\circ/90^\circ]_s$ laminate are illustrated in Figures 7.14 and 7.15.

The comparison between the SSA and FEM results indicates that the discrepancies become more significant for both interlaminar stresses and electric field intensity components when the free edge is approached. It is shown that when $y \geq 0.999b$, these discrepancies appear noticeable. It is also interesting to note that the interlaminar normal stress σ_z in the analysis of FEM is discontinuous at the interface between dissimilar material layers. Although this discontinuity at the interface is negligible in the inner region of a laminate even in a small region $0.98 \leq y/b < 0.999$, it is becoming prominent and cannot be neglected at the free edge (Figure 7.14 (a)).

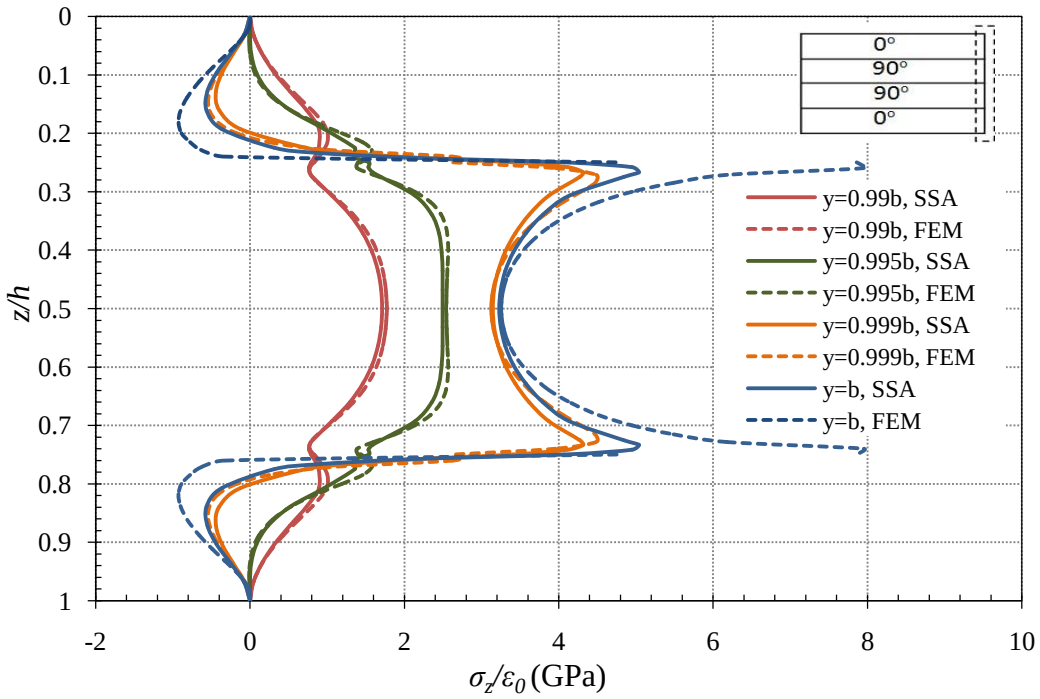

(a)

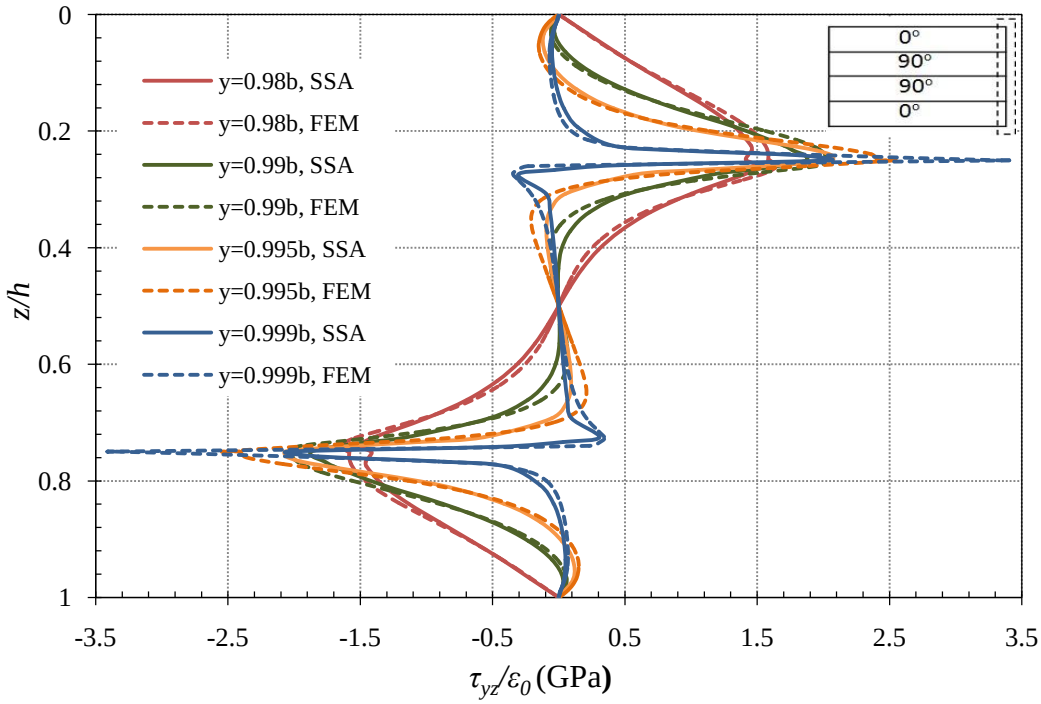

(b)

Figure 7.14: Variations of interlaminar stresses through the thickness in the $[0^{\circ}/90^{\circ}]_s$ laminate

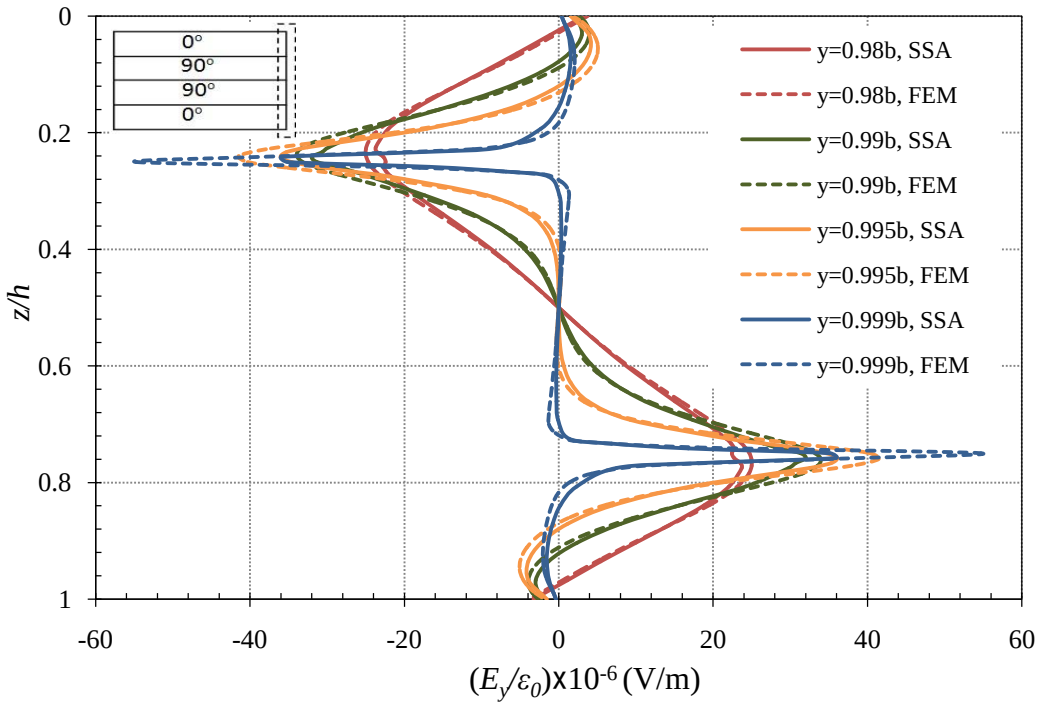

(a)

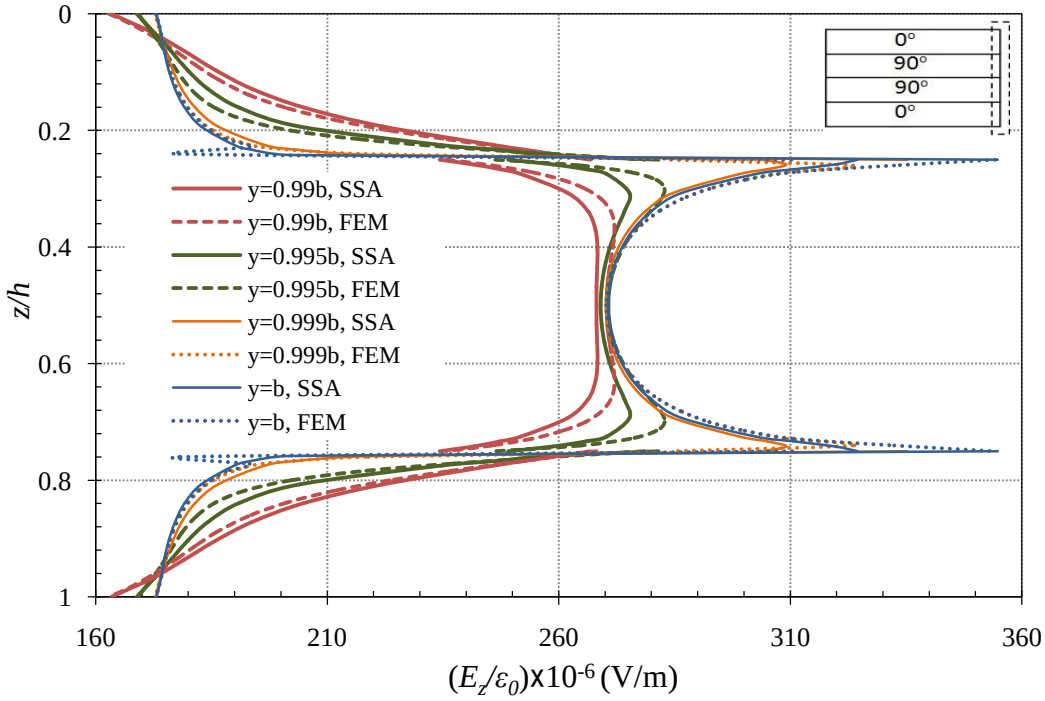

(b)

Figure 7.15: Variations of electric field intensity components through the thickness in the $[0^{\circ}/90^{\circ}]_s$ laminate

The free-edge and electromechanical coupling effects on the symmetric cross-ply piezoelectric laminates have drawn intense attention recently and the extensive investigation on these effects has been conducted in this thesis. Although the finite element models like Artel and Becker (2005) and FEM can demonstrate significant stress and electric field gradients with an enhanced mesh refinement in the vicinity of the free edge, they have difficulties in satisfying continuity conditions of interlaminar stresses at interfaces and fulfilling traction-free boundary conditions at free edges. Compared with published numerical and analytical models, the present models can capture the steep variations of interlaminar stresses and electric fields and also guarantee the continuity conditions and traction-free boundary conditions. Moreover, to obtain a more accurate description of the free-edge and electromechanical coupling effects, the non-uniform layer refinement technique proposed in Chapter 5 was adopted. With more mathematical sub-layers towards the interface of two different adjacent physical layers, the small region near the interface is relatively refined, leading to a more accurate prediction of the stresses and electric fields distributions.

7.2.2 Influence of stacking sequences in cross-ply laminates

To evaluate the influence of stacking sequence on the interlaminar stresses and electric field intensity components, the analyses of unsymmetric cross-ply $[0^\circ/90^\circ/0^\circ/90^\circ]$ and $[90^\circ/90^\circ/90^\circ/0^\circ]$ piezoelectric laminates are carried out. Since there are no published analytical or numerical solutions available, the present analytical results from SSA are illustrated in comparison with the finite element solution obtained by FEM. Specifically, the $0^\circ/90^\circ$ interface between the first and second layers in a $[0^\circ/90^\circ/0^\circ/90^\circ]$ laminate and the $90^\circ/0^\circ$ interface between the third and fourth layers in a $[90^\circ/90^\circ/90^\circ/0^\circ]$ laminate are investigated with and without electromechanical coupling.

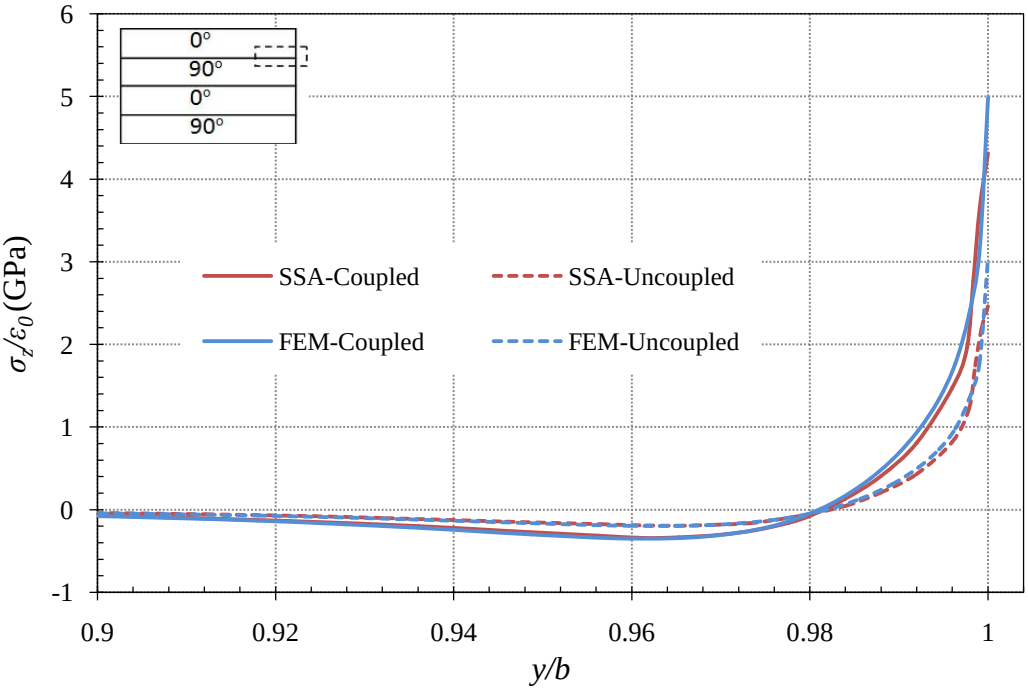

(a) [0˚/90˚/0˚/90˚]

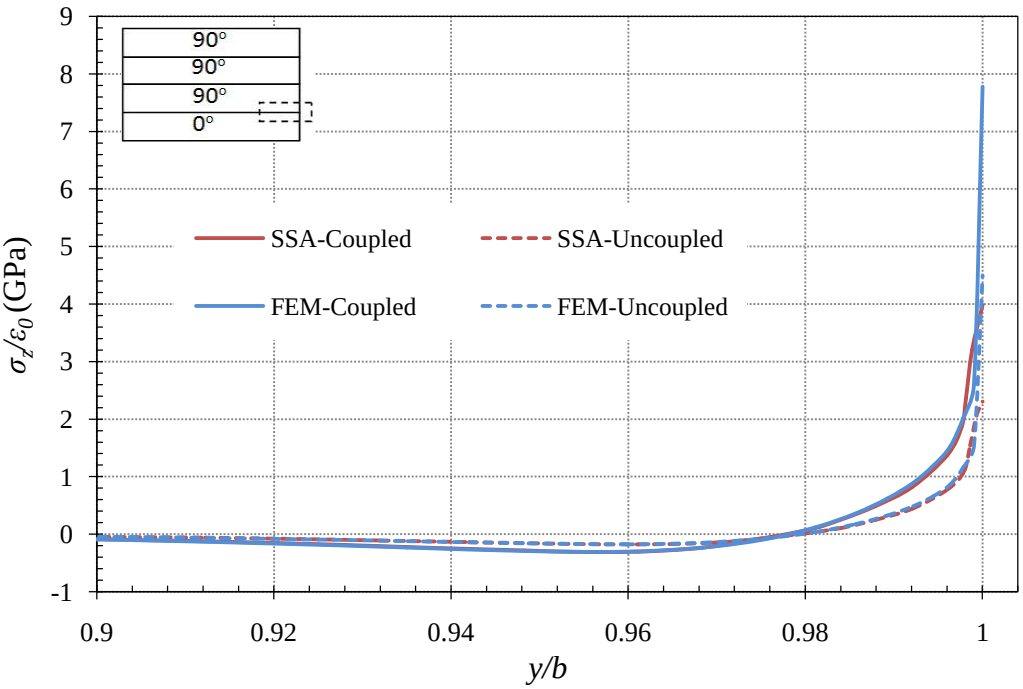

(b) [90˚/90˚/90˚/0˚]

Figure 7.16: Distributions of interlaminar normal stress σ_z at the interfaces in the [0˚/90˚/0˚/90˚] and [90˚/90˚/90˚/0˚] laminates

The plots shown in Figure 7.16 display behaviours of the interlaminar normal stress σ_z at the interfaces in the $[0^\circ/90^\circ/0^\circ/90^\circ]$ and $[90^\circ/90^\circ/90^\circ/0^\circ]$ laminates. As shown in this figure, σ_z in the electromechanical coupled analysis is larger than that in the uncoupled one. It is found that the interlaminar normal stress retains tensile and increases rapidly in the vicinity of the free edge at the interface for the $[0^\circ/90^\circ/0^\circ/90^\circ]$ and $[90^\circ/90^\circ/90^\circ/0^\circ]$ laminates while the maximum interlaminar normal stress of the $[0^\circ/90^\circ/0^\circ/90^\circ]$ laminate in the coupled case at the free edge is larger than those of other laminates. It appears that due to the existence of a higher interlaminar normal stress in tension the antisymmetric $[0^\circ/90^\circ/0^\circ/90^\circ]$ laminate is a little bit more vulnerable to delamination than other laminate configurations.

The effect of stacking sequences on the interlaminar normal stress can be observed from the through-thickness variations in Figure 7.17. It is found that the stress gradients occur near the intersections of the interface and the free edge and the value of the interlaminar normal stress tends to decline away from the free edge. As mentioned before, in contrast to the SSA result, the finite element solution cannot guarantee the continuity of the interlaminar normal stress at the interface between dissimilar material layers and more significant discontinuities are captured at the intersections of the interface and the free edge. In spite of this deficiency, the discontinuity of the interlaminar normal stress in the finite element solution is illustrated to be negligible away from the free edge from this figure. As a result, the discrepancies between the SSA results and those of FEM are reduced and good agreement is observed.

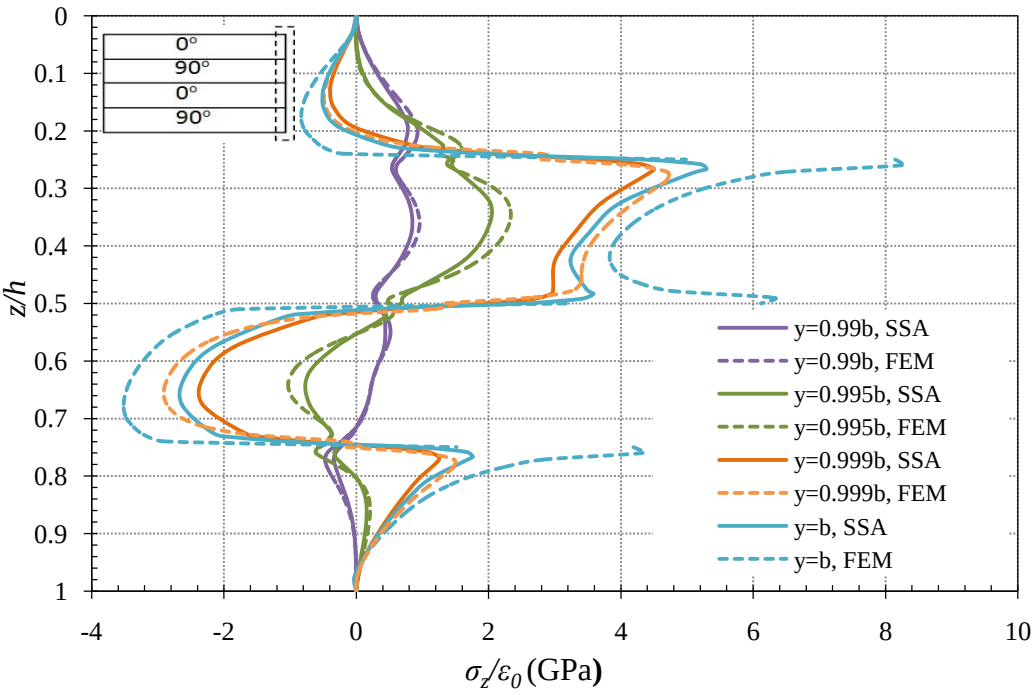

(a) [0°/90°/0°/90°]

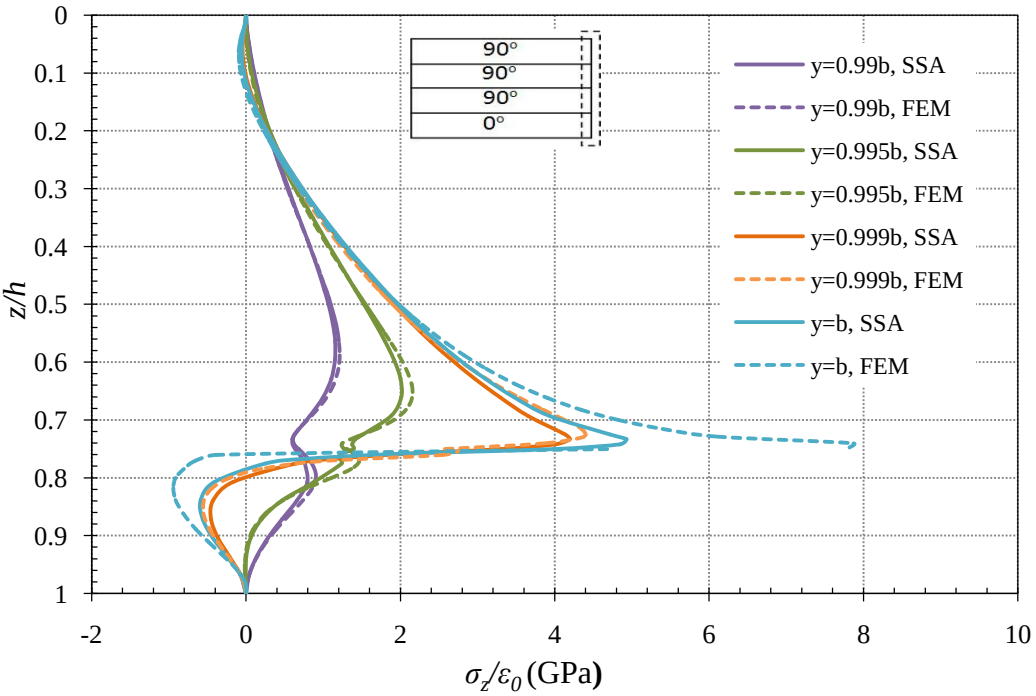

(b) [90°/90°/90°/0°]

Figure 7.17: Variations of interlaminar normal stress σ_z through the thickness in the [0°/90°/0°/90°] and [90°/90°/90°/0°] laminates

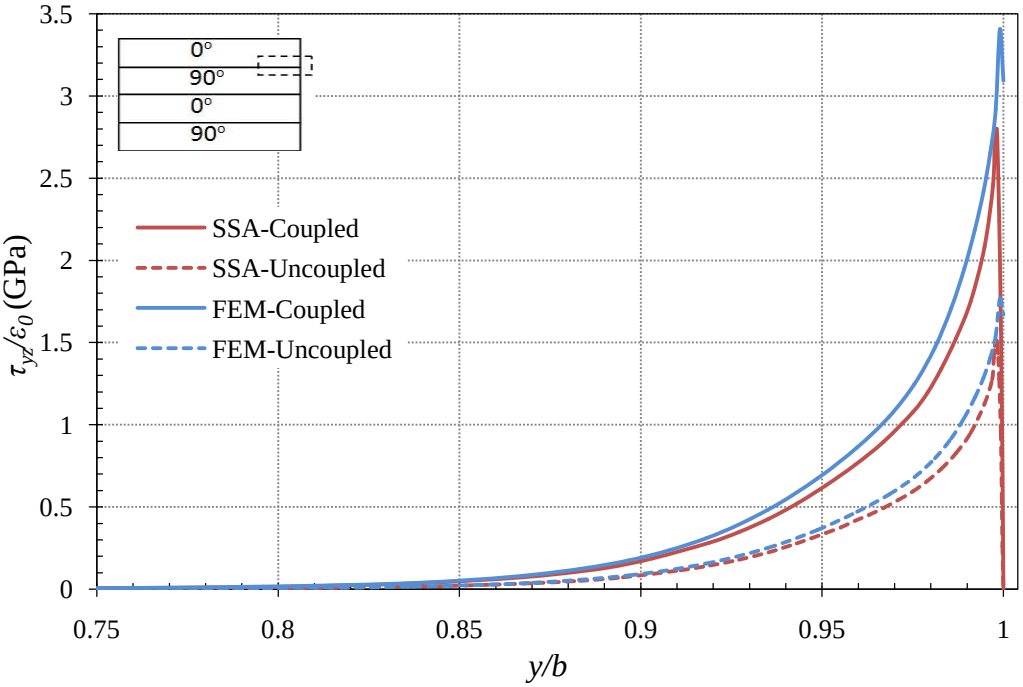

(a) [0°/90°/0°/90°]

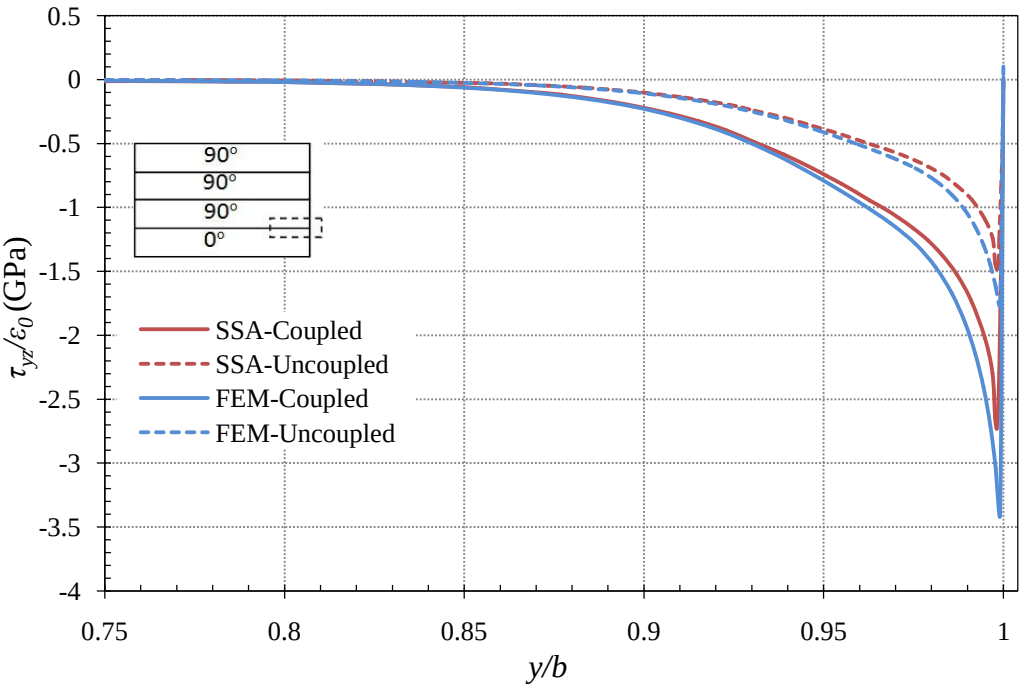

(b) [90°/90°/90°/0°]

Figure 7.18: Distributions of interlaminar shear stress τ_{yz} at the interfaces in the [0°/90°/0°/90°] and [90°/90°/90°/0°] laminates

As depicted in Figure 7.18, the interlaminar shear stress disturbance occurs near the free edge for both $[0^\circ/90^\circ/0^\circ/90^\circ]$ and $[90^\circ/90^\circ/90^\circ/0^\circ]$ laminates with and without electromechanical coupling. The SSA coupled results are approximately twice than the uncoupled ones. Although there are some differences in the interlaminar shear stress near the free edge between the SSA results and those of FEM, these differences tend to be reduced and consistent results can be obtained away from the singular points in this figure.

This finding can also be verified from the variations of the interlaminar shear stress through the thickness with respect to y in Figure 7.19. It is apparent that there are noticeable discrepancies within small regions very close to the intersections of the interface and the free edge but these discrepancies are reduced when *y/b* is smaller. Similar to the interlaminar normal stress, the singular problems of the interlaminar shear stress near the interfaces as well as the free edges lead to the redistributions of this stress through the thickness.

It is clear that the SSA solutions predict strong electric field gradients near the intersection of the interface and the free edge for E_y and E_z. Distinctive distributions of electric field intensity components across the thickness are illustrated in Figures 7.20 and 7.21. For the $[0^\circ/90^\circ/0^\circ/90^\circ]$ and $[90^\circ/90^\circ/90^\circ/0^\circ]$ laminates, noticeable electric field gradients are observed at the physical interfaces of dissimilar material layers.

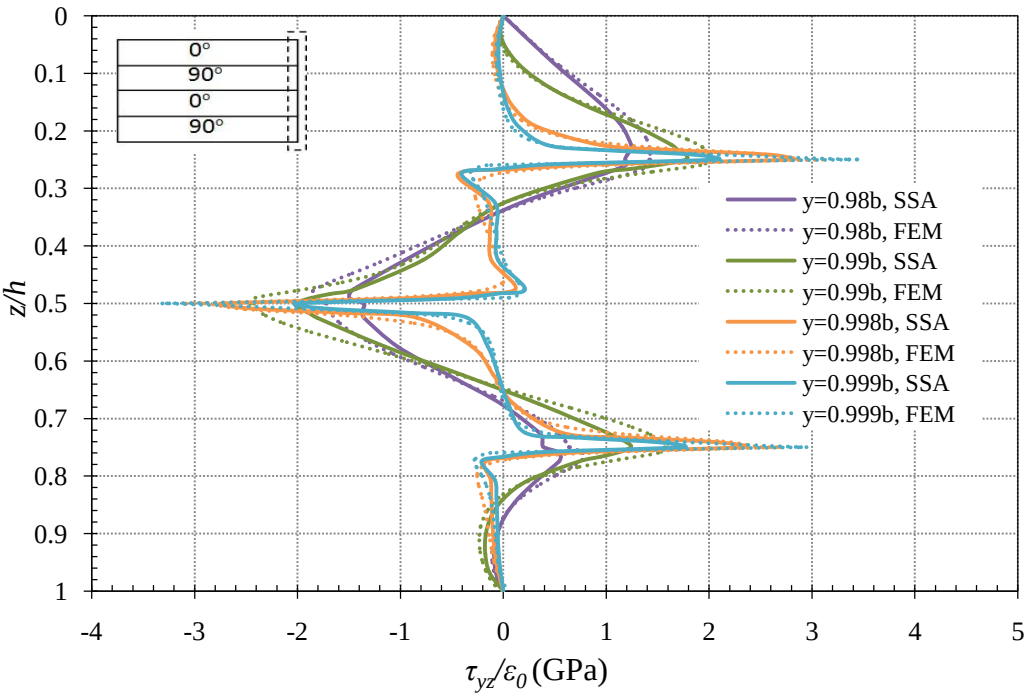

(a) [0°/90°/0°/90°]

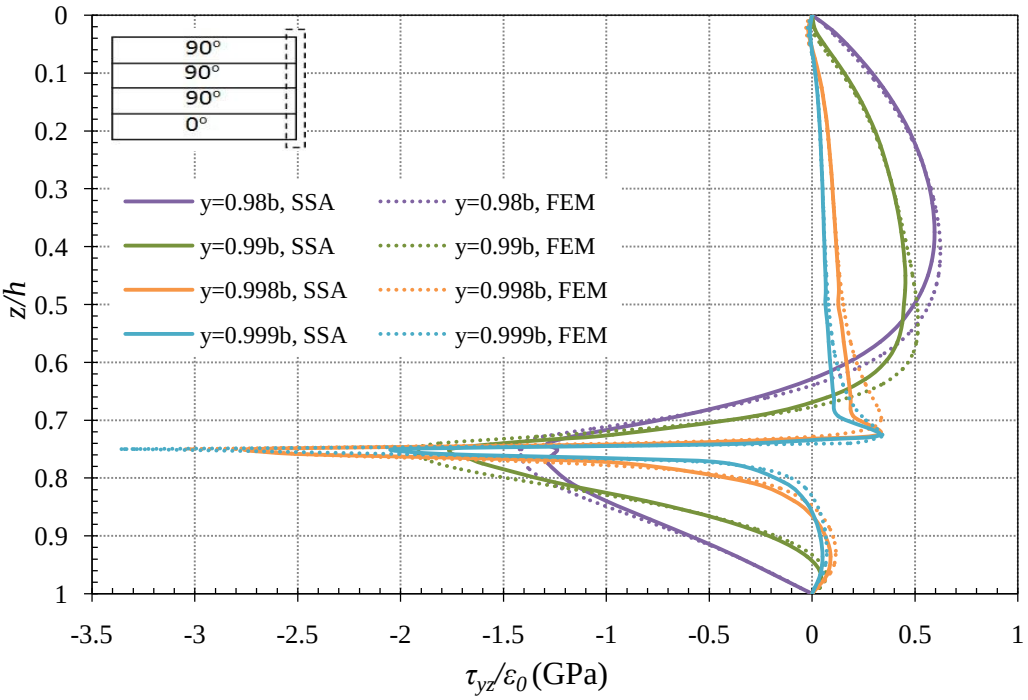

(b) [90°/90°/90°/0°]

Figure 7.19: Variations of interlaminar shear stress τ_{yz} through the thickness in the [0°/90°/0°/90°] and [90°/90°/90°/0°] laminates

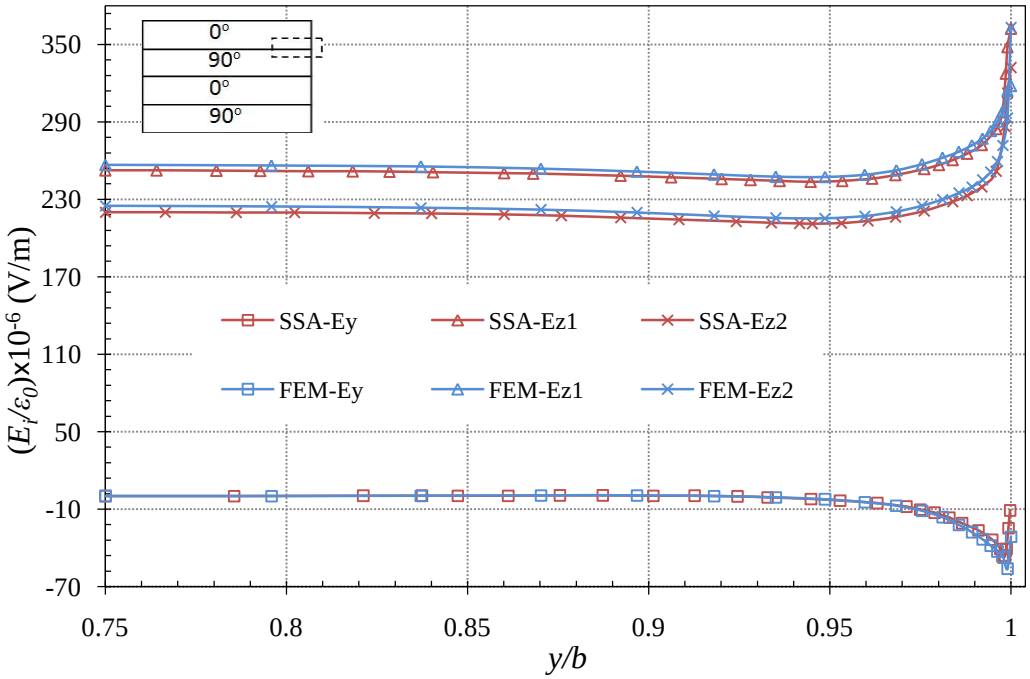

(a) [0°/90°/0°/90°]

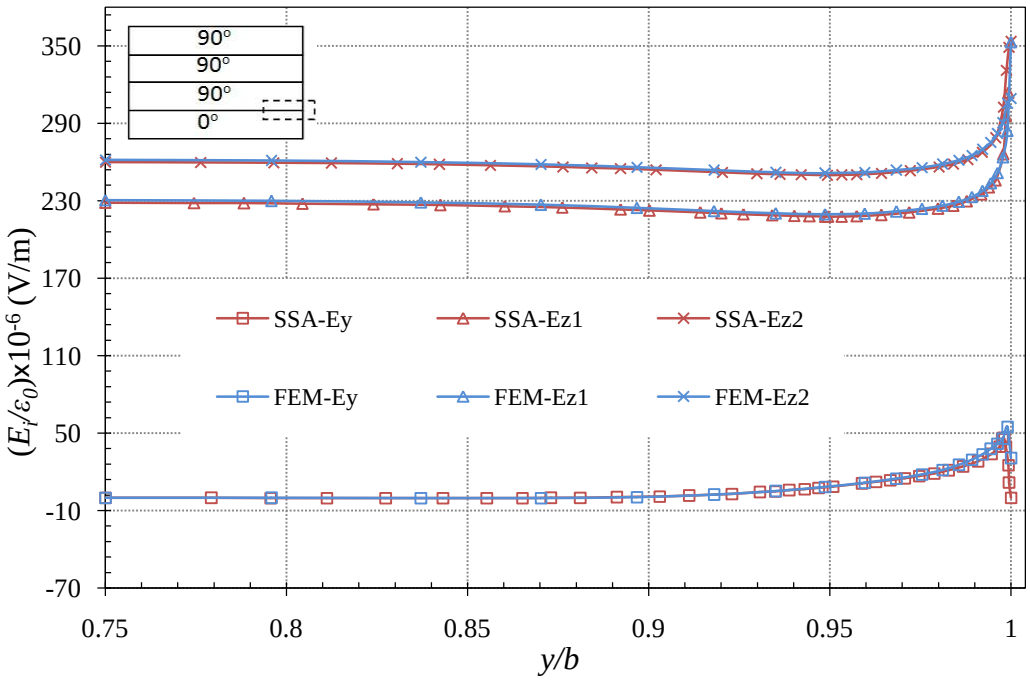

(b) [90°/90°/90°/0°]

Figure 7.20: Distributions of electric field intensity components E_y and E_z at the interfaces in the [0°/90°/0°/90°] and [90°/90°/90°/0°] laminates

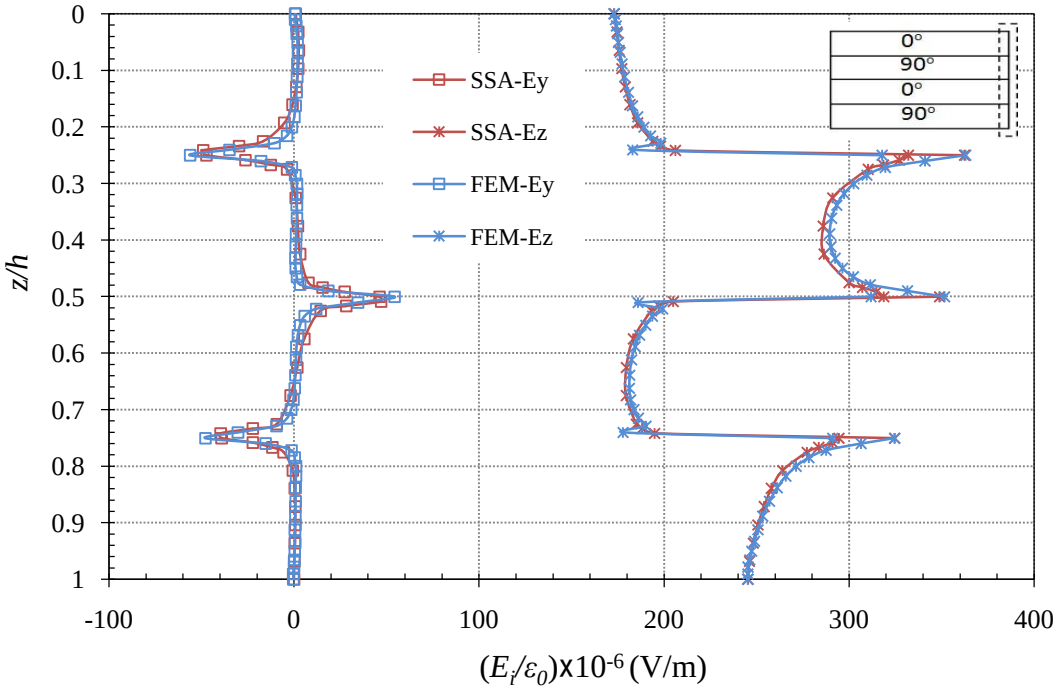

(a) [0°/90°/0°/90°]

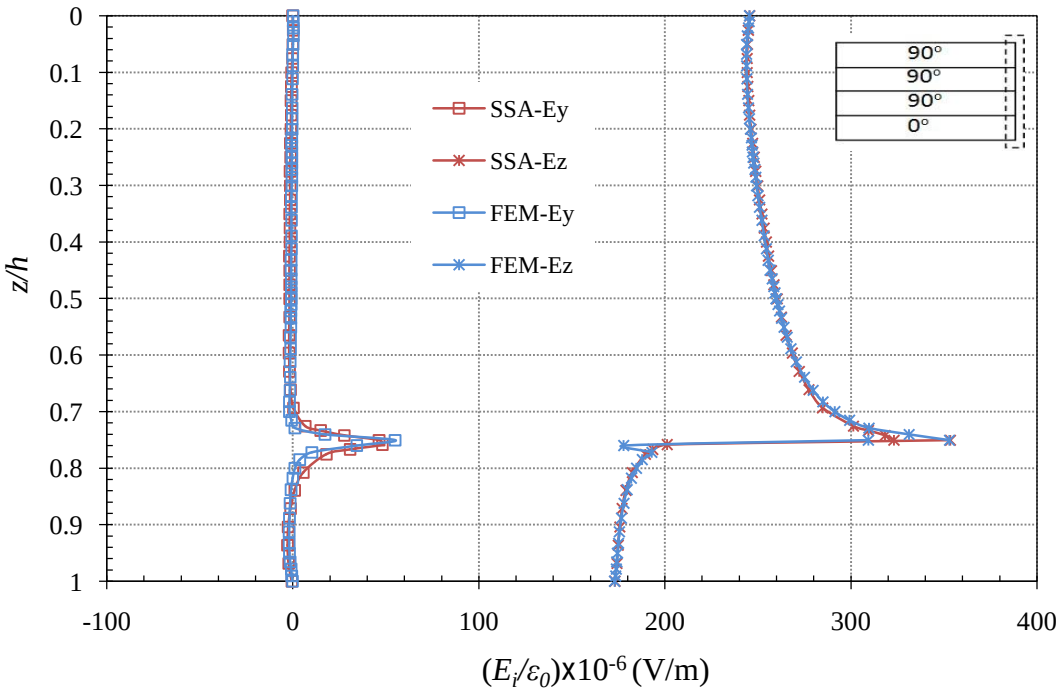

(b) [90°/90°/90°/0°]

Figure 7.21: Variations of electric field intensity components E_y and E_z through the thickness in the [0°/90°/0°/90°] and [90°/90°/90°/0°] laminates

7.3 Investigations on closed-circuit surface condition

As primary variables, the state vectors preserved in the state equations directly represent the mechanical and electric surface conditions on the top and bottom surfaces. When the closed-circuit conditions are imposed on the top and bottom surfaces, the state vector on the top surface can be solved by using the transfer matrix, recursive solution approach and continuity conditions between layers of the laminate.

Considering the relationship between the state vector of an arbitrary layer and that of the top surface, any state variable can be expressed in terms of the unknown boundary coefficients contained in the non-homogeneous vector. Once the mechanical and electric boundary conditions at the free edges are given, the unknown boundary coefficients can be determined by solving the corresponding algebraic equations.

As discussed above, the closed-circuit electric surface conditions are applied on the top and bottom surfaces of the four-layered laminate and there are four traction-free boundary conditions for this laminate: two free edges at $y=0$ and $y=b$, and two top and bottom surfaces at $z=0$ and $z=h$. Moreover, for the four layered laminate the length is assumed to be sufficiently long in the x-axis, and width b is chosen ten times larger than the thickness h, and the thickness of each layer in the laminate is identical.

Similarly, four stacking sequences: $[0^\circ/90^\circ]_s$, $[90^\circ/0^\circ]_s$, $[0^\circ/90^\circ/0^\circ/90^\circ]$ and $[90^\circ/90^\circ/90^\circ/0^\circ]$ with electromechanical coupling are considered and each laminate is subjected to a uniform axial strain ε_0. The mechanical and electrical material properties are given in Table 5.9. Additionally, the same abbreviation in Chapter 5 is used, and L1, L2, L3 and L4 are chosen to denote the four stacking sequences: $[0^\circ/90^\circ]_s$, $[90^\circ/0^\circ]_s$, $[0^\circ/90^\circ/0^\circ/90^\circ]$ and $[90^\circ/90^\circ/90^\circ/0^\circ]$, respectively.

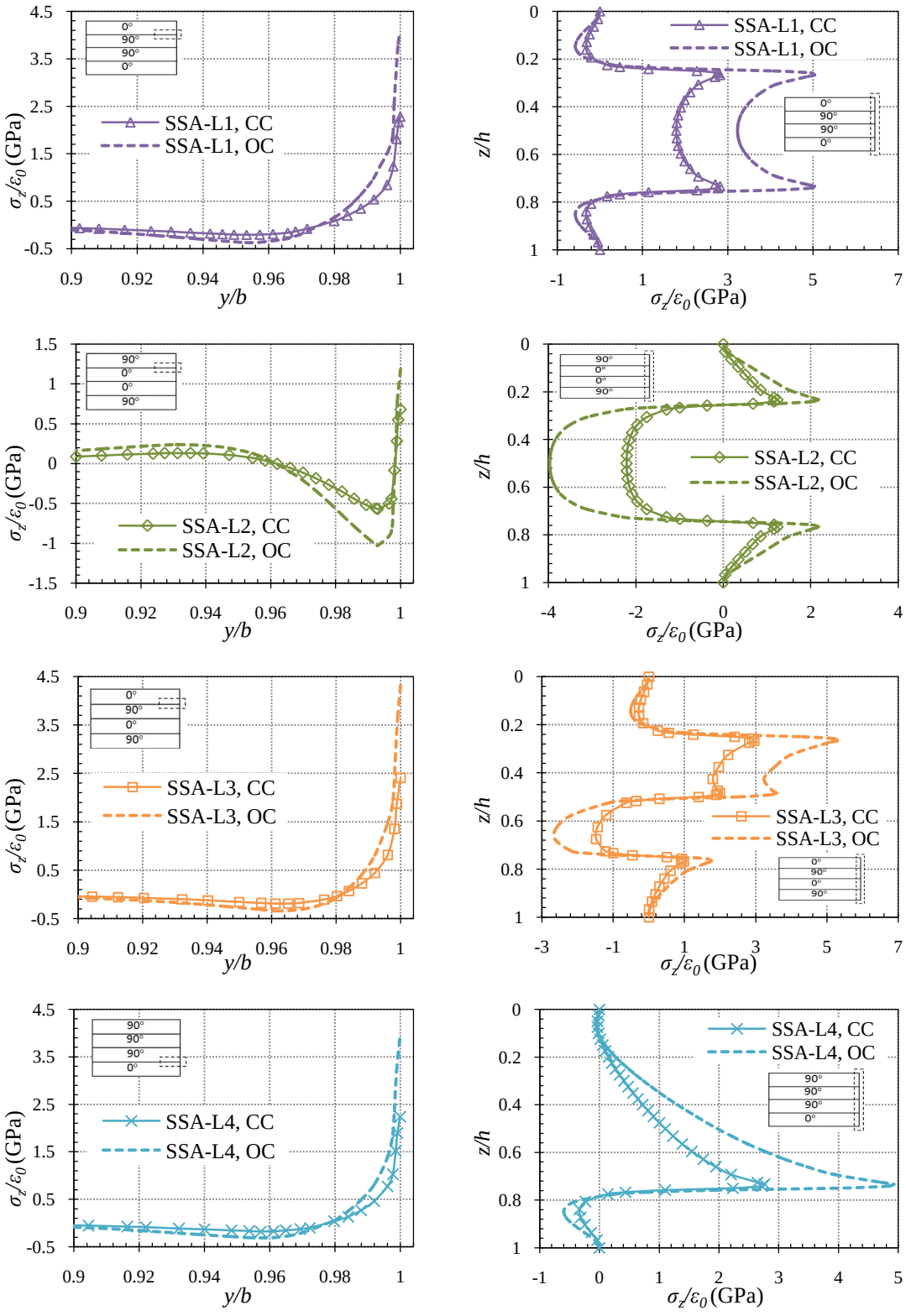

Figure 7.22: Variations of interlaminar normal stress σ_z along the interface (left) and through the thickness (right) in general cross-ply piezoelectric laminates under closed-circuit (CC) and open-circuit (OC) surface conditions

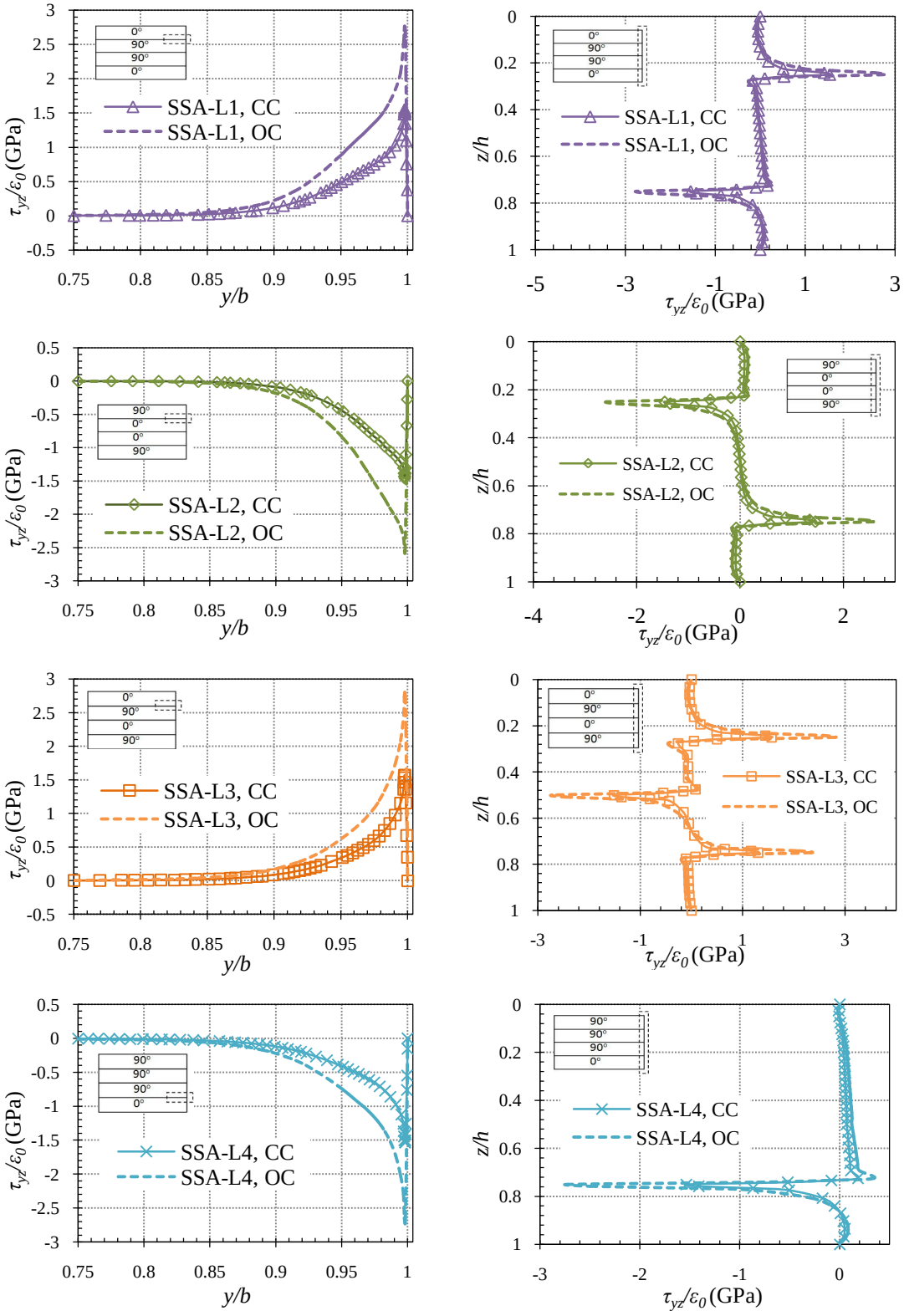

Figure 7.23: Variations of interlaminar shear stress τ_{yz} along the interface (left) and through the thickness (right) in general cross-ply piezoelectric laminates under closed-circuit (CC) and open-circuit (OC) surface conditions

Analogously, validation is also carried out by comparing present SSA results with those of FEM and there are no significant differences between these two solutions except for the region where a singularity occur.

Different electric surface conditions may lead to redistributions of electromechanical variables such as interlaminar stresses and electric field intensities. Since the influence of piezoelectric coupling on these mentioned variables near the free edge under open-circuit surface condition has been studied, it is inevitable to investigate the influence under closed-circuit surface condition and the difference between these two electric surface conditions.

To assess the distributions of interlaminar stresses σ_z and τ_{yz}, and electric field intensity components E_y and E_z along the y direction, the $0^\circ/90^\circ$ interface at z/h=0.25, $90^\circ/0^\circ$ interface at z/h=0.25, $0^\circ/90^\circ$ interface at z/h=0.25 and $90^\circ/0^\circ$ interface at z/h=0.75 are chosen for the $[0^\circ/90^\circ]_s$, $[90^\circ/0^\circ]_s$, $[0^\circ/90^\circ/0^\circ/90^\circ]$ and $[90^\circ/90^\circ/90^\circ/0^\circ]$ laminates, respectively. In addition, the through-thickness variations of these interlaminar stresses near the free edge are also presented.

As depicted in Figures 7.22 and 7.23, the stresses in the closed-circuit surface condition are qualitatively similar to those in the open-circuit surface condition where a notable interlaminar stress gradient is captured near the intersection of the interface and the free edge. However, it is observed that the stresses in the closed-circuit surface condition are approximately half of those in the open-circuit surface condition quantitatively. It also should be noted that the discrepancy between these two electric surface conditions becomes more noticeable when the free edge or the interface is approached.

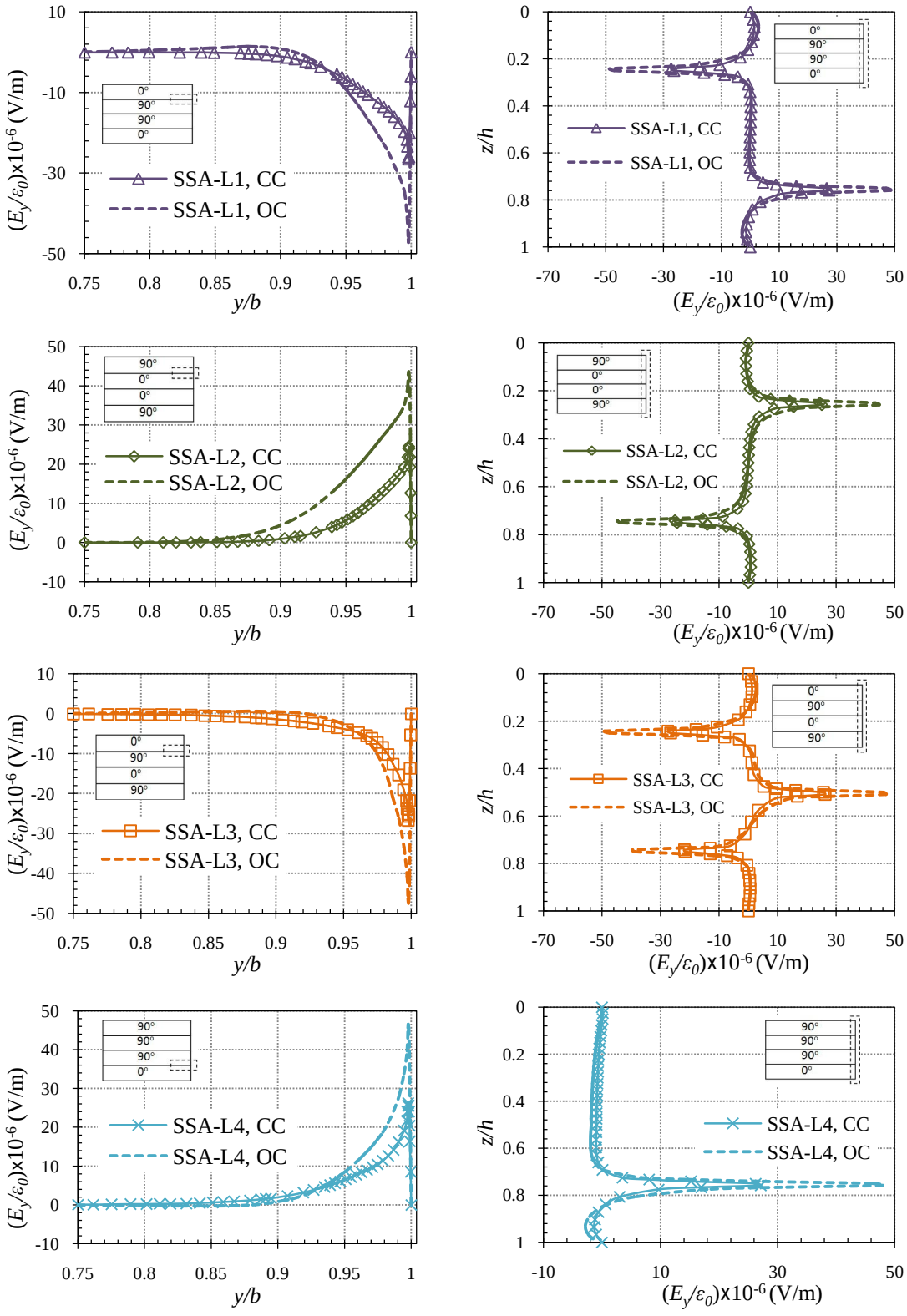

Figure 7.24: Variations of electric field intensity component E_y along the interface (left) and through the thickness (right) in general cross-ply piezoelectric laminates under closed-circuit (CC) and open-circuit (OC) surface conditions

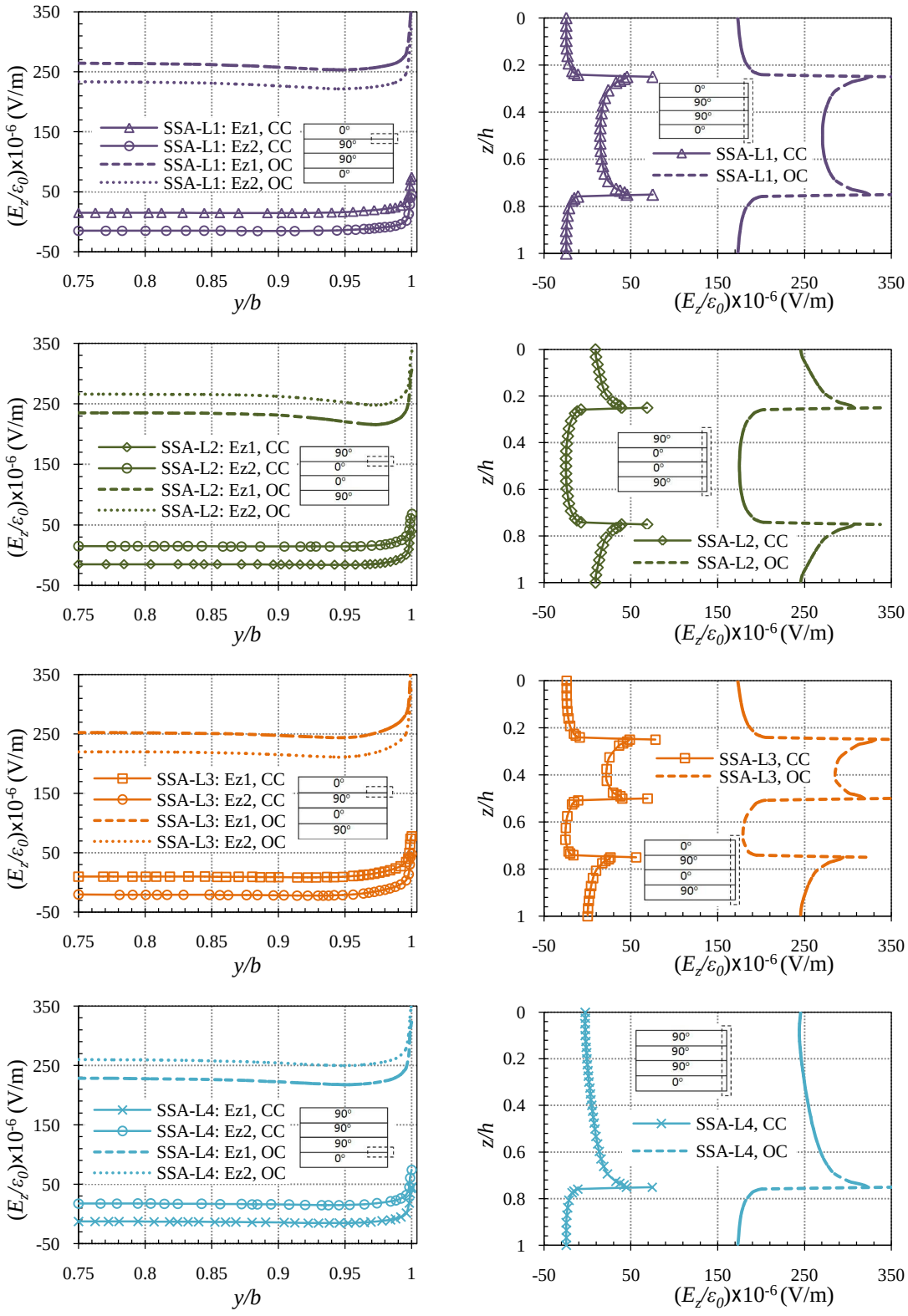

Figure 7.25: Variations of electric field intensity component E_z along the interface (left) and through the thickness (right) in general cross-ply piezoelectric laminates under closed-circuit (CC) and open-circuit (OC) surface conditions

The variations of electric field intensity components E_y and E_z along the interface and through the thickness under different electric surface conditions are shown in Figures 7.24 and 7.25. It is apparent that E_y in the closed-circuit surface condition are also approximately half of those in the open-circuit surface condition quantitatively near the intersection of the interface and the free edge.

Although the electric field intensity component E_z in the closed-circuit surface condition is qualitatively similar to that in the open-circuit surface condition and they both exhibit steep variations near the interface and the free edge, a significant difference is found between the two electric surface conditions. Compared to the open-circuit surface, the magnitude of E_z in the closed-circuit surface condition is much smaller not only near the free edge but also in the inner region of the piezoelectric laminate.

7.4 Conclusions

In this chapter, an extensive and in-depth investigation has been carried out to analyze the electromechanical and free edge effects on the interlaminar stresses and electric fields in the symmetric and unsymmetric cross-ply piezoelectric laminates under uniaxial extension. To evaluate the influence of the piezoelectric coupling effect in the vicinity of the free edges, both coupled and uncoupled analyses of the free-edge effect have been performed.

For the symmetric cross-ply piezoelectric laminates the present analytical SSA solution has been compared with the results available in the literature and FEM. The accuracy and effectiveness of the SSA solution in predicting the localized three-dimensional interlaminar stresses and electric fields were shown analytically. Since there are no published analytical or numerical solutions for the unsymmetric cross-ply piezoelectric laminates, the SSA results can be used as a benchmark which has been verified by the FEM solution from ABAQUS. There was good agreement between the SSA results and those from FEM except for the region very near the

free edge where a singularity was expected. Due to this singularity, the interlaminar stresses and electric fields showed significant gradients near the intersection of the interface and the free edge for both coupled and uncoupled cases.

It was also found that the interlaminar stresses in the coupled analysis exhibited higher magnitude than those in the uncoupled analysis, so the electromechanical coupling as well as the free edge effects had a notable influence on the interlaminar stresses and for determining the interlaminar stresses in the piezoelectric laminated plate, in particular near the free edges, the coupled analysis should be carried out. In addition, owing to much higher interlaminar stresses in the piezoelectric laminates than the laminates without electromechanical coupling the piezoelectric laminates are more vulnerable to edge delamination which may affect the structural integrity and reliability.

Furthermore the results of this investigation illustrated that the interlaminar stresses σ_z and τ_{yz}, and electric field intensity component E_y in the closed-circuit surface condition were half of those in the open-circuit surface while the electric field intensity component E_z declined significantly when applying the closed-circuit surface condition. The application of different electric boundary conditions had a significant influence on the distributions of interlaminar stresses, particularly near the free edge. The results indicate that in order to prevent the initiation of edge delamination the closed-circuit surface conditions on the piezoelectric laminates under uniaxial extension would be preferable.

CHAPTER 8 CONCLUSIONS AND RECOMMENDATIONS FOR FUTURE STUDIES

8.1 Introduction

Based on the theories of 3D elasticity and piezoelectricity, the state space method has been developed to investigate the global and local behaviour of piezoelectric laminated plates with free edges, in particular the electromechanical coupling and free-edge effects on the distributions of interlaminar stresses. Two main laminated models: simply-supported and free-edge piezoelectric laminated plates under transverse loads and infinite long piezoelectric laminates under uniaxial extension, have been established. In addition, by using the finite element package ABAQUS, numerical models have been performed and their results also have been compared with those of present analytical models. This chapter summarizes the main conclusions and contributions of the analytical and numerical investigations in the research and recommends some potential studies in the future.

8.2 Analytical and numerical investigations on simply-supported piezoelectric laminated thick plates with free edges

The following conclusions from this investigation can be drawn

- With the introduction of electric state variables (D_z and $\emptyset$) in terms of eigen-functions in the state equations the state space method preserves the three displacement components *u*, *v* and *w*, three interlaminar stresses σ_z, τ_{xz} and τ_{yz}, electric potential $\emptyset$ and transverse electric displacement D_z as the state vectors with respect to the theories of 3D piezoelasticity and all the independent elastic and piezoelectric constants for the orthotropic and piezoelectric materials are considered. The continuity conditions between different layers are also satisfied

and the traction-free and open-circuit boundary conditions at free edges are guaranteed. This state space method can provide exact 3D analytical solutions for the analyses of the electromechanical and free-edge effects on the piezoelectric laminates, and the present 3D analytical solutions delivered an improvement in precision over other 2D analytical and numerical solutions and could serve as a benchmark for these solutions.

- By using the 3D piezoelectric brick element in the finite element package ABAQUS, the finite element method yielded reasonable solutions to predict the distributions of the field variables in the piezoelectric laminate everywhere except for a region involving the two elements closest to the stress singularity. Due to the fact that the locations of Gauss point get closer to the node point locations (but never become the nodal locations) the continuity of interlaminar stresses and the traction-free boundary conditions are not guaranteed. The discrepancy between the interlaminar stresses at the interfaces could be reduced or neglected in the inner region of the plate. However, with the high inhomogeneity in mechanical and electric material properties and singularity near the free edge, this discontinuous behaviour became noticeable.
- By applying more mathematical sub-layers in the small region in the immediate vicinity of the interface without increasing the total number of the sub-layers, the non-uniform layer refinement was implemented in the state space approach for the first time. The accuracy of the local mechanical and electrical quantities was improved and more realistic gradients of these quantities were captured near the intersection of the interface and the free edge. This novel layer refinement was validated as a possible compromise between the accuracy and computation efficiency for the analysis of the free-edge effect.
- The comparison with the Levy analytical solution based on CLPT indicated that CLPT underestimated the maximum central deflection of laminated plates even for thin plates and gave poor results on stresses. The results from the present 3D analytical solution were in good agreement with those from FEM. The present analytical solution is suitable for the design and accurate analysis of piezoelectric laminated thin and thick plates with free-edge boundary conditions.

- For the three-layered piezoelectric laminates the interlaminar shear stress τ_{xz} played a dominant role along the simply-supported edges and increased steadily to the maximum value at the corners. Compared with τ_{xz}, τ_{yz} was quantitatively smaller but exhibited a significant variation. Due to the influences of different material properties, geometries and stacking sequences on the singular behaviour of τ_{yz}, this interlaminar shear stress near the free edge was not negligible and had a tendency to contribute to edge delamination in the piezoelectric laminate. Moreover, the highest tensile interlaminar normal stress σ_z was observed at the interface of the $[90^\circ/90^\circ/90^\circ/0^\circ]$ piezoelectric laminate that was more susceptible to delamination damage. As a recommendation, the edge reinforcement or edge modification should be adopted in practical design to prevent such edge delamination.
- The present analytical plate model can be utilized to evaluate the 3D bending behaviour of the simply-supported piezoelectric beam with all dimensions and elastic and electric constants for the orthotropic and piezoelectric material being considered. As the width to thickness ratio *b*/*h* increases, the variation of transverse shear stress τ_{xz} along the width became more noticeable. Due to the free-edge effect, the value of this transverse shear stress at the intersection of the free edge and simply-supported edge was approximately 33% larger than that at the middle of the simply-supported edge when *b/h*=1. The beam model based on the plane stress state assumption was not suitable for an accurate prediction of the transverse shear stresses. The present solution can provide alternative means for evaluating the full 3D state of stresses and electric fields in the design and analysis of piezoelectric beams and plates, and serve as a benchmark for other numerical methods. Moreover, the significant influence of the electrical material parameters on the singular behaviour of τ_{yz} was captured and τ_{xz} that was much larger than τ_{yz} varied steadily.

8.3 Analytical and numerical investigations on infinite long piezoelectric laminated plates under uniaxial extension

In this study, several conclusions can be made as follows:

- There were significant gradients of interlaminar stresses σ_z and τ_{yz}, and electric field intensity components E_y and E_z in the region near the intersection of the interface and the free edge. The tensile interlaminar stress σ_z was found in all general cross-ply piezoelectric laminates and this suggests that particular attention needs to be paid to this region.
- The interlaminar stresses in the electromechanical coupled analysis exhibited higher magnitude than those in the uncoupled analysis. It was caused by the additional electric boundary conditions and the electromechanical coupling. This influence of the electromechanical coupling and the free-edge effect on the interlaminar stresses was notable and the piezoelectric laminate was more susceptible to delamination damage than the laminate without electromechanical coupling. Hence, in order to monitor the structural performance the coupled analysis should be carried out for the piezoelectric laminated plates to accurately determine the interlaminar stresses and more attention should be devoted to the regions near free edges in the design of piezoelectric laminated structures. Also, it was found that the application of the closed-circuited surface condition led to smaller interlaminar stresses and electric fields and might prevent the edge delamination initiation which would affect the structural integrity and reliability of piezoelectric laminates.

8.4 Recommendations for future studies

Since the interlaminar stresses are the predominant cause of failure (delamination) in piezoelectric laminated structures, the development of efficient 3D analytical solutions which can accurately determine the distributions of those stresses is necessary. The present solutions of piezoelectric laminated plates with free edges by

using the non-uniform layer refinement can be used as a benchmark for predicting interlaminar stresses and electric fields accurately not only in the inner region but also near the intersection of the interface and the free edge. It can be used to evaluate the accuracy of other various approximate analytical and numerical solutions.

Further investigation should be performed for other boundary conditions such as fully clamped, clamped and free. In addition other loading conditions like traction loads and electric loads could be considered.

The 3D free-edge effect phenomenon will become more complex under the action of a combination of multi physical fields such as mechanical, thermal, electrical field. The state space method has been demonstrated to be very effective and accurate in predicting the electromechanical and free-edge effects on the interlaminar stresses. This method can be extended, in principle, to the electro-thermo-mechanical and free-edge problems with additional corresponding state variables and boundary conditions.

The present solution can be developed to analyze the free-edge effect of the functional graded plate with the material property parameters varying in the z direction. By using the layer refinement, the functional graded plate can be artificially divided into a certain number of mathematical layers with smaller thickness and the variable material coefficients of each layer can be reasonably approximated to be the constants in the sense of average layer thickness. With the transfer matrix method, the general solutions of the system equations can be obtained layer by layer.

REFERENCES

ABAQUS, 2010. ABAQUS/STANDARD User's Manual. Version 6.10.1.

AMBARTSUMIAN, S. 1958. On theory of bending plates. *Izv Otd Tech Nauk AN SSSR,* 5**,** 69-77.

ANDAKHSHIDEH, A. & TAHANI, M. 2013. Free-edge stress analysis of general rectangular composite laminates under bending, torsion and thermal loads. *European Journal of Mechanics-A/Solids,* 42**,** 229-240.

ARTEL, J. & BECKER, W. 2005. Coupled and uncoupled analyses of piezoelectric free-edge effect in laminated plates. *Composite Structures,* 69**,** 329-335.

ATTALLAH, K., YE, J. & SHENG, H. 2007. Three-dimensional finite strip analysis of laminated panels. *Computers & Structures,* 85**,** 1769-1781.

BECKER, W. 1993. Closed-form solution for the free-edge effect in cross-ply laminates. *Composite Structures,* 26**,** 39-45.

BJELETICH, J. G., CROSSMAN, F. W. & WARREN, W. J. 1979. The influence of stacking sequence on failure modes in quasi-isotropic graphite-epoxy laminates. *Failure Modes in Composites–IV, JR Cornie and FW Crossman (editors), American Institute of Mining, Metallurgical and Petroleum Engineers, New York, NY.*

BUFLER, H. 1971. Theory of elasticity of a multilayered medium. *Journal of Elasticity,* 1**,** 125-143.

CARREIRA, R. P., CARON, J.-F. & DIAZ DIAZ, A. 2002. Model of multilayered materials for interface stresses estimation and validation by finite element calculations. *Mechanics of Materials,* 34**,** 217-230.

CARRERA, E. 1996. C^0 Reissner-Mindlin multilayered plate elements including zig - zag and interlaminar stress continuity. *International Journal for Numerical Methods in Engineering,* 39**,** 1797-1820.

CARRERA, E. 1997. C^0z requirements-models for the two dimensional analysis of multilayered structures. *Composite Structures,* 37**,** 373-383.

CARRERA, E. 2000. A priori vs. a posteriori evaluation of transverse stresses in multilayered orthotropic plates. *Composite Structures,* 48**,** 245-260.

CARRERA, E. & CIUFFREDA, A. 2005. A unified formulation to assess theories of multilayered plates for various bending problems. *Composite Structures,* 69**,** 271-293.

CHAREF, A. & BOUCHERMA, D. 2011. Analytical solution of the linear fractional system of commensurate order. *Computers & Mathematics with Applications,* 62, 4415-4428.

CHENG, Z. Q. & BATRA, R. 2000. Three-dimensional asymptotic analysis of multiple-electroded piezoelectric laminates. *AIAA Journal,* 38**,** 317-324.

CHO, M. & OH, J. 2004. Higher order zig-zag theory for fully coupled thermo-electric–mechanical smart composite plates. *International Journal of Solids and Structures,* 41**,** 1331-1356.

CHO, M. & PARMERTER, R. 1993. Efficient higher order composite plate theory for general lamination configurations. *AIAA Journal,* 31**,** 1299-1306.

CHRISTOU, P. 2007. Advanced materials for turbine blade manufacture. *Reinforced Plastics,* 51, 22-24.

CHUNG, S. 2003. *Effects of interlaminar stress gradients on free edge delamination in composite laminates* PhD, Drexel University.

CROSSMAN, F. W. & WANG, A. S. D. 1982. The dependence of transverse cracking and delamination on ply thickness in graphite/epoxy laminates. Damage in composite materials, *ASTM STP,* 775, 118-139.

DI SCIUVA, M. 1986. Bending, vibration and buckling of simply supported thick multilayered orthotropic plates: an evaluation of a new displacement model. *Journal of Sound and Vibration,* 105**,** 425-442.

DONG, C. & SHENG, H. 2005. State space method for the analysis of free-edge stresses of laminated plates. *Chinese Journal of Applied Mechanics,* 22**,** 470-474.

DUAN, W. H., WANG, Q. & QUEK, S. T. 2010. Applications of piezoelectric materials in structural health monitoring and repair: Selected research examples. *Materials,* 3, 5169-5194.

FAGIANO, C. 2010. *Computational modeling of tow-placed composite laminates with fabrication features*, PhD thesis, Delft University of Technology, The Netherlands.

FAN, J. R. 1998. *Exact theory of laminated thick plates and shells,* Beijing, Science Press.

FAN, J. R. & DING, K. W. 1993. Exact solution for thick laminated closed cylindrical shells with two clamped edges. *Applied Mathematical Modelling,* 17**,** 632-641.

FAN, J. R. & SHENG, H. Y. 1992. Exact solution for thick laminates with clamped edges. *Acta. Mechanica. Sinica,* 24**,** 574-583.

FAN, J. R. & YE, J. Q. 1990a. An exact solution for the statics and dynamics of laminated thick plates with orthotropic layers. *International Journal of Solids and Structures,* 26**,** 655-662.

FAN, J. R. & YE, J. Q. 1990b. A series solution of the exact equation for thick orthotropic plates. *International Journal of Solids and Structures,* 26**,** 773-778.

FERNANDES, A. & POUGET, J. 2006. Structural response of composite plates equipped with piezoelectric actuators. *Computers & Structures,* 84**,** 1459-1470.

GAUTSCHI, G. 2002. *Piezoelectric sensorics: force, strain, pressure, acceleration and acoustic emission sensors, materials and amplifiers*, Springer.

HAYASHI, T. 1967. Analytical study of interlaminar shear stresses in a laminated composite plate(Interlaminar shear stresses in cross-plied three ply symmetric laminated composite plate, analyzing interlaminar stress distribution under simple tension). *Japan Society for Aeronautical and Space Sciences, transactions,* 10**,** 43-48.

HEYLIGER, P. 1994. Static behavior of laminated elastic/piezoelectric plates. *AIAA journal,* 32**,** 2481-2484.

ICARDI, U. & BERTETTO, A. M. 1995. An evaluation of the influence of geometry and of material properties at free edges and at corners of composite laminates. *Computers & Structures,* 57**,** 555-571.

IYENGAR, K. & PANDYA, S. 1983. Analysis of orthotropic rectangular thick plates. *Fibre Science and Technology,* 18**,** 19-36.

IZADI, M. & TAHANI, M. 2010. Analysis of interlaminar stresses in general cross-ply laminates with distributed piezoelectric actuators. *Composite Structures,* 92**,** 757-768.

JONES, R. M. 1998 . *Mechanics of Composite Materials*. CRC Press.

KANT, T. & PANDYA, B. 1988. A simple finite element formulation of a higher-order theory for unsymmetrically laminated composite plates. *Composite Structures,* 9**,** 215-246.

KAPURIA, S. 2004. A coupled zig-zag third-order theory for piezoelectric hybrid cross-ply plates. *Journal of Applied Mechanics,* 71**,** 604-614.

KAPURIA, S. & ACHARY, G. 2005. A coupled consistent third-order theory for hybrid piezoelectric plates. *Composite Structures,* 70**,** 120-133.

KAPURIA, S. & DUMIR, P. 2000. Coupled FSDT for piezothermoelectric hybrid rectangular plate. *International Journal of Solids and Structures,* 37**,** 6131-6153.

KAPURIA, S. & KUMARI, P. 2012. Boundary layer effects in Levy-type rectangular piezoelectric composite plates using a coupled efficient layerwise theory. *European Journal of Mechanics-A/Solids,* 36**,** 122-140.

KAPURIA, S., KUMARI, P. & NATH, J. 2010. Efficient modeling of smart piezoelectric composite laminates: a review. *Acta Mechanica,* 214**,** 31-48.

KASSAPOGLOU, C. 1990. Determination of interlaminar stresses in composite laminates under combined loads. *Journal of Reinforced Plastics and Composites,* 9**,** 33-58.

KASSAPOGLOU, C. & LAGACE, P. A. 1987. Closed form solutions for the interlaminar stress field in angle-ply and cross-ply laminates. *Journal of Composite Materials,* 21**,** 292-308.

KRISHNA MURTY, A. & HARI KUMAR, H. 1989. Modelling of symmetric laminates under extension. *Composite Structures,* 11**,** 15-32.

LEE, C. 1990. Theory of laminated piezoelectric plates for the design of distributed sensors/actuators. Part I: Governing equations and reciprocal relationships. *The Journal of the Acoustical Society of America,* 87**,** 1144.

LAGUNEGRAND, L., LORRIOT, T., HARRY, R., WARGNIER, H. & QUENISSET, J. M. 2006a. Initiation of free-edge delamination in composite laminates. *Composites Science and Technology,* 66, 1315-1327.

LAGUNEGRAND, L., LORRIOT, T., HARRY, R. & WARGNIER, H. 2006b. Design of an improved four point bending test on a sandwich beam for free edge delamination studies. *Composites Part B: Engineering,* 37, 127-136.

LEE, J. S. & JIANG, L. Z. 1996. Exact electroelastic analysis of piezoelectric laminae via state space approach. *International Journal of Solids and Structures,* 33**,** 977-990.

LEGUILLON, D. 1999. A method based on singularity theory to predict edge delamination of laminates. *International Journal of Fracture,* 100**,** 105-120.

LIN, Q. R., LIU, Z. X. & JIN, Z. L. 2000. A close-form solution to simply supported piezoelectric beams under uniform exterior pressure. *Applied Mathematics and Mechanics,* 21**,** 681-690.

LO, S., ZHEN, W. & SZE, K. 2012. An enhanced Reddy's theory for composite plates subjected to temperature load. *Mechanics of Advanced Materials and Structures,* 20, 834-841.

LÓPEZ, C., FIRMO, J. P., CORREIA, J. R. & TIAGO, C. 2013. Fire protection systems for reinforced concrete slabs strengthened with CFRP laminates. *Construction and Building Materials,* 47, 324-333.

LORRIOT, T., MARION, G., HARRY, R. & WARGNIER, H. 2003. Onset of free-edge delamination in composite laminates under tensile loading. *Composites Part B: Engineering,* 34, 459-471.

LÜ, C. F., CHEN, W. Q. & SHAO, J. W. 2008. Semi-analytical three-dimensional elasticity solutions for generally laminated composite plates. *European Journal of Mechanics-A/Solids,* 27**,** 899-917.

MANDELL, J. F., CAIRNS, D. S., SAMBORSKY, D. D., MOREHEAD, R. B., & HAUGEN, D. H. 2003. Prediction of delamination in wind turbine blade structural details. In *ASME 2003 Wind Energy Symposium,* 202-213.

MANNINI, A. & GAUDENZI, P. 2004. Multi-layer higher-order finite elements for the analysis of free-edge stresses in piezoelectric actuated laminates. *Composite Structures,* 63**,** 263-270.

MINDLIN, R. 1964. Micro-structure in linear elasticity. *Archive for Rational Mechanics and Analysis,* 16**,** 51-78.

MIRZABABAEE, M. & TAHANI, M. 2009. Accurate determination of coupling effects on free edge interlaminar stresses in piezoelectric laminated plates. *Materials & Design,* 30**,** 2963-2974.

MITCHELL, J. & REDDY, J. 1995. A refined hybrid plate theory for composite laminates with piezoelectric laminae. *International Journal of Solids and Structures,* 32**,** 2345-2367.

MITTELSTEDT, C. & BECKER, W. 2004. Interlaminar stress concentrations in layered structures: Part I-a selective literature survey on the free-edge effect since 1967. *Journal of Composite Materials,* 38**,** 1037-1062.

NGUYEN, V. T. & CARON, J. F. 2006. A new finite element for free edge effect analysis in laminated composites. *Computers & Structures,* 84**,** 1538-1546.

NODA, M. I., NAOTAKE 2000. Piezothermoelastic analysis of a cross-ply laminate considering the effects of transverse shear and coupling. *Journal of Thermal Stresses,* 23**,** 441-461.

NGUYEN, Q., NGO, T., MENDIS, P. & TRAN, P. 2013. Composite Materials for Next Generation Building Façade Systems. *Civil Engineering and Architecture,* 1, 88-95.

NOOR, A. K. & BURTON, W. S. 1989. Assessment of shear deformation theories for multilayered composite plates. *Applied Mechanics Reviews,* 42**,** 1-13.

NOSIER, A. & MALEKI, M. 2008. Free-edge stresses in general composite laminates. *International Journal of Mechanical Sciences,* 50**,** 1435-1447.

NYE, J. F. 1985. *Physical Properties of Cristals: Their Representation by Tensors and Matrices,* Oxford University Press.

ONG, M. T. & REED, E. J. 2012. Engineered piezoelectricity in graphene. *ACS Nano,* 6**,** 1387-1394.

PAGANO, N. J. 1969. Exact solutions for composite laminates in cylindrical bending. *Journal of Composite Materials,* 3**,** 398-411.

PAGANO, N. J. 1970. Exact solutions for rectangular bidirectional composites and sandwich plates. *Journal of Composite Materials,* 4**,** 20-34.

PAGANO, N. J. & PIPES, R. B. 1971. The influence of stacking sequence on laminate strength. *Journal of Composite Materials,* 5**,** 50-57.

PAGANO, N. J. & PIPES, R. B. 1973. Some observations on the interlaminar strength of composite laminates. *International Journal of Mechanical Sciences,* 15**,** 679-688.

PAN, E. 2001. Exact solution for simply supported and multilayered magneto-electro-elastic plates. *Transactions-American Society of Mechanical Engineers Journal of Applied Mechanics,* 68**,** 608-618.

PIPES, R. B. 1980. Boundary layer effects in composite laminates. *Fibre Science and Technology,* 13**,** 49-71.

PIPES, R. B. & PAGANO, N. 1970. Interlaminar stresses in composite laminates under uniform axial extension. *Journal of Composite Materials,* 4**,** 538-548.

PUPPO, A. & EVENSEN, H. 1970. Interlaminar shear in laminated composites under generalized plane stress. *Journal of Composite Materials,* 4**,** 204-220.

RAY, M., RAO, K. & SAMANTA, B. 1992. Exact analysis of coupled electroelastic behaviour of a piezoelectric plate under cylindrical bending. *Computers & Structures,* 45**,** 667-677.

RAY, M. C., RAO, K. & SAMANTA, B. 1993. Exact solution for static analysis of an intelligent structure under cylindrical bending. *Computers & Structures,* 47**,** 1031-1042.

REDDY, J. N. 2004. *Mechanics of Laminated Composite Plates and Shells: Theory and Analysis/JN Reddy*, CRC press.

REISSNER, E. 1945. The effect of transverse shear deformation on the bending of elastic plates. *Journal of Applied Mechanics,* 12**,** 69-77.

REISSNER, E. 1961. Bending and stretching of certain types of heterogeneous aeolotropic elastic plates. *Journal of Applied Mechanics,* 28**,** 402-408.

REISSNER, E. 1986. On a mixed variational theorem and on shear deformable plate theory. *International Journal for Numerical Methods in Engineering,* 23**,** 193-198.

ROGERS, T., WATSON, P. & SPENCER, A. 1995. Exact three-dimensional elasticity solutions for bending of moderately thick inhomogeneous and laminated strips under normal pressure. *International Journal of Solids and Structures,* 32**,** 1659-1673.

ROLFES, R., NOOR, A. & SPARR, H. 1998. Evaluation of transverse thermal stresses in composite plates based on first-order shear deformation theory. *Computer Methods in Applied Mechanics and Engineering,* 167**,** 355-368.

ROMERA, J. M., CANTERA, M. A., ADARRAGA, I. & MUJIKA, F. 2013. Application of the submodeling technique to the analysis of the edge effects of composite laminates. *Journal of Reinforced Plastics and Composites*, 32, 1099-1111.

SAEEDI, N., SAB, K. & CARON, J.-F. 2012a. Delaminated multilayered plates under uniaxial extension. Part I: Analytical analysis using a layerwise stress approach. *International Journal of Solids and Structures*, 49, 3711-3726.

SAEEDI, N., SAB, K. & CARON, J.-F. 2012b. Delaminated multilayered plates under uniaxial extension. Part II: Efficient layerwise mesh strategy for the prediction of delamination onset. *International Journal of Solids and Structures*, 49, 3727-3740.

SAVITHRI, S. & VARADAN, T. 1990. Accurate bending analysis of laminated orthotropic plates. *AIAA Journal,* 28**,** 1842-1844.

SEKOURI, E. M., HU, Y. R. & NGO, A. D. 2004. Modeling of a circular plate with piezoelectric actuators. *Mechatronics,* 14**,** 1007-1020.

SHAHROKH, H.-H., FADAEE, M. & TAHER, H. 2011. Exact solutions for free flexural vibration of Levy-type rectangular thick plates via third-order shear deformation plate theory. *Appl. Math. Mod,* 35**,** 708-727.

SHANG, F., KITAMURA, T., HIRAKATA, H., KANNO, I., KOTERA, H. & TERADA, K. 2005. Experimental and theoretical investigations of delamination at free edge of interface between piezoelectric thin films on a substrate. *International Journal of Solids and Structures,* 42**,** 1729-1741.

SHENG, H. Y., WANG, H. & YE, J. Q. 2007. State space solution for thick laminated piezoelectric plates with clamped and electric open-circuited boundary conditions. *International Journal of Mechanical Sciences,* 49**,** 806-818.

SHENG, H. Y. & YE, J. Q. 2002. A semi-analytical finite element for laminated composite plates. *Composite Structures,* 57**,** 117-123.

SHENG, H. Y. & YE, J. Q. 2005. State space solution for axisymmetric bending of angle-ply laminated cylinder with clamped edges. *Composite Structures,* 68**,** 119-128.

SOLDATOS, K. & HADJIGEORGIOU, V. 1990. Three-dimensional solution of the free vibration problem of homogeneous isotropic cylindrical shells and panels. *Journal of Sound and Vibration,* 137**,** 369-384.

SPILKER, R. L. & CHOU, S. 1980. Edge effects in symmetric composite laminates-Importance of satisfying the traction-free-edge condition. *Journal of Composite Materials,* 14**,** 2-20.

SRINIVAS, S. & RAO, A. 1970. Bending, vibration and buckling of simply supported thick orthotropic rectangular plates and laminates. *International Journal of Solids and Structures,* 6**,** 1463-1481.

TAHANI, M. & ANDAKHSHIDEH, A. 2012. Interlaminar stresses in thick rectangular laminated plates with arbitrary laminations and boundary conditions under transverse loads. *Composite Structures,* 94**,** 1793-1804.

TAHANI, M. & MIRZABABAEE, M. 2009. Higher-order coupled and uncoupled analyses of free edge effect in piezoelectric laminates under mechanical loadings. *Materials & Design,* 30**,** 2473-2482.

TAHANI, M. & NOSIER, A. 2003. Edge effects of uniformly loaded cross-ply composite laminates. *Materials & Design,* 24**,** 647-658.

TAHANI, M. & NOSIER, A. 2004. Accurate determination of interlaminar stresses in general cross-ply laminates. *Mechanics of Advanced Materials and Structures,* 11**,** 67-92.

TIMOSHENKO, S., TIMOSHENKO, S. & GOODIER, J. 1951. *Theory of Elasticity, by S. Timoshenko and JN Goodier*, McGraw-Hill Book Company.

TOLEDANO, A. & MURAKAMI, H. 1987. A high-order laminated plate theory with improved in-plane responses. *International Journal of Solids and Structures,* 23**,** 111-131.

VEL, S. & BATRA, R. 2000. Three-dimensional analytical solution for hybrid multilayered piezoelectric plates. *Journal of Applied Mechanics,* 67**,** 558-567.

VLASOV, V. 1957. Method of initial functions in problems of theory of thick plates and shells. *Proc. 9th Int. Cong. Appl. Mech., Brussels***,** 321.

WANG, Y. M., TARN, J. Q. & HSU, C.-K. 2000. State space approach for stress decay in laminates. *International Sournal of Solids and Structures,* 37**,** 3535-3553.

WEN, P., SLADEK, J. & SLADEK, V. 2011. Three-dimensional analysis of functionally graded plates. *International Journal for Numerical Methods in Engineering,* 87**,** 923-942.

WHITCOMB, J., RAJU, I. & GOREE, J. 1982. Reliability of the finite element method for calculating free edge stresses in composite laminates. *Computers & Structures,* 15**,** 23-37.

WHITE, N., GLYNNE-JONES, P. & BEEBY, S. 2001. A novel thick-film piezoelectric micro-generator. *Smart Materials and Structures,* 10**,** 850-852.

WHITNEY, J. & SUN, C. 1973. A higher order theory for extensional motion of laminated composites. *Journal of Sound and Vibration,* 30**,** 85-97.

WHITNEY, J. M. & LEISSA, A. W. 1969. Analysis of heterogeneous anisotropic plates. *Journal of Applied Mechanics,* 36**,** 261.

WU, C. P. & SYU, Y.-S. 2007. Exact solutions of functionally graded piezoelectric shells under cylindrical bending. *International Journal of Solids and Structures,* 44**,** 6450-6472.

WU, C. P. & TSAI, T.-C. 2012. Exact solutions of functionally graded piezoelectric material sandwich cylinders by a modified Pagano method. *Applied Mathematical Modelling,* 36**,** 1910-1930.

WU, C. P. & TSAI, Y. H. 2009. Cylindrical bending vibration of functionally graded piezoelectric shells using the method of perturbation. *Journal of Engineering Mathematics,* 63**,** 95-119.

WU, Z., CHEN, R. G. & CHEN, W. 2005. Refined laminated composite plate element based on global–local higher-order shear deformation theory. *Composite Structures,* 70**,** 135-152.

WU, Z. J., HAN, F. & WU, H. 2010. *Elasticity,* University Press of Beijing Institute of Technology.

WU, Z. J. & KAMIS, E. 2012. Influence of element type on the simulation of laminated composite plates with clamped edges. The 20th UK Conference of the Association for Computational Mechanics in Engineering.

WU, Z. J. & WARDENIER, J. 1998. Further investigation on the exact elasticity solution for anisotropic thick rectangular plates. *International Journal of Solids and Structures,* 35**,** 747-758.

YANG, Q. S., QIN, Q. H. & LIU, T. 2006. Interlayer stress in laminate beam of piezoelectric and elastic materials. *Composite Structures,* 75**,** 587-592.

YE, J. Q. 2003. *Laminated composite plates and shells: 3D modelling,* Springer.

YE, J. Q., SHENG, H. Y. & QIN, Q. H. 2004. A state space finite element for laminated composites with free edges and subjected to transverse and in-plane loads. *Computers & Structures,* 82**,** 1131-1141.

YIN, L., WANG, X. M. & SHEN, Y. P. 1996. Damage-monitoring in composite laminates by piezoelectric films. *Computers & Structures,* 59, 623-630.

ZHANG, B., ZHANG, J. & FAN, J. 2003. A coupled electromechanical analysis of a piezoelectric layer bonded to an elastic substrate: Part II, numerical solution and applications. *International Journal of Solids and Structures,* 40, 6799-6812.

ZHANG, D. X., YE, J. Q. & LAM, D. 2007. Free-edge and ply cracking effect in angle-ply laminated composites subjected to in-plane loads. *Journal of Engineering Mechanics,* 133**,** 1268-1277.

ZHANG, D. X., YE, J. Q. & SHENG, H. Y. 2006. Free-edge and ply cracking effect in cross-ply laminated composites under uniform extension and thermal loading. *Composite Structures,* 76**,** 314-325.

ZHONG, Z. & SHANG, E. 2003. Three-dimensional exact analysis of a simply supported functionally gradient piezoelectric plate. *International Journal of Solids and Structures,* 40**,** 5335-5352.

PUBLICATIONS

Han, C., Wu, Z. J. 2013. Free edge coupling effect of piezoelectric cross-ply laminated plates. *Proceedings of the 13th International Conference on Fracture. Beijing,* S04-018.

Han, C., Wu, Z. J. and Niu, Z. R. 2014. Accurate prediction of free-edge and electromechanical coupling effects in cross-ply piezoelectric laminates. *Composite Structures*, 113, 308-315.

Wu, Z. J., Han, C. and Niu, Z. R. 2014. Boundary effect on the interfacial stress distribution of asymmetric piezoelectric laminates with electromechanical coupling under pretension. Submitted to International Journal of Solid and Structures.

APPENDIX A: THE DERIVATION OF EQUATION (3-8)

From Equations (3-3), (3-4) and (3-5) , yields

$$\sigma_x = C_{11}\alpha u + C_{12}\beta v + C_{13}\frac{\partial w}{\partial z} + e_{31}\frac{\partial \emptyset}{\partial z}$$

$$\sigma_y = C_{12}\alpha u + C_{22}\beta v + C_{23}\frac{\partial w}{\partial z} + e_{32}\frac{\partial \emptyset}{\partial z}$$

$$\sigma_z = C_{13}\alpha u + C_{23}\beta v + C_{33}\frac{\partial w}{\partial z} + e_{33}\frac{\partial \emptyset}{\partial z}$$

$$\tau_{yz} = C_{44}(\beta w + \frac{\partial v}{\partial z}) + e_{24}\beta\emptyset$$

$$\tau_{xz} = C_{55}(\alpha w + \frac{\partial u}{\partial z}) + e_{15}\alpha\emptyset$$

$$\tau_{xy} = C_{66}(\beta u + \alpha v)$$

$$D_x = e_{15}\left(\alpha w + \frac{\partial u}{\partial z}\right) - \in_{11}\ \alpha\emptyset$$

$$D_y = e_{24}\left(\beta w + \frac{\partial v}{\partial z}\right) - \in_{22}\ \beta\emptyset$$

$$D_z = e_{31}\alpha u + e_{32}\beta v + e_{33}\frac{\partial w}{\partial z} - \in_{33}\frac{\partial \emptyset}{\partial z} \qquad \text{(A-1)}$$

Consider the third and ninth rows of Equation (A-1), $\frac{\partial w}{\partial z}$ and $\frac{\partial \emptyset}{\partial z}$ can be expressed as

$$\begin{aligned}\frac{\partial w}{\partial z} &= \left(\frac{-e_{31}e_{33} - C_{13}\in_{33}}{e_{33}^2 + C_{33}\in_{33}}\right)\alpha u + \left(\frac{-e_{32}e_{33} - C_{23}\in_{33}}{e_{33}^2 + C_{33}\in_{33}}\right)\beta v \\ &\quad + \left(\frac{e_{33}}{e_{33}^2 + C_{33}\in_{33}}\right)D_z + \left(\frac{\in_{33}}{e_{33}^2 + C_{33}\in_{33}}\right)\sigma_z \\ \frac{\partial \emptyset}{\partial z} &= \left(\frac{C_{33}e_{31} - C_{13}e_{33}}{e_{33}^2 + C_{33}\in_{33}}\right)\alpha u + \left(\frac{C_{33}e_{32} - C_{23}e_{33}}{e_{33}^2 + C_{33}\in_{33}}\right)\beta v \\ &\quad + \left(\frac{-C_{33}}{e_{33}^2 + C_{33}\in_{33}}\right)D_z + \left(\frac{e_{33}}{e_{33}^2 + C_{33}\in_{33}}\right)\sigma_z\end{aligned} \qquad \text{(A-2)}$$

APPENDIX B: THE DERIVATION OF THE FIRST-ORDER NON-HOMOGENEOUS ORDINARY DIFFERENTIAL EQUATION (3-26)

To solve the first-order non-homogeneous ordinary differential equation, the non-homogeneous vector needs to be determined first. Substituting Equations (3-21) and (3-22) into (3-12), the left and right columns of the first-order non-homogeneous equation can be expressed as follows, respectively.

$$\frac{\partial}{\partial z}\begin{Bmatrix} u(x,y,z) \\ v(x,y,z) \\ D_z(x,y,z) \\ \sigma_z(x,y,z) \\ \tau_{xz}(x,y,z) \\ \tau_{yz}(x,y,z) \\ \emptyset(x,y,z) \\ w(x,y,z) \end{Bmatrix} = \frac{\partial}{\partial z}\begin{Bmatrix} \tilde{u}(x,y,z) \\ \tilde{v}(x,y,z) \\ D_z(x,y,z) \\ \sigma_z(x,y,z) \\ \tau_{xz}(x,y,z) \\ \tau_{yz}(x,y,z) \\ \emptyset(x,y,z) \\ w(x,y,z) \end{Bmatrix} + \frac{\partial}{\partial z}\begin{Bmatrix} \frac{b}{2}\left(1-\frac{y}{b}\right)^2 \alpha v^{(0)}(x,z) - \frac{b}{2}\left(\frac{y}{b}\right)^2 \alpha v^{(b)}(x,z) \\ \left(1-\frac{y}{b}\right) v^{(0)}(x,z) + \frac{y}{b} v^{(b)}(x,z) \\ 0 \\ 0 \\ 0 \\ 0 \\ 0 \\ 0 \end{Bmatrix} \quad \text{(B-1)}$$

$$[A]\begin{Bmatrix} u(x,y,z) \\ v(x,y,z) \\ D_z(x,y,z) \\ \sigma_z(x,y,z) \\ \tau_{xz}(x,y,z) \\ \tau_{yz}(x,y,z) \\ \emptyset(x,y,z) \\ w(x,y,z) \end{Bmatrix} = [A]\begin{Bmatrix} \tilde{u}(x,y,z) \\ \tilde{v}(x,y,z) \\ D_z(x,y,z) \\ \sigma_z(x,y,z) \\ \tau_{xz}(x,y,z) \\ \tau_{yz}(x,y,z) \\ \emptyset(x,y,z) \\ w(x,y,z) \end{Bmatrix} + [A]\begin{Bmatrix} \frac{b}{2}\left(1-\frac{y}{b}\right)^2 \alpha v^{(0)}(x,z) - \frac{b}{2}\left(\frac{y}{b}\right)^2 \alpha v^{(b)}(x,z) \\ \left(1-\frac{y}{b}\right) v^{(0)}(x,z) + \frac{y}{b} v^{(b)}(x,z) \\ 0 \\ 0 \\ 0 \\ 0 \\ 0 \\ 0 \end{Bmatrix} \quad \text{(B-2)}$$

Form Equations (B-1) and (B-2), yields

$$\frac{\partial}{\partial z}\begin{Bmatrix}\tilde{u}(x,y,z)\\ \tilde{v}(x,y,z)\\ D_z(x,y,z)\\ \sigma_z(x,y,z)\\ \tau_{xz}(x,y,z)\\ \tau_{yz}(x,y,z)\\ \emptyset(x,y,z)\\ w(x,y,z)\end{Bmatrix} = [A]\begin{Bmatrix}\tilde{u}(x,y,z)\\ \tilde{v}(x,y,z)\\ D_z(x,y,z)\\ \sigma_z(x,y,z)\\ \tau_{xz}(x,y,z)\\ \tau_{yz}(x,y,z)\\ \emptyset(x,y,z)\\ w(x,y,z)\end{Bmatrix} + [A]\begin{Bmatrix}\frac{b}{2}\left(1-\frac{y}{b}\right)^2\alpha v^{(0)}(x,z) - \frac{b}{2}\left(\frac{y}{b}\right)^2\alpha v^{(b)}(x,z)\\ \left(1-\frac{y}{b}\right)v^{(0)}(x,z) + \frac{y}{b}v^{(b)}(x,z)\\ 0\\ 0\\ 0\\ 0\\ 0\\ 0\end{Bmatrix}$$
$$-\begin{Bmatrix}\frac{b}{2}\left(1-\frac{y}{b}\right)^2\alpha\frac{\partial v^{(0)}(x,z)}{\partial z} - \frac{b}{2}\left(\frac{y}{b}\right)^2\alpha\frac{\partial v^{(b)}(x,z)}{\partial z}\\ \left(1-\frac{y}{b}\right)\frac{\partial v^{(0)}(x,z)}{\partial z} + \frac{y}{b}\frac{\partial v^{(b)}(x,z)}{\partial z}\\ 0\\ 0\\ 0\\ 0\\ 0\\ 0\end{Bmatrix} \quad \text{(B-3)}$$

The third and fourth columns in Equation (B-3) needs to be determined, and let

$$\begin{Bmatrix}B_1(x,y,z)\\ B_2(x,y,z)\\ B_3(x,y,z)\\ B_4(x,y,z)\\ B_5(x,y,z)\\ B_6(x,y,z)\\ B_7(x,y,z)\\ B_8(x,y,z)\end{Bmatrix} = [A]\begin{Bmatrix}\frac{b}{2}\left(1-\frac{y}{b}\right)^2\alpha v^{(0)}(x,z) - \frac{b}{2}\left(\frac{y}{b}\right)^2\alpha v^{(b)}(x,z)\\ \left(1-\frac{y}{b}\right)v^{(0)}(x,z) + \frac{y}{b}v^{(b)}(x,z)\\ 0\\ 0\\ 0\\ 0\\ 0\\ 0\end{Bmatrix}$$
$$-\begin{Bmatrix}\frac{b}{2}\left(1-\frac{y}{b}\right)^2\alpha\frac{\partial v^{(0)}(x,z)}{\partial z} - \frac{b}{2}\left(\frac{y}{b}\right)^2\alpha\frac{\partial v^{(b)}(x,z)}{\partial z}\\ \left(1-\frac{y}{b}\right)\frac{\partial v^{(0)}(x,z)}{\partial z} + \frac{y}{b}\frac{\partial v^{(b)}(x,z)}{\partial z}\\ 0\\ 0\\ 0\\ 0\\ 0\\ 0\end{Bmatrix} \quad \text{(B-4)}$$

where

$$B_1(x,y,z) = -\frac{b}{2}\cdot\left(1-\frac{y}{b}\right)^2\cdot\alpha\frac{\partial v^{(0)}(x,z)}{\partial z}+\frac{b}{2}\cdot\left(\frac{y}{b}\right)^2\cdot\alpha\frac{\partial v^{(b)}(x,z)}{\partial z}$$

$$B_2(x,y,z) = -\left(1-\frac{y}{b}\right)\cdot\frac{\partial v^{(0)}(x,z)}{\partial z}-\frac{y}{b}\cdot\frac{\partial v^{(b)}(x,z)}{\partial z}$$

$$B_3(x,y,z) = 0$$

$$B_4(x,y,z) = 0$$

$$B_5(x,y,z) = -k_9\cdot\frac{b}{2}\cdot\left(1-\frac{y}{b}\right)^2\cdot\alpha^3 v^{(0)}(x,z)+k_9\cdot\frac{b}{2}\cdot\left(\frac{y}{b}\right)^2\cdot\alpha^3 v^{(b)}(x,z)$$
$$-\frac{k_{17}}{b}\cdot\alpha v^{(0)}(x,z)+\frac{k_{17}}{b}\cdot\alpha v^{(b)}(x,z)+\left(\frac{k_{10}+k_{17}}{b}\right)\cdot\alpha v^{(0)}(x,z)-\left(\frac{k_{10}+k_{17}}{b}\right)\cdot\alpha v^{(b)}(x,z)$$

$$B_6(x,y,z) = -(k_{17}+k_{13})\cdot\left(\frac{y}{b}-1\right)\cdot\alpha^2 v^{(0)}(x,z)+(k_{17}+k_{13})\cdot\left(\frac{y}{b}\right)\cdot\alpha^2 v^{(b)}(x,z)$$
$$-k_{17}\cdot\left(1-\frac{y}{b}\right)\cdot\alpha^2 v^{(0)}(x,z)-k_{17}\cdot\left(\frac{y}{b}\right)\cdot\alpha^2 v^{(b)}(x,z)$$

$$B_7(x,y,z) = k_5\cdot\frac{b}{2}\cdot\left(1-\frac{y}{b}\right)^2\cdot\alpha^2 v^{(0)}(x,z)-k_5\cdot\frac{b}{2}\cdot\left(\frac{y}{b}\right)^2\cdot\alpha^2 v^{(b)}(x,z)$$
$$-\frac{k_6}{b}\cdot v^{(0)}(x,z)+\frac{k_6}{b}\cdot v^{(b)}(x,z)$$

$$B_8(x,y,z) = k_1\cdot\frac{b}{2}\cdot\left(1-\frac{y}{b}\right)^2\cdot\alpha^2 v^{(0)}(x,z)-k_1\cdot\frac{b}{2}\cdot\left(\frac{y}{b}\right)^2\cdot\alpha^2 v^{(b)}(x,z)$$
$$-\frac{k_2}{b}\cdot v^{(0)}(x,z)+\frac{k_2}{b}\cdot v^{(b)}(x,z) \qquad \text{(B-5)}$$

Equation (B-3) can be expressed as

$$\frac{\partial}{\partial z}\begin{Bmatrix}\tilde{u}(x,y,z)\\ \tilde{v}(x,y,z)\\ D_z(x,y,z)\\ \sigma_z(x,y,z)\\ \tau_{xz}(x,y,z)\\ \tau_{yz}(x,y,z)\\ \emptyset(x,y,z)\\ w(x,y,z)\end{Bmatrix}=[A]\begin{Bmatrix}\tilde{u}(x,y,z)\\ \tilde{v}(x,y,z)\\ D_z(x,y,z)\\ \sigma_z(x,y,z)\\ \tau_{xz}(x,y,z)\\ \tau_{yz}(x,y,z)\\ \emptyset(x,y,z)\\ w(x,y,z)\end{Bmatrix}+\begin{Bmatrix}B_1(x,y,z)\\ B_2(x,y,z)\\ B_3(x,y,z)\\ B_4(x,y,z)\\ B_5(x,y,z)\\ B_6(x,y,z)\\ B_7(x,y,z)\\ B_8(x,y,z)\end{Bmatrix} \tag{B-6}$$

The eigen-functions in Equations (3-23)-(3-25) are given as follows

$$v^{(0)}(x,z)=\sum_m v_m^{(0)}(z)\sin\zeta x$$

$$v^{(b)}(x,z)=\sum_m v_m^{(b)}(z)\sin\zeta x$$

$$\begin{aligned}
\tilde{u}&=\sum_m\sum_n \tilde{u}_{mn}(z)\cos\zeta x\cos\eta y, & \tau_{xz}&=\sum_m\sum_n X_{mn}(z)\cos\zeta x\cos\eta y\\
\tilde{v}&=\sum_m\sum_n \tilde{v}_{mn}(z)\sin\zeta x\sin\eta y, & \tau_{yz}&=\sum_m\sum_n Y_{mn}(z)\sin\zeta x\sin\eta y\\
\sigma_z&=\sum_m\sum_n Z_{mn}(z)\sin\zeta x\cos\eta y, & w&=\sum_m\sum_n w_{mn}(z)\sin\zeta x\cos\eta y\\
D_z&=\sum_m\sum_n D_{mn}(z)\sin\zeta x\cos\eta y, & \emptyset&=\sum_m\sum_n \emptyset_{mn}(z)\sin\zeta x\cos\eta y
\end{aligned} \tag{B-7}$$

$$1-\frac{y}{b}=\sum_{n=1}^{\infty}\frac{2}{n\pi}\sin\eta y, \qquad (1-\frac{y}{b})^2=\frac{1}{3}+\sum_{n=1}^{\infty}\frac{4}{n^2\pi^2}\cos\eta y$$

$$\frac{y}{b}=\sum_{n=1}^{\infty}\frac{-2\cos n\pi}{n\pi}\sin\eta y, \quad (\frac{y}{b})^2=\frac{1}{3}+\sum_{n=1}^{\infty}\frac{4\cos n\pi}{n^2\pi^2}\cos\eta y$$

By introducing Equation (B-7) into Equation (B-6), Equation (3-26) can be obtained by matching the coefficients of eigen-functions at two sides of Equation (B-6)

$$\frac{d}{dz}\{R_{mn}(z)\}=[\bar{A}]\{R_{mn}(z)\}+\{B_{mn}(z)\} \tag{3-26}$$

APPENDIX C: THE VERIFICATIONS OF THE BOUNDARY CONDITIONS FOR SIMPLY-SUPPORTED PIEZOELECTRIC LAMINATES WITH FREE EDGES

Simply-supported and close-circuit boundary conditions at x=0 and a, and we have:

$$\begin{aligned}
\sigma_x &= \sum_m \sum_n [-k_9 \cdot \zeta \cdot \tilde{u}_{mn}(z) + k_{10} \cdot \eta \cdot \tilde{v}_{mn}(z) + k_{11} \cdot D_{mn}(z) \\
&\qquad + k_{12} \cdot Z_{mn}(z)] \sin \zeta x \cos \eta y \\
&\quad + \sum_m \{-\frac{k_9}{2} \cdot b \cdot [(1-\frac{y}{b})^2 + \left(\frac{y}{b}\right)^2] \cdot \zeta^2 - \frac{2k_{10}}{b}\} v_m^{(0)}(z) \sin \zeta x = 0 \\
v &= \sum_m \sum_n \tilde{v}_{mn}(z) \sin \zeta x \sin \eta y \\
&\quad + \left(1-\frac{y}{b}\right) \sum_m v_m^{(0)}(z) \sin \zeta x + \frac{y}{b} \sum_m v_m^{(b)}(z) \sin \zeta x = 0 \\
w &= \sum_m \sum_n w_{mn}(z) \sin \zeta x \cos \eta y = 0 \\
\emptyset &= \sum_m \sum_n \emptyset_{mn}(z) \sin \zeta x \cos \eta y = 0
\end{aligned} \tag{C-1}$$

Free-edge and open-circuit boundary conditions at y=0 and b, and we have

$$\begin{aligned}
\tau_{yz} &= \sum_m \sum_n Y_{mn}(z) \sin \zeta x \sin \eta y \\
\tau_{xy} &= -k_{17} \sum_m \sum_n \eta \tilde{u}_{mn}(z) \cos \zeta x \sin \eta y + k_{17} \left(\frac{y}{b} - 1\right) \sum_m \zeta v_m^{(0)}(z) \cos \zeta x \\
&\quad - \frac{k_{17} \cdot y}{b} \sum_m \zeta \cdot v_m^{(b)}(z) \cos \zeta x + k_{17} \sum_m \sum_n \zeta \tilde{v}_{mn}(z) \cos \zeta x \sin \eta y \\
&\quad + k_{17} \left(1-\frac{y}{b}\right) \sum_m \zeta v_m^{(0)}(z) \cos \zeta x + \frac{k_{17} \cdot y}{b} \sum_m \zeta \cdot v_m^{(b)}(z) \cos \zeta x \\
&= k_{17} \sum_m \sum_n [-\eta \tilde{u}_{mn}(z) + \zeta \tilde{v}_{mn}(z)] \cos \zeta x \sin \eta y = 0 \\
D_y &= k_{20} \sum_m \sum_n Y_{mn}(z) \sin \zeta x \sin \eta y - k_{21} \sum_m \sum_n \eta \emptyset_{mn}(z) \sin \zeta x \sin \eta y = 0
\end{aligned} \tag{C-2}$$

APPENDIX D: THE DERIVATION OF EQUATION (4-4)

From Equations (3-3), (3-4) and (4-1), yields

$$\sigma_x = C_{11}\varepsilon_0 + C_{12}\beta v + C_{13}\frac{\partial w}{\partial z} + e_{31}\frac{\partial \emptyset}{\partial z}$$

$$\sigma_y = C_{12}\varepsilon_0 + C_{22}\beta v + C_{23}\frac{\partial w}{\partial z} + e_{32}\frac{\partial \emptyset}{\partial z}$$

$$\sigma_z = C_{13}\varepsilon_0 + C_{23}\beta v + C_{33}\frac{\partial w}{\partial z} + e_{33}\frac{\partial \emptyset}{\partial z}$$

$$\tau_{yz} = C_{44}(\beta w + \frac{\partial v}{\partial z}) + e_{24}\beta \emptyset$$

$$\tau_{xz} = 0$$

$$\tau_{xy} = 0$$

$$D_x = 0$$

$$D_y = e_{24}\left(\beta w + \frac{\partial v}{\partial z}\right) - \in_{22} \beta \emptyset$$

$$D_z = e_{31}\varepsilon_0 + e_{32}\beta v + e_{33}\frac{\partial w}{\partial z} - \in_{33} \frac{\partial \emptyset}{\partial z} \qquad \text{(D-1)}$$

Considering the third and ninth rows of Equation (D-1), $\frac{\partial w}{\partial z}$ and $\frac{\partial \emptyset}{\partial z}$ can be expressed as

$$\frac{\partial w}{\partial z} = \left(\frac{-e_{32}e_{33} - C_{23} \in_{33}}{e_{33}^2 + C_{33} \in_{33}}\right)\beta v + \left(\frac{e_{33}}{e_{33}^2 + C_{33} \in_{33}}\right)D_z + \left(\frac{\in_{33}}{e_{33}^2 + C_{33} \in_{33}}\right)\sigma_z$$

$$\frac{\partial \emptyset}{\partial z} = \left(\frac{C_{33}e_{32} - C_{23}e_{33}}{e_{33}^2 + C_{33} \in_{33}}\right)\beta v + \left(\frac{-C_{33}}{e_{33}^2 + C_{33} \in_{33}}\right)D_z + \left(\frac{e_{33}}{e_{33}^2 + C_{33} \in_{33}}\right)\sigma_z \qquad \text{(D-2)}$$

APPENDIX E: THE DERIVATION OF THE FIRST-ORDER NON-HOMOGENEOUS ORDINARY DIFFERENTIAL EQUATION (4-18)

Substituting Equation (4-15) into (4-8), yields

$$\frac{\partial}{\partial z}\begin{Bmatrix}\tilde{v}(y,z)\\ D_z(y,z)\\ \sigma_z(y,z)\\ \tau_{yz}(y,z)\\ \emptyset(y,z)\\ w(y,z)\end{Bmatrix}+\frac{\partial}{\partial z}\begin{Bmatrix}v^{(0)}(z)\cdot(1-\frac{2y}{b})\\ 0\\ 0\\ 0\\ 0\\ 0\end{Bmatrix}$$
$$=[A]\begin{Bmatrix}\tilde{v}(y,z)\\ D_z(y,z)\\ \sigma_z(y,z)\\ \tau_{yz}(y,z)\\ \emptyset(y,z)\\ w(y,z)\end{Bmatrix}+[A]\begin{Bmatrix}v^{(0)}(z)\cdot(1-\frac{2y}{b})\\ 0\\ 0\\ 0\\ 0\\ 0\end{Bmatrix}+\begin{Bmatrix}0\\ 0\\ 0\\ 0\\ k_8\\ k_4\end{Bmatrix}\varepsilon_0 \tag{E-1}$$

Then Equation (E-1) can be simplified as

$$\frac{\partial}{\partial z}\begin{Bmatrix}\tilde{v}(y,z)\\ D_z(y,z)\\ \sigma_z(y,z)\\ \tau_{yz}(y,z)\\ \emptyset(y,z)\\ w(y,z)\end{Bmatrix}=[A]\begin{Bmatrix}\tilde{v}(y,z)\\ D_z(y,z)\\ \sigma_z(y,z)\\ \tau_{yz}(y,z)\\ \emptyset(y,z)\\ w(y,z)\end{Bmatrix}+\begin{Bmatrix}-\frac{dv^{(0)}(z)}{dz}\cdot(1-\frac{2y}{b})\\ 0\\ 0\\ 0\\ -\frac{2}{b}\cdot k_5\cdot v^{(0)}(z)+k_8\cdot\varepsilon_0\\ -\frac{2}{b}\cdot k_1\cdot v^{(0)}(z)+k_4\cdot\varepsilon_0\end{Bmatrix} \tag{E-2}$$

The eigen-functions in Equations (4-16) and (4-17) are given as follows

$$\tilde{v}(y,z) = \sum_n \tilde{v}_n(z)\sin\eta y, \qquad \tau_{yz}(y,z) = \sum_n Y_n(z)\sin\eta y$$

$$D_z(y,z) = \sum_n D_n(z)\cos\eta y, \qquad \emptyset(y,z) = \sum_n \emptyset_n(z)\cos\eta y$$

$$\sigma_z(y,z) = \sum_n Z_n(z)\cos\eta y, \qquad w(y,z) = \sum_n w_n(z)\cos\eta y$$

$$y = -\sum_{n=0}^{\infty} \frac{2\,b\cos n\pi}{n\pi}\sin\eta y \tag{E-3}$$

By introducing Equation (E-3) into Equation (E-2), Equation (4-18) can be obtained by matching the coefficients of eigen-functions at two sides of Equation (E-2)

$$\frac{d}{dz}\{R_n(z)\} = [\bar{A}]\{R_n(z)\} + \{\bar{B}(z)\} \tag{4-18}$$

APPENDIX F: COMPARISON BETWEEN SSA AND FEM RESULTS ON ELECTRIC QUANTITIES

Table F.1: Electric potential under open-circuit conditions against different *h/a*

		h/a=0.2		*h/a*=0.4		*h/a*=0.6	
		SSA	FEM	SSA	FEM	SSA	FEM
$\bar{\phi}$	T+	0.83019	0.83015	0.24217	0.24210	0.13069	0.13057
x=*a*/2	T-	0.99747	0.99747	0.26830	0.26832	0.13299	0.13304
y=*b*/2	C+	0.99747	0.99747	0.26830	0.26832	0.13299	0.13304
	C-	0.94557	0.94557	0.21695	0.21694	0.08232	0.08229
	B+	0.94557	0.94557	0.21695	0.21694	0.08232	0.08229
	B-	0.75246	0.75250	0.16514	0.16510	0.05784	0.05777
$\bar{\phi}$	T+	0.86513	0.86522	0.25347	0.25351	0.13668	0.13659
x=*a*/2	T-	0.99804	0.99855	0.27078	0.27158	0.13501	0.13590
y=0	C+	0.99804	0.99855	0.27078	0.27158	0.13501	0.13590
	C-	0.93942	0.93904	0.21360	0.21327	0.08052	0.08023
	B+	0.93942	0.93904	0.21360	0.21327	0.08052	0.08023
	B-	0.78193	0.78191	0.17215	0.17195	0.06068	0.06054

Table F.2: Electric field intensity components under open-circuit conditions against different *h/a*

		h/a=0.2		*h/a*=0.4		*h/a*=0.6	
		SSA	FEM	SSA	FEM	SSA	FEM
$\bar{E}_x$	T+	-0.31439	-0.31750	-0.17241	-0.17546	-0.13761	-0.14058
x=a/4	T-	-0.38902	-0.38931	-0.20215	-0.20215	-0.15182	-0.15187
y=b/2	C+	-0.38902	-0.38931	-0.20215	-0.20215	-0.15182	-0.15187
	C-	-0.38783	-0.38783	-0.18660	-0.18661	-0.10853	-0.10850
	B+	-0.38783	-0.38783	-0.18660	-0.18661	-0.10853	-0.10850
	B-	-0.31338	-0.31341	-0.14397	-0.14395	-0.07671	-0.07665
$\bar{E}_y$	T+	0.01445	0.01451	0.01060	0.01070	0.00897	0.00899
x=a/2	T-	-0.00028	-0.00023	0.00186	0.00213	0.00179	0.00213
y=b/4	C+	-0.00028	-0.00023	0.00186	0.00213	0.00179	0.00213
	C-	-0.00172	-0.00175	-0.00318	-0.00340	-0.00287	-0.00309
	B+	-0.00172	-0.00175	-0.00318	-0.00340	-0.00287	-0.00309
	B-	0.01191	0.01192	0.00571	0.00558	0.00361	0.00349
$\bar{E}_z$	T+	-1.10321	-1.10364	-0.21754	-0.21839	-0.06928	-0.07078
x=a/2	T-	-0.57430	-0.57420	-0.04780	-0.04788	0.04335	0.04295
y=b/2	C+	-0.20861	-0.20858	0.05468	0.05466	0.09815	0.09802
	C-	0.38177	0.38163	0.11556	0.11561	0.06297	0.06307
	B+	0.70322	0.70302	0.17062	0.17068	0.06937	0.06945
	B-	1.23249	1.23220	0.35245	0.35267	0.18128	0.18136

Table F.3: Electric displacements under open-circuit conditions against different *h/a*

		h/a=0.2		*h/a*=0.4		*h/a*=0.6	
		SSA	FEM	SSA	FEM	SSA	FEM
$\overline{D}_x$	T+	-2.16157	-2.18186	-1.18541	-1.20639	-0.94614	-0.96669
x=*a*/4	T-	-1.18083	-1.17776	-0.67999	-0.67965	-0.57837	-0.57813
y=*b*/2	C+	0.31307	0.31524	0.02990	0.03063	-0.11290	-0.11098
	C-	0.35124	0.35246	0.41869	0.42004	0.45615	0.45707
	B+	-1.15765	-1.15402	-0.43212	-0.43022	-0.14502	-0.14325
	B-	-2.15466	-2.15080	-0.98984	-0.98799	-0.52743	-0.52542
$\overline{D}_y$	T+	0.09934	0.10019	0.07286	0.07361	0.06169	0.06182
x=*a*/2	T-	0.22632	0.22843	0.06398	0.06291	0.01700	0.01389
y=*b*/4	C+	0.45460	0.45633	0.11518	0.11092	0.02167	0.01312
	C-	0.44889	0.45063	0.17057	0.17384	0.10180	0.10656
	B+	0.21854	0.22034	0.07435	0.07562	0.04104	0.04299
	B-	0.08190	0.08331	0.03926	0.03887	0.02481	0.02445
$\overline{D}_z$	T+	0.00000	0.00018	0.00000	0.00006	0.00000	0.00002
x=*a/2*	T-	-0.23735	-0.23572	-0.25548	-0.25500	-0.34356	-0.34406
y=*b*/2	C+	-0.23735	-0.23589	-0.25548	-0.25501	-0.34356	-0.34404
	C-	0.23602	0.23584	0.21769	0.21765	0.13699	0.13622
	B+	0.23602	0.23568	0.21769	0.21767	0.13699	0.13628
	B-	0.00000	-0.00039	0.00000	0.00003	0.00000	0.00020